The influence of basement structure and volcanics on the evolution of the Uruguayan margin

Holly Jayne Rowlands

Submitted in accordance with the requirements for the degree of

Doctor of Philosophy

The University of Leeds

Institute of Applied Geoscience

School of Earth and Environment

August 2020

The candidate confirms that the work submitted is her own and that appropriate credit has been given where reference has been made to the work of others.

Acknowledgements

I would very much like to thank my supervisors, Douglas Paton and Estelle Mortimer for their guidance, advice and technical discussions over this time. It has been a pleasure to gain from their experience and knowledge. More importantly, I would like to thank them for their patience, support and understanding over the past, (extremely challenging) few years. (I made it in the end!).

I would like to thank Gerencia de Exploración y Producción, ANCAP of Montevideo, Uruguay and BG Group (now Shell) as well as ION Geophysical for providing the data used in this thesis.

I am grateful to Jonathan Turner for his advice and guidance and for being my external supervisor whilst BG Group was still in existence. I would also like to thank Phil Thompson (formerly BG Group, now Shell) for technical discussions and advice, especially earlier in this project and at conferences and presentations. My thanks also go out to Carlos Urien and Pablo Gristo in Montevideo for discussions at conferences and their interest in my work.

I would like to thank all students, staff and postgrads, past and present at the Basin Structure Group at Leeds, for keeping me sane with office discussions (work related and otherwise) and as a sounding board when needed. Special mention to Ben Craven, James Norcliffe, Simon Oldfield and Emma Bramham for discussions and encouragement.

I'm very grateful to have had the support of the University of Leeds Student counselling service, especially Liz Oxley and also Alison Plant of the lifestyle and wellbeing program. I would also like to acknowledge Ian Burke and Fiona Gill for their independent advice and support. I am also very grateful to Michelle Lesnianski for all the help, encouragement, support and university liaison work she has provided to me, as well as her understanding office chats.

This thesis is dedicated to my best friend (and the best mum ever), who unfortunately passed during this process. Thank you for your unwavering love, support and belief in me. I truly could not have done this without you, or without believing you are still at my side in spirit.

Abstract

A common characterisation of rifted margins is into those which are magma-rich and those which are magma-poor. Despite a global abundance of magma-rich margins, there are still gaps in our understanding as to how these margins evolve. The Uruguay margin is traditionally considered magma-rich, along with the conjugate South African margin. In this thesis, new insights are gained into the volcanic basement of offshore Uruguay. Outstanding research questions that are answered involve the variable contributions of tectonism and magmatism to the margin architecture and the influence of inherited fabrics on the siting of nascent rifting. Also investigated is the poorly- understood, continent-ocean boundary within transitional crust, one of the last major unsolved regions of plate tectonics. It is demonstrated that a geologically brief period of margin-oblique rifting is preserved in the offshore basement, agreeing with previous work that the Uruguayan Punta del Esté Basin represents an extensional aulacogen. This study reveals highly atypical crustal morphology across the margin, integrally linked to pre-existing pan-African crustal heterogeneities. Locally, magmatic crust is demonstrated as comprising the basement of the offshore margin, replacing pre-existing continental crust and a rare, well-defined, magma chamber has been identified in 3D within the transitional domain that provides key information on early Cretaceous South Atlantic rifting and the subsequent tectono-magmatic evolution of the margin. The exact timing of magma emplacement is still unknown, leaving open the possibility of a phase of early rifting confined to a margin-oblique orientation. However, this work suggests that the majority of oblique rifting and magmatism was contemporaneous with the start of early Atlantic rifting and quickly abandoned as the South Atlantic pole of rotation changed with the progression of northward propagating rifting. This has

provided a rare 3D window into the early rifting of a complex, magma-rich rifted margin.

Table of Contents

List of Figures

List of Tables

Key

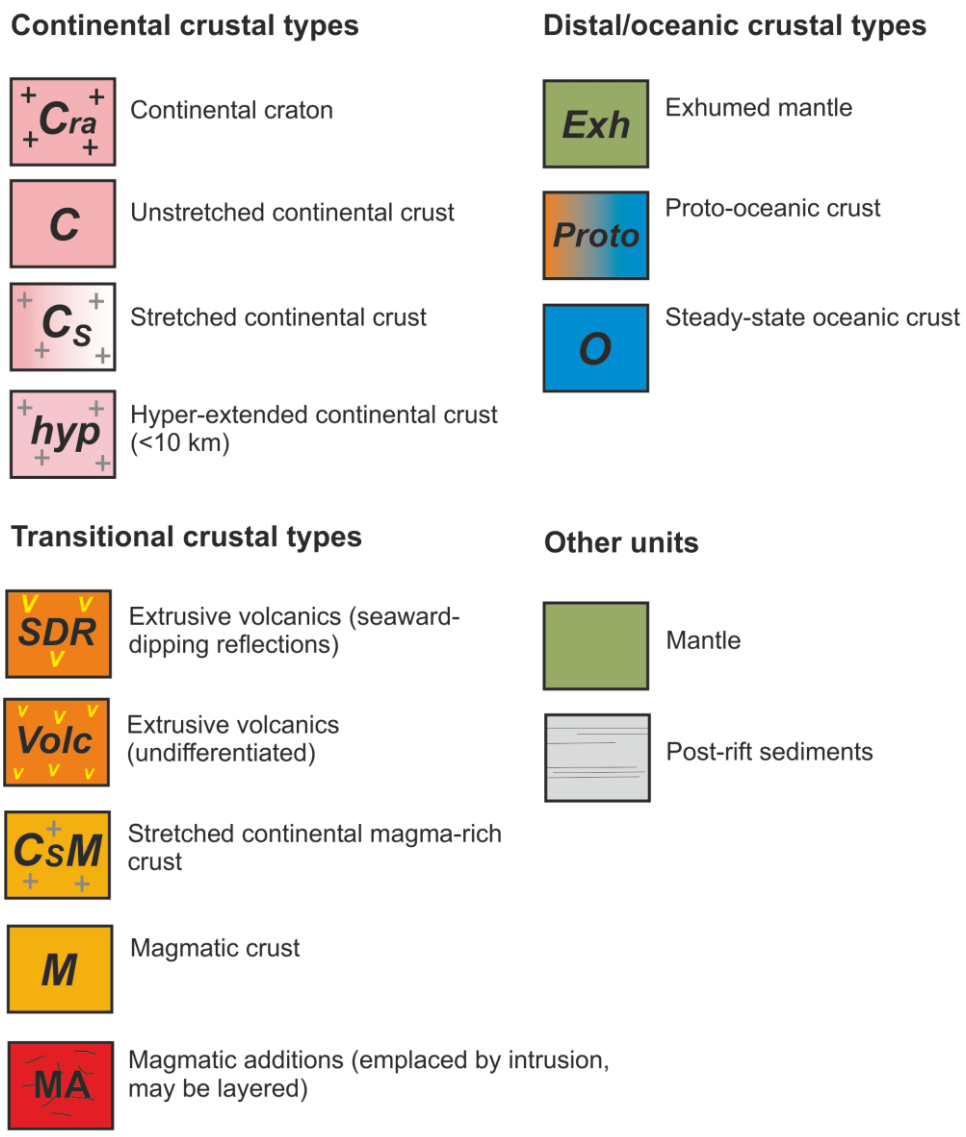
Continental crustal types
Cra
Continental craton
C
Unstretched continental crust
Cs
Stretched continental crust
hyp
Hyper-extended continental crust (<10 km)
Distal/oceanic crustal types
Exh
Exhumed mantle
Proto
Proto-oceanic crust
O
Steady-state oceanic crust
Transitional crustal types
SDR
Extrusive volcanics (seaward-dipping reflections)
Volc
Extrusive volcanics (undifferentiated)
CsM
Stretched continental magma-rich crust
M
Magmatic crust
MA
Magmatic additions (emplaced by intrusion, may be layered)
Other units
Mantle
Post-rift sediments

Abbreviations

COT	Continent-ocean transition
HVLC	High velocity lower crust
LCB	Lower crustal body
ODP	Ocean Drilling Program
Penrose	Refers to the full ‘layer-cake’ model of oceanic crust derived from ophiolite studies Vine & Moores, (1972)
PdE	Punta del Esté Basin
RdP	Rio de la Plata craton
RPTS	Rio de la Plata Transfer System
SDR/s	Seaward-dipping reflections

Chapter 1A: Background to scientific rationale

1.1 Rationale

Models for the development of rifted margins have been commonly divided into archetypal end members, volcanic or non-volcanic (McCarthy et al., 1988; White and Mckenzie, 1989). However, more recently there has been an appreciation of a range of magmatic budgets during rifting leading to the terminology, magma-poor and magma-rich (Tugend et al., 2018; Lundin et al., 2018; Harkin et al., 2019). The process of rifting on magma-poor margins is well understood because we are able to directly observe and measure elements such as the exhumation of mantle in the distal portions of non-volcanic margins (i.e the Iberian margin) through ocean drilling programs (Boillot et al., 1980; Boillot et al., 1987), field analogues (Florineth and Froitzheim, 1994; Manatschal and Müntener, 2009), and numerical modelling (Lavier and Manatschal, 2006; Pérez-Gussinyé et al., 2006; Gillard et al., 2017). As such, there is a wealth of studies pertaining to magma-poor margins (Cannat et al., 2009; Manatschal and Müntener, 2009; Perez-Gussinye, 2012; Davis and Lavier, 2017; Decarlis et al., 2018) however, Magma-rich margins are less well-studied, with seismic signals from basement structures often obscured by syn-rift volcanism (Reston, 2005; Abdelmalak et al., 2016; Osmundsen and Péron-Pinvidic, 2018). The Atlantic margins have received considerable attention over recent years with the identification of large hydrocarbon reserves associated with passive margins on both sides (most notably, in the Santos and Campos Basins of Brazil and offshore West Africa). This resurgence of interest has driven research by a suite of authors into how magma-rich margins develop (Eldholm et al., 2000; Franke et al., 2002; Planke et al., 2003; Franke et al., 2007; Franke et al., 2010; Soto et al., 2011; Blaich et al., 2013). It has also necessitated the collection of new, high resolution 2D and 3D datasets to identify potential new prospects and mitigate the risks associated

with further exploration and development. This has benefited academia with the advent of these state-of-the-art datasets becoming accessible. This study is the first investigation into the volcanic basement of offshore Uruguay. The basement of a rifted passive margin is an often under-studied region that can give important insights into early rift processes and the key transitional crust region created between continental rifting and oceanic spreading. The volcanic basement and its interaction with rift faulting can also give a window into the early tectono-magmatic evolution of the margin, with wider implications for heat flow and the thermal profile of the margin. This can have ramifications for the location and maturation of overlying source rocks. Offshore Uruguay has remained a frontier area and as such has been poorly studied, certainly in comparison to its South American neighbours, Argentina and Brazil. This has been primarily due to uncertainties surrounding its hydrocarbon potential and until recently, a lack of good quality data both in the form of seismic data and well data. Very little is known about the pre-rift and basement of offshore Uruguay, with only two wells high on the continental shelf which did not penetrate deeper strata. Legacy, 2D multi-channel seismic reflection surveys have struggled to record a good signal at depths beyond ~10 km and apart from the identification of a transfer system in 2011 (Soto et al., 2011) there has been no work focused upon deciphering the nature of the basement in the region. The recent (2014-) data advancements now allow for a comprehensive, regional 2D study of the region to depths of ~30 km. Of particular interest is understanding the transitional zone between continental crust and the creation of new oceanic crust on magma-rich margins, which remains a poorly understood area of study (Gillard et al., 2017). Offshore Uruguay provides the ideal location for this study as it is a known magmatic margin with both the 2D and 3D datasets covering the transitional domain. In particular the 3D dataset is positioned over the transfer system between the two

major, Seaward-dipping reflections (SDR) wedges and the continent-ocean boundary. The region provides an example of the underlying complexities of magmatic margins, which are both under-recognised and under-studied. This thesis will use multi-client, multi-channel seismic reflection datasets in 2D and 3D from offshore Uruguay, to provide new insights into the break-up and subsequent continental margin development of offshore Uruguay. A particular focus is also given to the smaller-scale interactions between tectonism and rift magmatism. Significant advances in geophysical techniques now allow for the imaging of magma plumbing systems globally (Magee et al., 2018) and this study identifies key elements of an unrecognised magmatic system in the Uruguayan offshore basement. Understanding the transition between pre-existing continent and the creation of new oceanic crust is one of the last major unsolved problems of plate tectonics (Gillard et al., 2017).

1.2 Aims and objectives

The specific objectives of the project are:

1. *To determine the role of structural inheritance in margin evolution.*
2. *To answer, does Uruguay conform to a typical magmatic margin?*
3. *To provide insights into the 3D evolution of magmatic plumbing systems through mapping of a magma chamber and associated connective elements.*

The aim of the study is to provide a 2D regional framework to understand the regional development of the volcanic basement of offshore Uruguay. The margin is first considered in a regional context, using a high resolution, long recording time 2D PSDM dataset from ION Geophysical that covers 2,800 km of the Uruguayan margin. A regional scale crustal characterisation and seismic facies mapping will be undertaken, identifying crustal scale fabrics and structures. This will highlight tectono-magmatic features which are both typical and atypical of volcanic margin

development and are newly recognised in offshore Uruguay. This will answer the question as to whether the Uruguay margin conforms to a typical magmatic margin. 3D conceptual models will be used to explain observations and decipher the tectono-magmatic arrangement of offshore Uruguay. A state-of-the-art, 3D PSDM seismic reflection dataset was shot in 2014-15 which fits within the 2D ION SPAN PSDM data and in conjunction, covers 13,000 km^2 of the margin. This data coverage allows the first 3D investigation of an offshore rift system, previously identified as the Rio de la Plata Transfer System (RPTS) by Soto et al., (2011). A new, complex syn-rift magmatic plumbing system will be identified and a large magma chamber will be mapped in detail. Conduits and feeder dykes are identified as connective elements and suggest a wider volcanic plumbing system that has been previously unrecognised. A unique window is created into the three-dimensional development of a highly volcanic margin, firstly in a regional, 2D context followed by a more focused, 3D data investigation that provides a detailed investigation of a magma chamber and a wider magmatic plumbing system that ties into seaward-dipping reflections and syn-rift magmatism.

1.3 Location of the study area

The study area is in offshore Uruguay, off the South American, Atlantic coast at approximately 35.5ºS, 53.5ºW. Figure 1.1, modified from Hernández-Molina et al. (2016) presents a regional map of the Uruguayan continental margin with base topography and bathymetry provided by SRTM 15m topographic data overlain on Google Earth™. Structural highs are shown as red dashed lines, transparent white areas delimit areas of shallow basement and the location of the only two known wells, Lobo and Gaviotín are also indicated on the continental shelf. The landward limit of the voluminous extrusive volcanics, known as Seaward-dipping reflectors (SDRs) is based upon Franke et al. (2007) and is shown as a dashed black line,

behind the SDRs which are outlined in Orange. Onshore basins are outlined in White and the major offshore basins in Black. Oceanic fracture zones are shown as continuous black lines, then dashed where uncertainty exists as to their continuation.

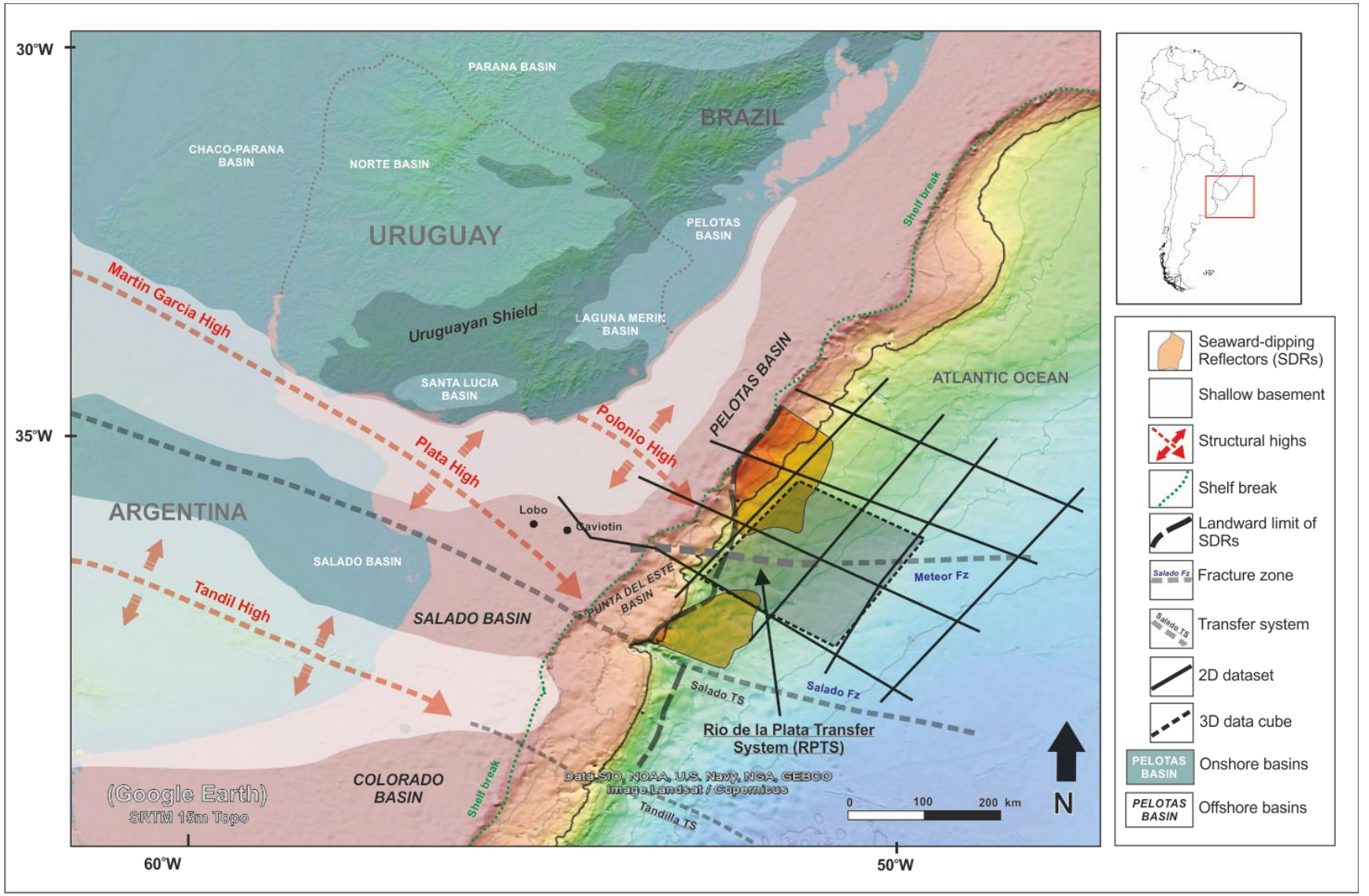

Figure 1.1: Regional scale location map of offshore Uruguay showing onshore and offshore basins, structural highs and geological features. The landward extent of the Seaward-dipping reflections (SDR) is based upon Franke et al., (2007). Modified from Franke et al., (2007) and Hernández-Molina et al., (2016).

Chapter 1B: The architecture and evolution of rifted passive margins

1.1 Magma-poor margins

Magma-poor margins consist of up to 50% of all rifted margins globally (Manatschal and Müntener, 2009). They exhibit very little syn-rift magmatism, (a defining feature of magma-rich margins) (Pérez-Gussinyé et al., 2006; Reston, 2007; Reston, 2009; Bronner et al., 2009; Reston and McDermott, 2011; Franke, 2013). These magma-poor settings reveal more about the rift initiation process than magma-rich margins, as tectonic features are not buried by voluminous volcanics (Reston, 2005). The crustal architecture of a magma-poor margin includes a succession of zones which show gradation from the proximal realm, with limited crustal stretching (Doré and Lundin, 2015) but attenuated continental crust and upper-crustal, listric detachment faults (Figure 1.2) (Franke, 2013). This continues through to hyper-extension of the crust and exhumed mantle and ultimately, steady-state (Penrose) oceanic crust (Doré and Lundin, 2015).

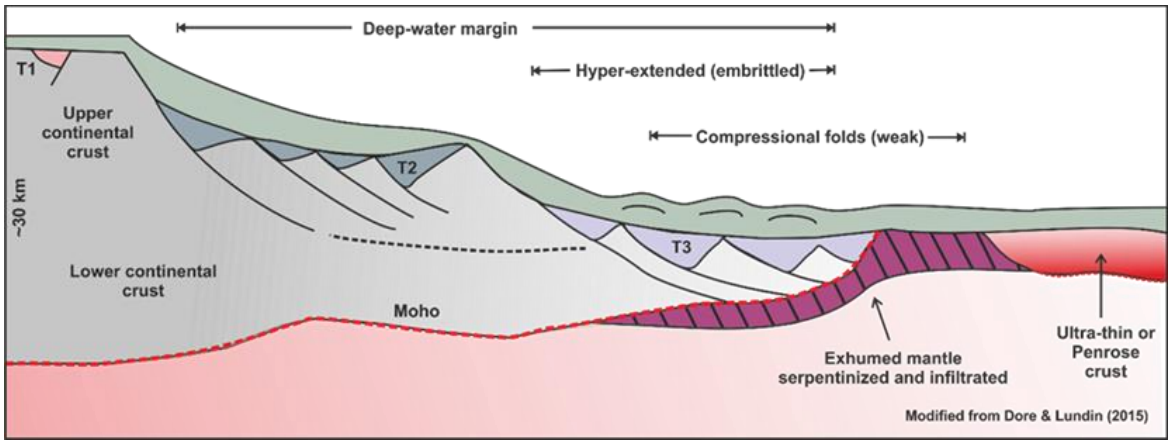

Figure 1.2: Characteristics of a magma-poor margin, modified from Doré and Lundin, (2015)**.**

This sequence plays out over a width of +100 km from the continent to the oceanic realm and has been widely studied in regions such as the Atlantic conjugates of western Iberia and Newfoundland (Whitmarsh et al., 2001; Reston, 2005; Reston, 2007; Perez-Gussinye, 2012; Loegering et al., 2013; Peron-Pinvidic et al., 2013;

Doré and Lundin, 2015). Further examples include those of Brazil and Angola (Brune et al., 2014) and the south China sea (Franke, 2013). Exhumed mantle material occurs over the continent-ocean transition zone (COT) (Pérez-Gussinyé et al., 2006; Reston, 2007; Gillard et al., 2015) which is a genetic and geographical link between the margin and the first oceanic crust (Cannat et al., 2009). During the early stages of mantle exhumation, the supply of magma is most likely passively controlled by mechanical processes and faulting but later competes with/interacts with, thermal processes (Decarlis et al., 2018). An example may be a rising mantle plume, which can help to localise deformation or a raised asthenosphere.

1.1.1 Evolution of a magma-poor margin

Traditionally, plate-driven models of extension are invoked to explain the development of non-volcanic margins (Gillard, Manatschal, et al., 2016). Perhaps the most common model to explain the asymmetry of distal regions of magma-poor margins is the ‘rolling-hinge model’ (Buck, 1988). The model by Buck, (1988) noted that it is difficult to reconcile an active system of low-angle faults with rock mechanics, earthquake focal mechanisms or geochronology. The rolling-hinge model, negates the need for active fault slip on low-angle faults. The model results in an abandoned, horizontal normal fault or ‘detachment’ (figure 1.3).

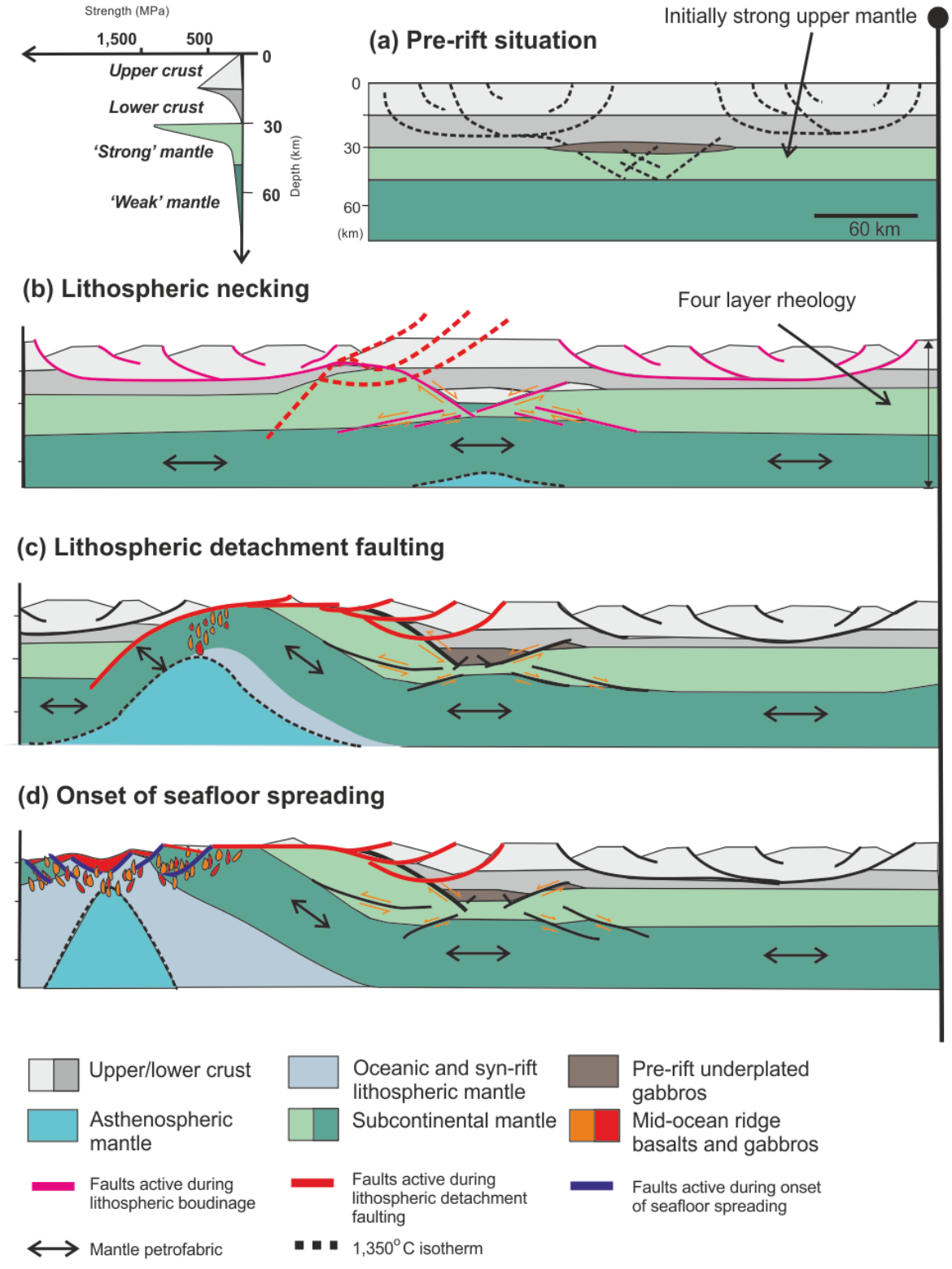

Figure 1.3: Conceptual lithospheric scale model of the development of a rifted magma-poor margin, relative to a fixed right hand edge (basin thickness not to scale) modified from Whitmarsh et al., (2001). (a) Pre-rift situation (b) Lithospheric necking (c) Lithospheric detachment faulting (d) Onset of seafloor spreading. See text for further details.

This leads to passive continental break-up controlled by a far-field stress regime (Franke, 2013). There is general agreement that extension is predominant within a coupled system of upper and lower crustal deformation (Reston, 2007; Franke,

2013). This may manifest in lower crustal ductility, sometimes to the upper asthenosphere but with little production of syn-rift igneous material (Reston, 2007; Reston, 2009; Bronner et al., 2009; Reston and McDermott, 2011; Perez-Gussinye, 2012). Figure 1.3 presents a conceptual, lithospheric scale model of the development of a rifted magma-poor margin from Whitmarsh et al., (2001). The model has been fixed at the right hand edge and shows an initial pre-rift situation (a, Figure 1.3) with a four layer rheology and a crust which may be locally thickened by under-plated gabbro (Whitmarsh et al., 2001). The upper mantle is initially strong, but is then 'necked' beneath the gabbro, where it has the least strength (b) this allows for the Asthenosphere to rise (Whitmarsh et al., 2001). In areas where rift basins have formed at the surface, this is suggested to be due to lower crustal ductile flow (Whitmarsh et al., 2001). Areas adjacent to the necked region are actually the first to thin, followed by a response to the asthenospheric rise, which alters the thermal regime and begins to influence rifting (c). This is localised to one side of the weakened lower crustal region, accompanied by a change from listric extensional faulting into one or more convex, detachment faults (c) due to the change in the distribution of weak layers (Whitmarsh et al., 2001). Whitmarsh, et al., (2001) propose that this style of faulting is more likely to be favoured by sub-vertical weaknesses or faults, which may be exploited by rising magma associated with an increased thermal gradient above a narrowing asthenospheric bulge. By (d), Figure 1.3, the Asthenosphere has risen close to the surface, creating mid-ocean ridge basalts which are intruded (or extruded onto) the sub-continental mantle (Whitmarsh et al., 2001). The deeper layers of mantle are exhumed oceanward and with increasing melt from the rising asthenosphere. Oceanic upper mantle is eventually created and the process of seafloor spreading begins proper (Whitmarsh et al., 2001). During the necking stage there can be created a section of tectonically

influenced continental block in the necking zone between adjacent areas of continental crust and bound by ‘oceanward’-dipping, conjugate master faults (Geoffroy et al., 2015). This is referred to by some authors as an H-Block. Description of the thinning, necking and evolutionary process for a magma-poor region is perhaps just as important as that of a magma-rich margin, as it illustrates that definition of ‘end-members’ to rifting can be problematic as there is always some degree of volcanism/magmatism and seafloor spreading itself is magmatic (Russell and Whitmarsh, 2003) - it is the marked absence of large amounts of syn-rift extrusive volcanics which is definitive on these margins.

1.1.2 Hyper-extension on a magma-poor margin

The term ‘hyper-extended’ is defined as significant stretching of the crust until the upper and lower crust become coupled and hardened (Doré and Lundin, 2015). Large faults are then able to penetrate the mantle through embrittlement, transporting fluids to the upper mantle (Harkin et al., 2019) and creating serpentinisation (of the upper mantle) through hydration (Lundin and Dore, 2011; Doré and Lundin, 2015). Hyper-extension is predominantly associated with magma-poor regions and has been documented in other parts of the South Atlantic, such as the west African continental margin (Contrucci et al., 2004; Doré and Lundin, 2015), Western Australia (Direen et al., 2007) and the Red Sea (Cochran and Karner, 2007). Doré and Lundin, (2015) and Perez-Gussinye and Reston, (2001) suggest that it requires a stretching factor of 3-4 with crustal thinning to 8 km or less. Harkin et al., (2019) suggest that continental crust which has been thinned to less than 10 km is hyper-extended and becomes embrittled. Additional magmatism is also recognised to occur in exhumed mantle domains, with sub-continental mantle being revealed in regions such as the Iberia-Newfoundland margin and the Alpine-Tethys margin (Lavier and Manatschal, 2006; Manatschal and Müntener, 2009). Field

evidence from recent work in the northern Apennines/Italy now suggests that magma is actually present throughout the exhumation process of a magma-poor margin (Decarlis et al., 2018).

1.1.3 Mantle exhumation

Exhumed mantle is predominantly associated with the transitional zone or continent-ocean boundary of magma-poor regions. It was first identified ~30 years ago in the distal region of the magma-poor, Iberian margin (Boillot et al., 1980; Péron-Pinvidic et al., 2009). On this margin, it occurs as a result of focused extension and the embrittlement of continental crust, which creates concave-downward detachment faults, which then exhume mantle rock to the sea floor (Whitmarsh et al., 2001; Lavier and Manatschal, 2006; Reston, 2007; Davy et al., 2016). These detachment faults are integral to the commonly used, 'rolling-hinge model' for magma-poor margins, first proposed by Buck, (1988) and are still a feature of newer models (figure 1.3) (Whitmarsh et al., 2001). Exhumation of the mantle is a challenging aspect as it cannot be isotopically dated and does not show linear magnetic anomalies (Doré and Lundin, 2015). However, there is well data to back up interpretations of exhumed mantle on the Iberian margin, in the form of the ODP well data (Ocean Drilling Program well data, sites 1068 and 1070) (Sibuet et al., 2007). Seismic velocities for exhumed, serpentinised mantle may range from 5-8 km s^{-1} (Reston, 2009; Harkin et al., 2019) with surface densities (depth-dependant) from 2650 to 2850 kg m^{-3} and 3000 kg m^{-3} at depth (Harkin et al., 2019). Exhumed mantle has been observed in seismic sections of rifted margins globally, these include; the distal region of the Australian-Antarctic margin (figure 1.4) (Gillard et al., 2015; Gillard, Autin et al., 2016) the previously mentioned and widely studied, Iberia-Newfoundland rifted margin (Boillot et al., 1980; Seifert and Brunotte, 1997; Whitmarsh et al., 2001; Manatschal et al., 2001; Russell and Whitmarsh, 2003;

Henning et al., 2004; Lavier and Manatschal, 2006; Reston, 2007; Sibuet et al., 2007; Kusznir and Karner, 2007; Péron-Pinvidic and Manatschal, 2009; Perez-Gussinye, 2012; Sutra et al., 2013; Davy et al., 2016; Brune et al., 2017; García-Senz et al., 2019); the East Indian-Antarctica rifted margin (the Krishna-Godvari Basin in particular, see figure 1.5) (Mangipudi et al., 2014; Sinha et al., 2016; Harkin et al., 2019; Tugend et al., 2020). Also, the remnants of the Alpine-Tethys rifted passive continental margin (Müntener and Hermann, 2001). There are many factors which influence continental break-up, the presence of any exhumed mantle on a predominantly 'magma-rich' margin would suggest a multi-phase, complex development which may have initially been non-magmatic.

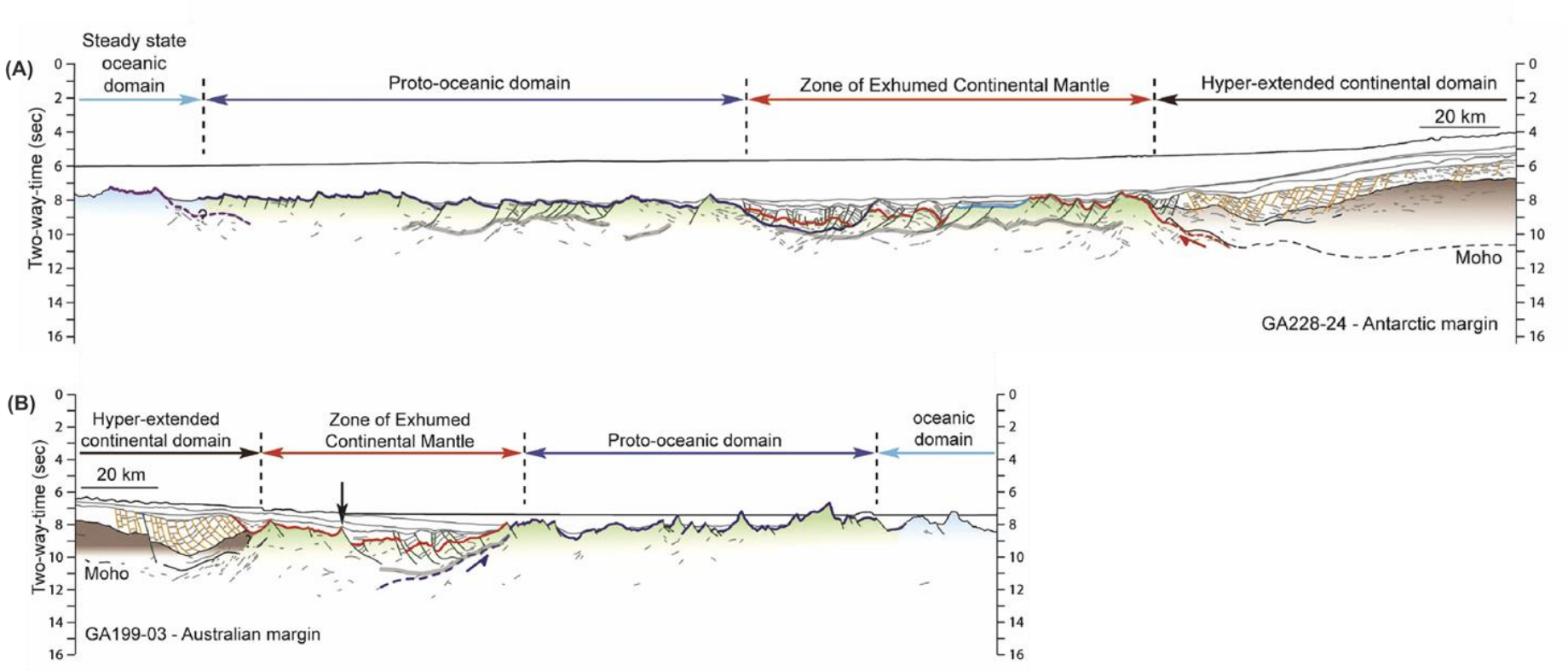

Figure 1.4: Line interpretations and fault mapping of two seismic sections (TWT) along the Australian and Antarctic margins with crustal domains, including zones of exhumed continental mantle. Modified from Gillard, Autin, et al., (2016). (A) Suggests a larger region of exhumed mantle on the Antarctic side of the margin, (B) shows a smaller region of exhumed mantle along the Australian margin.

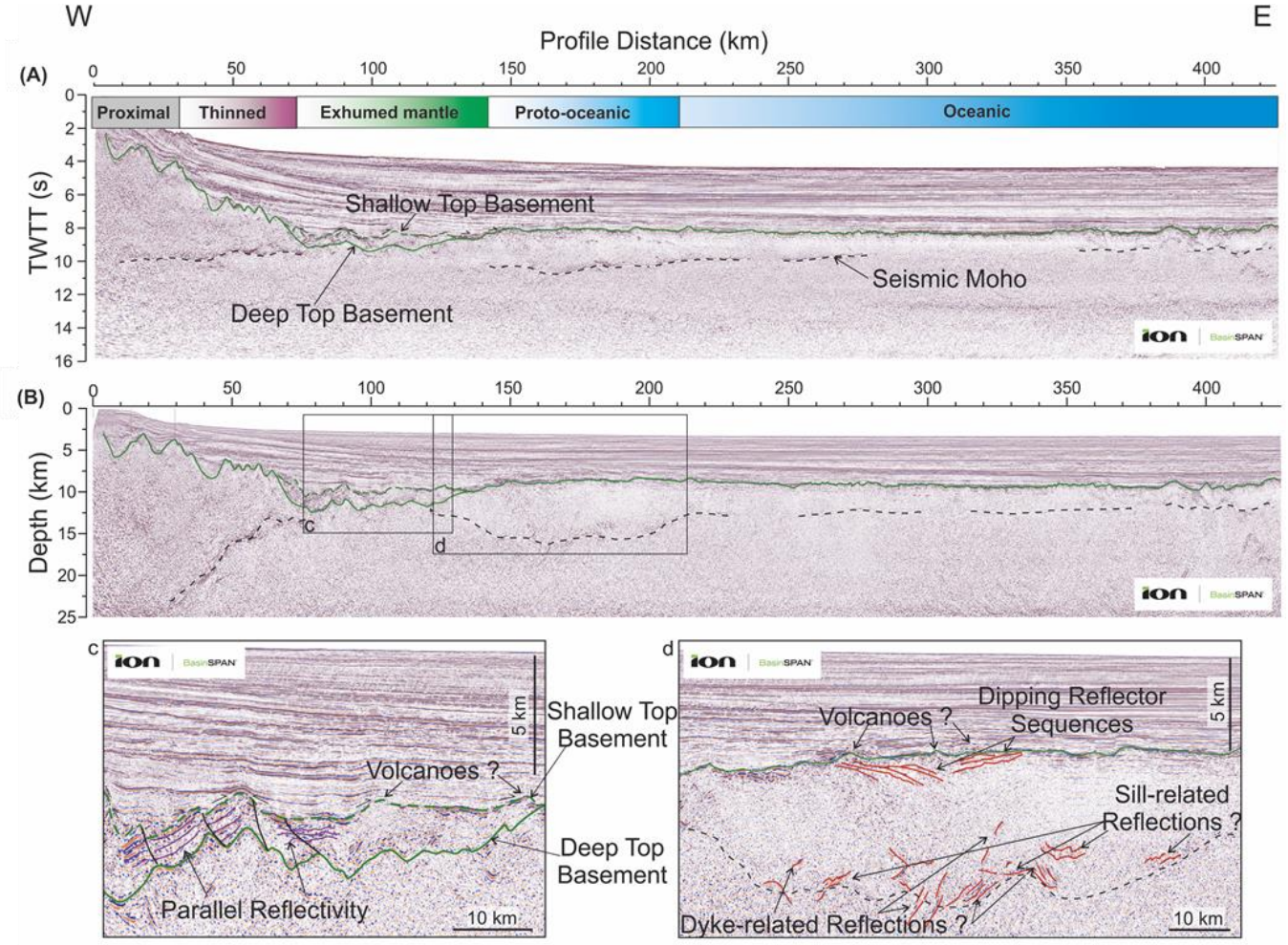

Figure 1.5: Seismic observations of ION line INE-1000 in the Krishna-Godvari Basin by Harkin et al., (2019) Crustal domain divisions taken from same line from Tugend et al., (2018)**.** (A) Pre-stacked time migrated (PSTM) (B) Pre-stacked depth migrated (PSDM) (c) and (d) are enlargements of boxes shown in (B). (c) Shows the top section of a region of exhumed mantle.

1.2 Magma-rich margins

1.2.1 Characteristics of a magma-rich margin

In contrast to magma-poor margins, those of a volcanic origin have been ascribed to active, plume-driven processes, initiating rifting with large volumes of igneous extrusives accompanying break-up (Menzies and Klemperer, 2002; Geoffroy, 2005). These extrusives can be of a significant extent and therefore represent a well-recognised and dominant morphological feature of volcanic rifted margins. Figure 1.6 modified from Geoffroy, (2005), presents an across-strike section through a typical magma-rich passive margin.

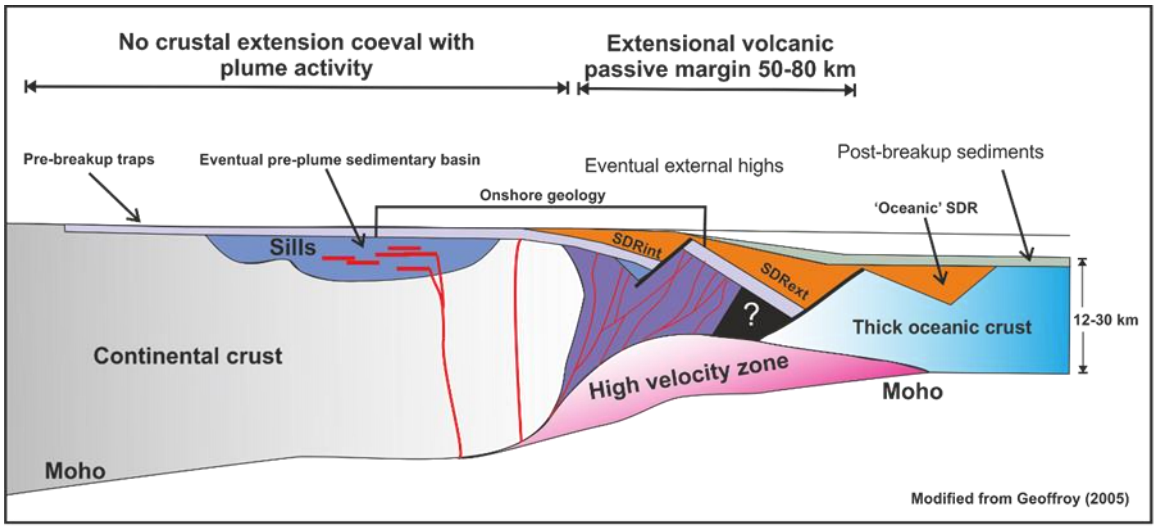

Figure 1.6: Diagram of the commonly seen features associated with a classic magma-rich, rifted margin, modified from Geoffroy, (2005).

Key features of the margin section are a 50-80 km wide seaward-dipping reflection sequence with an underlying high velocity zone, often termed the (HVLC - High Velocity Lower Crust. Geoffroy, (2005) also suggests an 'Oceanic' SDR overlying a thick sequence of oceanic crust, 12-30 km in thickness. Figure 1.7 presents a schematic diagram, interpreted from an example dip-line through the Argentine continental margin (to the south of the study area) (Franke et al., 2010).

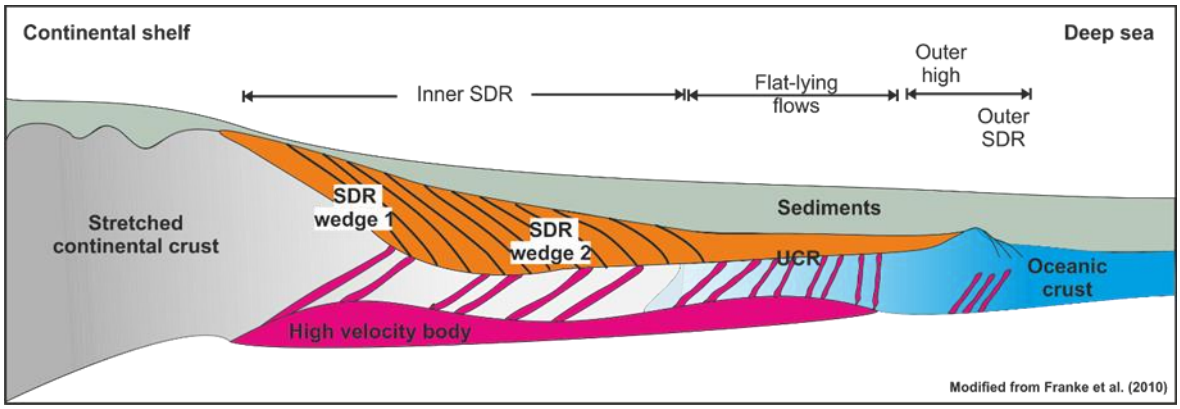

Figure 1.7: Diagram illustrating the main volcanic/magmatic features of the Argentine continental margin, modified from Franke et al., (2010).

This is an illustration of a 'classic magma-rich margin' geometry, with associated features such as a stretched crust in the proximal region moving into a large wedge of volcanic seaward-dipping reflections (SDRs). These are underlain by a region of high velocity lower crust (HVLC) or high velocity body which transitions into flat-lying volcanic flows and then into oceanic crust (with or without an associated outer high). Franke et al., (2010) also define a wedge of 'Inner SDRs' which are proximal to the outer high, and that of 'Outer SDRs' which lie oceanward of the outer high. Paton et al., (2017) go further in suggesting inner SDRs are emplaced onto attenuated continental crust and outer SDRs are contained within a 'magmatic crust', similar to oceanic crust.

1.2.2 Large Igneous Provinces (LIPs)

At magma-rich margins, lithospheric break-up also occurs before, or at the same time within the crust (Franke, 2013). This may be expressed by the creation of large igneous provinces (LIP) such as the Parana-Etendeka complex of the South Atlantic, (Torsvik et al., 2009; Will and Frimmel, 2013; Heine et al., 2013; Taposeea et al., 2017) or commonly, with wedges of seaward-dipping reflections (SDR) (Mutter et al., 1982; Mutter, 1985; Roger et al., 1988). Both SDRs and flood basalts/LIPs occur within a relatively short geological time periods ~2 Ma for SDRs (Mutter et al., 1982) but produce significant syn-rift volcanics and create lasting

geomorphological features on magma-rich margins. Figure 1.8 (A) presents another interpretation of a typical magmatic margin by Paton et al., (2017), with significant magmatism in the form of a large wedge of SDRs, which are underlain by gabbroic, melt-depleted magma-chambers (Paton et al., 2017). Figure 1.8 (B) presents a dip line, seismic reflection data section (PSDM) which shows the expected margin geometry and associated first order seismic facies associations. These relate to a region of proximal, continental crust and the following features noted in figure 1.8, B; (1) Seaward-dipping reflections with convex-up reflections, (2) a shallowing Moho towards oceanic crust; attenuated and intruded continental crust, (3) Steep Moho reflections (4) thick post-rift sediments (5) oceanic crust (6) and a region of transitional crust in the zone between the continental and oceanic domains (7).

1.2.3 Evolution of a magma-rich margin

The evolution of a magma-rich margin is an ‘active process’, controlled by various levels of extrusive flood volcanism, intrusive magmatism, uplift/erosion and extension (Menzies and Klemperer, 2002). Inherited lithospheric elements such as composition, thickness and thermal structure, or mantle temperatures (White and McKenzie, 1989; Reston and Morgan, 2004) influence the early evolution of magma-rich margins (Menzies and Klemperer, 2002), along with the thermal and rheological characteristics of the upper mantle.

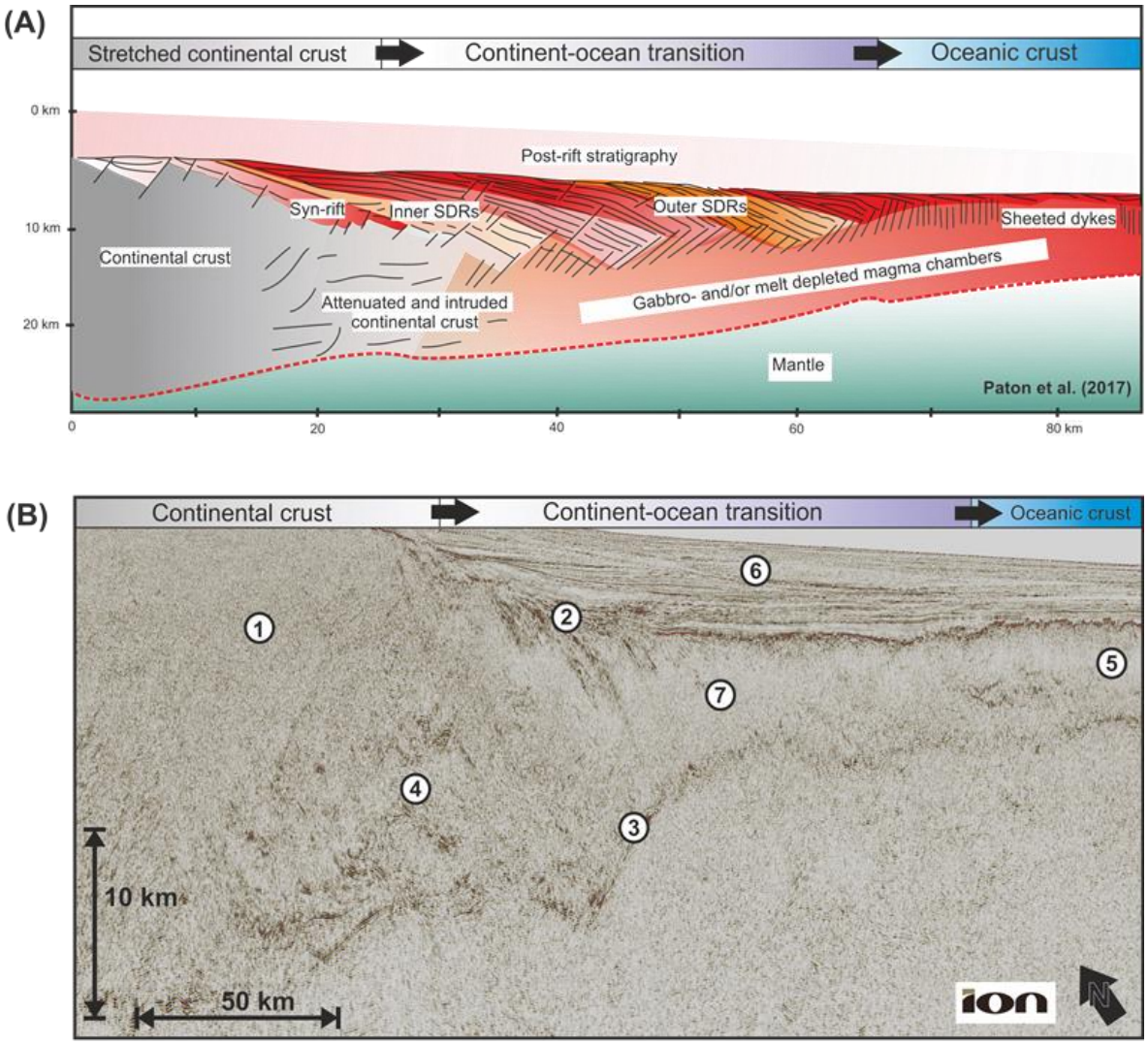

Figure 1.8: (A) Summary interpretation of a typical volcanic passive margin with significant magmatism in the form of SDRs (Seaward-dipping reflections) modified from Paton et al., (2017). (B) Example seismic reflection (PSDM) data line showing typical magmatic margin geometry (dip line section from the Uruguay SPAN (ION) dataset. (1) Continental crust (2) Seaward-dipping reflections (3) Steep Moho reflections (4) Attenuated and intruded continental crust (5) Oceanic crust (6) Thick post-rift sediments (7) Transitional crust.

Magma-rich margins, in contrast to those which are magma-poor, are traditionally associated with lithospheric necking and have high extension rates of ~25-30 mm/yr (Hopper et al., 2004; Geoffroy, 2005; Doré and Lundin, 2015). This produces significant mantle melting, and creates a thickening of igneous crust (Geoffroy, 2005). Extension is predominantly driven by the active process of an upwelling of asthenospheric magma (figure 1.9). The mantle plume model of magma-rich margin formation (figure 1.9) has predominated as the first-order explanation for the generation of large volume volcanics, associated with break-up (Geoffroy et al.,

2015). However, many believe there remains a ‘missing’ satisfactory explanation for the true genesis of magmatic margins (Quirk et al., 2014; Funck et al., 2017). It has been challenged by alternatives, such as small scale convection cells (Meyer et al., 2007; van Wijk et al., 2008) or secondary convection (King & Anderson., 1998) and multi-scale, mantle-mixing and mantle temperature/compositional heterogeneities (Korenaga, 2004; Foulger et al., 2007). There remains many outstanding questions on magma-rich rifted margins, not least because of the over-printing of rift structures by magmatism and until recently, a lack of quality data (Funck et al., 2017). One constant between both magma-poor and magma-rich margins is that they require some form of far-field extensional stress to initiate rift development (Geoffroy, 2005).

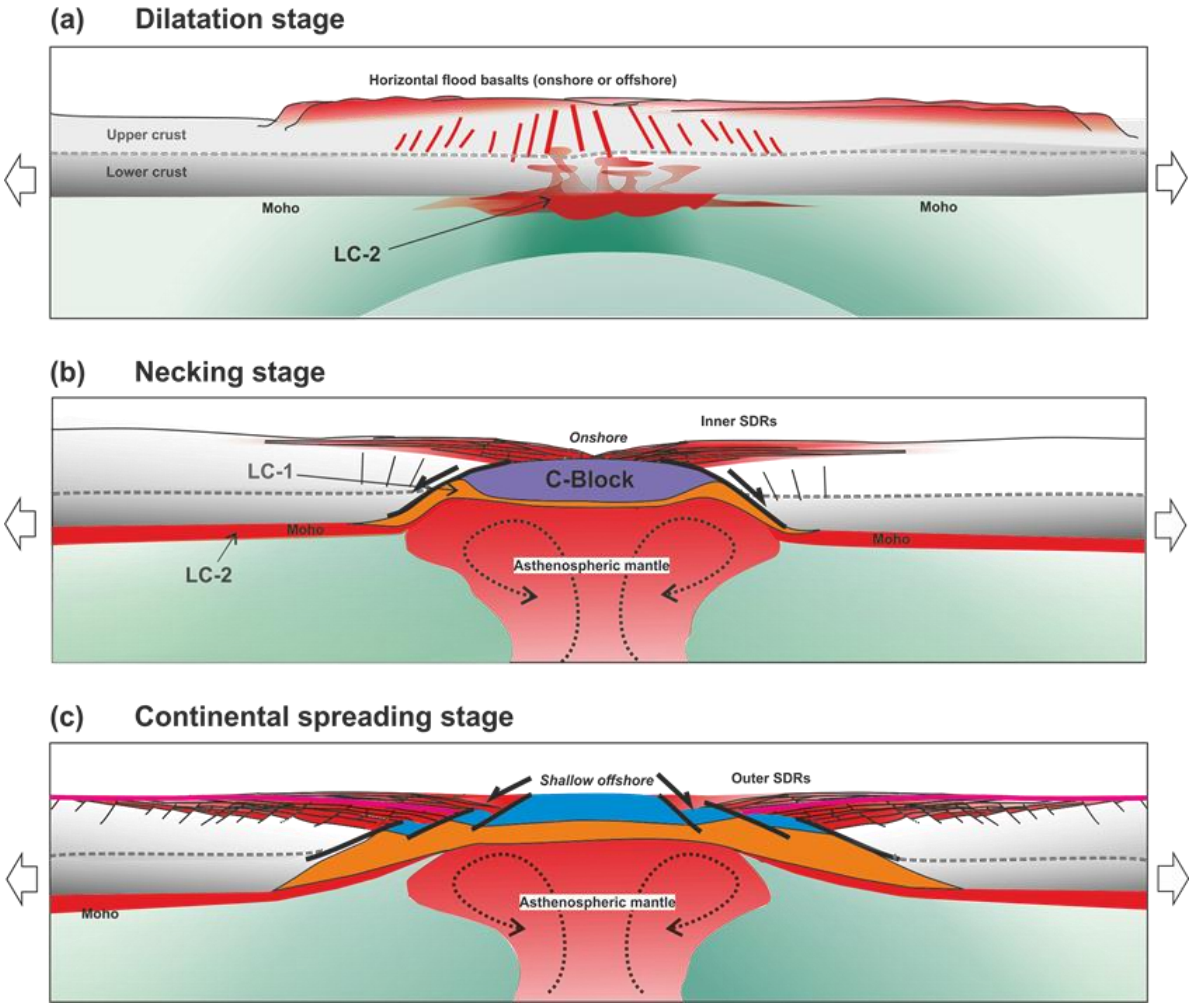

Figure 1.9: Proposed model of conjugate volcanic passive margin formation modified from Geoffroy et al., (2015) showing an upwelling plume of asthenospheric mantle. (a) Initial stage of extension and dilation of the crust by mafic magmas, producing sills and dykes respectively in the upper and lower crust. Flat-lying basaltic traps or a horizontal volcanics (~2km thick) may also be extruded. (b) Extreme crustal thinning during the 'Necking stage' with the individualisation of inner SDR packages and a central continental block (C-Block) to be compared with the 'H-Block' referred to on magma-poor margins. (c) Continental spreading through the breaking apart of the C-Block by the bulk, pure-shear process and formation of the outer SDR.

1.2.4 The continent-ocean transition (COT)

The boundary between continental and oceanic crust at extended, rifted continental margins is the genesis of continental breakup (Keen et al., 1988). As such, large volumes of syn-rift magmatic materials are often associated with this continent-ocean transition (Péron-Pinvidic et al., 2009). The mapping of the continent-ocean transition (COT or sometimes OCB, ocean-continent boundary) as a simple, linear boundary is now known to be an oversimplification (Eagles et al., 2015). However,

as noted by Eagles et al., (2015) and Funck et al., (2017), it is still widely mapped as such, primarily to provide a fixed reference for kinematic and palinspastic plate reconstructions. The inconsistent interpretation of this boundary has been studied in 150 publications by Eagles et al., (2015) who noted that expected, observational uncertainty associated with geophysical data (in an average of the global maximum) was found to be 167 km, and perhaps surprisingly this was found to be largely within studies of the last decade (Eagles et al., 2015). They attribute this considerable range to be due to author's variable understanding of the expected features and how they are interpreted at rifted continental margins. This is important to note, as it can speak to the reliability of plate reconstructions, as well as our understanding of the processes associated with breakup (Eagles et al., 2015). In some typical dip-line sections across a margin, there may be a relatively abrupt transition from continent to oceanic crust (Bronner et al., 2009) with an 'easy-to-pick' division between the two types of crust, based upon changes in crustal character, depth to the Moho and changes in seismic reflection characteristics. However, on many margins and those with a low magma supply (Bronner et al., 2009), reflection profiles of this region are dominated by much more, open-to-interpretation, 'transitional' regions where the crustal type lies in between continental and oceanic. Eagles et al., (2015) also highlight that different interpretations may exist for the same observations, resulting in the broad range of COT mapping locations as mentioned above, predominantly delineated by 'interpreter choice' (Eagles et al., 2015). In magma-poor regions such as the Iberia margin (Seifert and Brunotte, 1997; Eagles et al., 2015) and the Alps (Boillot et al., 1987), where mantle lithologies dominate, drilling or field study has enabled constraints to be applied in terms of geochemically differentiating crustal type. However, within magma-rich margins, the COT is often a thick region of ~20km seismically isotropic crust (Eagles et al., 2015)

with seismic reflection/refraction data the only source of data across the COT. It is also complicated by continental crustal remnants, which may be indistinguishable from oceanic crust, due to a magmatic ‘over-print’ of break-up related volcanics (Reston, 2005; Funck et al., 2017). The 3D complexity of a magmatic margin such as the Norwegian, Vøring margin has been suggested to be inadequately mapped by 2D seismic refraction profiles, which did not map deep crustal structures in detail (Funck et al., 2017) agreeing with the inconsistencies noted by Eagles et al., (2015).

1.2.5 Gravity and magnetics in relation to break-up

Traditionally, the timing and location of continental breakup has been determined by the first magnetic anomaly (Bronner et al., 2009) which is generated by the first magma extruded from a mid-oceanic ridge. However, the seafloor-spreading origin of magnetic anomalies within the transitional region, (that can often be broad) is questioned by some authors (Funck, 2003; Russell and Whitmarsh, 2003; Bronner et al., 2009). Bronner et al., (2009) have suggested that an earlier pulse of magmatism triggered continental separation in the North Atlantic, before seafloor spreading. The record of magnetic anomalies by polarity changes of the Earth’s magnetic field is complex in domains that do not result from ‘simple’ steady-state seafloor spreading (Gillard et al., 2015). This is particularly true for magnetic anomalies formed over exhumed mantle or magma-starved domains (Gillard et al., 2015). The difficult identification of magnetic anomalies in these poorly defined domains, questions the traditional way of dating the first magmatic oceanic crust by using the oldest magnetic anomaly (Gillard et al., 2015). Bronner et al., (2014) show that basement formed by serpentinized mantle rocks are unlikely to carry a strong, organized magnetic signal (Gillard et al., 2015) and were shown in the Southwest Indian Ridge (SWIR) to be weak and of a highly variable magnetic pattern, despite an ultra-slow spreading rate (Bronner et al., 2014).

1.3 Rift-related volcanics

1.3.1 Seaward-dipping reflections

Seaward-dipping reflections are a ubiquitous feature of magma-rich rifted margins. They are commonly observed down large areas of the Atlantic margins for hundreds of kilometres at, or near, the continent-ocean boundary. On seismic profiles, they present a wedge-shaped geometry of up to 15 km thick (Franke, 2013) of mid-high amplitude, arcuate reflections (Mutter et al., 1982; Mutter, 1985). The Norwegian Ocean drilling program of the 1970's showed them to be of a thoeliitic basaltic composition, similar to that found at mid-ocean ridges. They are considered to form as horizontal volcanics at, or within ~2 Ma, of break-up with packages subsequently rotated post-emplacement, due to differential subsidence. Within SDR wedges themselves are identified several sequences and seismically distinct, individual packages, separated by periods of erosion or non-extrusion (Koopmann, Franke, et al., 2014). It is established that there are significant variations in the along margin distribution of SDRs on the South American margin (Franke et al., 2007; Blaich et al., 2009; Blaich et al., 2011; Blaich et al., 2013; Koopmann, Brune, et al., 2014). This is in addition to a variable general margin geometry, that can be recognised in both volcanic and non-volcanic areas of the South American margin (Alves et al., 2009). Despite almost 50 years of research, the exact nature of SDR development and differing seismic signatures are still debated (Mutter et al., 1982; Mutter, 1985; Paton et al., 2017). Figure 1.10 shows the general features of SDRs on the Norwegian outer Vøring Plateau with their associated magnetic profile (Mutter et al., 1982).

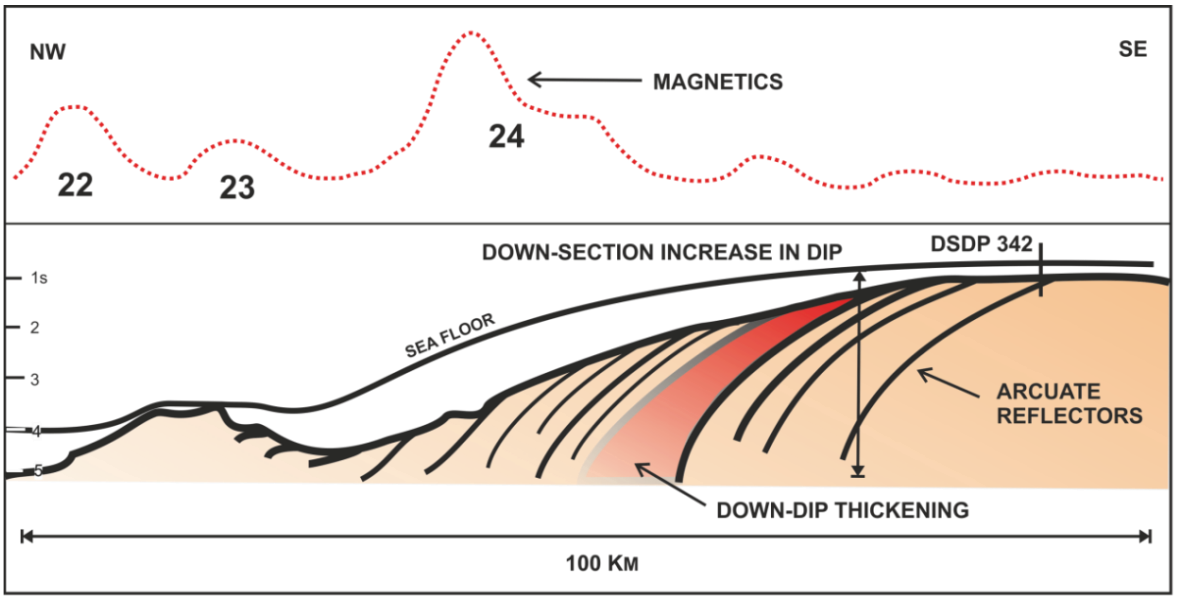

Figure 1.10: Modified schematic drawing of SDR on the Outer Vøring Plateau with the associated magnetic anomaly profile (Mutter et al., 1982).

1.3.2 Lower crustal bodies (LCB) and magmatic additions

The identification of lower crustal bodies (LCB) have been recognised on several magma-rich margins, including the mid-Norwegian margin (being more pronounced on the Møre and Vøring margin segments) (Reynisson et al., 2011). These are of an anomalously high density and velocity (Vp values of ~7km/s (Peron-Pinvidic et al., 2013) and are usually suggested as being magmatic or high-grade metamorphic in nature (Reynisson et al., 2011). High velocity lower crust (HVLC) is another form of LCB which is commonly detected under voluminous extrusives such as SDRs along the Argentine margin (Franke et al., 2010). Traditionally, these have been ascribed to magmatic underplating (Skogseid et al., 1992; Eldholm and Grue, 1994) but in recent years, various alternatives have been proposed as dataset quality has improved. Through the use of seismic refraction, we are able to learn more about the nature of often sub-volcanic regions. Alternate hypotheses for LCB in the north-east Atlantic have been proposed as, igneous transitional crust or thickened oceanic crust (Holbrook et al., 2001; Peron-Pinvidic et al., 2013), granulites or ecologites (Gernigon et al., 2004), highly intruded continental crust (White et al., 2008) – or

serpentinised mantle (Lundin and Dore, 2011). As in work by Lundin and Dore, (2011), HVLC bodies are suggested to underlie hyper-extended basins as serpentinised upper mantle. Reynisson et al., (2011) have proposed that despite the term, ‘crust’ the upper mantle can also be a part of LCBs. Magmatic additions and lithospheric breakup may also occur within an exhumed mantle domain itself, with the presence of sub-continental mantle present on both conjugate margins of the Iberia-Newfoundland (Boillot et al., 1980; Müntener and Manatschal, 2006) and Alpine-Tethys margins (Manatschal and Müntener, 2009; Gillard, Autin, et al., 2016). Exhumed mantle rocks from the Alps show intrusions of both gabbros and basaltic melt (Müntener and Hermann, 2001; Reston, 2007). Some authors have also recognised the contribution of long-lived, lithospheric weakening (Lundin and Dore, 2011) or of older mafic rocks (Reynisson et al., 2011) to LCBs. Magmatic intrusion into the lower crust has also been suggested as a compensatory method for the lack of an expected Moho uplift, as seen in the Siberian, Baikal rift which also produces a highly reflective, high velocity zone (Thybo and Nielsen, 2009). Thybo and Nielsen, (2009) note that this form of magmatism plays a previously unknown role in rifting, with implications for sedimentary basin modelling and extension estimates around failed rifts. Decarlis et al., (2018), suggest that seismic reflection data underestimates the importance of magmatic intrusions, which are often not resolvable. However with the advent of superior quality datasets, especially in 3D, this can now be considerably mitigated.

1.3.3 Magmatic plumbing systems

Over the last few decades there have been advancements in geophysical techniques that have enabled the mapping of magma plumbing systems (Magee et al., 2018). This has included identification of zones of melt, and the migration system associated with the transport of magma. Mapping the architecture of a sub-surface

magma system is important as this has implications for the location and timing of magmatic extrusives in the area (Magee et al., 2015). Various methods such as InSAR (Interferometric Synthetic Aperture Radar), GPS and other satellite tracking systems can now track contemporary magma movements in near real-time (Magee et al., 2018). Seismic imaging, gravimetry and electromagnetic data has also proved useful for mapping contemporary magma reservoirs (Magee et al., 2018). 3D seismic reflection data in particular has enabled the mapping of sill emplacement and the magmatic plumbing system associated with the Palaegene, Faroe-Shetland Sill Complex (FSSC) (Schofield et al., 2017). Fossilised systems such as the Bushveld Complex in South Africa are also still yielding important information on the composition of fossilised systems, however the mechanisms for the separation of melt and crystal-rich magma in plutonic magmatic systems are still debated with a hotly debated topic being the amount of melt versus 'crystal-mush' composing magma chambers.

1.4 The regional evolution of the South American margin

The formation of the larger South American Atlantic margin can be traced to rifting which initiated within the western side of the Gondwanan super-continent during the late Jurassic to early Cretaceous (Nürnberg and Müller, 1991; Jackson et al., 2000; Eagles, 2007; Schnabel et al., 2008; Aslanian and Moulin, 2010). However, the area has had a complex history of Pre-Cambrian geology and tectonics which has also left its mark on the structural fabric of the region.

1.4.1 Onshore Geology: Neoproterozoic continental terranes.

The correlation and origins of pre-rift strata and the arrangement of SW Gondwana in the Pre-Cambrian of this region of the South Atlantic margin have remained elusive until recently (Basei et al., 2005; Rapela et al., 2011). However, pre-existing, and predominantly Precambrian structures and lithospheric weaknesses have

played a significant role in determining the locus of continental break-up of the Gondwanan super-continent (Macdonald et al., 2003; Will and Frimmel, 2013). The effect of far-field forces has been suggested as the main impetus for the break-up (Will and Frimmel, 2018), with rheological weaknesses in thinned and softened lithosphere along the axis of former back-arc basins providing the locus for Gondwanan rifting (Will and Frimmel, 2018). These basins closed during the mid-late Neoproterozoic (Mesoproterozoic and Ediacaran) (Will and Frimmel, 2018) and into the early Cambrian, through a series of continental mass collisions (Casquet et al., 2012). It has been suggested that two major collisional orogenies have contributed to the geodynamics of the region; 1) Kaoko-Dom Feliciano (580-680 Ma) (Ediacaran/Neoproterzoic era) and 2) Gariep-Saldania (480-580 Ma Late Cambrian-early Ordovician) (Rapela et al., 2011) (Figure 1.11). More recent work by (Will and Frimmel, 2018) have dates of 650-580 Ma and 550-500 Ma respectively. Several prominent cratons have played a role in shaping the area for a long time, with the Rio de la Plata craton (RdP) and the Kalahari craton having been dated to ~1.0 Ga (Rabassa, 2010).

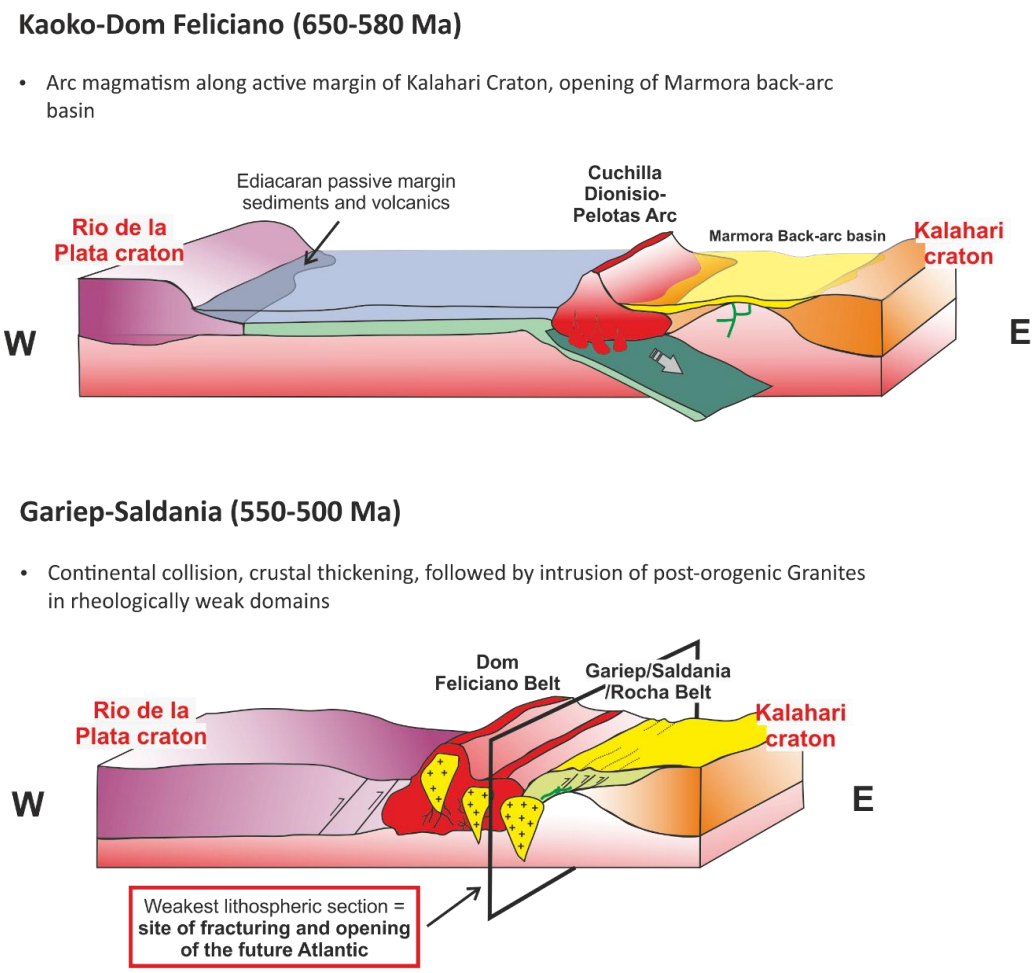

Figure 1.11: Schematic cross-sections of the main stages in the evolution of Pan-African/Brasiliano orogenic belts on the South Atlantic margins during the Mesoproterozoic and Ediacaran. Modified from Will and Frimmel, (2018). South African Gariep Basin is located to the south-east of these diagrams. ***Note**, the zone of weakness and site of future Atlantic rifting along the axis of a former back-arc basin*.

The location of some zones of crustal weakness of this era is still debated (Eagles et al., 2015). The major stratigraphic and tectonic elements of the 2D evolution of offshore Uruguay are inextricably linked to the 'mega-scale' cratonic developments and crustal re-organisations of the Proterozoic era, primarily discovered through research involving detrital zircons in basin sediments (Hartmann et al., 2001; Basei et al., 2008; Hueck et al., 2017). For example, the development of the Rio de la Plata craton and associated bounding, transcurrent (strike-slip) faults (Rapela et al., 2011) which formed during the Neoproterozoic. Many Gondwanan age sutures are also the focus for rift events on the conjugate, South African margin (Macdonald et al., 2003; Paton, 2006). A recent borehole in the eastern section of the Tandilia belt

of northern Argentina (38º South) has prompted a re-evaluation of Neoproterozoic sediments and terrane associations (Rapela et al., 2011) in an area which is still debated by Gondwanan researchers. The extent and placement of key terranes of this era has underpinned Mesozoic structural and stratigraphic developments, such as the opening of the South Atlantic. Fracturing of the basement has also been identified as a regionally extensive phenomenon during the late Jurassic (Zambrano and Urien, 1970) and as a precursor to the break-up of the western edge of the super-continent. The repeated reactivation of inherited basement fault systems peaked during the Triassic-Jurassic (Jacques, 2003).

1.4.2 Onshore Geology: Gondwanan fold belts

The onshore Rocha Group of the Punta del Esté Terrane, (part of the Dom Feliciano Belt in Uruguay (Figure 1.12) and successions of the Gariep Belt of South Africa (Oranjemund) have been found to be linked through radiometric dating (U-Pb – Uranium-Lead and detrital zircon analysis) and likely originated in the same basin (Basei et al., 2005). The Rocha Group is therefore considered part of a re-activated Ediacaran Gariep Basin, associated with the magmatic arc of the Dom Feliciano Belt (Basei et al., 2005) (figure 1.11). The Gariep Basin has relevance to the geological evolution of the area, as it provides evidence for a failed continental rift and re-activation as a back-arc basin (Dom Feliciano arc) (Basei et al., 2005). The southernmost extent of deposits associated with the Rio de la Plata Craton are found in the Tandilia belt which is located 300 km south of Buenos Aires, trending NW-SE with Neoproterozoic deposits (Sierras Bayas Group) and Ordovician-Silurian deposits (Balcarce Formation) (Rapela et al., 2011). Rapela et al., (2011) suggest that the Dom Feliciano belt is correlative with the Punta Mogotes sequence in north-eastern Argentina, meaning the Dom Feliciano orogenic belt must extend

to at least 38^{o} South - a noteworthy observation of Precambrian continental terranes which has direct relevance to later chapters of this thesis.

1.4.3 Onshore Geology: Mesozoic rift basins

Two Mesozoic rift basins related to South Atlantic opening are observed in the onshore geology of Uruguay. These are the southern, Santa Lucía Basin and the eastern part of the Laguna Merín Basin (figure 1.12) (Panario et al., 2014; Rabassa and Ollier, 2014). These basins are elongated in an east to north-east orientation and are considered to have formed during Gondwanan break-up (therefore ~132 Ma) as failed rifts (Panario et al., 2014). They are considered to be controlled by the SaLAM, the **Sa**nta **L**uciả – **A**igua-**M**erín tectonic alignment (Rossello et al., 2000) which relates to the Parana-Etendeka volcanic province (Panario et al., 2014). Studies using $^{40}Ar/^{39}Ar$ dating of igneous rocks on the proto-Atlantic coastal margins range from 134 to 128 Ma and indicate that melt generation in the east of the Parana province was either synchronous or slightly later than the main pulse of tholeiitic volcanism (between 134 and 132 Ma) (Gibson et al., 2006). The relationship between onshore and offshore structures is not always simple to discern. However, a precedent was set in the area regarding the continuation of onshore rifting into more distal oceanic domains in Argentinian basins (such as the Colorado Basin) through observation and modelling studies (Keeley and Light, 1993; Franke et al., 2006; Autin, Scheck-Wenderoth, et al., 2013). Two predominant fault systems within the onshore basement of the Uruguayan shield and Martin Garcia High region were recognised as ENE-WSW (nearly E-W) and ESE-WNW (Zambrano and Urien, 1970). Rearrangement of these intersecting fault systems is proposed to have given rise to block rotations during the late Jurassic (Zambrano and Urien, 1970). The Tandil High separates the Salado Basin to the south of the study area from the Rio de la Plata embayment and represents an only lightly deformed, Palaeozoic

sequence (Zambrano and Urien, 1970). Faulting in this area is only partially consistent with an ENE-WSW orientation. This has been suggested as being contemporaneous with an earlier rift phase, responsible for the Salado Basin (Zambrano and Urien, 1970). Crustal heterogeneity has played an important role in determining the location of crustal break-up (Ring, 1994; Piqué and Laville, 1996). This work builds upon the idea that pre-existing structures have significantly affected the volcano-tectonic morphology of early rifting (Geoffroy et al., 2001; Callot et al., 2002; Gaina et al., 2009).

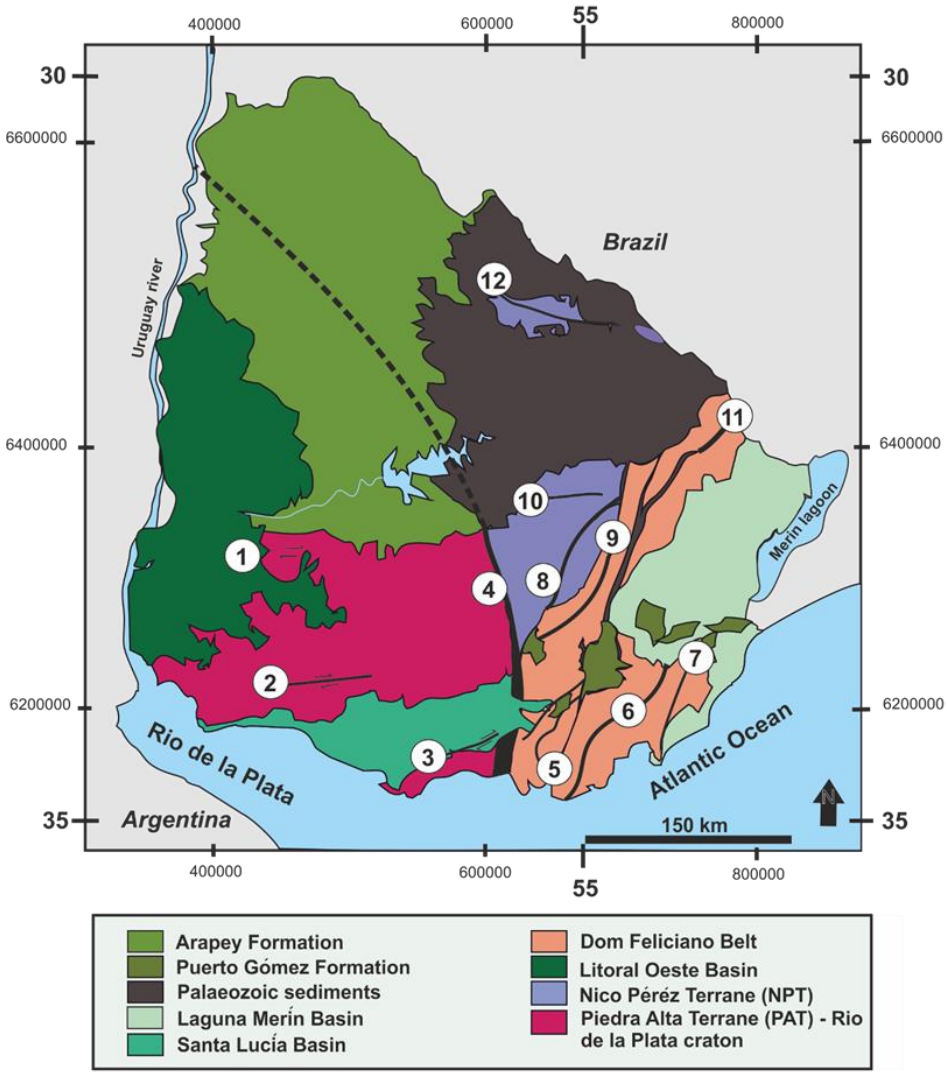

Figure 1.12: Main terranes and shear zones of Precambrian onshore Geology, Uruguay. Modified from Rabassa and Ollier, (2014). Shear zones – 1. Paso Lugo 2. Cufré 3.Mosquitos 4. Sarandí del Yí 5. Sierra Ballena 6. Cordillera 7. Rocha 8. Cueva del Tigre 9. Fraile Muerto-María Albina 10. Tupambaé 11. Cerro Amaro 12. Rivera. (Location of the South African Gariep Basin lies outside the coverage of this diagram to the south east).

1.4.4 Margin segmentation

Intracontinental lineaments and diffuse zones of transcontinental deformation accommodated early intraplate stress within the early stages of the splitting of the Gondwanan supercontinent (Eagles, 2007). These super-shear zones then accommodated block rotation along regions of dextral shear during early Atlantic opening (Tankard et al., 1995) and have been suggested to be linked either directly, or indirectly seaward, to oceanic fractures zones such as the Meteor Fracture zone (Hernández-Molina et al., 2016). A focus for recent studies on a regional scale has been the effect of margin segmentation and how this affects both upper and lower crustal structure of the South Atlantic (Eagles, 2007; Franke et al., 2007; Blaich et al., 2009; Franke et al., 2010; Aslanian and Moulin, 2010; Blaich et al., 2011; Becker et al., 2012; Blaich et al., 2013; Koopmann, Brune, et al., 2014). The Argentinian margin has also been the main focus for studies relating to margin segmentation, a phenomenon widely recognised by clear evidence of crustal-scale transform faults such as the Falkland Transfer, the Ventana Transfer and those bounding the Salado and Colorado basins (Figure 1.13) (Macdonald et al., 2003; Ghiglione et al., 2010; Aslanian and Moulin, 2010; Páengaro and Ramos, 2012; Autin, Scheck-Wenderoth,

et al., 2013; Autin, Bellahsen, et al., 2013; Koopmann, Franke, et al., 2014; Koopmann, Brune, et al., 2014).

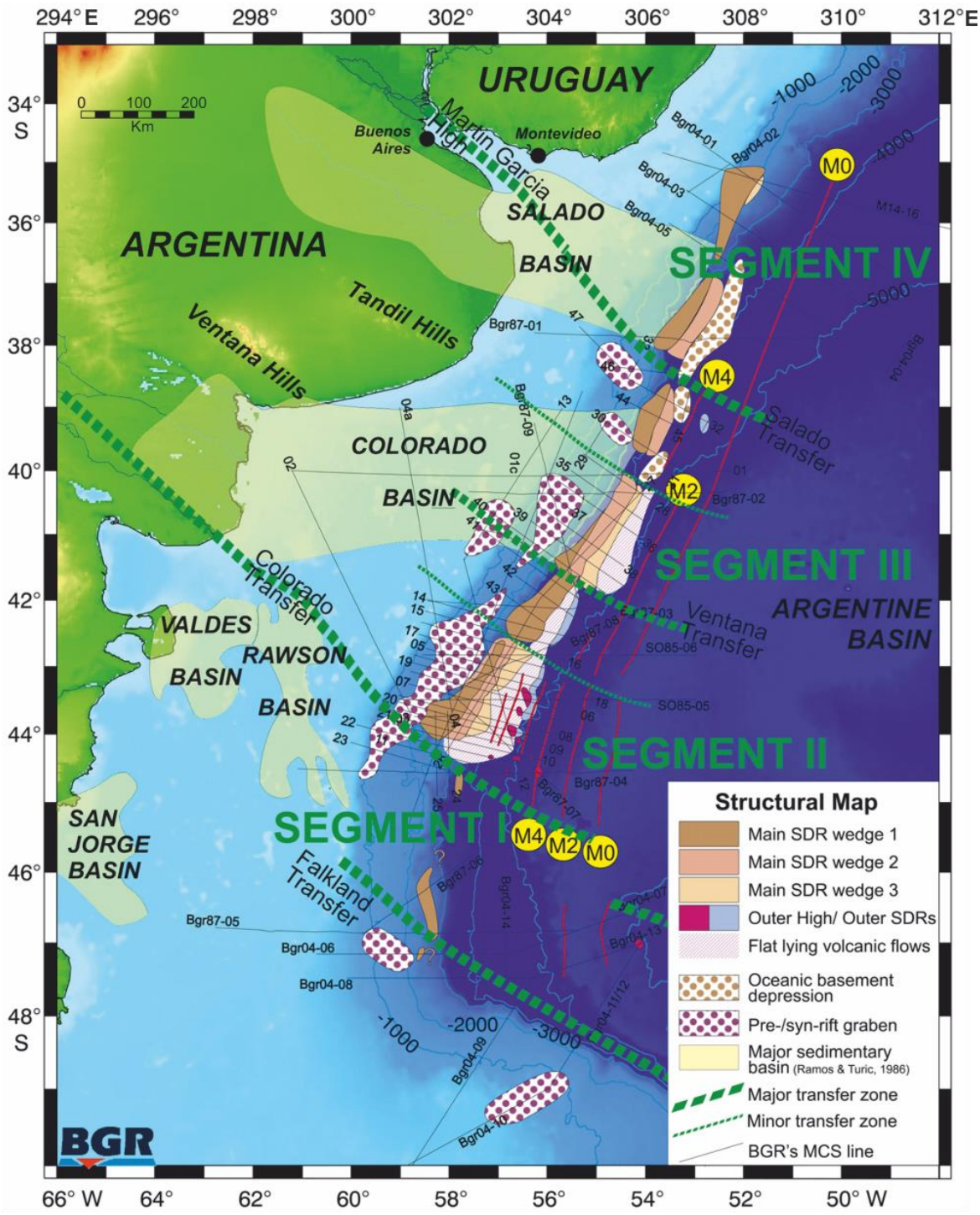

Figure 1.13: Transfer zones and margin segmentation. Modified from Franke et al., (2007). Margin segmentation is interpreted from volcano-tectonic character, post-rift sediment distribution, potential field data and earlier studies. Also showing structural features and the distribution of volcanics, especially SDRs. Major sedimentary basins on the shelf have been adopted from Turic et al., (1996) (Franke et al., 2007).

A ‘transfer zone’ refers to an area of accommodation where strain is transferred from one structural element to another. These form part of the extensional system, allowing the accommodation of extension between individual fault and basin segments along the length of the zone of deformation (Perez-Diaz and Eagles, 2014). The term ‘transfer zone’ was first used to describe relays of en-echelon fault systems in the East African Rift (Chorowicz, 1989). It is used later in this work to describe a zone of faulting oblique to the margin, which includes an extensional and strike-slip system and associated structures. This regional segmentation by transfer zones (Franke et al., 2007) and the associated volcano-tectonic architecture, remains a focus of recent work on Atlantic margins (Franke et al., 2007; Blaich et al., 2009; Blaich et al., 2013; Autin, Bellahsen, et al., 2013; Koopmann, Franke, et al., 2014; Koopmann, Brune, et al., 2014). Koopmann, Franke, et al., (2014) divide this region of the margin into four, first-order segments along ~2400 km. These exhibit varying volume and widths of SDR, with a sharp transition (10’s of kilometres) between a southerly, magma-poor margin, to that of a highly volcanic margin. Koopmann, Franke, et al., (2014), suggest that this variation is due to the influence of initial, oblique rifting during early break-up transitioning to later, margin-perpendicular oceanic spreading from ~130 Ma onwards (corresponding with magnetic chron M4). This is also supported by magnetic data (Koopmann, Franke, et al., 2014). The utilisation and reactivation of associated transform structures has also been shown to occur elsewhere along the margin, i.e The Colorado Basin (Autin, Bellahsen, et al., 2013). Soto et al., (2011) recognised two distinct tectono-structural segments in the offshore Uruguayan margin, divided by a previously unrecognised, transfer zone, the Rio de la Plata Transfer zone (RPTS). The proximity of a transfer zone has been proposed as a significant factor in limiting the magma supply along the southern Argentine margin (Becker et al., 2012) and

therefore, the absence of SDRs. South Atlantic ‘unzipping’ in terms of the northward propagation of Cretaceous rifting reached the Uruguayan latitude at ~132-134 Ma (Rabinowitz and LaBrecque, 1979; Uchupi, 1989; Franke et al., 2007). The interaction of volcanics and the pre-existing structural fabric have played a crucial role in the evolution and development of most South American basins, but to date, this has only been fully recognised in areas such as the Colorado Basin and the Salado Basin to the south (Blaich et al., 2009; Autin, 2010; Autin, Scheck-Wenderoth, et al., 2013; Autin, Bellahsen, et al., 2013). New data now allows this study to be the first to provide new insights and a detailed model of the tectono-magmatic evolution of the offshore Uruguay margin, building upon previous observations by several authors (Zambrano and Urien, 1970; Tomasini et al., 2011; Soto et al., 2011; Hernández-Molina et al., 2016; Creaser et al., 2017; Morales et al., 2017).

Chapter 2: Methods: Defining crustal types, facies and domains

2.1 Introduction

This chapter presents the primary data and methodologies which are applied in order to define the crustal architecture of the offshore region. Both uninterpreted and interpreted seismic reflection lines from the ION SPAN Uruguay survey (see figure 2.1 for survey location) are presented. The approach of this chapter is to initially document the seismic facies associations which are subsequently associated with crustal types. This form of analysis helps to fully capture the broad range of seismic reflection responses in the high resolution dataset, which in turn, gives evidence of the nature of crustal type and distribution across the study region. From these associations, it is then possible to build a framework of distinct crustal domains. This chapter will also highlight, investigate and discuss any anomalous crustal geometries and occurrences which are observed along the margin. These will be compared and contrasted to global analogues, outside of the constraints of 'traditional' passive margin classifications (i.e., margins which are both magma-rich and magma-poor will be considered). Observations of the strike line sections will also be noted and interpreted. These are seldom utilised (or available) in existing studies; however, in this study they provide a valuable perspective and insight of the crustal architecture in the offshore region in the third dimension. In conjunction with dip-line sections, they give important indications of margin-oblique tectonics, which play a crucial role in margin development. Using both orientations of line also gives a higher degree of confidence when mapping and interpreting anomalous geometries and oblique structures. All eight lines in the ION SPAN dataset are presented across chapters 2 and 3 to show the full range of crustal architectures and how these change along the Uruguayan margin.

2.2 Data

The primary data source was a 2D dataset acquired by ION Geophysical (Uruguay SPAN survey) in 2016. This provides a high resolution, regional framework for the area, covering approximately 2,800 km of long-offset depth data (figure 2.1).

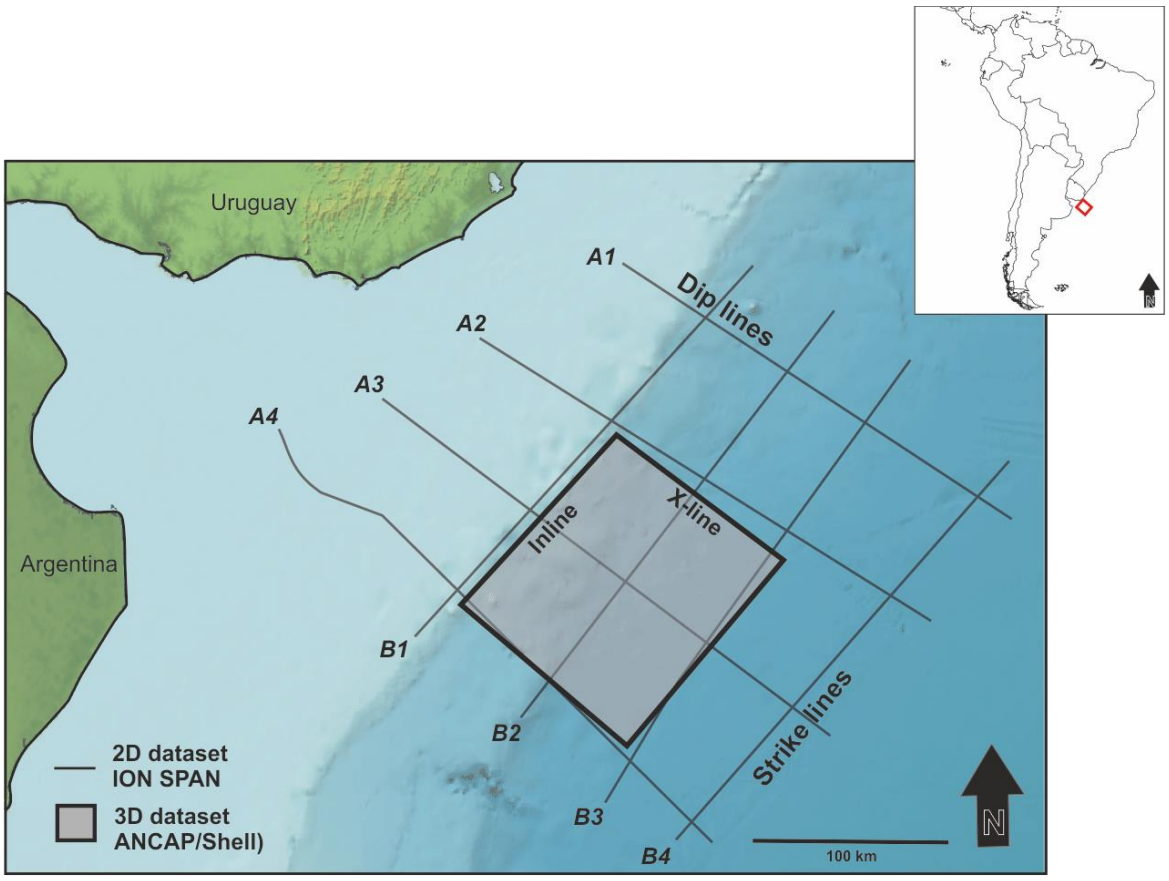

Figure 2.1: Location of eight grid lines from the ION SPAN Uruguay dataset and the 3D data cube (ANCAP/Shell) in the offshore region of Uruguay.

The survey was shot to fit into the existing Argentine, Brazilian and Pelotas SPAN datasets and provides coverage of the Punta del Esté Basin, as well as tying with existing exploration wells on the shelf. The dataset consists of a grid of eight, long-offset, high resolution PSDM and PSTM ultra-deep, 2D profiles recording to depths of ~40 km, and for several hundred kilometres along and across the margin (figure 2.1). The data was acquired with a unique setup, including offsets of 10,000 to 12,000 meters, a specially designed source array, and recording lengths of 18 seconds (ION). This dataset is largely unpublished (2020). Another primary data resource is a 3D dataset of PSDM seismic reflection data provided by BG Group

and shot by ANCAP in 2013/14 (figure 2.1). The survey was provided in two separate sections, firstly the most proximal and then the most distal section. The dataset provides high resolution, depth converted seismic reflection data of the highest standard from the seabed to a maximum depth of 13 km and covers an area of ~140 km by 160 km. In some regions the data has been provided with a mute at the base of the dataset which has unfortunately removed some of the lower-most reflections. The dataset also ties with the 2D ION SPAN dataset and thus, provides a form of two-way confirmation between the datasets of key observations (i.e. the Moho). The combination of these datasets provides excellent coverage of the margin, both in plan and cross-sectional views. These data contribute greatly to our understanding of both the spatial and temporal evolution of the tectono-magmatic evolution of the Uruguayan margin, both at a regional and local scale. They also represent relatively rare data, shot across a magma-rich rifted margin in high resolution and to unprecedented crustal depths. There was also significant amounts of 2D seismic reflection legacy data available from previous surveys. However, this was shot only to relatively shallow depths and excluded much of the basement (which is of primary interest) or was of very poor reflectivity/quality. In some cases lines were used to confirm the presence of a volcanic centre or of seaward-dipping reflections, however, due to the previous factors and lack of significant contribution to the project, these data have not been included.

2.3 Horizons interpreted

Figure 2.2 (A) shows an uninterpreted PSDM dip line profile from the ION SPAN dataset. The same line is repeated in (B) showing the horizons which were picked in Petrel software ©Schlumberger. Table 1 records the interpreted horizons with a brief description of the defining seismic characteristics or features.

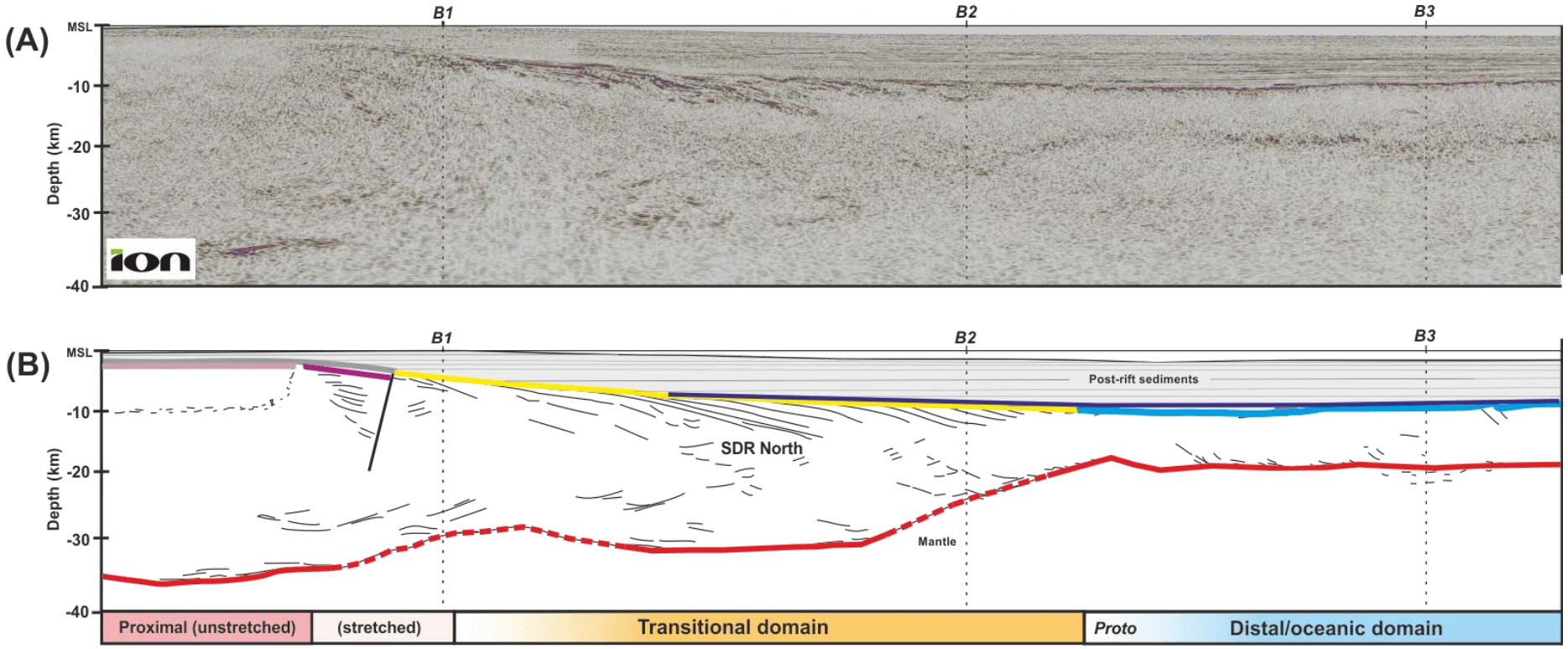

Figure 2.2: (A) Uninterpreted PSDM dip line A2 from the ION SPAN dataset showing a 'typical' magma-rich margin geometry and oriented NW (Proximal) to SE (Distal). (B) Horizons: Grey, top continental crust; Pink, top of cratonic continental crust; Purple, top syn-rift sediments on the continental shoulder; Yellow, top SDRs; Dark Blue, top syn-rift; Light Blue, top Oceanic crust; Red, Moho.

Table 1: Interpreted horizons and their defining criteria.

Interpreted horizon	Colour	Defining seismic character/features	Crust type	Domain
Moho	**Red**	Lowest, high amplitude reflections, sub-continous	–	–
Top cratonic crust	**Pink**	Above chaotic continental seismic facies, below post-rift sediments	Continental crust	Proximal (unstretched)
Top continental crust	**Dark Grey**	Above continental seismic facies, below post-rift sediments	Continental crust	Proximal (stretched)
Top syn-rift sediments (divergent reflections)	**Purple**	Top divergent reflections, below post-rift sediments	Continental crust	Proximal (stretched)
Top syn-rift sediments (inferred, no divergent reflections)	**Blue**	Top syn-rift sediments across basin, onlaps proximal continental crust (inferred from the 3D dataset)	– –	– –
Top magma-rich transitional crust	**Brown**	Top magmatic additions/new magmatic crust	Transitional crust	Transitional
Top seaward-dipping reflections (SDR)	**Yellow**	Top seaward-dipping reflections/extrusive magma deposits	Transitional crust	Transitional
Top transitional/hyper-extended crust	**Orange**	Top hyper-extended (<10 km) continental crust in transitional realm	Transitional crust	Transitional
Top exhumed mantle	**Green**	Top surface of exhumed mantle, immediately below post-rift	*Exhumed mantle*	Distal/oceanic
Top oceanic crust	**Navy Blue**	Top high amplitude reflections, above oceanic facies	Oceanic crust	Distal/oceanic
Seabed	**Black**	High amplitude seabed reflection, ocean above	–	–

Figure 2.3 is a colour key for the various crustal types which are used in the following seismic facies section and in the rest of this thesis.

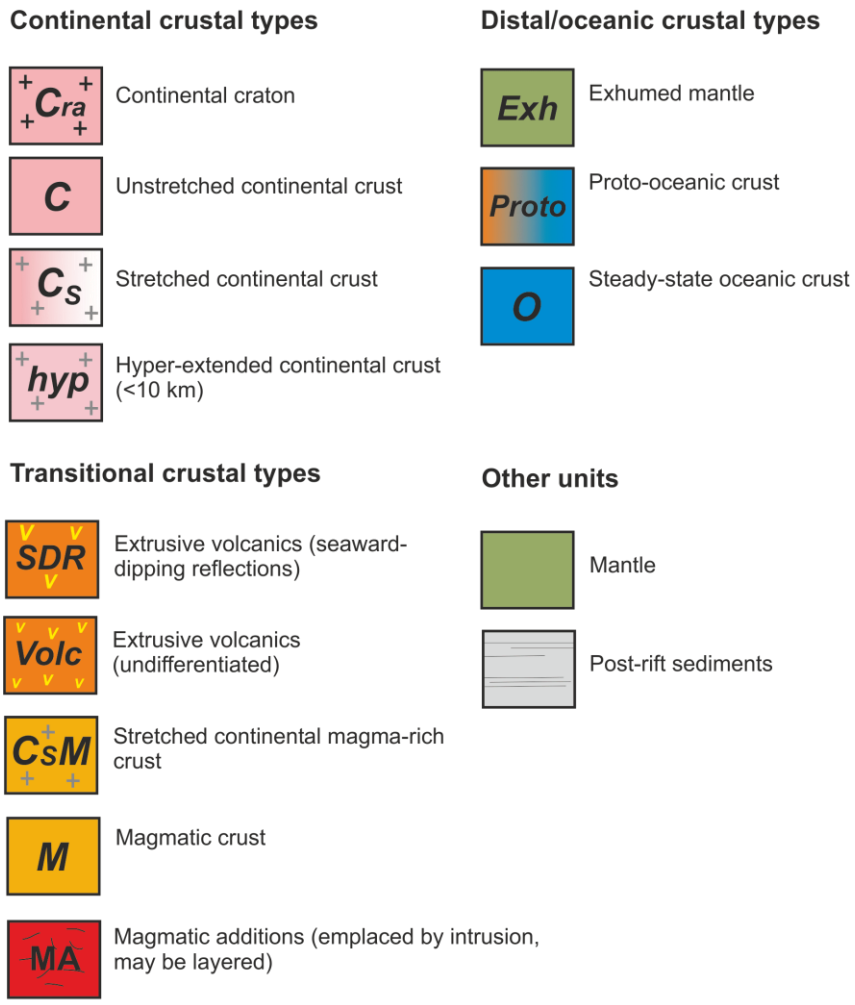

Figure 2.3: Crustal types colour key with continental, transitional and distal/oceanic crust types which are used in the following section and the rest of this thesis. This key can also be found in the preface on page xxi.

2.4 Seismic facies observations

Through use of the ION SPAN dataset a series of distinct seismic facies can be identified. Seismic facies analysis involves the use of different seismic parameters to determine geology and structures. Seismic facies units are compared to adjacent facies for differences in the characteristics such as reflection amplitude, continuity, reflection frequency, polarity and internal velocity (Roksandic, 1978). They have been used for sedimentary and volcanic classifications, in particular volcano-seismic facies on the Norwegian and Australian margins (Planke et al., 1999; Planke et al., 2005; Rey et al., 2008). The seismic facies of this study are presented in table form below, within the classification of crustal types as defined in figure 2.3 and are examined from the most proximal region to the outer or distal region. This methodology allows the definition of specific crustal domains, which are explored further, towards the end of this chapter.

2.4.1 Continental craton (*Cra*)

Cratonic continental crust (*Cra*) is defined by two primary seismic facies, *Cra*-1 and *Cra*-2 (Table 2). Seismic facies *Cra*-3 to 5 represent different forms of reflections of this crustal type at different depths. This crustal type covers a region of ~18 x 14 x 80 km. It lies within undifferentiated, unstretched, continental crust and is only observed in the proximal region of the margin.

Table 2: Key seismic facies and reflection relationships for the crustal type 'Cratonic continental crust' (*Cra*). Highlighted Red defines the specific reflections of interest. Coloured boxes refer to crustal types (see removable key).

Crustal type	Seismic facies	Key reflection relationships	Reflection characteristics	Seismic Facies Association
Cra	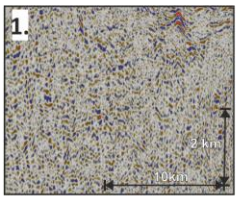	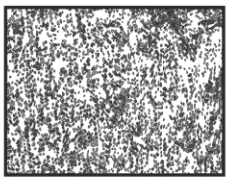	**Cra 1** Discontinuous, chaotic reflections of a mid-high amplitude. No discernable internal structure or reflections. Indicative of deep continental crust.	Continental cratonic, Igneous crust.
Cra	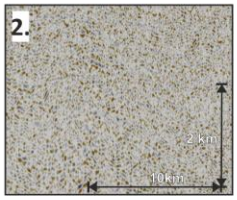	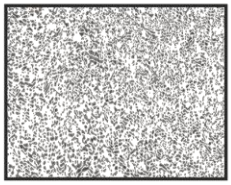	**Cra 2** Very low amplitude, discontinuous, chaotic reflections with no discernable structure or internal geometries.	Continental cratonic, Igneous crust.
Cra	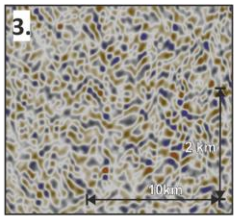	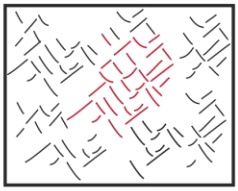	**Cra 3** Mid-low amplitude, discontinuous, reflections which cross-cut in an approximately orthogonal pattern.	Mid-lower depth continental cratonic, Igneous crust.
Cra	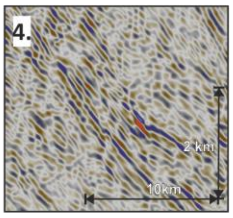	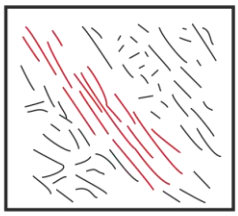	**Cra 4** High amplitude, partially continuous reflections steeply dipping ~50° within lower amplitude chaotic reflections.	Toward the base of continental cratonic, Igneous crust.
Cra	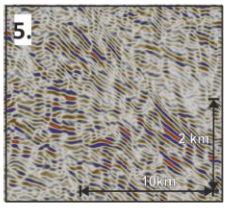	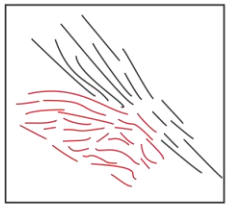	**Cra 5** High amplitude, partially continuous reflections intersecting with Cra 4.	Continental cratonic, Igneous crust Moho.

The north-western, proximal boundary of the cratonic continental crust is defined by the edge of the ION SPAN dataset. The reflection characteristics of the seismic facies associated with this crustal type are predominantly chaotic and discontinuous in nature and range from low to mid-amplitudes. The lowest depth of this crustal type is approximated at ~18 km, which is interpreted from (line B1, see Figure 3.6). This is suggested due to a horizontal band of higher amplitude reflections, which are interpreted as representing the base of the primary internal section of continental craton. However, the full depth to the Moho of cratonic continental crust is more

challenging to define on the dip line sections (A1-4) due to the unusual, often steeply-dipping reflectivity represented by seismic facies *Cra*-4 (Table 2) which may be indicative of out-of-plane tectonics and intrusions of mantle-sourced material. The 'root' of the craton may extend to the full depth of the stretched continental crust (see next section) which surrounds cratonic facies – and appears to be essentially 'tethered' to the upper-mantle/continental Moho at approximately 28 km depth.

2.4.2 Unstretched continental crust (*C*)

Unstretched continental crust (*C*) is present on dip lines A1, A2, A3 and is characterised by a region of undifferentiated, mid-low amplitude reflectivity of a discontinuous nature and a constant thickness of 30-35 km (*C*1, *C*2 Table 3). This varies in distribution from the proximal start of the line from ~36 km to ~118 km. Some reflections may be cross-cutting or curvilinear (*C*-2) but remain of a discontinuous nature with broadly chaotic reflections throughout the region. Unstretched continental crust is also observed directly beneath the cratonic seismic facies (*Cra*) and is most evident on strike line section B1. It is defined as 'unstretched' due to the lack (or scarcity) of large areas of dipping reflections (which are deemed indicative of extension, or oblique tectonics) an absence of faulting and where the facies correspond with a characteristic, constant crustal thickness.

Table 3: Key seismic facies and reflection relationships for the crustal type 'Unstretched continental crust' (*C*). Red defines specific reflections, or packages of reflections which are indicative of the facies.

Crustal type	Seismic facies	Key reflection relationships	Reflection characteristics	Seismic Facies Association
C	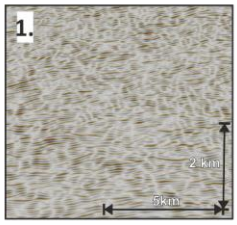	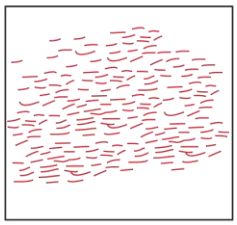	**C 1** Discontinuous, chaotic reflections of a mid-high amplitude. No discernable internal structure or reflections. Indicative of deep, unstretched continental crust.	Unstretched continental crust.
C	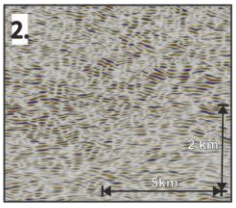	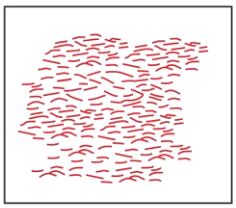	**C 2** Discontinuous, chaotic reflections of a high amplitude reflections. Cross-cutting and curvi-linear in nature. Indicative of deep, unstretched continental crust.	Unstretched continental crust.

2.4.3 Stretched continental crust (*CS*) and stretched continental magma-rich crust (*CsM*)

Stretched continental crust (Table 4) is also predominantly thinned continental crust as by definition, crustal thinning implies extensional processes. This crustal type comprises the majority of the proximal crust region along with the craton. As noted by the facies in section 1.4, there are few areas in the study region where 'typical' continental crust exists that is not in some way affected by thinning or stretching (at some depth) within the crust. This crust type is represented by an area comprising approximately 240 km along the margin and which varies between, 90 km to 180 km from the continent to the ocean (from the most continentward, ION SPAN north-western data boundary). The key seismic facies that comprise this crust are noted in Table 4. Facies *CS* 1 exhibits steeply dipping reflections within the continental crust, which are especially observed at depth or branching from mid-high amplitude sets of reflections, interpreted as being the continental Moho. Facies *CS* 2 is interpreted as continental blocks within the stretched continental crust zone. *CS* 3 is anomalous in that it has convex-up reflections. This is predominantly observed at the base of the 3D dataset. Hyp-1 facies is included as this represents a zone of

hyper-extended (thinned to less than 10 km) continental crust (note thumbnails are in x3 vertical exaggeration). Seismic facies *CsM* 1-3 are similar in that they correspond to areas of both stretched continental crust and are both highly magma-rich. This magma-richness is interpreted from the steeply dipping, high amplitude reflections, often near the base of the crust or detaching to the Moho.

Table 4: Key seismic facies and reflection relationships for 'Stretched continental crust' (*CS*) Hyper-extended continental crust (<10 km) (*hyp*) and magma-rich stretched continental crust (*CsM*). Red defines specific reflections, or packages of reflections which are indicative of the facies.

Crustal type	Seismic facies	Key reflection relationships	Reflection characteristics	Seismic Facies Association
Cs	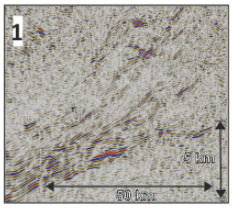	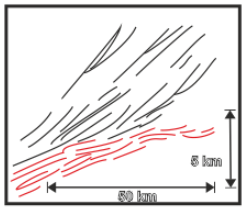	**CS 1** High amplitude sets of reflections, sub-horizontal and above a low amplitude matrix. Cs3 reflections branch away from this set of reflections.	Continental crust that is affected by extension/shearing /thinning representing Moho.
Cs	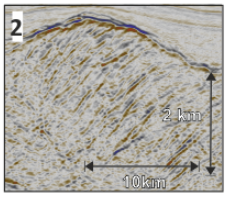	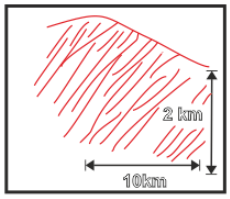	**CS 2** High-mid amplitude, reflections closely parallel spaced and dipping. Top of facies is represented by several high amplitude, partially continuous reflections	Continental crust in resistant, basement horsts
Cs	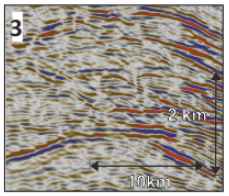	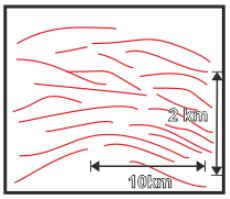	**CS 3** High amplitude reflections, convex-up, forming broadly symmetrical folds and with partially continuous reflections, also some dipping reflections internally	Continental crust (compression?)
hyp	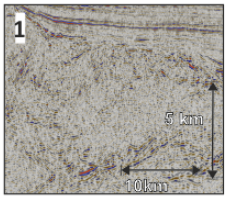	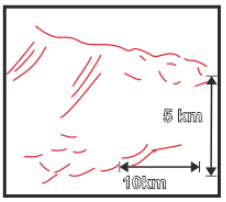	**Hyp 1** Mid-high amplitude reflections to the top and bottom of the facies which has an internal section of low reflectivity with mostly discontinuous reflections and some dipping reflections	Hyper-extended, volcanic continental crust (<10 km thickness)
CsM	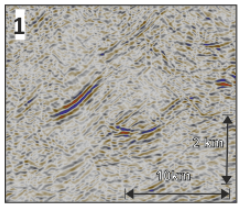	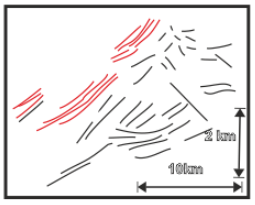	**CsM 1** High amplitude sets of 3-5 reflections, dipping and partially continuous within a low-mid amplitude sub-chaotic matrix with some mid-amplitude reflections	Continental crust that is affected by extension/shear ing/thinning
CsM	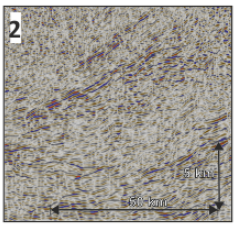	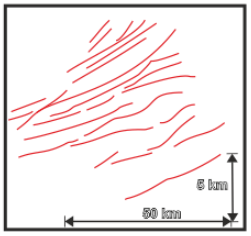	**CsM 2** High amplitude sets of dipping reflections, longer than 1. also partially continuous within a low-mid amplitude sub-chaotic matrix that has both low and mid-amplitude reflections	Continental crust that is affected by extension/sheari ng/thinning
CsM	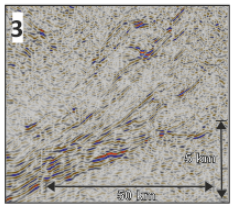	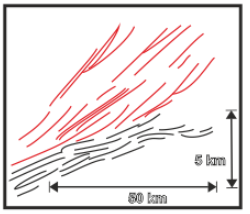	**CsM 3** High amplitude sets of dipping reflections in packages several reflections wide, within a partially continuous low amplitude chaotic matrix of reflections	Continental crust that is affected by extension/shearing /thinning

2.4.4 Extrusive volcanics (seaward-dipping reflections (SDR), magmatic additions and magmatic crust (*M*)

Seismic facies that are interpreted as the crustal type ‘extrusive volcanics’ are located in a thick wedge 80-90 km wide by ~4 km thickness in a broadly north-south orientation down the offshore margin (Table 5). The primary facies and reflections characteristics which define this crustal type, are sets of high amplitude, convex-up reflections, which dip seaward (commonly known as ‘Seaward-dipping reflections’, or SDR (Table 5). These are represented by orange with yellow ‘v’ and the lettering, ‘SDR’. Extrusive volcanics which are not able to be unequivocally defined as seaward-dipping reflections (but may be associated with them) are labelled as ‘Volc’. Reflection characteristics of the seismic facies which comprise the extrusive volcanics crustal type may be affected by various elements which include, hydrothermal processes, sill intrusions and sediments or faulting. Each of these elements has produced different reflection characteristics which are noted in Table 5 and are continued in Table 6. Magmatic additions are represented by a red background with the lettering ‘*MA’.* These volcanics may be emplaced by magmatic intrusion and may have a layered structure. These are also noted in Table 6. This division include regions where there is a prominent extrusive volcanic feature and volcanic flows on either side that are related. This division also includes features such as magma-chambers which are also suggested as sources which have fed magmatic addition flows. Magmatic crust is represented by orange and is defined as newly-created crust during the creation of SDR and which often underlies them, as part of this there may be feeder dykes within the magmatic crust that have supplied the overlying SDR packages. The distinction of magmatic crust is separated from stretched continental crust (with high levels of magmatism) due to the fundamental differences in the environment of creation of the SDRs. Different definitions of inner and outer SDR are used in the existing literature (see background

chapter). However, for the purposes of this thesis Inner-SDR refers to SDR which overlie stretched continental crust and Outer-SDR are those which have magmatic crust underneath.

Table 5: Key seismic facies and reflection relationships for the crustal types, Extrusive volcanics (*Volc*) and Seaward-dipping reflections (*SDR*). Red defines specific reflections, or packages of reflections which are indicative of the facies.

Crustal type	Seismic facies	Key reflection relationships	Reflection characteristics	Seismic Facies Association
SDR	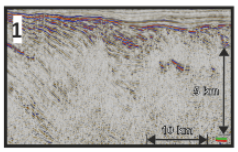	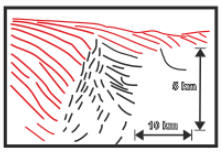	**1** High amplitude, mostly continuous curvi-linear reflections, with a shallow dip to the right of the section and interrupted by S-1.	Volcanic extrusive packages
SDR	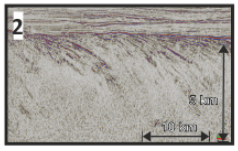	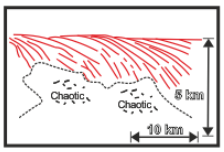	**2** High amplitude, mostly continuous, curvi-linear reflections, dipping to the right of the section with a basal section of low amplitude chaotic reflections.	Volcanic extrusive packages with a steeper dip than 1.
SDR	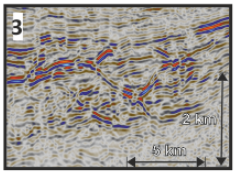	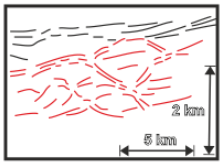	**3** High amplitude, curvi-linear reflections in a circular 'eye' - shaped arrangement with opposing direction dipping reflections.	Volcanic extrusive packages affected by hydrothermal fluidisation.
SDR	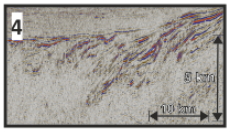	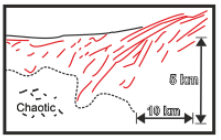	**4** High amplitude, discontinuous curvi-linear reflections, dipping to the left of the section. Basal section of low amplitude chaotic reflections.	Volcanic extrusive packages affected by sills and faulting.
Volc	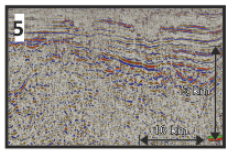	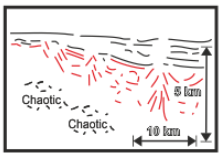	**5** Mid-high amplitude, discontinuous reflections, with a broadly chaotic nature with some dipping internal features.	Volcanic packages affected by sediments and faulting.
SDR	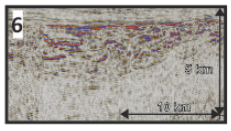	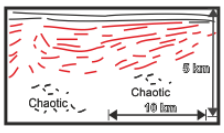	**6** Mid-high amplitude, discontinuous reflections dipping to the left of section, steeper reflections at the left of the section.	Seaward-dipping reflections affected by sediments and faulting.
SDR	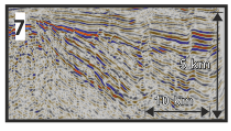	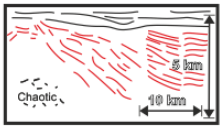	**7** High amplitude, discontinuous reflections dipping to the right of section, broken by distinct almost vertical fractures.	Steeply faulted seaward-dipping reflections.
SDR	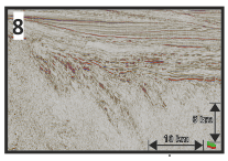	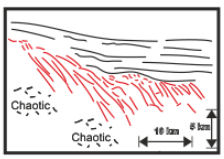	**8** Mid-High amplitude, sub-continuous reflections dipping to the right of section with a base of low amplitude chaotic reflections.	Highly faulted seaward-dipping reflections.
SDR	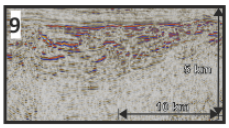	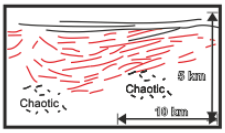	**9** Mid-High amplitude, sub-continuous reflections dipping to the left of section, with low amplitude chaotic reflections on the bottom right of section.	Seaward-dipping reflections affected by sediments, fluidisation and faulting.

Table 6: Key seismic facies and reflection relationships for the crustal types, Extrusive volcanics (*Volc*) and Seaward-dipping reflections (*SDR*) continued. 'Magmatic additions' (*MA*) and 'Magmatic crust' (*M*). Red defines specific reflections, or packages of reflections which are indicative of the facies.

Crustal type	Seismic facies	Key reflection relationships	Reflection characteristics	Seismic Facies Association
Volc	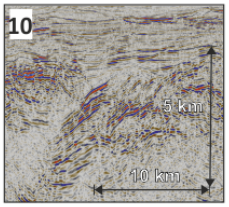	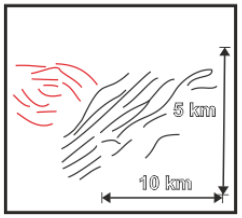	**10** High-amplitude, sub-continuous curved, (both convex and concave) reflections.	Extrusive volcanics
Volc	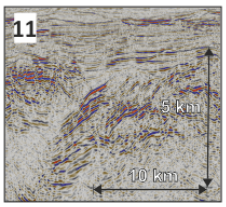	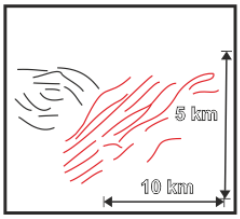	**11** Package of mid-high amplitude, partially continuous dipping reflections, broadly parallel and lying adjacent to 10	Interaction of extrusive volcanic centre and margin oblique faulting.
MA	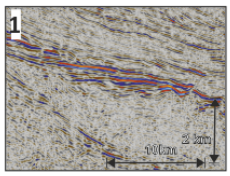	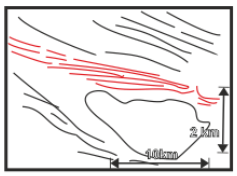	**1** High amplitude sets of reflections, broadly continuous above a low amplitude chaotic matrix	Extrusive volcanic flows (flat-lying or low dip)
MA	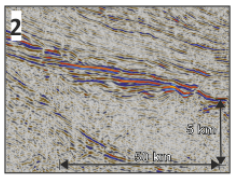	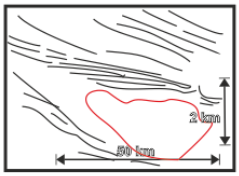	**2** Amorphous area of very low amplitude, discontinuous reflections which are chaotic. Also confined by $T_{ext}1$ ontop.	Extrusive volcanic pond/magma chamber
MA	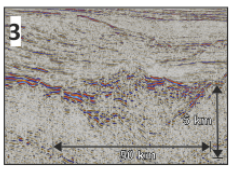	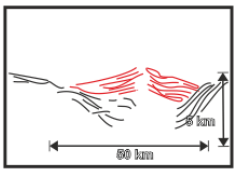	**3** High amplitude partially continuous reflections dipping in opposing directions around a central area.	Reflections representing the sides of an extrusive volcanic vent
MA	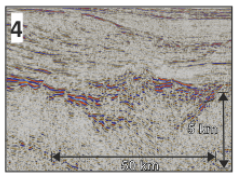	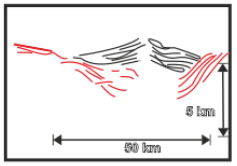	**4** Mid-high amplitude reflections, partly continuous and dipping towards a central axis	Extrusive volcanics in-filling topographic lows
M	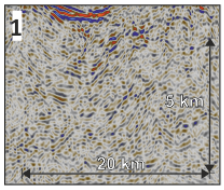	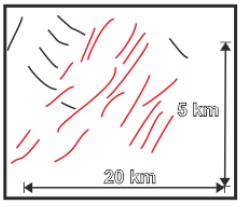	**1** Mid-amplitude, sub-continuous, high angle reflections, within a low amplitude, low coherency matrix of reflections.	Transitional crust/ 'magmatic crust' highly intruded
M	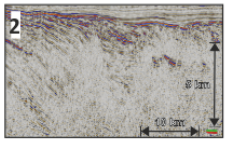	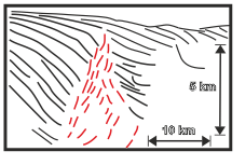	**2** Low amplitude, chaotic discontinuous dipping reflections to both the left and right of section in the centre of the section.	Volcanic vent/upwelling/ intrusion through seaward-dipping reflection packages.

2.4.5 Exhumed mantle (*Exh*)

Exhumed mantle facies have a variety of distinctive and characteristic seismic reflection characteristics (Table 7). These include high amplitude reflections, which create a rugose surface that lies directly below syn-rift sediments (*Exh* 4) and is only found where the Moho is notably absent below. These are suggested as basalt flows or serpentinised upper-mantle, sensu Gillard et al., (2015). These facies are explored in greater depth later in this chapter and in following chapters.

Table 7: Key seismic facies and reflection relationships for the crustal type 'Exhumed mantle' (*Exh*). Red defines specific reflections, or packages of reflections which are indicative of the facies.

Crustal type	Seismic facies	Key reflection relationships	Reflection characteristics	Seismic Facies Association
Exh	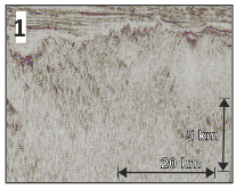	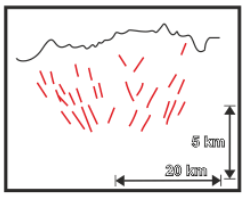	**1** Package of mid-high amplitude, partially continuous, dipping reflections, broadly diverging upwards from the centre of the section.	Internal reflections of exhumed Mantle
Exh	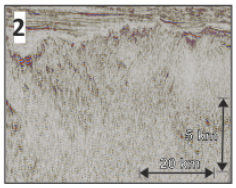	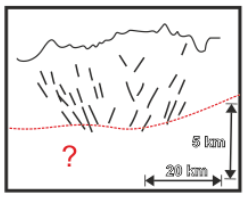	**2** Zone of discontinuous, chaotic low amplitude reflections with no structure. Absence of expected Moho representative reflections.	Lower section of exhumed Mantle
Exh *hyp*	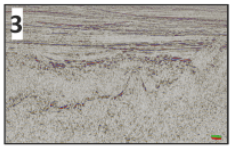	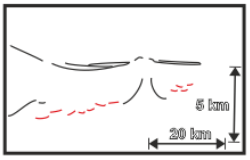	**3** Zone of discontinuous, chaotic low amplitude reflections with no structure. Absence of expected Moho representative reflections.	Upper Mantle reflections/fault plane reflections
Exh	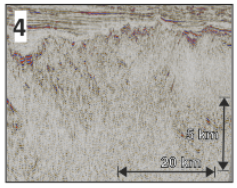	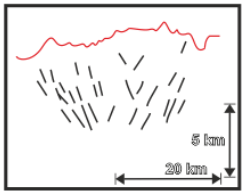	**4** High amplitude reflections forming a distinct rugose surface which may also be convex in some areas. Directly below post-rift sediment.	Serpentinised upper Mantle surface, or Basalt flows

2.4.6 Oceanic crust (*O*)

Oceanic crust (*O*) of a predominantly ‘typical’ thickness of 7-8 km comprises the majority of the distal, eastern section of the study area. A clear oceanic Moho is defined by a high amplitude reflection (or package of several reflections) that are the lower boundary to oceanic crust. Although typical in general thickness and the broad arrangement of reflections across the crustal type, there are also distinct seismic facies which can be distinguished that are noted in Table 8. This includes changes to the nature of the upper crustal reflections and fracture/faulting patterns and internal reflections that dip in opposing directions. Also of note is Oceanic facies 4 which shows steep dipping reflections on the lower section which cut the oceanic Moho.

Table 8: Key seismic facies and reflection relationships for the crustal type 'Oceanic crust' (*O*). Red defines specific reflections, or packages of reflections which are indicative of the facies.

Crustal type	Seismic facies	Key reflection relationships	Reflection characteristics	Seismic Facies Association
O	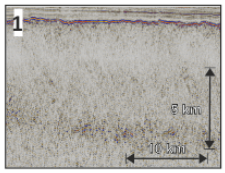	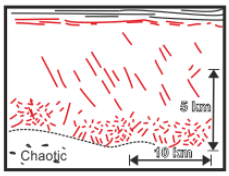	**1** High amplitude, continuous reflections, parallel at the top of the package. Right-dipping mid-low coherency and low amplitude reflections within chaotic reflections with high amplitudes at the base.	Oceanic crust of a normal thickness with volcanic flows. Unusual right-dipping internal reflections.
O	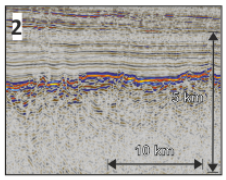	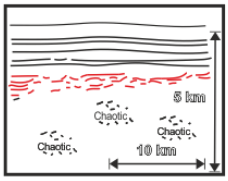	**2** High amplitude, discontinuous but horizontal reflections, parallel at the top of the package. Below is a large package of low amplitude chaotic reflections.	Highly faulted oceanic crust.
O	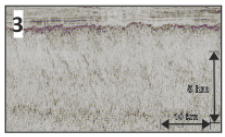	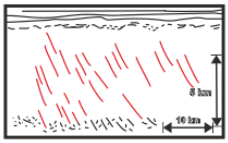	**3** High amplitude, sub-continuous reflections, Right-dipping mid-low amplitude reflections within a low amplitude chaotic matrix.	Oceanic crust of normal thickness. Unusual dipping internal reflections.
O	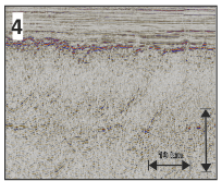	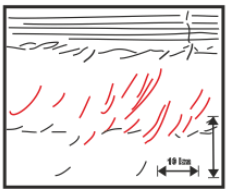	**4** Mid-high amplitude, sub-continuous reflections, Dipping to the left (of section) within a low amplitude chaotic matrix. Section is topped by horizontal high amplitude reflections and to the base.	Oceanic crust not uniform in thickness. Unusual left-dipping internal reflections.
O	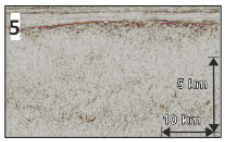	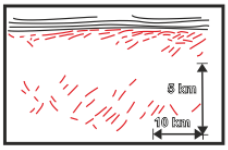	**5** High amplitude, discontinuous curvi-linear reflections dipping to the left of section (top). Similar reflections at the base with a central low amplitude, chaotic matrix.	Oceanic crust of average thickness with elements of SDR geometries.
O	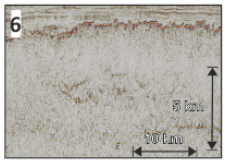	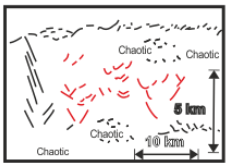	**6** High amplitude, discontinuous curvi-linear reflections within a surrounding low amplitude chaotic matrix of reflections.	Sill intrusions to oceanic crust

2.5 Domains

2.5.1 Introduction and rationale for domain categorisation

Peron-Pinvidic et al., (2013) observed that there is a consistent arrangement of first-order structural domains across both magma-poor and magma-rich margins, despite their inherent differences and smaller-scale variations. This has been borne-out through the work of many authors who have observed this typical distribution (of domains). Examples of some of the key areas that have helped define the domains include, the Iberia-Newfoundland margin (Manatschal et al., 2001; Henning et al., 2004; Brune et al., 2017) and the mid-Norway-East Greenland (Mjelde et al., 2009; Theissen-Krah et al., 2017). Seismic refraction has been used (Reston, 2009) to broadly classify rifted margins. However, potential field data, along with well data and seismic reflection profiles allow for the most detailed examinations of basement structure (Peron-Pinvidic et al., 2013). Peron-Pinvidic et al., (2013) notes a rift exists between margins which have been drilled (i.e. Iberia-Newfoundland, through the Ocean Drilling Program (ODP) and those which have not. The ODP has provided invaluable evidence for rifted margin studies, especially regarding lithological changes on magma-poor margins, however this only provides ‘spot’ sampling and does not allow for wider constraints on margin architecture and evolution. The Iberian margin has become a highly studied and ‘type example’ of continental breakup in a low magma system. This has also provided data for recent revisions to widely held assumptions on rifted margins (Péron-Pinvidic and Manatschal, 2009). This includes the establishment of a series of recognisable domains from the continental region, seaward. These include, proximal, necking, distal and outer zones which are common to all rifted margins and have comparable structural characteristics (Peron-Pinvidic et al., 2013). These were defined in work by Peron-Pinvidic et al., (2013) and such a system has been adopted in this thesis for the

observational classification of the Uruguayan margin using the ION SPAN 2D dataset. In this study the high fidelity and long recording times of the ION SPAN dataset are invaluable in expanding the understanding of basement development and the development of rifted margins as a whole. The grid arrangement of lines at 80 km intervals provides a close segmentation of the margin (not usually found in 2D surveys) to study the crustal geometry and how this changes, both along the margin and from continent to ocean.

2.5.2 Defining crustal domains and a domain framework

Now that the seismic facies and reflection characteristics have been recorded it is possible to build a framework of distinct crustal domains. The identification of specific crustal domains from the continent, oceanward, is a key stage in the categorisation of rifted margins which has been adopted by in studies dealing with both magma-rich and magma-poor rifted margins. Peron-Pinvidic et al., (2013) note that each domain presents a set of individual and comparable structural characteristics. It is then possible to capture the changes in crustal architecture from the continental to oceanic domains. Crustal type observations can then be linked to different processes responsible for their creation and ultimately the evolution of the margin can be uncovered. The major domains commonly identified include those of ***proximal***, ***necking***, ***transitional*** and ***distal*/outer/oceanic**.

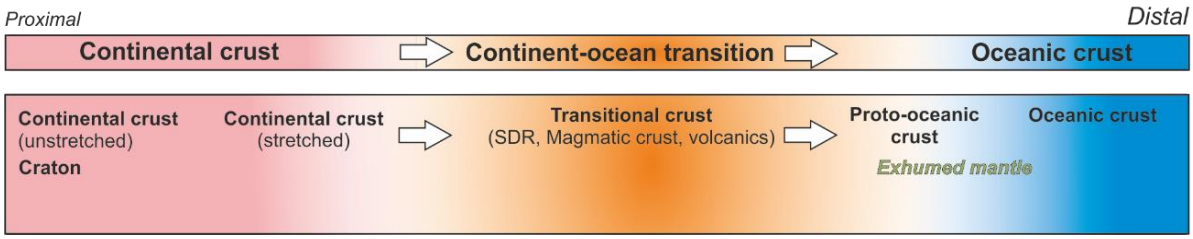

Figure 2.4: Crustal domain divisions and sub-divisions used in this study .From left to right, (1) Continental craton and continental crust (unstretched) (2) Continental crust (stretched) (3) Transitional crust (4) Proto-oceanic crust (5) Oceanic crust.

Figure 2.4 includes the crustal type divisions and sub-divisions from the proximal to the distal domain which are used in this study. In accordance with similar studies investigating the 2D crustal architecture of margins, the 2D architecture of the offshore Uruguay margin is divided into distinct zones which represent commonly observed crustal processes. The primary crustal domains consist of (from the proximal region oceanward); 1) Unstretched continental crust (inclusive of cratonic crust) 2) Stretched continental crust 3) A zone of transition (including magmatic accretion) 4) A zone of oceanization. These represent commonly observed crustal regions which are observable on dip-line seismic reflections sections across a magma-rich passive margin. Within these regions a sub-division of proto-oceanic crust is also recognised in some areas but may not always be observed.

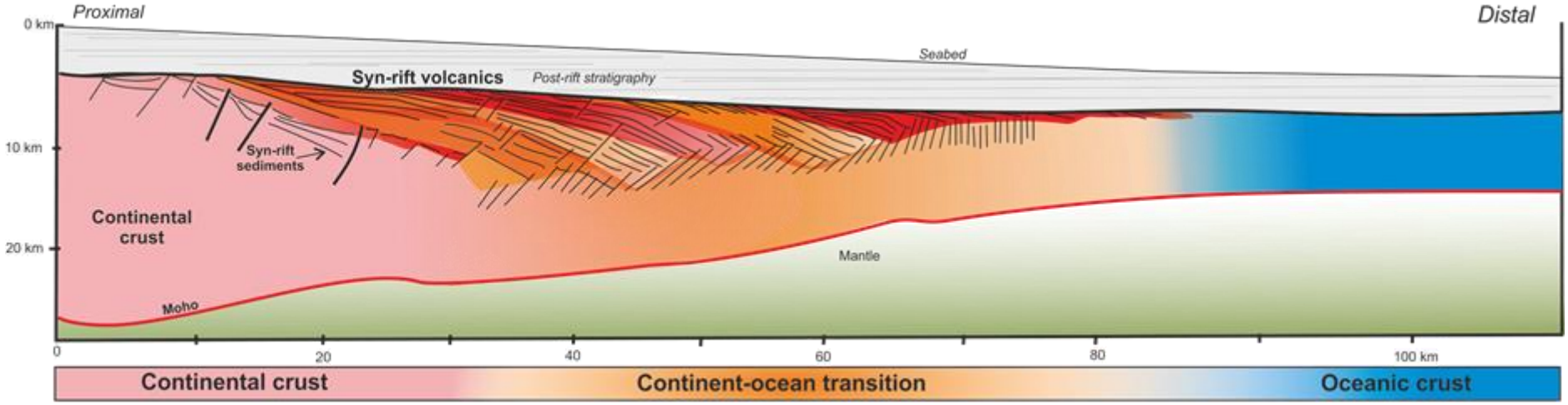

Figure 2.5: (Expanded section of figure 2.2) Type section showing major crustal types across a magma-rich margin, modified from Paton et al., (2017). (Excludes sub-divisions noted in text).

Figure 2.5 shows these stages on a typical dip-line section through a magma-rich passive margin (Paton et al., 2017) and is shown as a simplified figure, without the sub-divisions previously noted. This shows a proximal zone of thick, continental crust which is at first, unstretched and may also comprise a region of ancient cratonic crust which is usually also undeformed. Moving seaward, the continental region may become stretched during rifting, in a volcanic setting this becomes a transitional crust region, characterised by magmatic accretion in the form of a classic representation of a wedge of seaward-dipping reflections (SDR) and a characteristic thickening of the crust beneath the SDR. This transitions to an outer, oceanic zone in the distal region, where steady-state oceanic spreading is observed. The width and individual reflection characteristics of these stages may vary from margin to margin, but it is typical that most magmatic-rifted margins will broadly conform to this geometry.

2.6 Observations of crustal geometry

A first-order geometry exists in rifted margins, regardless of the volume of magmatic products. This includes the presence of a seismic basement which is thickest in a proximal region with an expected thickness of ~30 km and which thins oceanward to ~7-8 km in the distal realm (or as thin as 5 km in the Iberian-Newfoundland margin) (Peron-Pinvidic et al., 2013). Expected structural features in the proximal region include half-graben with syn-tectonic sequence/s and in the distal zone, the presence of a sedimentary ‘sag’ basin (which is either sediment or water filled) (Peron-Pinvidic et al., 2013).

2.6.1 The proximal domain

The proximal domain is identified as the most inboard continental crust, which is either unstretched or has only undergone light stretching. Peron-Pinvidic et al., (2013) suggest that despite some variation, there is also little to no crustal thinning,

the suggested lowest thickness of this domain is 25 km in established literature (Peron-Pinvidic et al., 2013). The top section of the domain is typically affected by brittle faulting and characterised by tilted blocks bound by high-angle extensional faults, or sediment-filled half-graben. Faults predominantly root into a brittle-ductile transition at a mid-crustal level and do not affect the Moho (Peron-Pinvidic et al., 2013) and tectonics are decoupled at a lithospheric scale (Weinberg et al., 2007; Sutra and Manatschal, 2012; Peron-Pinvidic et al., 2013). These faults accommodate minimal extension, however there may be significant basement relief (such as in the Lusitanian Basin) uplift and magmatic activity (from late-stage structural reactivation (Peron-Pinvidic et al., 2013).

2.6.2 The necking domain

This domain is characterised by a wedge-shape to the crust and a distinct basinward increase in accommodation space (Sutra and Manatschal, 2012; Peron-Pinvidic et al., 2013). An inflection point is also characteristic of this zone with a sharp decrease in crustal thickness to less than ~10 km (Péron-Pinvidic and Manatschal, 2009; Mohn et al., 2010; Peron-Pinvidic et al., 2013). This point when it is closest to the coastline is also referred to by Peron-Pinvidic et al., (2013) and Osmundsen and Redfield, (2011) as a ‘taper break’. It may also correspond to the ‘coupling point’ where the first brittle faults cut the entire crust and decollé into the Mantle. This juncture is important as it represents the boundary from the proximal continental region, where mid-crustal decoupling of tectonics occurs, and the transition into the oceanic realm where deformation is coupled and there are no separate ductile layers within the crust (Peron-Pinvidic et al., 2013).

2.6.3 The transitional domain

The basement of the transitional region in studies to date may be either; upper and/or lower continental crust, exhumed serpentinised Mantle or embryonic oceanic

crust (Peron-Pinvidic et al., 2013). Magmatic intrusions may also be present. The defining characteristic of the transition into this domain according to Peron-Pinvidic et al., (2013) is that no ‘remnant ductile layers’ are present and all faulting must be through the whole of the crust to the Mantle. This definition is satisfied in this work for delineation of the transitional domain. A separate transitional domain has been interpreted in this study, separate to the distal domain, which is characterised by unequivocal oceanic crust only (see outer/oceanic domain). This is in order to discern internal variability in this region that may be crucial to understanding the tectono-magmatic evolution of the margin. In this study there are considerable amounts of extrusive volcanics known and observed. These comprise a large area of the transitional zone. Due to the long recording times of available data, we are now able to define a lower boundary to much of the transitional domain and in some orientations, beneath packages of extrusive volcanics. It should also be noted that the full observation of features through a transitional zone has not been achieved in an across-margin orientation in any known study previously. In this study, this exposes a lower-crustal/Mantle ‘*intrusive component’* vertically beneath extrusive products (which has been recorded as a separate crustal type on interpretations of seismic profiles, in particular on strike lines). It was considered important to make this distinction for later interpretations of the tectono-magmatic evolution and timing of magmatic generation in the region and specifically within the transitional zone. Note: for plan-view, crustal type classification, both intrusive and extrusive products have been noted in the same geographical position.

2.6.4 The outer/oceanic domain

This domain identification is considered most important in the distinction between magma-rich and magma-poor environments. In this study it is defined as beginning at the same point at which unambiguous oceanic crust is observed. This also includes any anomalous features which are still interpreted as being within oceanic crust (i.e sills within oceanic crust, slight thickening of oceanic crust). There is variability between studies, authors and settings as to what is considered the distal region. Some studies include a continent-ocean transition, a transitional domain, or on magma-poor margins, the (ZECM) the Zone of Exhumed Continental Mantle. The distal domain is also commonly referred to as the hyper-extended region on magma-poor margins such as the Iberian margin (Peron-Pinvidic et al., 2013).

2.6.5 Uncertainties of the continent-ocean boundary (COB)

Increasing ambiguity and controversy over the positioning of a distinct continent-ocean boundary on rifted margins has arisen in recent years (Eagles et al., 2015). This ‘boundary’ may be a diffuse zone or marked only by geochemical changes (Peron-Pinvidic et al., 2013). It may also be masked by extensive, intrusive or extrusive volcanics, such as on the Norwegian, Møre and Vøring margins (Skogseid et al., 1992; Peron-Pinvidic et al., 2013) which is a key defining characteristic of the transitional region of magma-rich margins. Defining instead a simple boundary between continent and ocean however, has benefits for both palinspastic and plate kinematic reconstructions and it is therefore, continued to be mapped as such (Eagles et al., 2015).

Chapter 3: The 2D crustal architecture of the offshore Uruguay margin

3.1 Introduction

So far, the overriding crustal architecture of the offshore Uruguay margin has been observed and recorded using dip line sections, a common methodology for investigating magma-rich margins. However, this thesis includes an equally thorough examination of the strike line profiles of the Uruguay ION SPAN dataset. These have also been used as each strike line contained unexpected and anomalous crustal geometries which, if not included, would leave much of the complexity of the margin unrecognised and the three-dimensional story of the margins evolution, incomplete. By including both dip and strike line profiles, this study is able to capture both smaller-scale features and margin-oblique structures which may prove crucial to understanding the full development of the margin. The following section records the nature and character of seismic reflectivity on the eight lines which comprise the ION SPAN dataset (figure 3.1). The dip lines for this dataset are considered first and comprise lines A1-A4 from the north to the south. This study then includes detailed analysis of the Strike lines B1-B4 from the west to the east. The start of the line is taken as the proximal (most landward) side, creating a profile section which is approximately perpendicular to the margin. Strike line sections are lines B1-B4 and are considered from the most proximal line location to the most distal, along the margin and from south to north on each profile. Lines are spaced at ~80 km and span a distance of ~335 km from north to south. They are presented as PSDM profiles in 1:1 scale and observations are recorded in terms of the overall line geometry, major features, structures and crustal architecture of the margin.

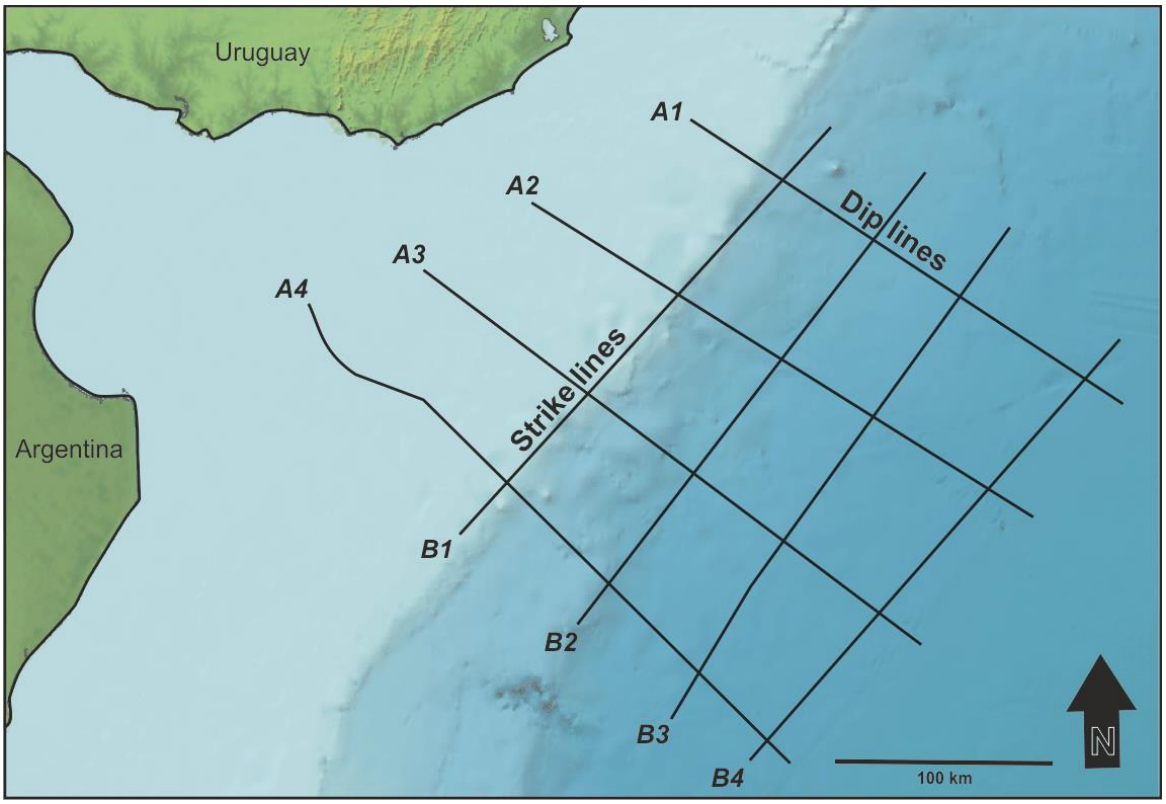

Figure 3.1: Grid line locations in offshore Uruguay of the seismic reflections profiles of the ION SPAN dataset.

Dip lines are lines A1-A4 which are considered in order from north to south. The start of the line is taken as the proximal (most landward) side, creating a profile section which is approximately perpendicular to the margin. Strike line sections are lines B1-B4 and are considered from most proximal line location to most distal, along the margin and from south to north on each profile.

The crustal domains outlined in the previous chapter have also been identified and mapped. These include continental and cratonic crust in the proximal domain, as well as stretched continental crust, transitional crust (inclusive of seaward-dipping reflections) and distal oceanic crust. Crustal thickness measurements have been taken from the top crustal horizon of a domain (e.g top continental crust, top oceanic crust) to the centre of basal packages of reflections of the Moho. The distance along the line where measurements were taken is also noted. Comments are made in relation to the identification of anomalous or unexpected features. However, the interpretation and reasons for these anomalies will be discussed in detail in section 3.4.

3.2 Dip lines

3.2.1 Line A1

The overall geometry observed in line A1 (figure 3.2) shows a broadly thinning crustal wedge from proximal continental crust, into a zone of transitional crust to distal oceanic crust. The proximal crustal zone comprises a thick (32 km) section of continental crust. The upper-crustal section of this line is dominated by an area of distinct, chaotic reflections with a low-mid amplitude and high reflection discontinuity, this is suggested to be cratonic in nature. This facies extends for 30 km from the most proximal edge of the line and to a depth of 5.5-6 km, below this, continental crust extends to 32 km thickness with an internal character of predominantly mid-amplitude, discontinuous reflections. There are also intra-crustal zones of high amplitude reflections which are curvilinear towards the base of the section. Directly seaward of the cratonic facies is an area of high amplitude reflections which dip seaward and are interspersed with low amplitude reflections. These terminate on either side suggesting a large, controlling syn-rift structure (a sediment-filled half-graben) which extends to 10 km in depth with a width of 16 km. This high angle fault represents the primary faulting observed in the continental crust

on this line. Underneath this half-graben and for a zone of 40 km oceanwards, there is an absence of defined Moho reflections. There are also intra-crustal reflections of a mid-amplitude. Immediately seaward of the large half-graben structure, the upper crust transitions into broad wedge of high amplitude, seaward-dipping reflections (SDR) which continue for 80-85 km and to a depth of 4-5 km. These reflections are considered magmatic and broadly continuous with a zone of low amplitude reflectivity directly below them. Crustal thickness beneath this transitional region of crust is consistent at ~22 km until between 42 km and 83 km from the start of the line where there is an area of low coherency and an absence of Moho reflections. This accompanies mid-amplitude, steeply dipping reflections which form on either side of this zone producing a triangular feature of low-mid amplitude reflections. The general positioning of the wedge of SDRs within a region that exhibits transitional crust and lies seaward of continental crust and inboard of full oceanic crust, can be considered typical for a dip line profile across a magma-rich margin. At ~60 km from the proximal initiation of the seaward-dipping reflections, thinning of the crust is observed with the shallowing of high amplitude, Moho reflections. This thinning occurs until the end of the SDR wedge, at a total distance of 147 km from the start of the line, and marks the relatively abrupt transition to a zone of proto-oceanic crust. This proto-oceanic crust has an initial thickness of 6-6.2 km for ~20 km, before full Penrose oceanic crust is established which has a thickness of 7.5 km and is constant until the distal termination of the line. There are occasional intra-crustal, oceanic crustal reflections but most notable are breaks in the Moho reflections along the base of the oceanic crust. This faulting becomes more prominent in the most distal 25 km of the line, where whole-crustal faulting is observed through the oceanic crust and displacement is seen in the high amplitude reflections, characteristic of the upper oceanic crust. This faulting does not continue into the post-rift sediments,

which are draped over any displaced sections of upper oceanic crust. This line shows the expected broad crustal architecture through a magma-rich margin, with features such as the thick section of proximal continental crust and crustal extension accommodated in this region by a large, extensional half-graben on the continental shoulder. The wedge of SDR (termed SDR North) is also typical in both geometry, length and thickness to other SDR observed down the Argentinian margin to the south and aside from a small section of proto-oceanic crust, the oceanic crust has an expected location, thickness and typical reflection characteristics. Overall, this line shows very little unexpected architecture, however there are some anomalous features of note. These are the absence of Moho reflections within the basal proximal zone of mildly stretched/transitional crust where the initiation of the SDR wedge occurs. Steeply-dipping, whole-crustal faults are also prominent and unexpectedly observed in the distal region of the oceanic crust.

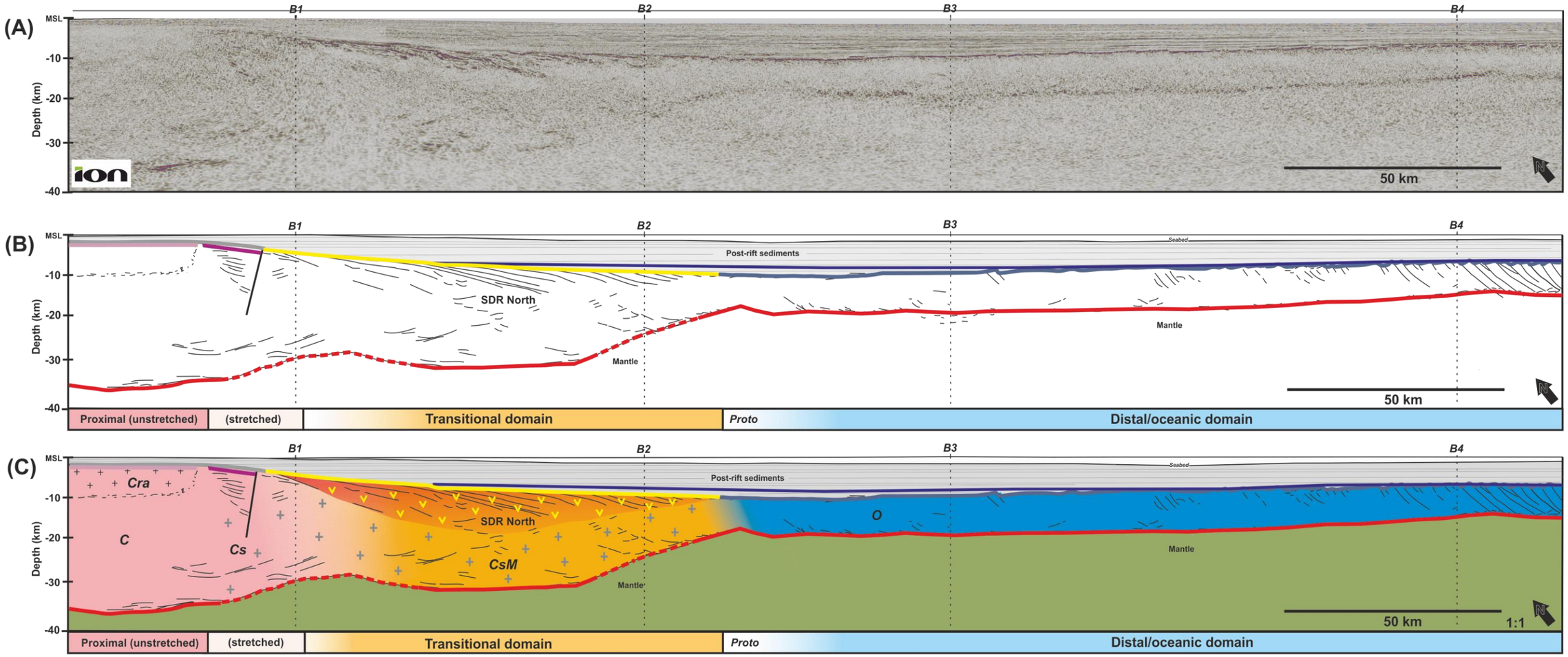

Figure 3.2: (A) Line A1 uninterpreted 2D PSDM seismic reflection line (ION SPAN) (B) Line drawing interpretation of the major structural and geological features with major crustal horizons (C) Interpretation of line A1 with major structures and crustal domains. Please refer to key in Table 1 for horizons and corresponding crustal types and domains in figure 2.3.

3.2.2 Line A2

The overall geometry observed in line A2 (figure 3.3) is similar to line A1 in that it shows a thinning crustal wedge from proximal continental crust, into a zone of transitional crust to distal oceanic crust. Line A2 broadly conforms to the expected crustal geometry with some small exceptions. The line consists of a gradually thinning crustal architecture, as expected, from a thick section of proximal continental crust of 32 km thickness, into a region of transitional crust (~22 km) to a thin zone of distal oceanic crust (~7km). However, the base crust reflection geometry of this line shows higher complexity than A1 and is accompanied by an immediately obvious increase in the width of the continental and cratonic crust (*Cra*) of the proximal domain. The upper-crustal section of the line is dominated by chaotic, low amplitude, discontinuous reflections which are representative of cratonic crust (*Cra*). This zone extends for a distance of 115 km from the start of the line and has a thickness of ~5-7 km. Beneath this region is an area of discontinuous, mid-amplitude reflections at mid-crustal and lower crustal levels. There are areas of high-amplitude reflections at mid-crustal levels which dip continent-ward (towards the start of the line). Although discontinuous in places, it is possible to discern continental crustal Moho reflections at a depth of ~32 km. This thickness of crust continues until approximately 88 km from the beginning of the line whereby crustal thinning occurs to 19-22 km thickness. This is accompanied by an increase in lower crustal reflectivity, and at the top of the crust there are dipping reflections that may be related to a large continent-dipping fault and a half-graben structure (although this is not clearly defined). Immediately seaward of this structure there is the initiation of a large wedge of seaward-dipping reflections that extends seaward for ~60 km. The crust thickens to 20 km under the SDR probably due to the addition of magma and then thins rapidly over 40 km to a thickness of 8 km at the most-distal

point of the SDRs. Immediately basinward of the SDR is the occurrence of typical oceanic crust with a thickness of ~7.5-8 km. The transition from SDRs into oceanic crust is more gradual than in line A1 and is characterised by high amplitude Moho reflections that shallow gradationally from the SDRs into the oceanic domain. After a ~60 km long section of 'typical' oceanic crust (but with more dispersed Moho reflections), the upper reflections of the top of the oceanic crust become interrupted, and remain highly vertically faulted and fractured until the distal end of the section. Also, in this distal region are high amplitude, convex-up reflections within the low amplitude internal region of the oceanic crust, which is in contrast to the previous line (A1). This continues over a distance of ~48 km but disappears in the most distal 20 km of oceanic crust.

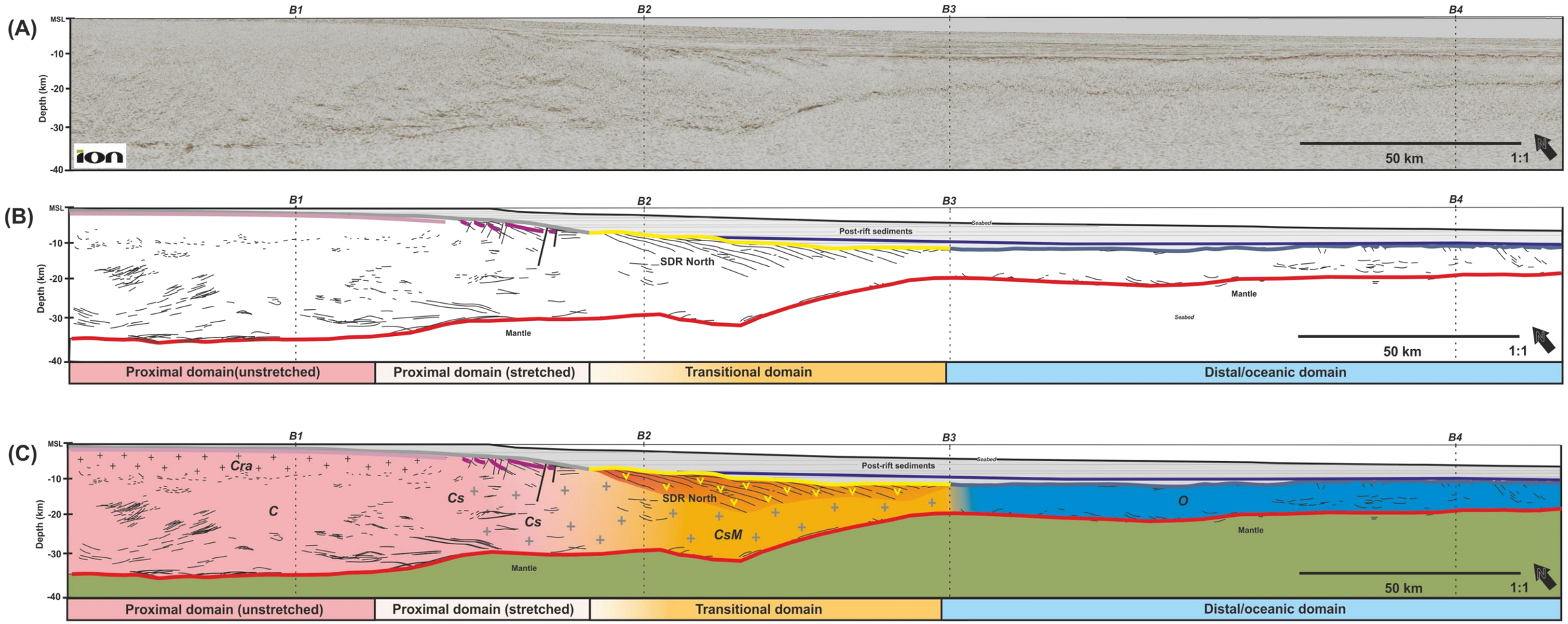

Figure 3.3: (A) Line A2 uninterpreted 2D PSDM seismic reflection line (ION SPAN) (B) Line drawing interpretation of the major structures and geological features with major crustal horizons (C) Interpretation of line A2 with major structures and domain boundaries. Please refer to key in Table 1 for horizons and corresponding crustal types and domains in figure 2.3.

3.2.3 Line A3

The overall geometry observed in line A3 (figure 3.4) is of a broadly thinning crustal wedge from continental crust in the proximal domain, into a zone of 'transitional' crust to oceanic crust. However, the transitional region of crust contains anomalous reflectivity. Line A3 has a wide (~107 km) proximal section of thick continental crust similar to the previous lines (A1 and A2). This continental crust extends to a depth of ~35 km for 107 km from the proximal start of the line. At the top of the proximal continental crust are low amplitude, chaotic reflections of a low to mid amplitude which are pervasive to a depth of 6-7 km and are considered representative of cratonic crust (*Cra*). Dispersed, high-amplitude, sub-horizontal reflectivity is observed within the middle section of the crust and at the base of the crust within Moho reflections. At approximately 107 km from the proximal start of the line, there is a shallowing of the continental Moho that continues to ~150 km from the initiation of the line. The upper crust is then significantly faulted by large extensional structures that form distinct half-graben, these are accompanied by further crustal thinning until a thickness of only ~6km is reached. The crust becomes 'hyper-extended' with faults decolling to the Moho and the total crustal thickness reduced to less than ~6 km over a short horizontal distance of ~40 km (from the thickest section of continental crust). In contrast to the previous lines, there is a notable absence of any seaward-dipping, high amplitude reflections (SDR wedge) where they would be geometrically expected. A further inflection point within the Moho is observed where the character of the basal crustal reflectivity undergoes a distinct change. Reflections at the base of the following section for ~30 km occur in discreet, discontinuous packages, and are present at a level below the previous reflections (for which there is high degree of confidence that these are Moho). The height of these reflection packages is also not continuous. As a result of this zone of intense

crustal complexity and uncertainty, this thesis presents alternate interpretations of the nature of the crust in this region (see figure 3.4). Additionally, there are two prominent, steeply-dipping high amplitude reflections within this anomalous section. This anomalous crustal zone extends for 60-80 km (depending on the crustal domain interpretation). At ~284 km from the start of the line there is an area of discontinuous low-mid amplitude reflections with no discernible Moho for a distance of approximately 30 km. The upper section of this zone becomes characteristic of upper oceanic crust with horizontal high amplitude reflections sitting below the post-rift sediments. There are also some mid-high amplitude reflections within the central area of oceanic crust; however, it is not until 302 km along the line that unequivocal oceanic crust is observed with the typical reflection characteristics, as well as an expected thickness of ~7.8 km. Oceanic crust extends from this point to the end of the line at ~390 km, and there is an increase in faulting of the upper oceanic crust reflections.

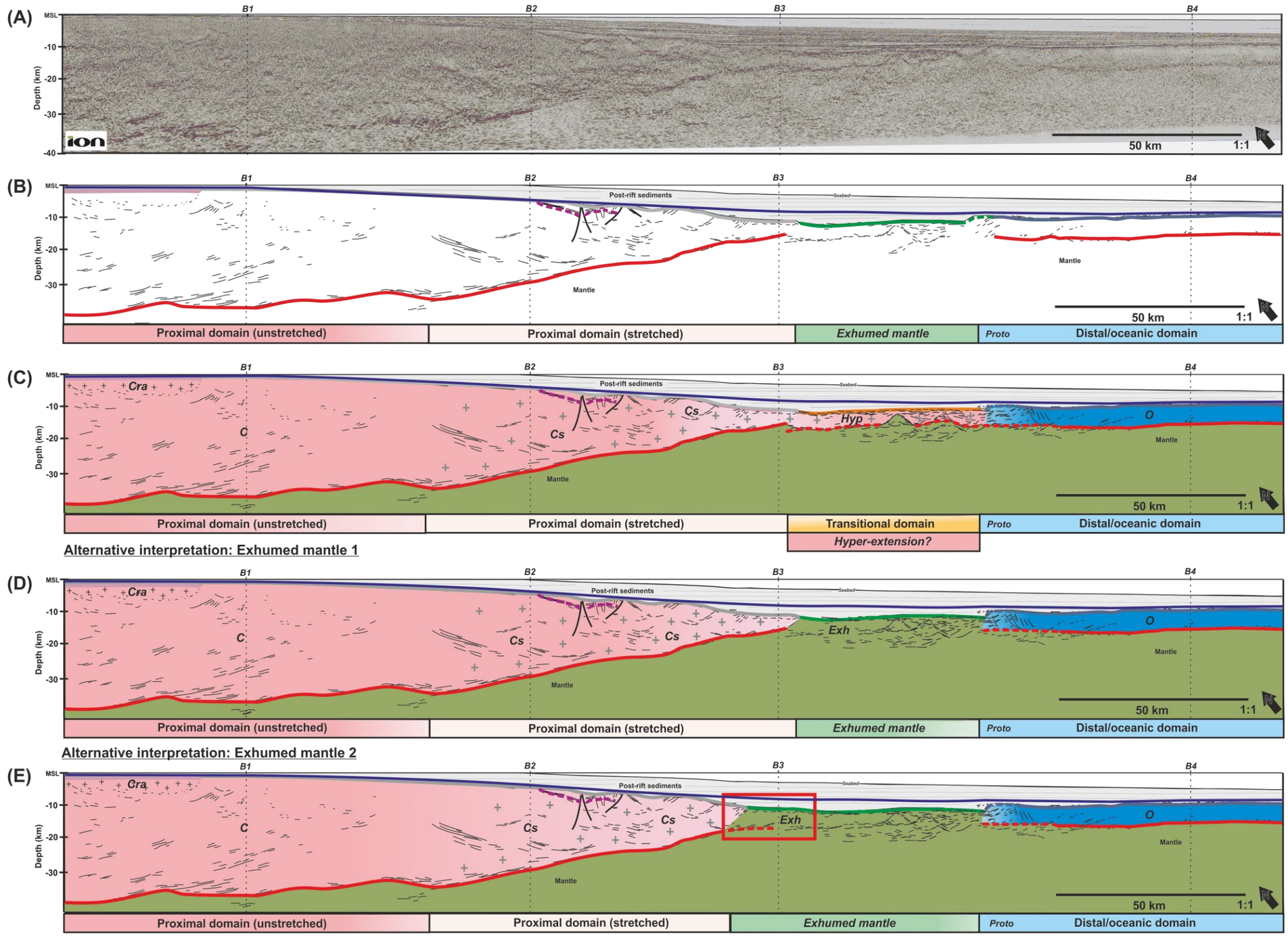

Figure 3.4: (A) Line A3 uninterpreted 2D PSDM seismic reflection line (ION SPAN) (B) Line drawing interpretation of the major structural and geological features with major crustal horizons (C) Interpretation of line A3 with major structures, crustal types and crustal domain boundaries and hyper-extended continental crust (D) Alternate, **preferred** domain interpretation: Exhumed mantle (E) Alternate domain interpretation: Exhumed mantle 2 (extended section of exhumed mantle). Please refer to key in Table 1 for horizons and corresponding crustal types and domains in figure 2.3.

3.2.4 Line A4

The overall geometry observed in line A4 (figure 3.5) is also characterised by a broadly thinning crustal wedge of proximal continental crust, a zone of transitional crust, and a distal domain of oceanic crust. However, there is significant anomalous crustal thinning observed in the region between the most distal section of continental crust and the initiation of transitional crust. In the proximal region, line A4 is characterised by a section of approximately 30 km thick continental crust which conforms to the previous lines and expected margin geometry. The upper section of the continental crust is dominated by a zone of mid-low amplitude reflections which are chaotic and discontinuous in nature and are proposed to be cratonic crust. Higher amplitude reflections are observed beneath and around this area, which are steeply dipping at an angle of 60-70^{o}. In mid-crustal regions, there are also areas of distinct cross-cutting reflectivity of a mid-high amplitude. The base of this proximal section of continental crust is broadly horizontal and defined by a series of high amplitude, partially continuous reflections. There are large (~8-10 km) upper-crustal blocks in the top section of the crust, structurally tilted and rotated across 50 km. This line is the only line of the dataset to have a large bend in its acquisition (see line A4, figure 3.1). This has been considered in the interpretation of reflectivity in this part of the line. It is especially relevant in relation to the interpretation of mid and lower crustal reflectivity associated with extensional processes as some reflectivity may be an artificial product of the change in line orientation rather than indicative of any real crustal process. Moving distally there is some thinning of the crust to ~23 km and a large sediment-filled half-graben on the edge of the continental ‘shoulder’ with a large, continent-dipping fault. The observed half-graben has an atypical internal geometry, with only occasional divergent reflections but it contains a fill that extends to a depth of 15-16 km. Immediately seaward of the half-graben is an

inflection point, beyond which the crust thins considerably to ~14 km at a distance of 210 km from the proximal start of the line. This area of anomalous crust and crustal thinning is notably not present on the other dip lines. High amplitude reflections are observed branching upwards from the continental Moho. The upper section of crust has high amplitude reflections which dip towards a central area. This central zone has horizontal, or low-angle, dipping reflections on top of a low amplitude area. Low amplitude 'bars' are observed either side of a central, high amplitude zone and bound by high amplitude packages of 3-5 reflections. Directly below this region the Moho reflections are absent. Immediately seaward of this feature the reflectivity returns to high amplitude reflections at the base of a thinned crustal segment, which are steeply dipping seaward over a distance of ~3 km. In the upper crust where these base reflections become horizontal, there is the start of the SDR with convex-up, high amplitude, seaward-dipping reflections which appear outboard of the previous SDR North wedge. Under the SDR wedge the crust gradually shallows and thins from a thickness of ~20 km to ~8-9 km at the terminal end of the seaward-dipping reflection package (termed the SDR South). A slightly raised area of crust exists at the seaward termination of the SDRs which is capped by horizontal high amplitude reflections and has a thickness of 8-9 km. Beyond this raised section, the crust thins to 6 km and then thickens again to a more typical thickness for oceanic crust of ~7.5 km. There are also partially continuous high amplitude reflections on the top section of crust with low, poor reflectivity beneath this and a basal section of high amplitude reflections that extends into the low amplitude zone above it. Unequivocal oceanic crust is then present until the distal termination of the line at ~410 km.

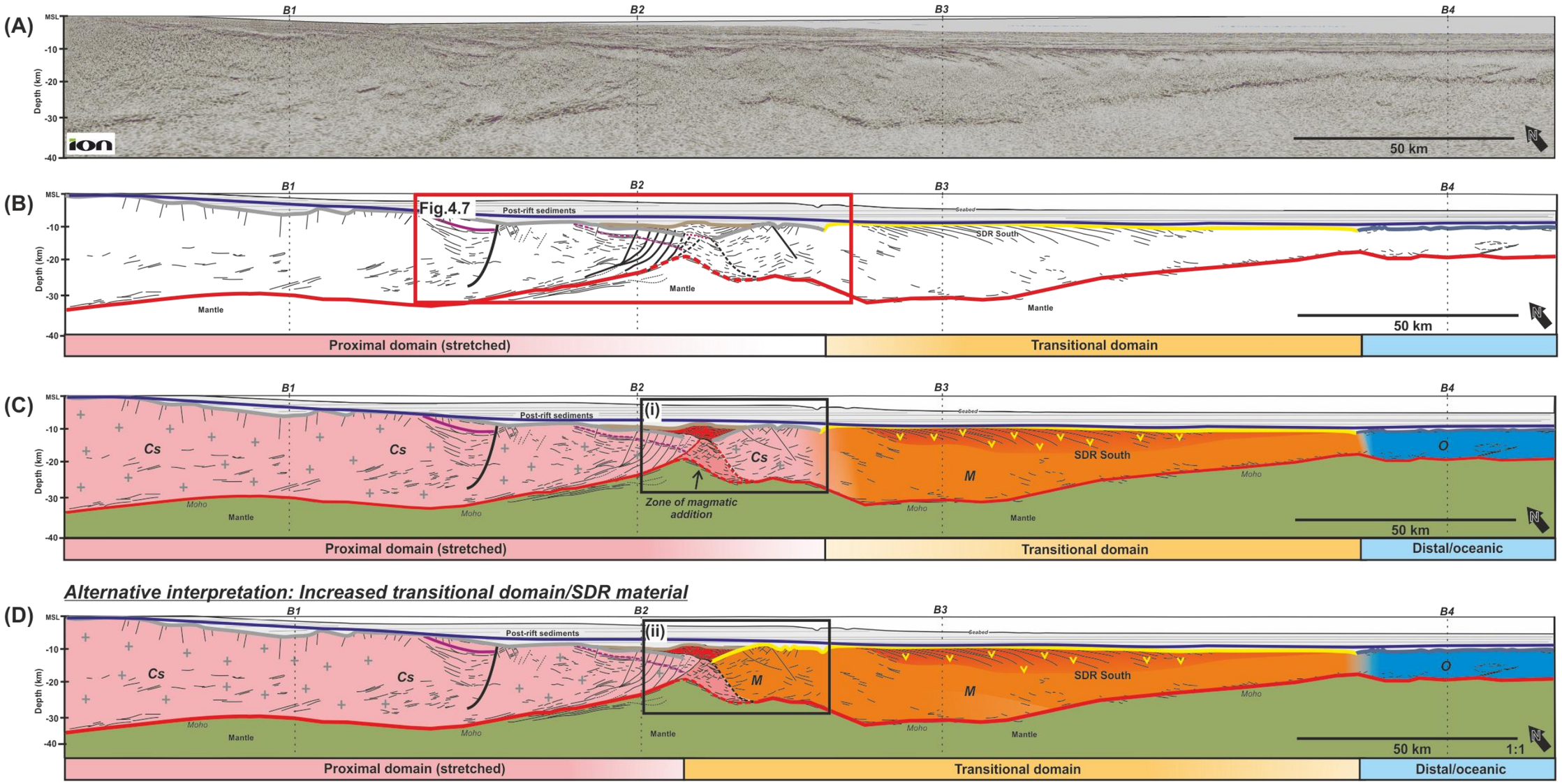

Figure 3.5: (A) Line A4 uninterpreted 2D PSDM seismic reflection dip line from the ION SPAN dataset (B) Line drawing interpretation of the major structural and geological features with major crustal horizons. Shown in red is the location of figure 4.7 (see Chapter 4) note the difference in vertical exaggeration (C) Interpretation of line A4 with major structures, crustal types and crustal domain boundaries (i) Interpretation with larger section of stretched continental crust (Cs) (D) Alternative interpretation (ii) with increased transitional domain/SDR material replacing a separate block of stretched continental crust (Cs) shown in (C). Please refer to key in Table 1 for horizons and corresponding crustal types and domains in figure 2.3.

3.3 Strike lines

The following observations record the seismic nature and reflection characteristics of all four strike line sections, at a line spacing of ~80 km's. Each line adds different information relating to both the structural and crustal domain mapping of the offshore region. Lines are addressed from the most proximal, B1 to the most distal, B4 and from left to right (south to north).

3.3.1 Line B1

The crustal thickness at the start of line B1 (figure 3.6) is 16-17 km, which is interpreted as an anomalously thinned region of continental crust. This thickness is approximate as the upper crust is dominated by tilted and rotated packages of fault-bound blocks with high amplitude, partly continuous reflections. These create discrete upper-crustal blocks with local highs and areas of both high and low reflectivity. These packages begin abruptly at the start of the line. These faulted crustal blocks dip south at the start of this section and then northward, producing significant upper-crustal tectonics. At mid-crustal levels, there are mid-high amplitude, discontinuous reflections which are cross-cutting and primarily chaotic in arrangement. Both the mid and lower sections of the crust are permeated by high amplitude, partly continuous reflections that are cross-cutting. Moho reflections are of a high amplitude, partly continuous, with some upward branching reflections. This crustal character continues for 85 km from the south of the line. At this point, the upper-crustal zone becomes comprised of low amplitude, highly chaotic, discontinuous reflections which are suggestive of cratonic continental crust. This represents an area of the upper crust for 145 km distance along the line and has a thickness of 5-6 km which remains relatively consistent. Beneath this zone reflections have a higher amplitude within mid-crustal levels. At 16 km depth there is a change to a more continuous section of high amplitude reflections and this zone

continues for ~70 km along the line at a mid-crustal depth of ~15-21 km. A band of lower reflectivity is observed beneath this zone, followed by a change back to high amplitude, continuous reflections at a depth of 27 km. Also of note, is that there is a return to lower amplitude reflections at a level deeper than the Moho, beneath both continental and continental cratonic crust. At a distance of 181 km from the start of the line, mid-crustal reflectivity begins dipping to the south at ~20^{o}. There are also upward-branching reflections observed from the Moho. At ~240 km from the start of the line, (correlating with the termination of the upper-crustal cratonic region) mid-crustal reflectivity is of a high amplitude and dips northward in several areas. Cross-cutting reflectivity is observed with some reflectivity being south-dipping. At this point, there is a shallowing of the crust from ~27 km to ~19 km at the thinnest point. Towards the end of the line, southwards-dipping, mid-crustal reflectivity continues. The upper crust has mid-high amplitude reflections which dip at a shallow angle to the north. In totality, this line predominantly exhibits continental and cratonic crust. However there is a variable crustal thickness observed, both to the south and north of the central region of cratonic crust. In the southern section in particular there is the notable presence of large-scale, discrete, crustal ‘block’ tilting and rotation via deep, (~10 km) faults observable in the upper crust and corresponding to a shallowing of the Moho. In an expected strike line at this distance from the coastline, little to no crustal thickness variation should be observed and continental crust should be relatively homogeneous. Instead, there are considerable anomalous zones of complex reflectivity throughout the line.

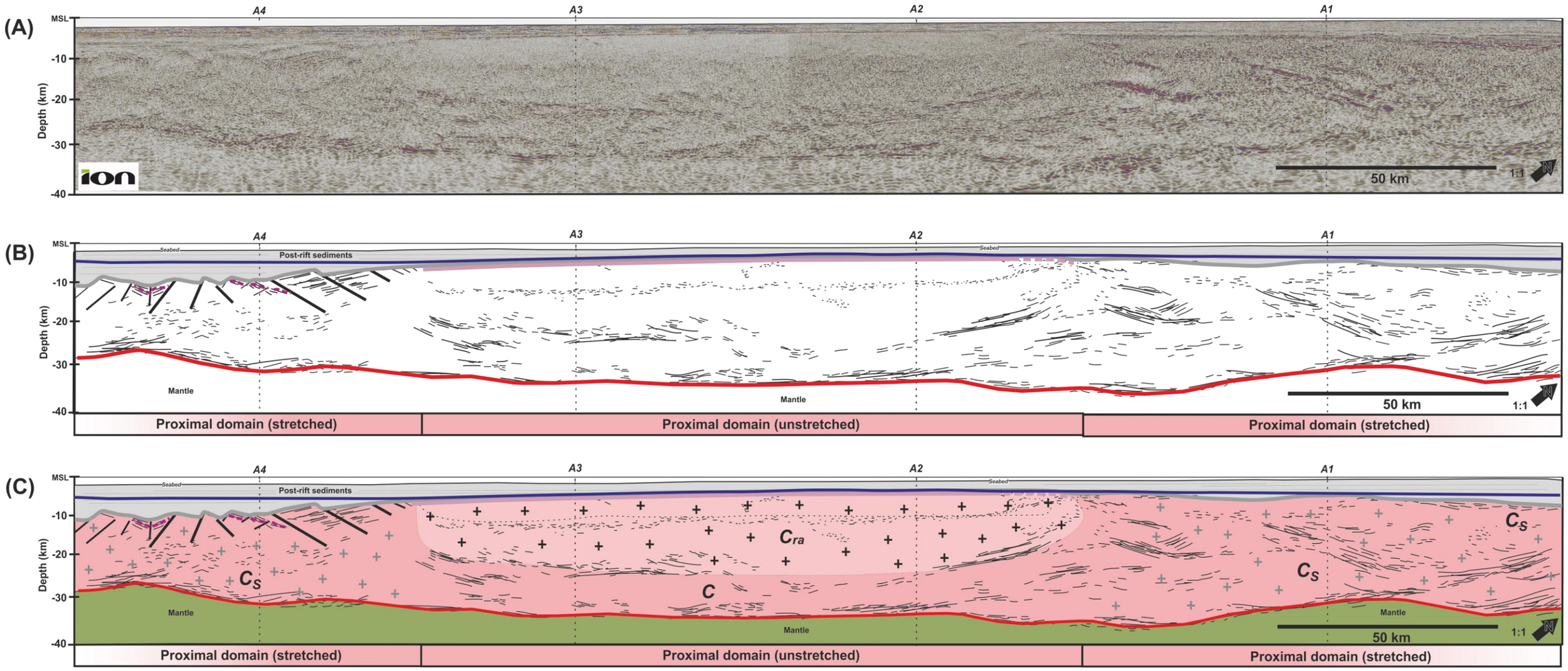

Figure 3.6: (A) Line B1 uninterpreted 2D PSDM seismic reflection line from the ION SPAN dataset (B) Line drawing interpretation of the major structural and geological features with major crustal horizons (C) Interpretation of line B1 with major structures, crustal types and crustal domain boundaries. Please refer to key in Table 1 for horizons and corresponding crustal types and domains in figure 2.3.

3.3.2 Line B2

In the second strike line section from the continent, B2 (figure 3.7), there are many unexpected crustal anomalies in terms of both observable large-scale structures and crustal thickness. For a line at this distance from the continent, it would be typical to see a continuous thickness section of transitional crust, likely wholly comprising seaward-dipping reflections (for which no dip would be observed as it is a strike line orientation). However, this is not what is observed. From the start of the line (the most southern edge) transitional crust is observed with high amplitude reflections in the upper crust which are dipping to the south (continuing off the edge of the line). Under these is a large zone of low amplitude reflections. The morphology and seismic nature of the high amplitude reflections are similar to the seaward-dipping reflections observed on dip lines A1, A2 and A4, but appear in contrast to dip to the south. There is an abrupt transition in the upper crust into large-scale (to ~5 km depth) curvilinear, extensional faulting (primarily north dipping). This continues for ~75 km from the start of the line with some south-dipping faults also becoming evident. For the first ~50 km of the line there are only sporadic lower crustal reflections but these tentatively suggest a transitional crustal thickness of ~17 km. Beyond this point, the Moho begins to shallow and has a notable increase in high amplitude reflections. This is accompanied by a zone of higher amplitude reflectivity at mid-crustal levels. At ~80 km from the start of the line there are high amplitude, horizontal reflections in the upper crust and another significant shallowing of the Moho to a thickness of only ~3 km over a horizontal distance of only ~20 km. There is then a large, south-dipping, whole-crustal fault whose fault plane is represented by higher amplitude reflections. Directly adjacent to the north, there is an uplifted footwall section of crust and a crustal thickness of ~4-5 km. There is also a zone immediately below the fault in which Moho is *not* clearly observed.

This zone of questionable Moho reflections continues to the north of the large structure for approximately 18 km. This also corresponds with unusual reflectivity in the upper crust across this zone. Also evident, is a cross-cutting of internal reflectivity which makes discerning any internal individual structures difficult at this scale. Beyond this zone there is another increase in high amplitude reflections at the Moho as crustal thickness begins to increase again from 4-5 km to 11 km. Large-scale upper-crustal faulting which is curvilinear in nature resumes, with the majority of structures now dipping to the north for a region approximately 25 km wide. To the north of these structures is a high amplitude section of upper-crustal reflections that is highly anomalous. Within this region, there are packages of high amplitude reflections which dip to the south directly adjacent to a low amplitude region. Beyond this, crustal thickness begins to increase again to 19-20 km and there is the upper-crustal establishment of northward-dipping, high amplitude reflections. These are sub-horizontal and resemble SDR in seismic reflection nature and morphology. A distinct northward dip however, is observed for ~40 km from the large anomalous feature until reflections then become horizontal. Crustal thickness remains at a relatively constant, 19 km. Towards the north end of these reflections there is a zone of high angle, high amplitude, dipping reflectivity in the mid-crust. These reflections also interfere with the overlying, horizontal reflectivity. Crustal thickness is variable until the end of the line but sits between 17 and 19 km.

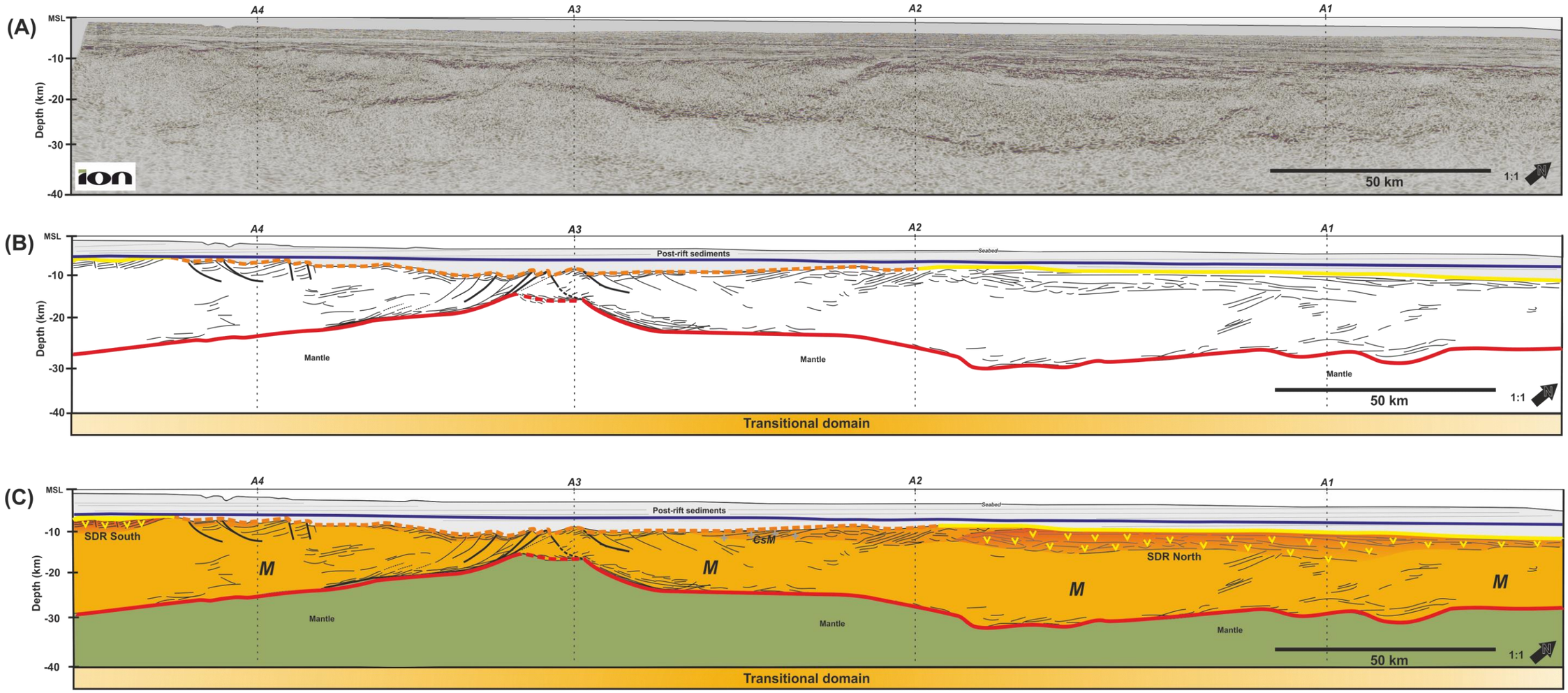

Figure 3.7: (A) Line B2 uninterpreted 2D PSDM seismic reflection line from the ION SPAN dataset (B) Line drawing interpretation of the major structural and geological features with major crustal horizons (C) Interpretation of line B2 with major structures and crustal domains. Please refer to key in Table 1 for horizons and corresponding crustal types and domains in figure 2.3.

3.3.3 Line B3

Within this third strike line from the continent, Line B3 (figure 3.8) it is immediately evident that there is further anomalous crustal geometry side by side with more familiar crustal features and domains. It is also the first time in the strike line sections where we are able to observe unequivocal oceanic crust. The first 40 km of the upper crust from the southern start of the line is comprised of high amplitude, partially continuous reflections which have a shallow but distinct dip to the south. This section also has a thickness of ~3 km. There are high amplitude reflections of the Moho at a depth of ~10-11 km along with a zone of low amplitude chaotic reflections directly below the high amplitude packages. There is also some mid-high amplitude mid-crustal reflectivity. At ~40 km from the start of the line there is a change in the nature of the upper-crustal reflectivity as it swaps dip direction and dips northward. There is also mid-crustal reflectivity which is sub-vertical and similar to that observed on the previous line, B2. At ~70 km from the start of the line, the upper-crustal sub-horizontal reflectivity changes again, to dip to the south. There is also less of a distinct boundary between the upper-crustal reflections and mid-crustal level reflections. High amplitude reflections are present at the base of the section and are indicative of the Moho, but are not entirely continuous. The crustal thickness remains at between, 10-12 km throughout this zone. At ~96 km from the start of the line there is a raised area of anomalous crust and with a direct transition to high amplitude, reflections to the north. This is also marked by a corresponding shallowing of the Moho resulting in a reduced crustal thickness of ~7 km. This appears as a large-scale southwards-tilted, crustal block with a high amplitude top, similar in

character to oceanic crust. To the north of this anomalous crustal block, the crust is permeated by whole-crustal extensional faults, which have a dip to the north. These are also of a low angle for extensional faults, but appear to have an extensional geometry. The throw of these faults varies from ~1 km to 5 km and below, there is an absence of Moho reflections, which leads to the interpretation of this as exhumed mantle. There are high amplitude horizontal reflections evident in the hanging-walls of two of the largest faults. There is then a south-dipping fault and an abrupt transition to a highly unusual zone of reflectivity which is internally dissected, has no discernible Moho and a rugose upper surface, indicative of exhumed mantle. Faulting in this segment is initially northwards, but swaps to predominantly southwards about 30 km along this ~50 km section. To the north of this zone is a small area where the Moho appears to be re-established in a proto-oceanic segment which is ~ 7-8 km long and 7-8 km thick. There is then the establishment of unequivocal Penrose oceanic crust with recognisable packages of reflections of this crustal type. Although the Moho reflections of this region of oceanic crust are not contained within a thin package, it is still possible to see an oceanic Moho that exists at the base of the typical oceanic crust thickness of ~7 km and is continuous until the north end of the line.

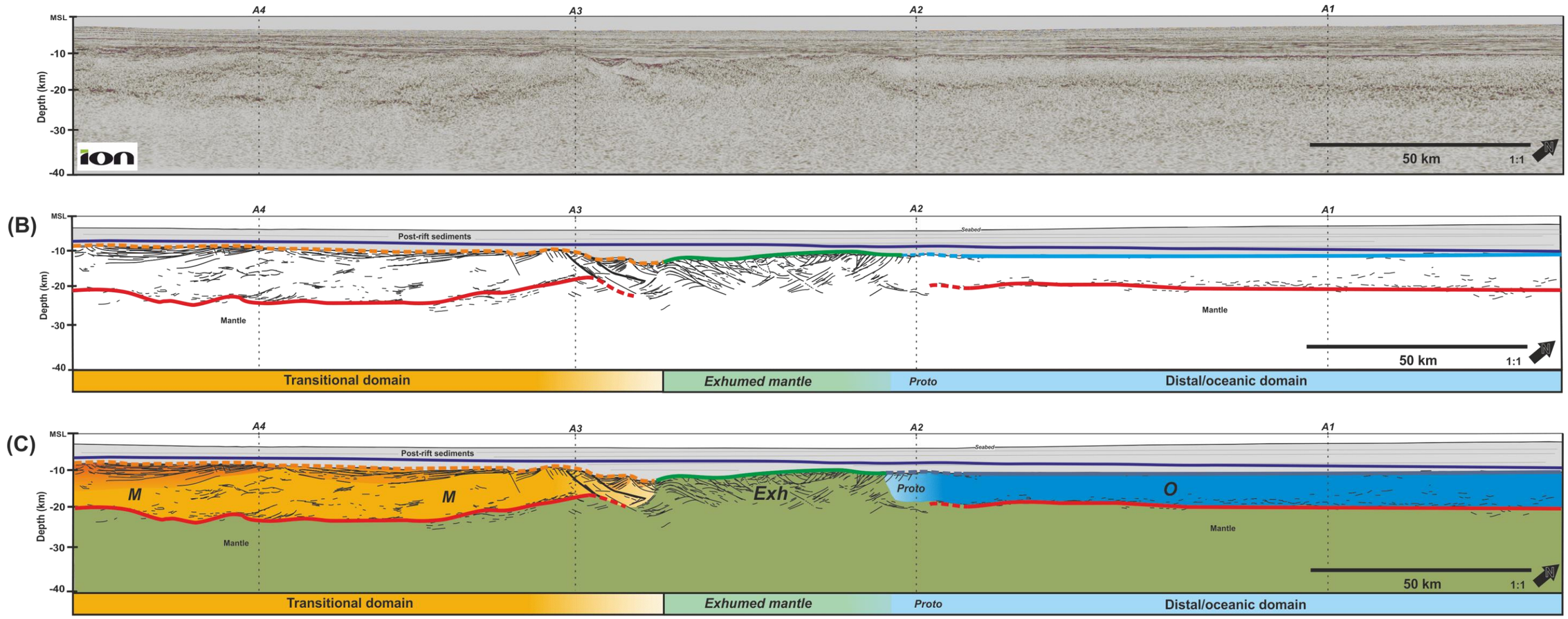

Figure 3.8: (A) Line B3 uninterpreted 2D PSDM seismic reflection line from the ION SPAN dataset (B) Line drawing interpretation of the major structural and geological features with major crustal horizons (C) Interpretation of line B3 with major structures, crustal types and crustal domains. Please refer to key in Table 1 for horizons and corresponding crustal types and domains in figure 2.3.

3.3.4 Line B4

This strike line, Line B4 (figure 3.9) is positioned within unequivocal oceanic crust, which conforms to expected oceanic crustal geometry and has a consistent thickness of ~7 km for the entirety of the line. However, it also reveals whole-crustal structures which change in dip orientation along the line, but do not affect the overlying sediments. A standard section of oceanic crust exists for approximately 250 km which has an increasing amount of whole-crustal faulting, evident through predominantly mid-crustal seismic reflections of a high angle and of locally increased amplitude. This then swaps to a similar style of whole-crustal faulting but with a southwards dip. This continues until the end of the line. Some of this south-dipping reflectivity is also noted to continue into the upper-mantle.

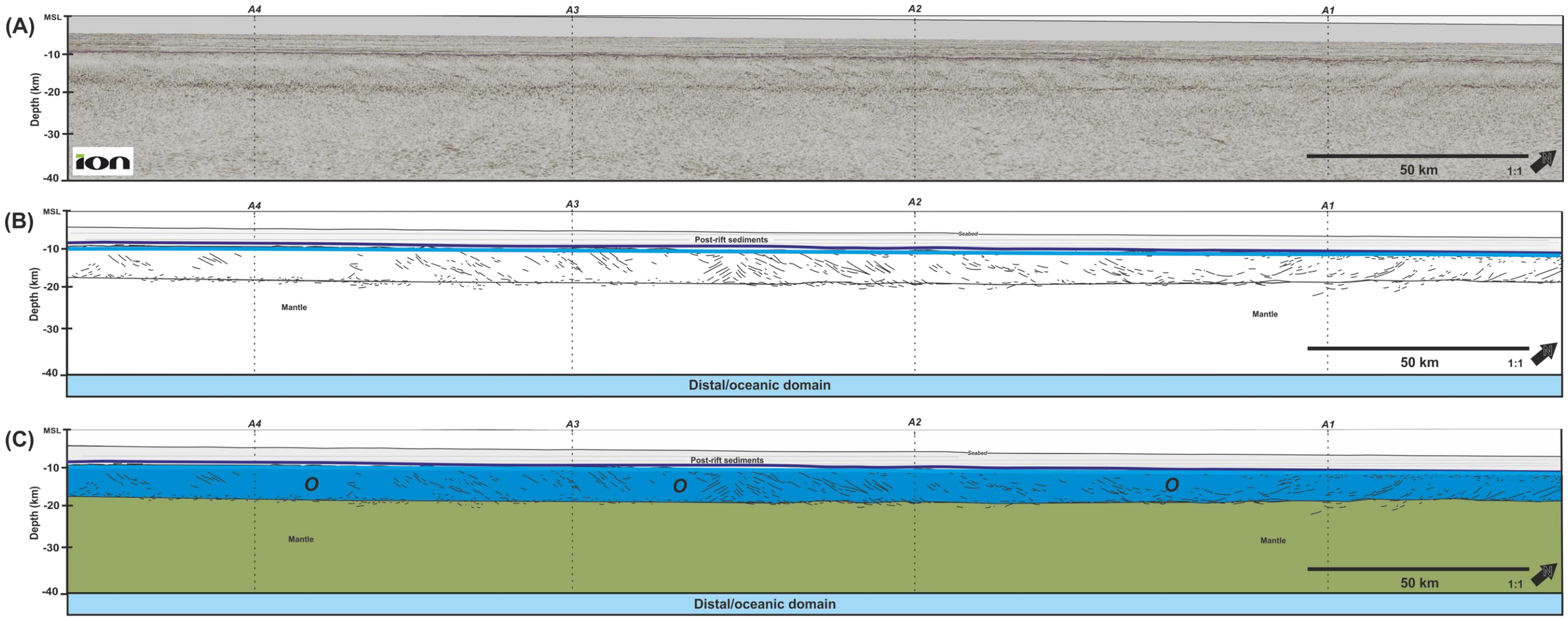

Figure 3.9: (A) Line B4 uninterpreted 2D PSDM seismic reflection line from the ION SPAN dataset (B) Line drawing interpretation of the major structures and geological features with major crustal horizons (C) Interpretation of line B4 with major structures, crustal types and crustal domains. Please refer to key in Table 1 for horizons and corresponding crustal types and domains in figure 2.3.

3.4 Summary of the 2D crustal architecture along the margin

This chapter has used a series of 2D seismic reflection profiles of long recording times in both dip and strike orientations, in order to understand the deep crustal architecture of the offshore Uruguayan margin. This has been achieved over a region of ~2,800 km of the offshore Uruguayan margin and has been studied in its entirety for the first time in this work. New revelations have been revealed about the magma-rich rifted passive margin of offshore Uruguay, which displays both typical, and atypical crustal geometries. Typical crustal geometries are observed in the north of the study area. These are dip lines A1 and A2 that both conform to the expected crustal architecture for a magma-rich margin. The proximal domain is characterised by a thick section of unstretched continental crust (*C*) (~30 km thickness) and includes crust identified as cratonic (*Cra*). Immediately seaward begins a wedge of seaward-dipping reflections (SDR), underlain by stretched continental crust (*CS*) with syn-rift extensional half-graben structures. This zone may also be highly intruded, especially as the crust thins during extension. This is followed by a distal zone of unequivocal oceanic crust of a uniform and expected thickness of ~7 km. Both northern dip line sections share this conformable geometry. However, line A3, ~80 km to the south of line A2, shows features highly atypical for a magmatic margin. A broad section of thick proximal continental crust extends to >100 km from the coast, this quickly transitions to extremely thin ‘crust’ which is less than 10 km in thickness. The expected wedge of seaward-dipping reflections is noticeably absent. The nature of the crust (or upper-mantle) in this abnormal crustal region can be interpreted in several ways. Alternative domain interpretations have been provided (figure 3.4); 1) a section of hyper-thinned continental crust, or 2) an area of unroofed upper-mantle. Each interpretation of this section has a wider impact on the position of the crustal domain boundaries and on the evolution of rifting in the area. Line A4

is the most southern dip line section and also shows atypical geometry. The SDR wedge is again visible, appearing to be more distally located than in the north. However, a zone of significant crustal thinning is observed proximal to the SDR. This area is interpreted as a zone of syn-rift magmatic addition across a region of stretched continental crust (*CS*) (Figure 3.10) or, with the alternative interpretation of a larger segment of magmatic crust on the distal edge of the anomalous magmatic feature. Another key point is that the SDR are now interpreted as overlying newly-created, syn-rift magmatic crust. Strike line sections across rifted margins are rarely utilised as they often add very little to the story of the margins evolution. Here, strike line sections are crucial as they are atypical (for magmatic rifted margins) and give much more information on oblique structures, shown in lines B2, B3. The relationship to the regionally significant craton in the proximal domain, and the influence of margin oblique features such as anomalous crustal thinning is also key, as seen on Line B2. Line B3 has a central zone which is interpreted as exhumed mantle, based upon the clear absence of a Moho (in contrast to crustal types on either side) and distinctive seismic facies, especially in the upper region of this domain. Figure 3.10 is discussed in greater detail in Chapter 6 as to whether this confirms of contradicts alternative published models.

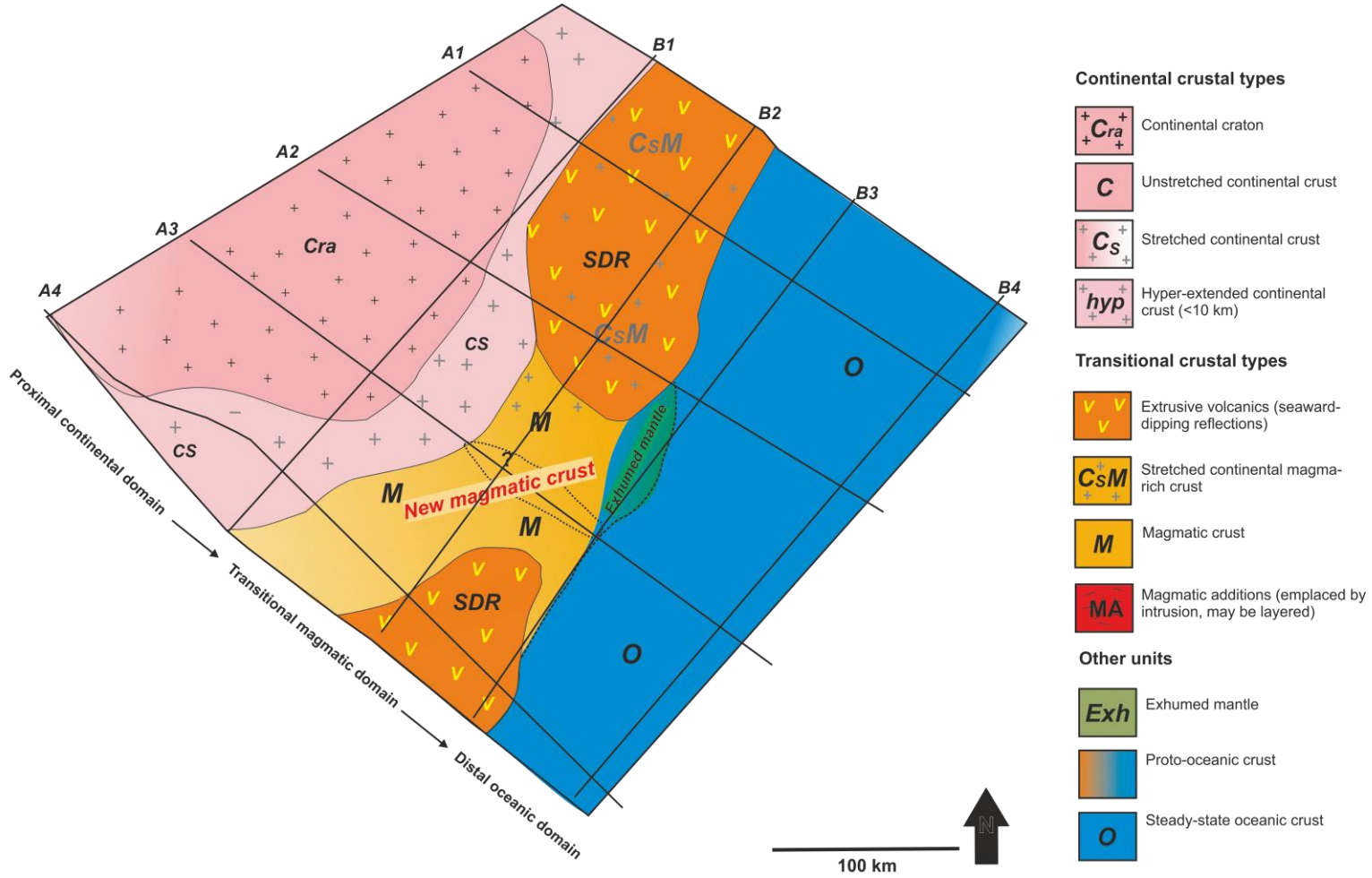

Figure 3.10: 2D crustal architecture of the offshore Uruguay region showing major crustal domains and crustal types.

Chapter 4: The regional evolution of the offshore Uruguay margin.

4.1 Introduction

This chapter integrates the structural framework and sediment/seismic package distribution to determine the tectono-stratigraphic evolution of the margin. Chapter 3 showed that there is considerable, atypical crustal geometry across the Uruguayan offshore region. To understand the successive evolution of the margin, the major structures and tectonic trends need to be associated with the evolutionary stages of the basin from the pre-rift to syn-rift and drift phases. The aims of this chapter are to map the major trends and fault structures across the 2D dataset and to analyse how these are related to the major stratigraphic and volcanic packages. In this chapter, fault mapping will first determine the location of a series of fault domains, then later, through QC with the 3D dataset, these will be related to each other and their possible correlation interpreted to provide a more complete tectonic map of the margin. (The detailed structure of the 3D region is comprehensibly covered in chapter 5). Across both this chapter and chapter 5, the margins evolution is divided into stages and in each, the role of the major structures in controlling the evolution will be explored. The main focus of this chapter is on the syn-rift phase and the timing and role this has played in the margins evolution. The processes and characterisation of the magmatic syn-rift phase is explored in further detail in chapter 5. Figure 4.1 shows the crustal type map which was created in Chapter 3. This section now adds the significant tectonic features that have affected the margin. Developing further from this, a stage-by-stage basin evolution of the margin will be proposed.

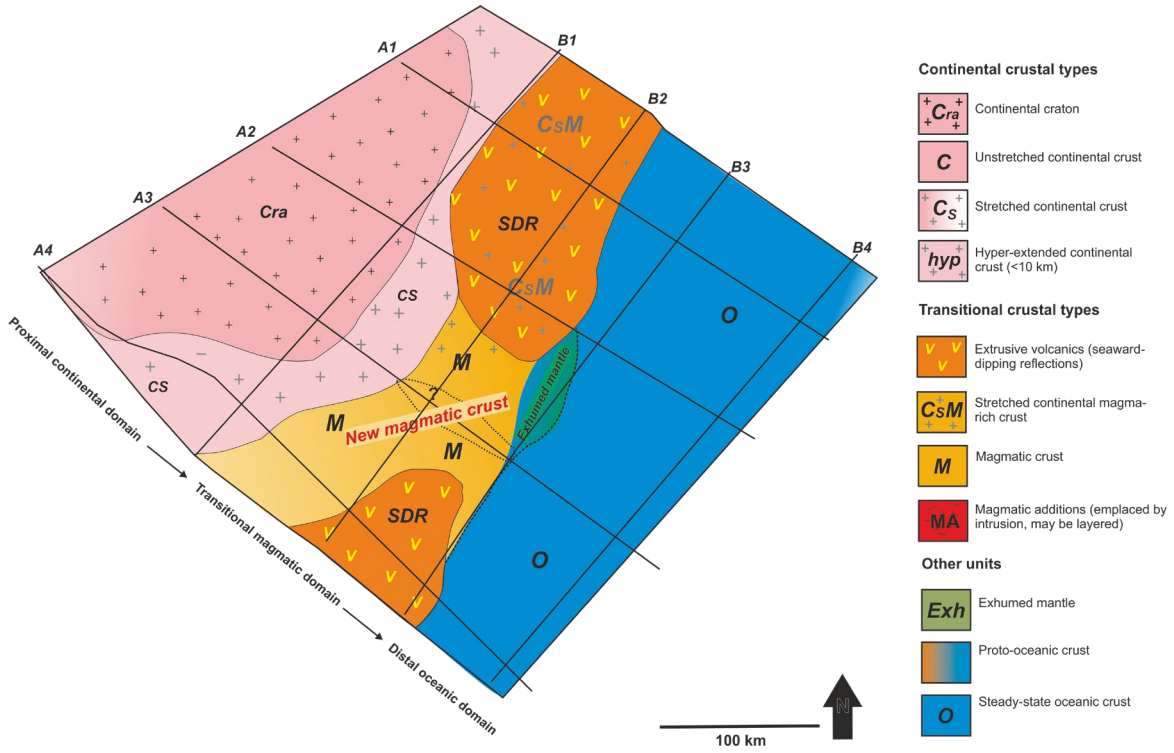

Figure 4.1: Crustal types map across the 2D dataset and covering the offshore region of the margin. Note, proximal, transitional and distal domains as well as an area of exhumed mantle.

4.2 Methodology

Initially, faults were mapped along the profile sections of the ION SPAN dataset. Due to the similarities between adjacent faults in particular areas of the dataset, faults were divided into related fault domains (figure 4.2).

4.2.1 Fault domains

Figure 4.2 (A) provides a plan view map of EMAG_2 data from Maus et al., (2009) across a regional view of the 2D data area. EMAG_2 data is a global, 2-arc-minute resolution grid of the anomaly of the magnetic intensity at an altitude of 4 km above mean sea level (CIRES, 2015). It is compiled from various sources including satellite data and marine, aeromagnetic and ground magnetic surveys (CIRES, 2015). Variations in the magmatic intensity where the local magnetic field is either depressed or enhanced produces magnetic anomalies which correspond to geological features in the subsurface. Magnetic signatures which are parallel to

oceanic isochrons can provide information on the temporal evolution of oceanic crust, both its creation and destruction (CIRES, 2015). It should be noted that the magnetic record of polarity changes for magnetic anomalies may be complex in regions which are not a result of simple, steady-state oceanic spreading (Gillard et al., 2015). Section (B) shows the major faults interpreted within the ION SPAN dataset. In figure 4.2 (C) the faults have been grouped into a number of domains, according to either their dip, trend or the stratigraphic interval they cut. Some fault domains are likely to be linked, but have been initially categorised as separate, until later analysis suggests otherwise. Building upon these associated fault domains and the integration of sediment package distribution, the active tectonics for a specific time period in the margins evolution can be established. The faults mapped and shown in Figure 4.2 have deliberately not been connected or extrapolated in order to show (and honour) the considerable regions of uncertainty between profile lines.

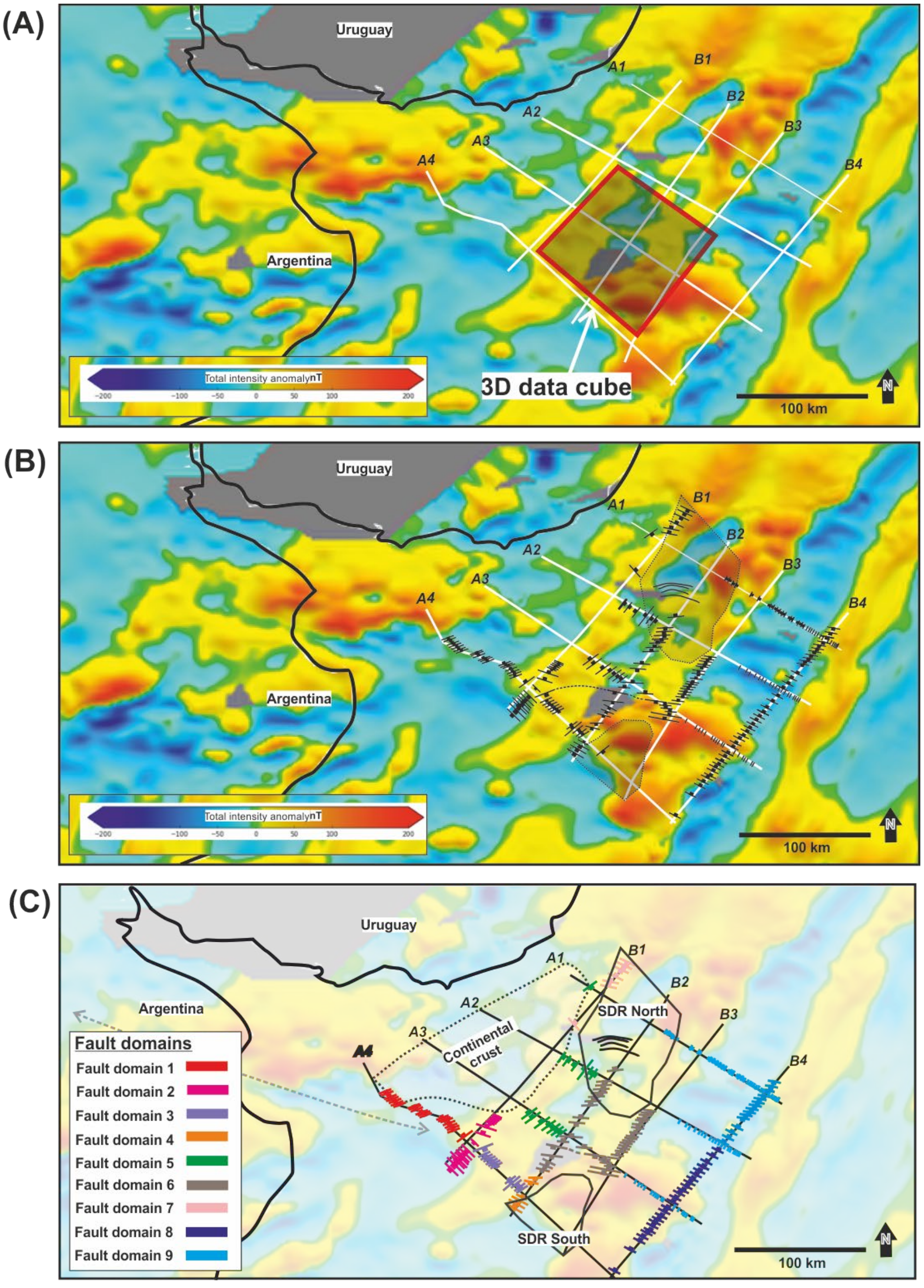

Figure 4.2: (A) EMAG_2 data for a wide region of the offshore Uruguay margin, the ION SPAN data grid is shown in white from Maus *et al.*, (2009). The 3D data cube (ANCAP/Shell) is shown outlined in red (B) Map view of the major structures across the 2D dataset. (C) Fault domains shown marked in different colours, also noted are the SDR wedges and the limit of continental crust.

4.2.2 Depth maps

Depth maps were created using the PSDM ION SPAN dataset at various important, evolutionary intervals across the 2D dataset. The horizons which are mapped include the Moho, Top crust, Top SDRs (North and South), Top syn-rift, Top oceanic crust and the Top seabed. Figure 4.3 and the following figures in this chapter incorporate observations from the 3D dataset, which is fully investigated and mapped in Chapter 5. Figure 4.3 shows an early stage of mapping in Petrel software, before surface generation, where data has been combined from the 2D dataset and the 3D cube for the top syn-rift depth map. here there is no data available, (i.e no data or no syn-rift horizon identified), this region has then been blanked out in the resulting surface map.

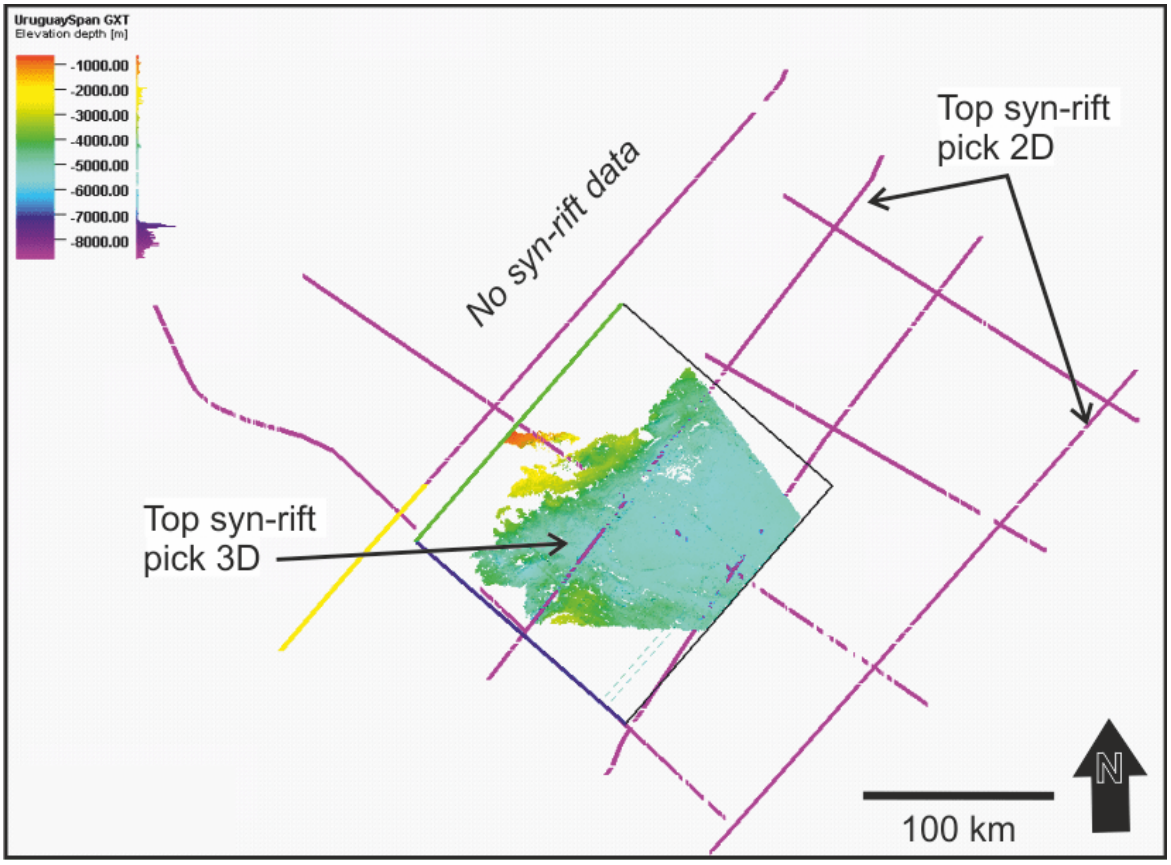

Figure 4.3: 2D and 3D pick for the top syn-rift horizon before creation of the depth map surface. Note the difference in data concentration with the 2D picks being more widely spaced due to the 2D data line spacing in combination with the more detailed, 3D data pick. Where there was no syn-rift interpreted this area was left blank and subsequently blanked out in the resultant surface map.

4.2.3 Areas of uncertainty and establishing a structural overview

The ION SPAN dataset has lines acquired at ~80 km apart, this makes the tracing of multiple, regional structures, challenging. Fault length-displacement relationships can provide an estimate for the total extent of easily identifiable faults. However, as this chapter reveals, a complex and inter-related fault network exists over much of the study region. Correlation of faults was not possible using the 2D data alone and accurate throw calculations were also difficult due to the presence of syn-rift volcanics, intra-package faulting and volcano-sedimentary deposits of low amplitudes. The mapping of faults on one line only also means that the construction

of a fault model was not realistic within Petrel software. Fault orientations across the 2D dataset are constrained where possible using the 3D dataset. Chapter 5 expands investigations into the detailed structures present in the 3D data and allows for the QC of major through-going structures, identified in this chapter. The lack of a fault model also means that faults had to be individually identified as to what stratigraphic intervals they affected.

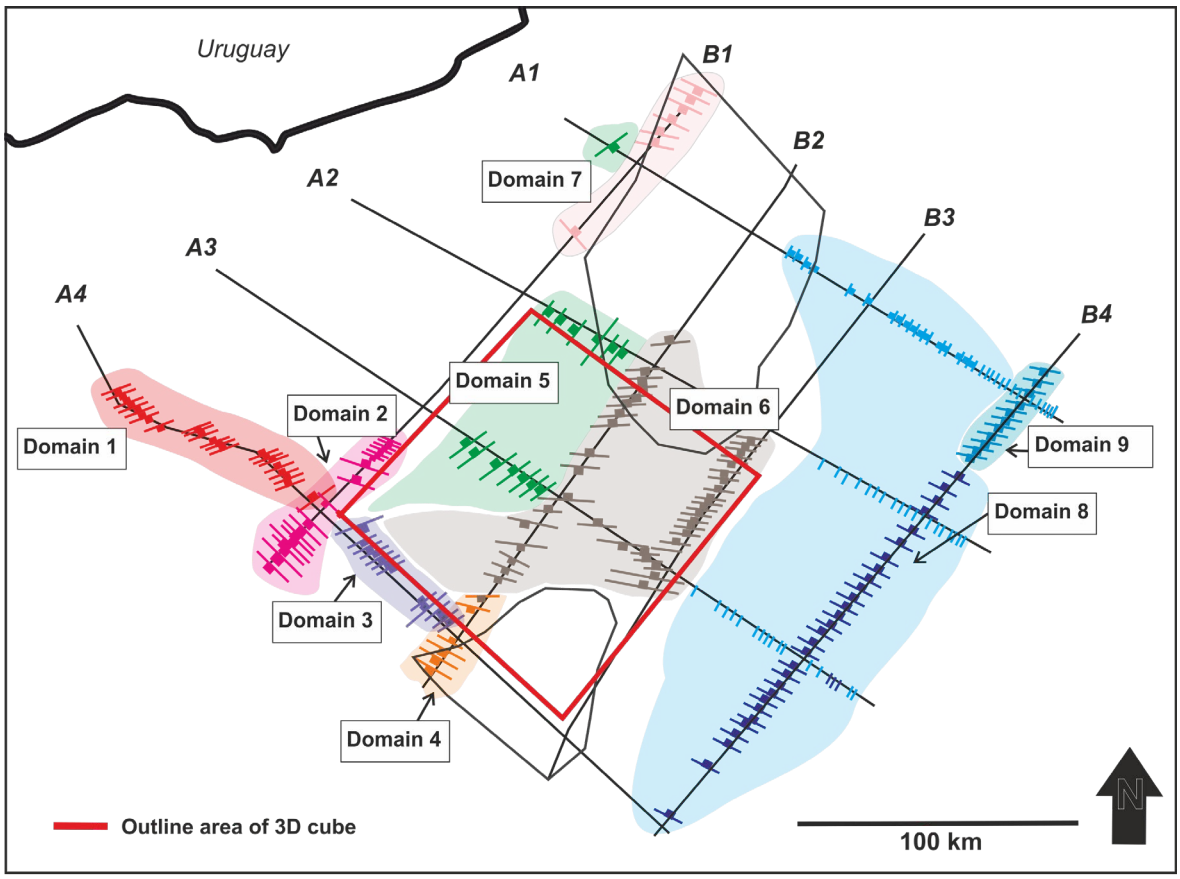

Figure 4.4: Fault domains mapped across the ION SPAN 2D data grid. See also Table 9.

4.3 Fault domains

Table 9 summarises 9 fault domains which have been mapped across the 2D data grid (figures 4.2, 4.4). The trend and dip direction of the multiple faults have been mapped through observations made on one line only with ~80 km between lines. As such, these measurements are approximated, with less constraint than those which also overlap with the 3D data coverage. Faults in some parts of Domains 5 and Domain 6 are also across the 3D dataset, allowing for more constraint. These faults

in particular are investigated in greater detail in the next chapter. Identifying fault anomalies, changes in dip and strike direction of faults in close proximity to one another are important in relation to the correlation of major structures and are analysed further in section 4.4 of this chapter.

Table 9: Major fault domains across the ION SPAN data grid. Dip directions and displacement amounts are approximate only.

Fault domain	**Colour**	**Fault trend**	**~ dip direction**	**Displacement (approx.)**	***Character***	***Figure no.***
Domain 1	Red	NE-SW	NW or SE	~200-500 m	Extensional fault-bound blocks, tilted	Fig. 4.5
Domain 2	Dark Pink	NW-SE	SW (anomaly NE)	<500 m	Extensional fault-bound blocks, tilted	Fig. 4.6
Domain 3	Purple	NE-SW	SE	~2-400 m	Extensional	Fig. 4.7
Domain 4	Orange	NW-SE	SW	<500 m	Extensional faults within SDR South	-
Domain 5	Green	NE-SW	NW or SE	~500 m -1 km	Extensional half-graben faults within continental crust	Fig. 4.8
Domain 6	Brown	~E-W	N or S	>1 km (major shear) or <500 m	Multiple extensional faults	Fig. 4.9
Domain 7	Light pink	NW-SE	NE or SW	<500 m	Extensional faults within SDR North	-
Domain 8	Dark Blue	NW-SE	NE	<500 m, steep angle almost vertical fractures	Oceanic fractures/high angle extensional faults in top oceanic crust	Fig.4.10
Domain 9	Light Blue	WNE-ESE	SW	<500 m, steep angle almost vertical fractures	Oceanic fractures/high angle extensional faults in top oceanic crust	Fig.4.10

4.3.1 Domain 1

Domain 1 is located in the west of the 2D dataset and mapped on line A4, the most southern line of the ION SPAN dataset (red, figure 4.4 and Table 9). This region is not correlated with additional 2D line data and is outside the area covered by the 3D dataset, therefore dip orientations are approximated. There are multiple dip orientations in this domain (figure 4.4) however, the primary direction is NW-SE with a fault trend of ~NE-SW. It is the most proximal domain of extensional faulting, where crustal blocks are segmented and fault bound with faults that extend for ~2 km into continental crust. These have vertical displacement distances of between ~200 m and ~500 m, however due to an unconformable 'top pre-rift' with some continuous reflections it is difficult to determine a precise throw or displacement on this line. These are also tilted and rotated and comprise internal sections of parallel high amplitude reflectivity, interpreted to be un-deformed (within the crustal block) pre-rift sediments. Smaller-scale faulting is also present, with multiple dip orientations in the most proximal section of the line where individual faults are harder to define. Faulted blocks of high amplitude reflections are overlain by more continuous and un-faulted syn-rift sediments (the top syn-rift horizon is QC'd with the 3D dataset) of low-mid amplitudes. Early syn-rift sediments have notably lower amplitudes and less continuous reflectivity. This domain has a possible connection or relationship with the faults observed on line B1 and recorded as Domain 2. They are similar in terms of their geometry, with tilted, internally un-deformed, fault-bound, crustal blocks within continental crust - however, direct correlation/linkage was not possible, due to the large line spacing and numerous faults of variable dips, so these have been classified separately. However, changes in dip orientation in the middle of a fault domain may be indicative of a through-going major structure. Figure 4.5

shows the main faults and associated interpreted horizons in Domain 1. The interpreted ‘top pre-rift’ horizon is erosional and unconformable with reflections appearing curvi-linear and partly continuous in places, which has made accurate measurement of fault throw and displacement, difficult. The top pre-rift is interpreted due to the change in seismic reflection character from high amplitude, parallel reflections of the internally un-deformed pre-rift within crustal blocks - to low amplitude, less continuous reflections (interpreted as the early syn-rift). In other areas of the continental crust the top pre-rift horizon is not as easily defined. This has meant that a more reliable ‘top crust’ horizon has been primarily used across

the wider 2D dataset, based upon the change from chaotic, discontinuous reflections of the 'basement' to the stratified sediments above.

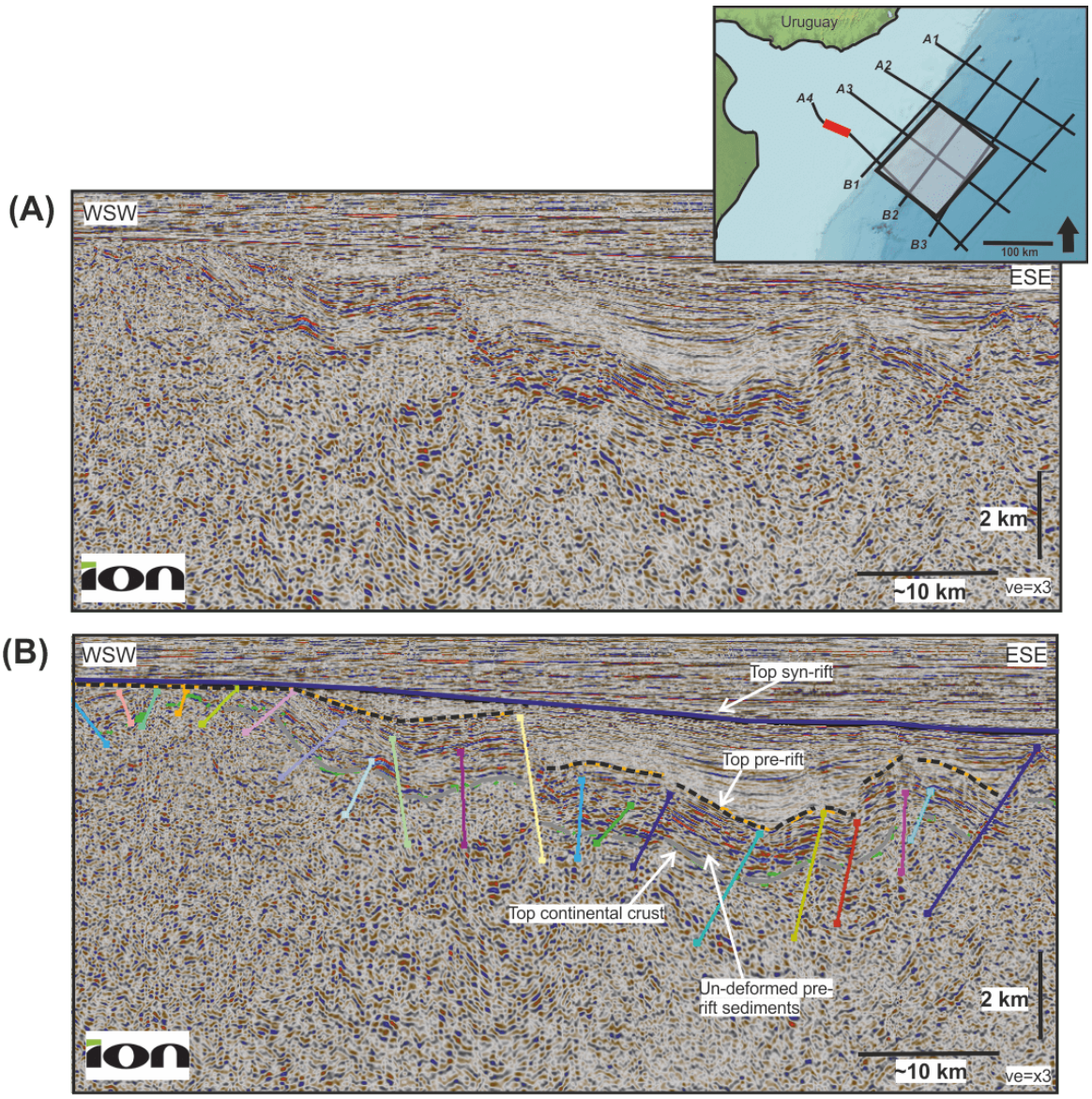

Figure 4.5: A section of line A4 from the ION SPAN dataset showing multiple faults of Domain 1 and the key horizons. Note: The top pre-rift has been defined (dashed black lines) as well as the top continental crust, based upon identification of un-deformed sediments at the top of fault-bound blocks, however this is not always recognised.

4.3.2 Domain 2

Domain 2 is also located in the west of the region at the most southern part of the proximal line B1 (figure 4.6). This section of line is not able to be QC'd with the 3D dataset as it falls outside the 3D cube extent. Faults in this domain are predominantly SW dipping extensional faults which trend NW-SE. However, in this

domain there are two notable anomalies which form a fault-bound block that dips to the ~NE. This suggests that a major through-going lineament may be responsible for this opposing dip change. High amplitude internal reflectivity creates a parallel, un-deformed section of crust which is interpreted as pre-rift sediments.

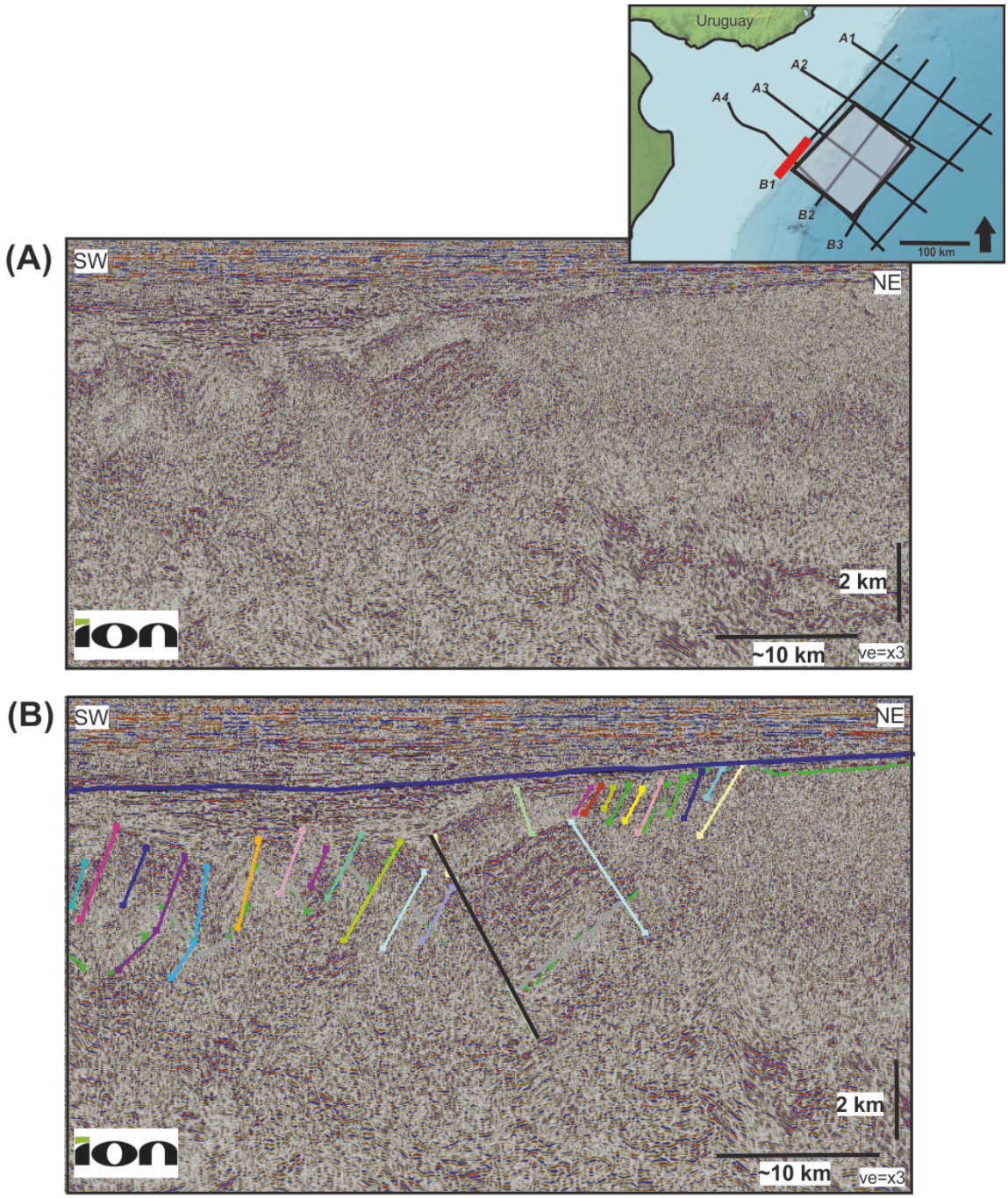

Figure 4.6: South section of line B1 from the ION SPAN dataset showing the faults in Domain 2.

4.3.3 Domains 3, 4 & 5

Domain 3 (figure 4.7) has a fault trend of ~NE-SW with faults dipping either NW or SE. Most faults have a small amount of displacement of less than ~400 m. However, two faults in particular are more unusual and appear to have longer and shallower fault planes, as such, these may be termed shear or detachment faults due to their low angle geometry. These anomalies may be indicative of larger, through-going regional structures.

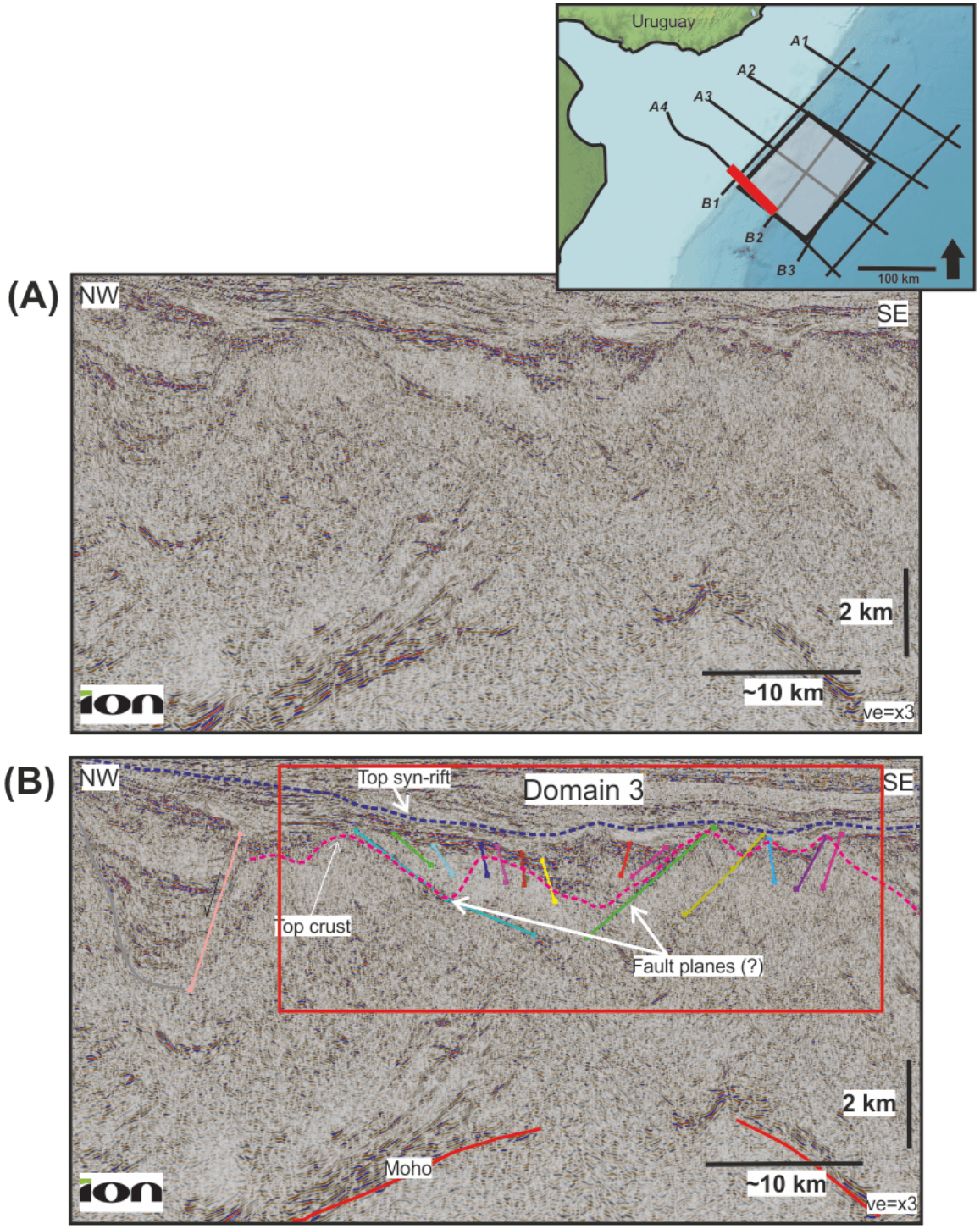

Figure 4.7: Faults from domain 3 which include two anomalies in the form of more shallow-dipping fault planes. These anomalies may be indicative of larger, through-going regional structures.

Domain 4 shows extensional faulting through the SDR South packages with high-angle extensional faults and low displacement values. Domain 5 (figure 4.8) represents large, half-graben extensional structures on the continental shoulder (on the edge of continental crust or the stretched region of continental crust). There are two or three major faults which can be identified in this section which have divergent wedges of internal syn-rift sediments. Determining precise throw or displacement on these structures is hampered by the poor internal reflectivity of syn-rift deposits. Top continental crust is determined by the base of syn-rift reflectivity and a change to chaotic, discontinous basement reflectivity. Also noted as part of this domain are high-angle extensional faults within the continental pre-rift horst blocks, although these have different dip orientations, these may overlap with some of the more proximal faults of Domain 6.

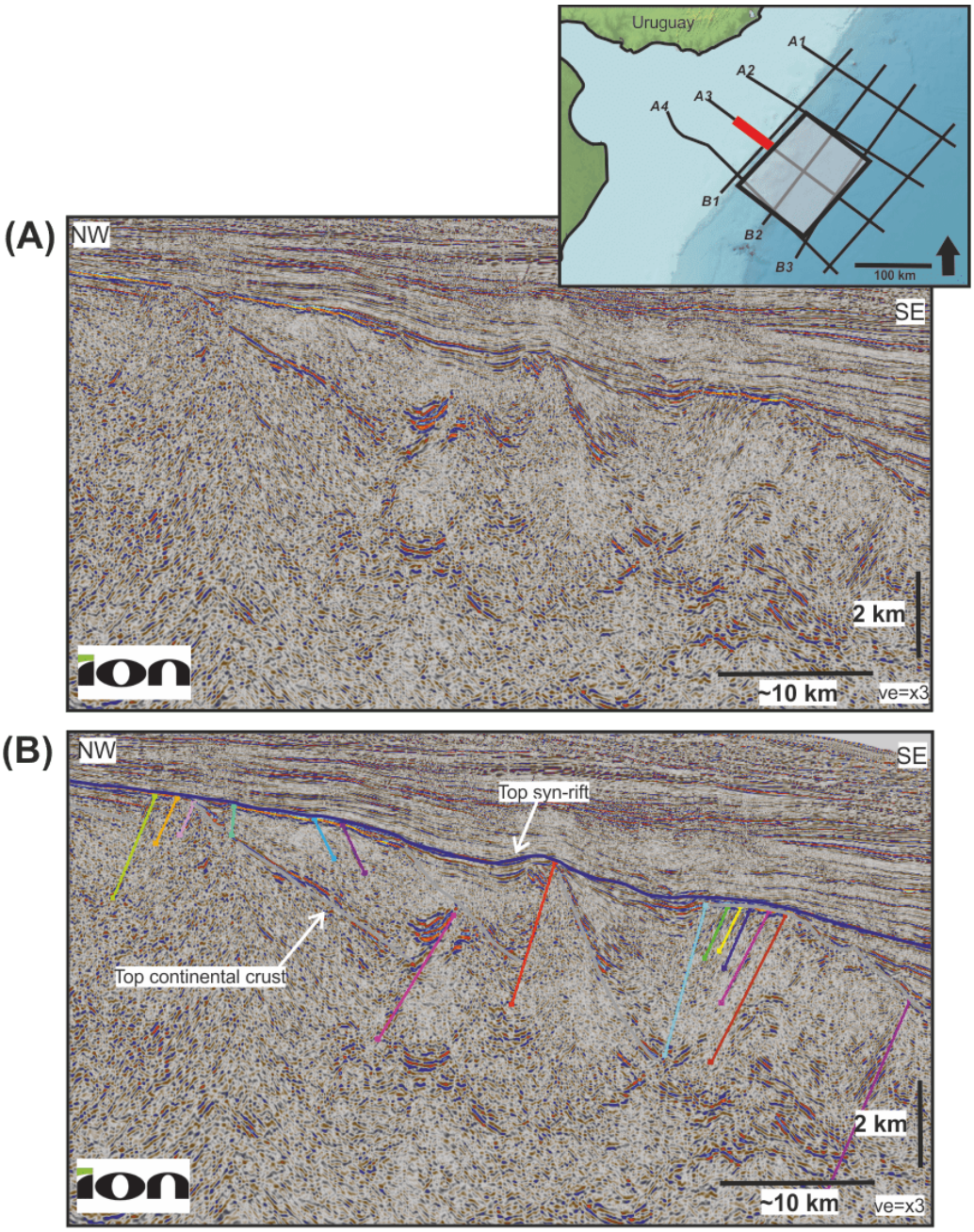

Figure 4.8: Faults of Domain 5 with large half-graben extensional faults within continental crust. Despite divergent reflectivity being observed, poor reflectivity makes the determination of precise throw or displacement difficult. Also noted are high angle extensional faults within the continental pre-rift horst blocks.

4.3.4 Domain 6

Domain 6 (figure 4.9) is located in the central region of the 2D dataset and is almost entirely also covered by the 3D data cube. The numerous smaller faults across this region are only evident in the 3D dataset, as such, this has been used to QC the faults across this area. There is a major fault or shear-zone which is evident in the

profile section of line B2 (figure 4.9) which is likely to be through-going, or regionally significant.

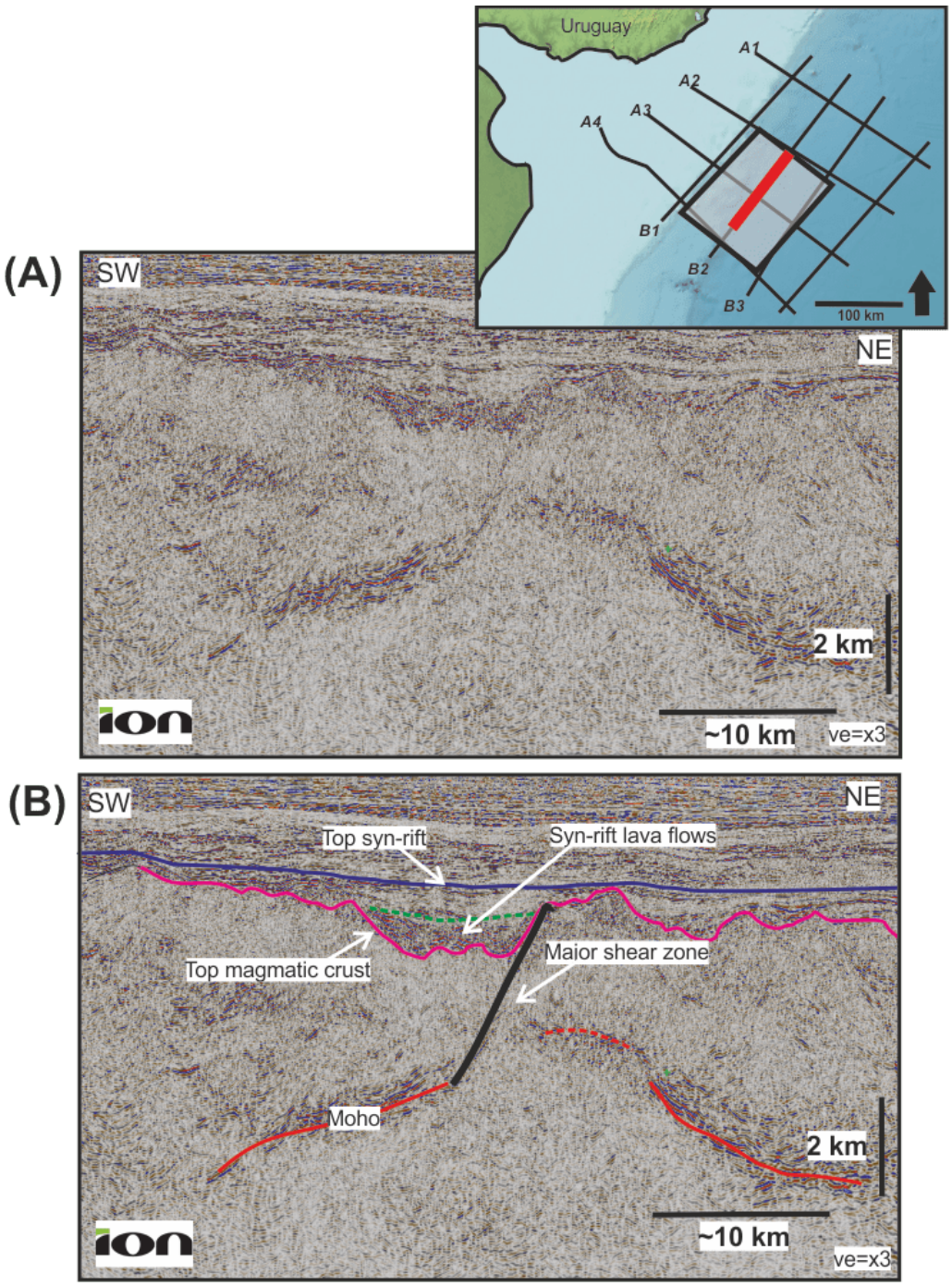

Figure 4.9: Faults of Domain 6 on a section of line B2 of the ION SPAN dataset. Small faults are not easily recognised within the 2D data, but there is a major fault or shear-zone which is evident in the profile section of line B2.

4.3.5 Domains 7, 8 & 9

Domain 7 is an isolated region of extensional faulting in the northern section of the 2D dataset and is almost entirely confined to the SDR North. Faults are trending

~NW-SE with NE or SW dips and low amounts of displacement. Domains 8 and 9 represent either vertical or high-angle extensional faulting in the oceanic crust. Domain 8 (figure 4.10) has dips which are all to the NE and Domain 9 (figure 4.10) has been separated, as there is a notable dip change to the SW.

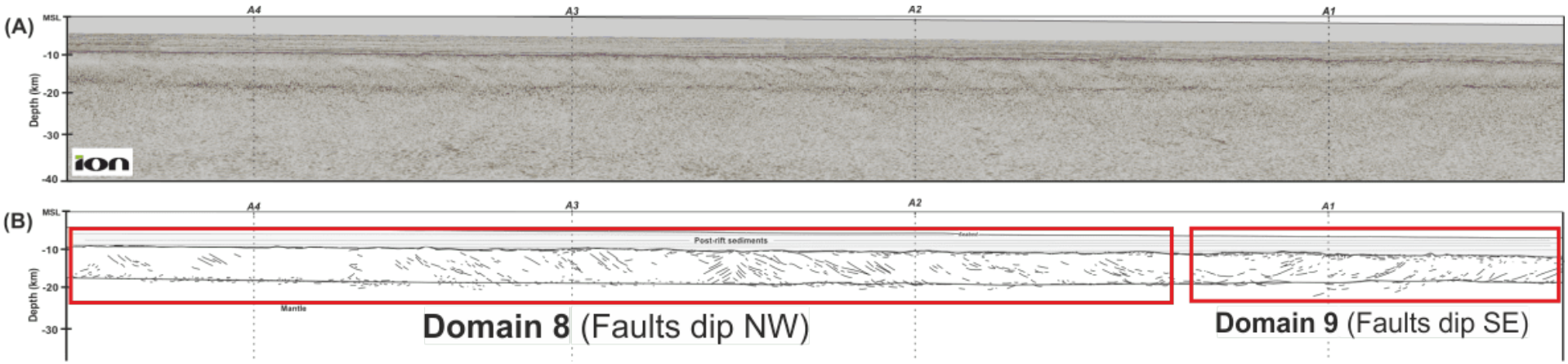

Figure 4.10: (A) 1:1 scale profile of strike line B4 of the ION SPAN dataset (B) Line drawing of (A) showing opposing sets of dipping faults within the oceanic crust.

4.4 Fault trends, anomalies and correlations

Figure 4.11 shows areas of fault anomalies within black circles, this highlights areas between fault domains where there is a considerable change in either fault character, dip or orientation. These can then be correlated to suggest the presence of through-going, regionally significant structures.

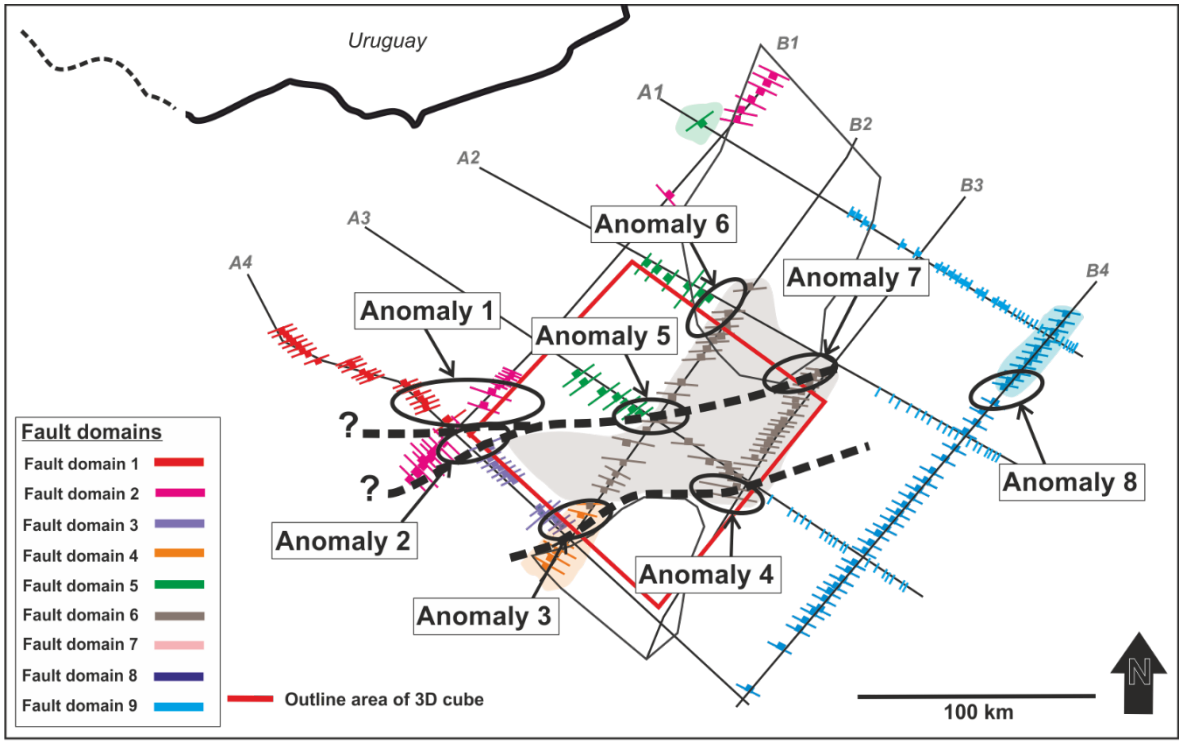

Figure 4.11: Fault anomaly map across the 2D grid, highlighting anomalous areas where there is a sudden fault orientation, dip or character change. These are key areas which help to map through-going and important regional structures. Black dashed lines are suggested major through-going structures.

Figure 4.12 shows a further linkage and interpretation of a connected fault network across the region, overlain on a background of a vertical gravity gradient map. The vertical gravity gradient represents the rate of change of the vertical gravity component with height. The density of features of the subsurface is thereby found by measuring the rate of change of gravitational acceleration (DiFrancesco et al., 2009). It can reveal the location of seamounts, oceanic fracture zones and plate boundaries where there is an absence of other bathymetric data as it varies

depending on local topography/bathymetry (Hunt et al., 2002). This data shows a gravity low across the region of fault domain 6 and the across the 3D data cube. Many of the faults that are south-east dipping on line A4 and on line B1 between A4 and A3, are likely to be connected. This is due to both a similar geometry, the stratigraphy they effect and their position around the southern edge of the craton. However, this is not an exclusive interpretation and does not necessarily associate the timing of their formation to more central structures. Fault anomalies (figure 4.11) such as anomalies 1, 2, 5 and 7 have been interpreted as representative of a larger through-going structure (figure 4.11). Fault anomalies, 3 and 4 and the location of the northern edge of the SDR South are also interpreted as representing another large scale structure. These are represented by larger black dashed lines in figure 4.12.

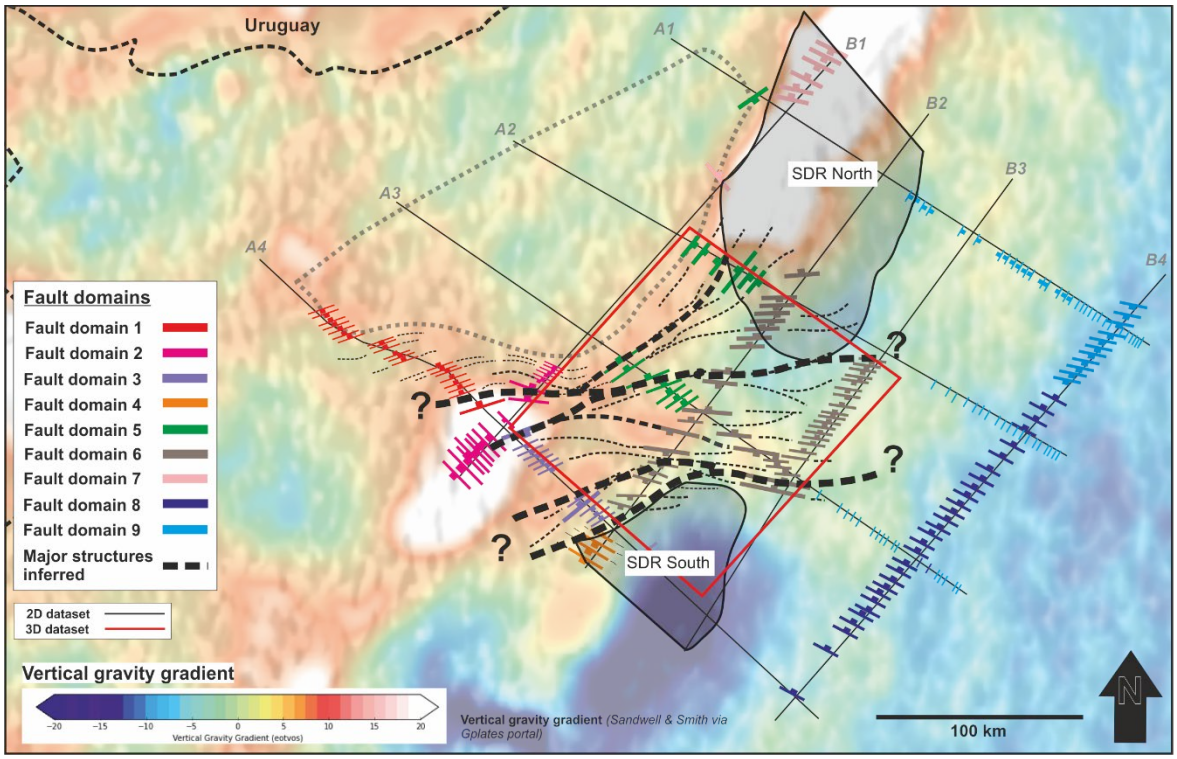

Figure 4.12: Interpretation of a linked fault network and possible major fault traces. Background map shows the vertical gravity gradient from Sandwell and Smith, (2009) from the Gplates portal. www.portal.gplates.org. See text for details on vertical gravity gradient.

Figure 4.13 shows the main faults which have been interpreted across the 2D region. These have been named, Major Extensional Fault 1 (MEF-1) and Major Extensional Fault 2 (MEF-2). Other extensional faults in figure 4.13, include those around the southern edge of the craton, shown in feature 1, figure 4.13 - these were then adjusted in trend for a more realistic orientation, when considering their location on the edge of the highly resistant craton (although this cannot be specifically constrained due to line spacing). Note: not all faults have been recorded in the simplified map. Similarly in features 2 and 3 of figure 4.13, the faults have been oriented taking into account their position relative to the craton and in feature 2 they have been interpreted as partly continuous around the craton.

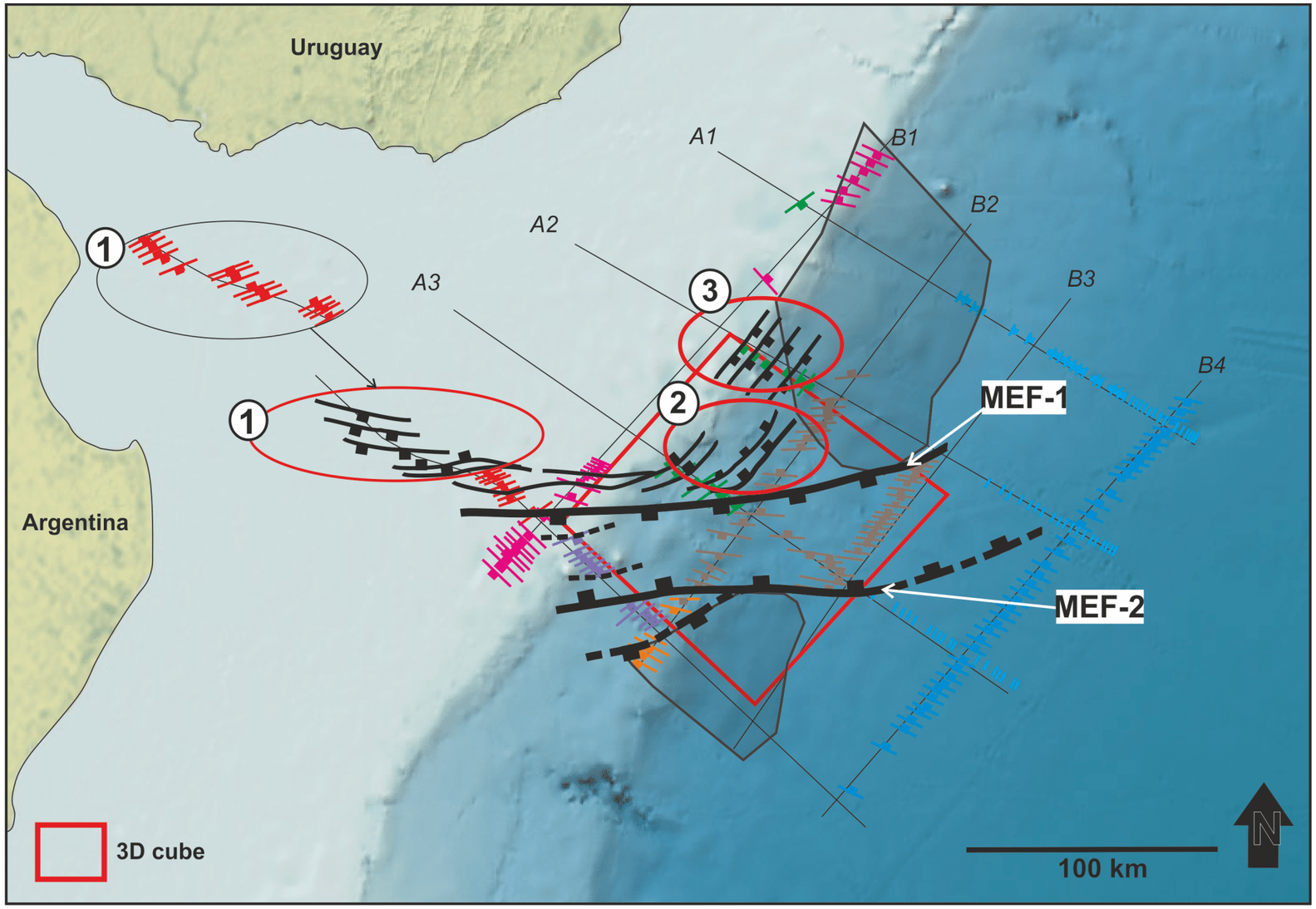

Figure 4.13: Major extensional faults simplified from the overall fault map to show major extensional faults, MEF-1 and MEF-2 and those which ring the craton. Grey polygons represent the area covered in the 2D dataset by the SDR North and SDR South.

4.5 Depth surface maps

Table 10 identifies the horizons for which depth maps have been created, noting whether 3D information has been included in the horizon pick. The horizons which are mapped include the Moho, top crust, top SDRs (North and South), top syn-rift, top oceanic crust and the top seabed.

Table 10: Horizon information for mapped depth surfaces.

Mapped horizon/s	**Nature of the horizon pick**	**Figure no.**
Moho	2D pick only	Figure 4.14
Top crust	Top crust – 2D pick only (does not include magmatic crust indentified in 3D dataset)	Figures 4.15, 4. 16
Top syn-rift	2D pick combined with 3D	Figures 4.17,4.18
Top SDRs (N&S)	Combined with 3D surfaces	Figure 4.19
Top oceanic crust	2D pick only	Figure 4.20
Top seabed	2D pick only (3D shown in inset map)	Figures 4.21, 4.22

4.5.1 The Moho

Figure 4.14 (A) shows a depth surface map created from the 2D pick of the Moho across the ION SPAN PSDM dataset. Immediately notable is a triangular region of higher elevation Moho (corresponding to a thinner crust). This area trends E-W through the south-central part of the 2D data grid (figure 4.14, B). As expected, the most proximal region to the north-west is dominated by a thick region of crust (lower elevation of the Moho pick) which correlates with the cratonic and continental crust. Figure 4.15 shows a 3D view of this surface with a vertical exaggeration of x2 for

the Moho surface, this is to indicate how pronounced the thinning is over a relatively small region of the margin.

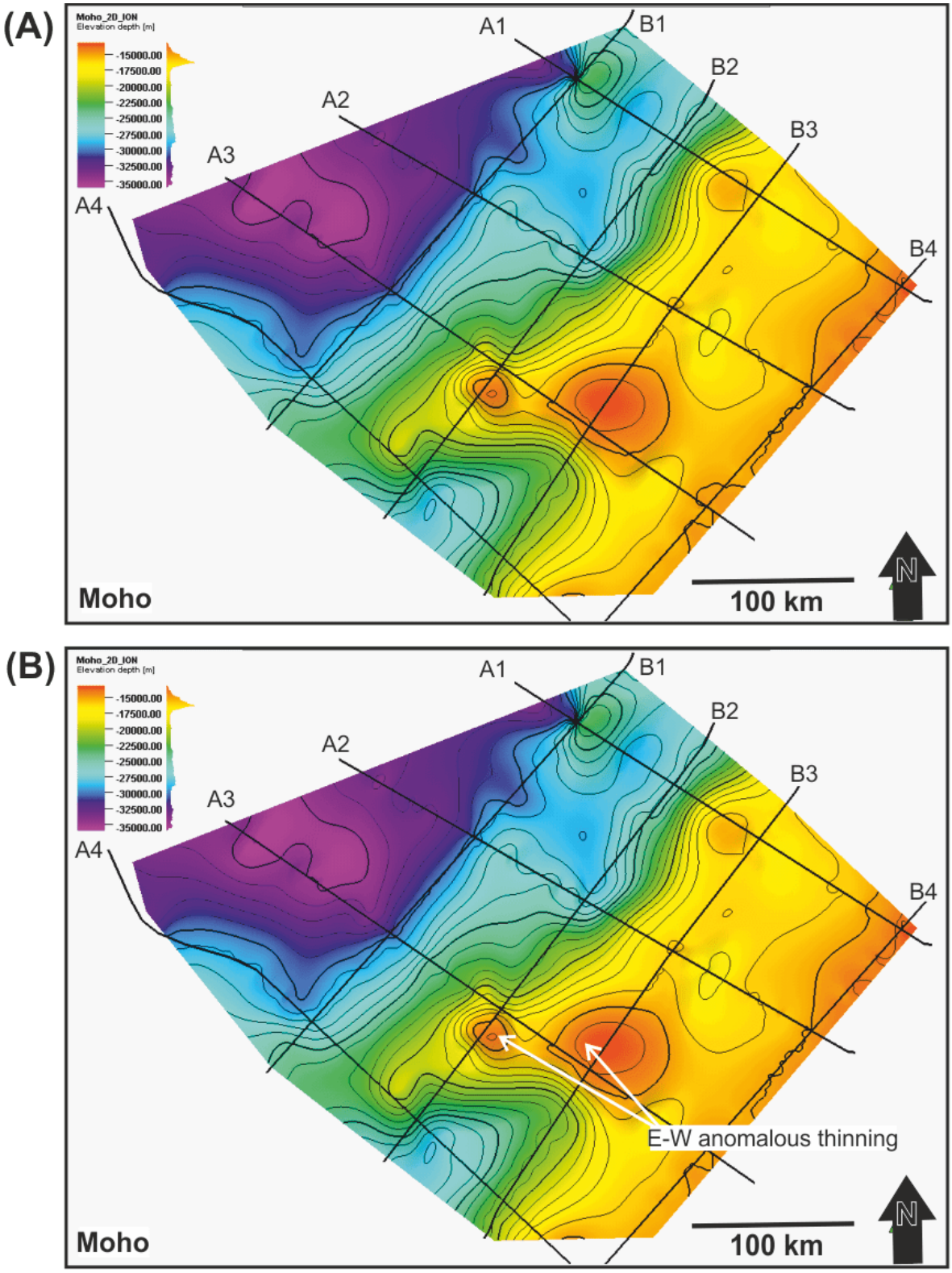

Figure 4.14: (A) Depth map of the Moho (m), mapped from the ION SPAN PSDM dataset (B) note, zone of anomalous thinning trends ~E-W. (Compiled from the 2D dataset only).

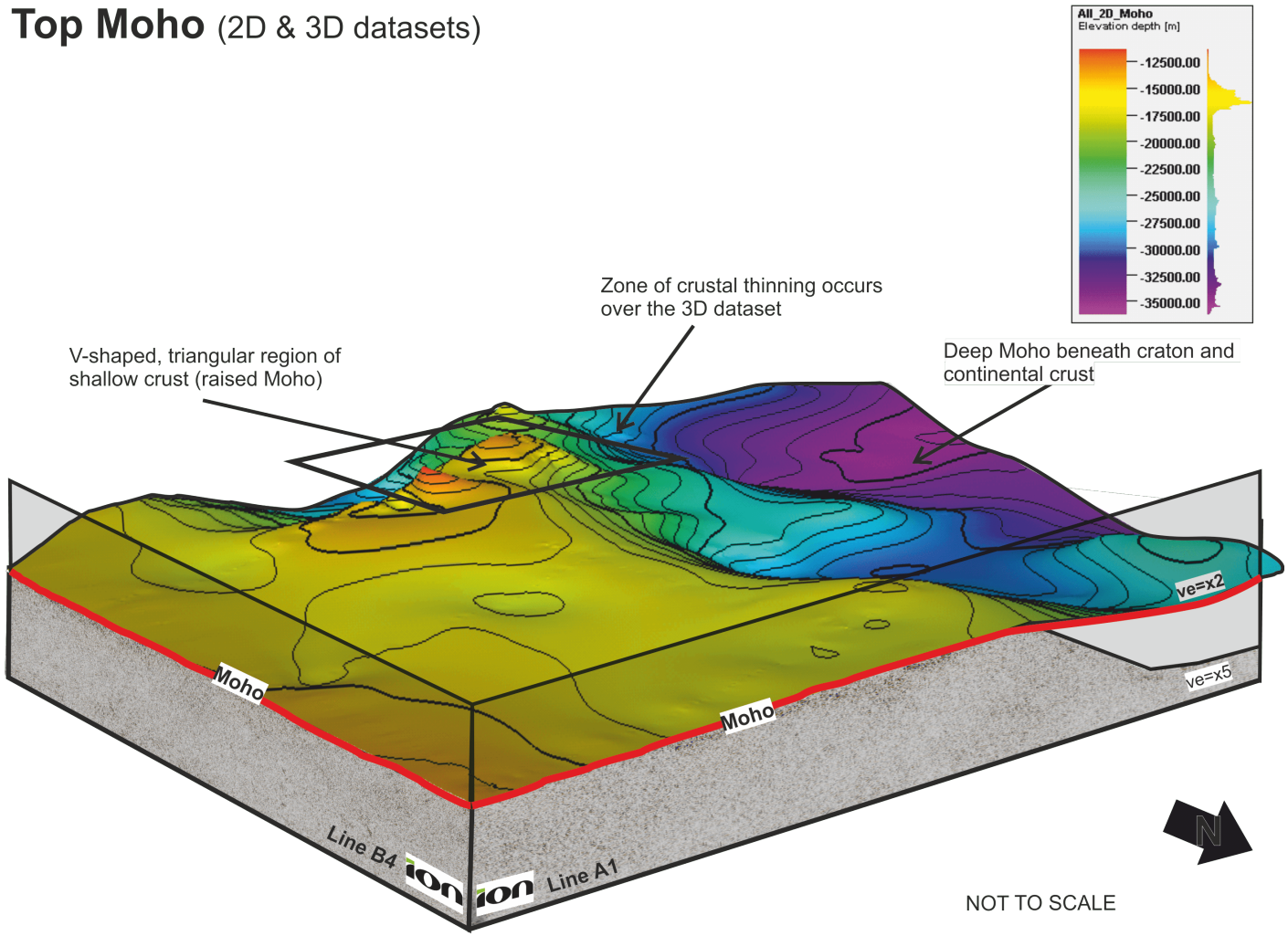

Figure 4.15: 3D view of the depth map, top Moho shows at x2 vertical exaggeration to highlight the extent of crustal thinning over a small area. (Compiled from the 2D dataset only).

4.5.2 Top crust

Figure 4.16 (A) shows the top crust horizon which was created from the ION SPAN PSDM dataset. The top crust horizon was separately mapped before the discovery of magmatic crust within the 3D region. This map does not consider the magmatic crust or a separate, top magmatic crust region (which is later recognised in the 3D dataset). It is an overall pick of the top 'pre-rift basement' across the 2D data grid. However, due to the discovery of new, replacement magmatic crust in the 3D dataset, a true 'pre-rift basement' horizon is technically not applicable across the entire 2D region. This means that the orientation of a crustal low running ~NE-SW is truly accurate in only the north-east section of the map. However, this does indicate that there was a pre-existing crustal depression which ran along a NNE-SSW trend to the margin and oceanwards of the regional high, maintained by the cratonic and continental crust in the proximal region. It is likely that there was some degree of continuation of this to the south of the craton which is indicated by more localised depocentres (figure 4.16, B).

4.5.3 Top syn-rift

Figure 4.17 (A) shows the top syn-rift horizon, mapped across both the 2D PSDM ION SPAN dataset and the 3D cube. This has resulted in a region of increased data resolution across the 3D area, showing a clear, triangular or funnel-shaped sediment depocentre (Figure 4.17, B) which is trending E-W through the 3D cube. This is consistent with the location and nature of the Punta del Esté Basin, recognised by previous authors (Ancap, 2011; Soto et al., 2011; Morales et al., 2017). In particular, the north-western boundary of the 3D depocentre shows a sharp transition from a stratigraphic low to a raised section of crust. This is interpreted to be the transition from syn-rift, magmatic crust which underlies the

'funnel' section of the triangular Punta del Esté Basin and the more resistant, pre-rift continental crust. Two large half-graben faults are evident on the edge of the continental crust which are filled with syn-rift sediments.

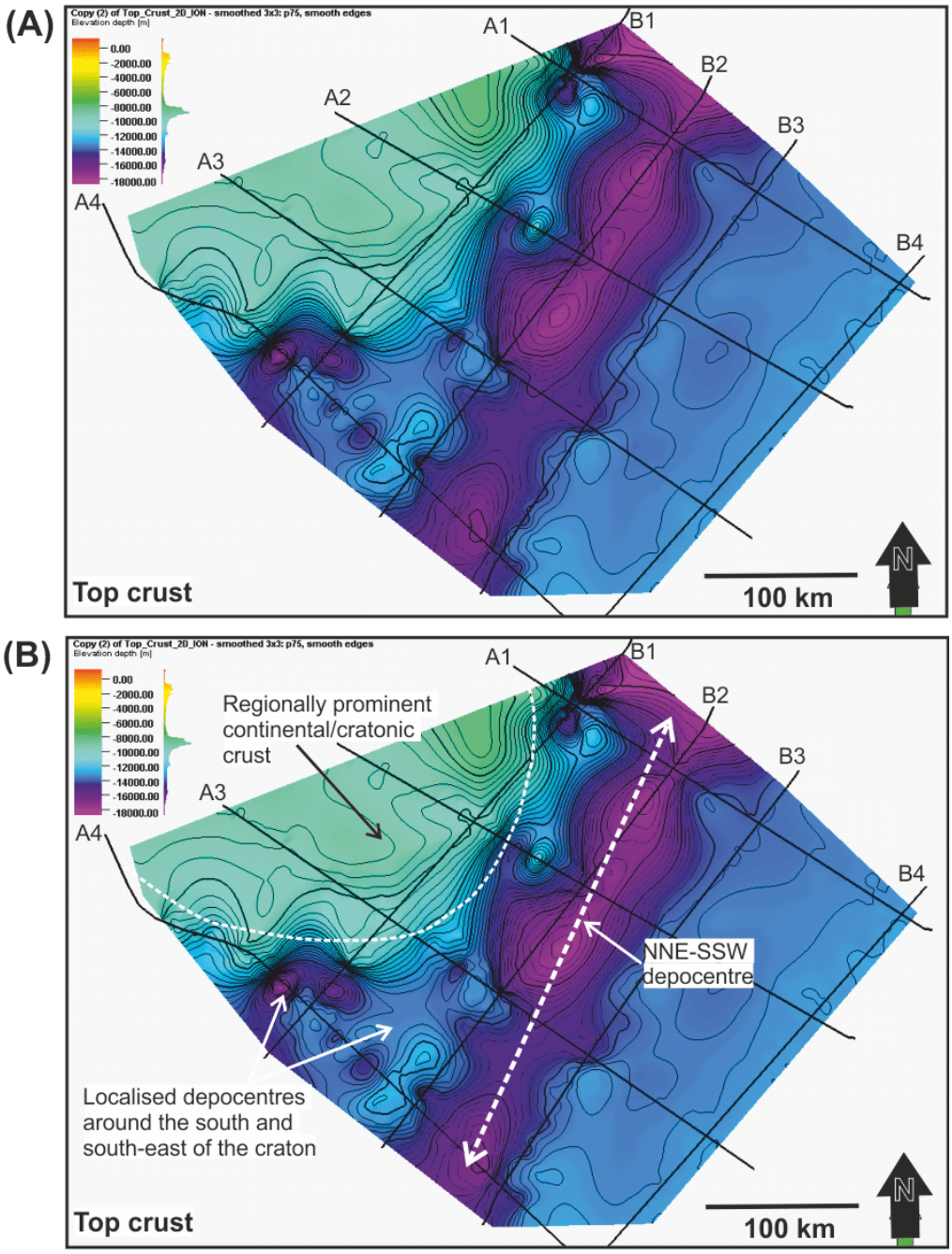

Figure 4.16: Depth map of the top crust. Mapped independently of the 3D dataset and the discovery of new, magmatic crust. NNE-SSW depocentre and localised depocentres around the south of the craton/continental crust are likely significant. (Compiled from the 2D dataset only).

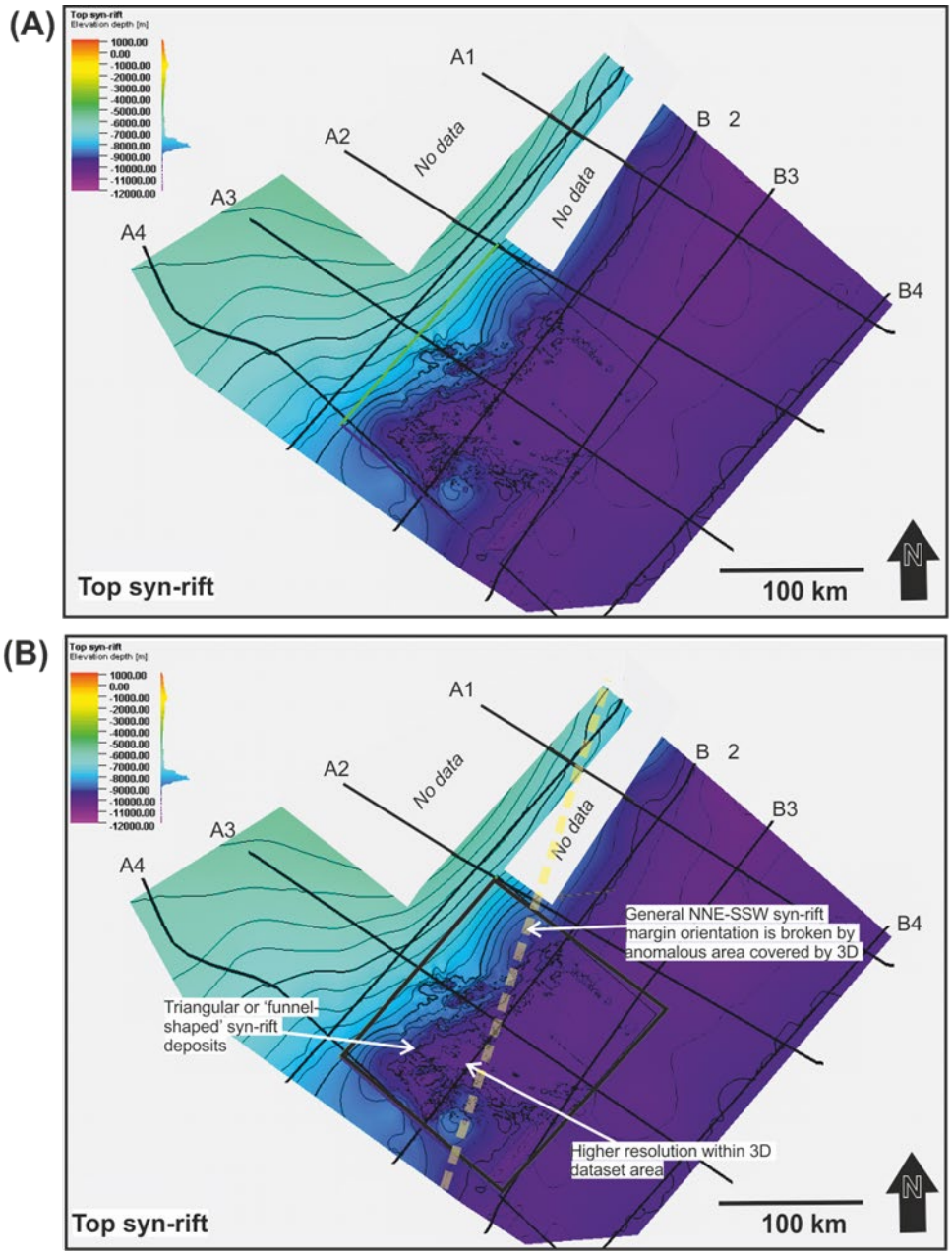

Figure 4.17: Depth map of the top syn-rift horizon, mapped both through the ION SPAN 2D PSDM dataset and the 3D PSDM data cube. Regions of no data have been blanked out. (Compiled from the 2D and 3D datasets).

Figure 4.18 shows a 3D view of the top syn-rift horizon with an inset map showing the area of a triangular depression in more detail.

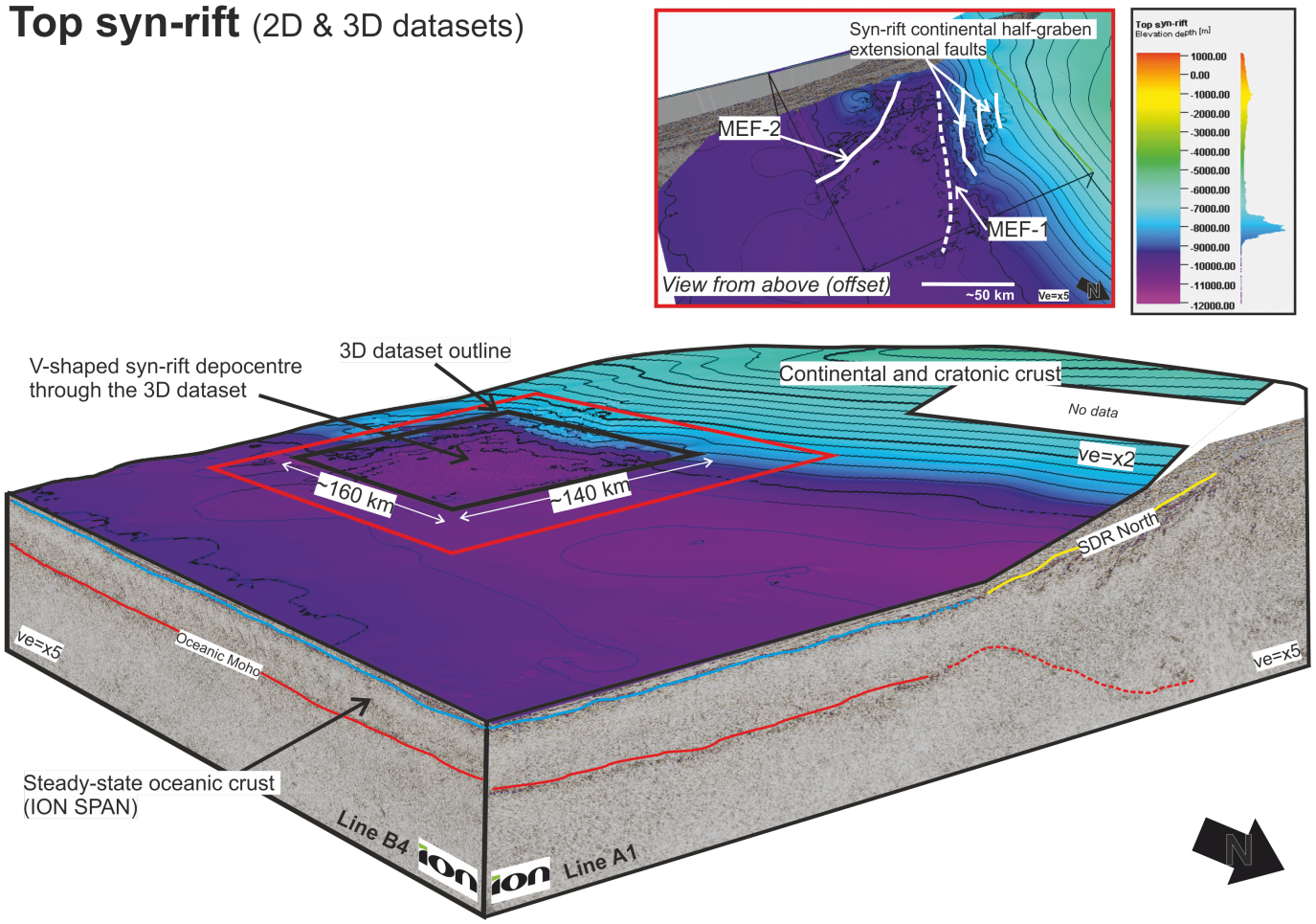

Figure 4.18: 3D view of the top syn-rift depth map along with line B4 and A1 from the ION SPAN dataset. Depth map was created from both the 2D and 3D datasets. Red box denotes the highlighted area that is shown within the inset box, of the triangular depression. (Compiled from the 2D and 3D datasets).

4.5.4 Top SDR (North and South)

Figure 4.19 shows both of the top surfaces to the SDR North packages and SDR South. Also included, but not in great detail, are the 3D surfaces (these are studied more closely in Chapter 5). The top surface of the SDR North is aligned, ~NE-SW along the orientation of the present day margin. SDR South covers a smaller region but shows more variability in the orientation of packages.

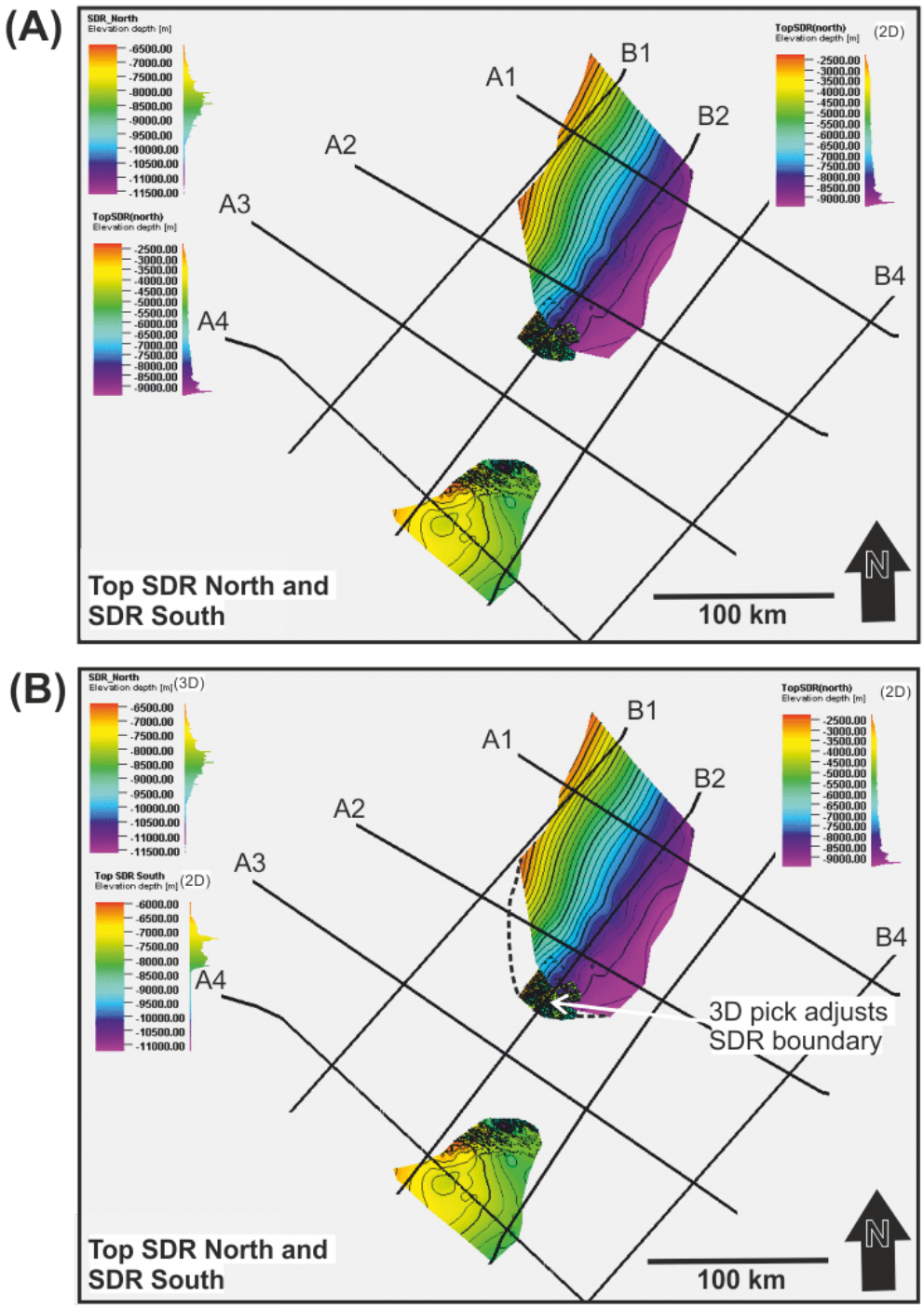

Figure 4.19: Depth maps for the top surfaces of the SDR South and SDR North. Also noted are the 3D data mapped regions of SDR. Note, boundary to the SDR North may be adjusted through 3D mapping. (Compiled from the 2D and 3D datasets).

4.5.5 Top oceanic crust

Figure 4.20 shows the depth map corresponding to the top oceanic crust, picked using the 2D dataset only. There is an anomalous region of increased thickness of the oceanic crust in the north-east region of the map.

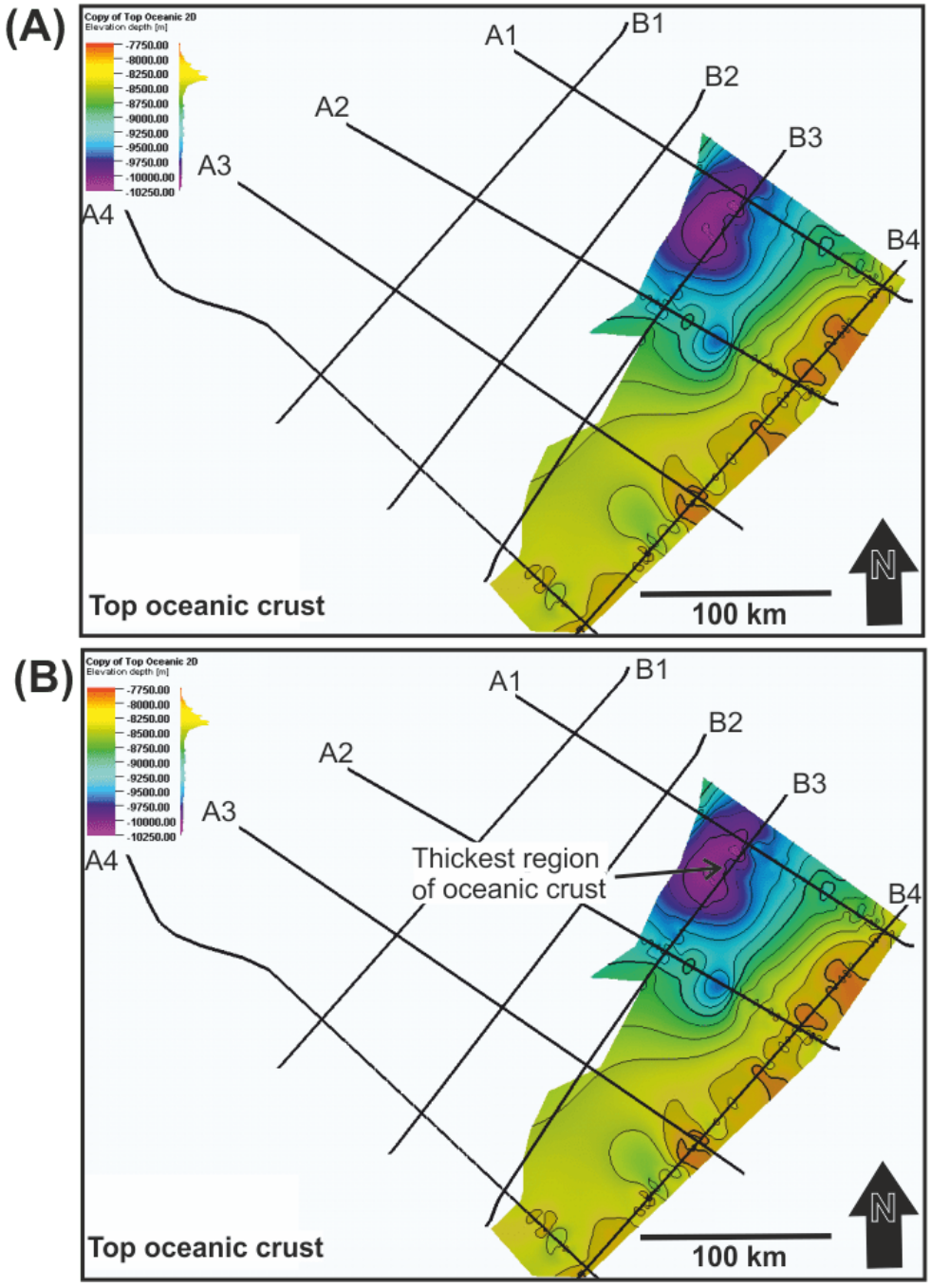

Figure 4.20: Depth map of the top oceanic crust mapped from the 2D dataset only.

Figure 4.21 shows the present day top seabed, mapped in the 2D data which shows no anomalous regions and a uniform margin trending NE-SW. Figure 4.22 shows a 3D version of this map with an inset map of the same surface, picked across the 3D dataset.

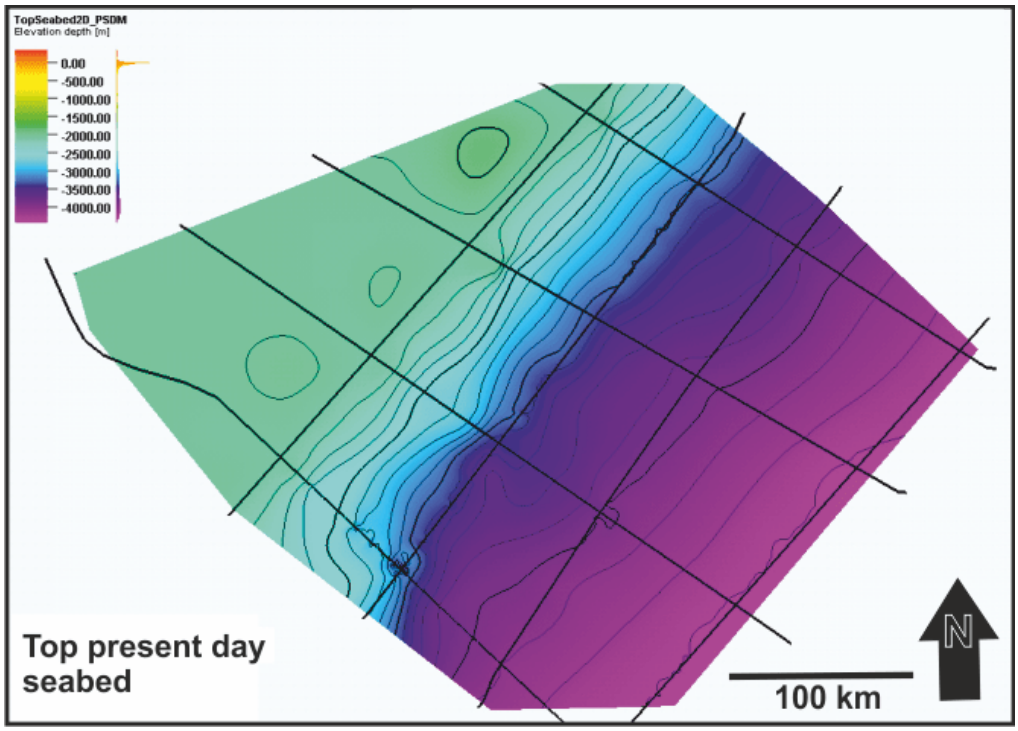

Figure 4.21: Depth surface map for the top seabed picked within the 2D ION dataset. (Compiled from the 2D dataset only).

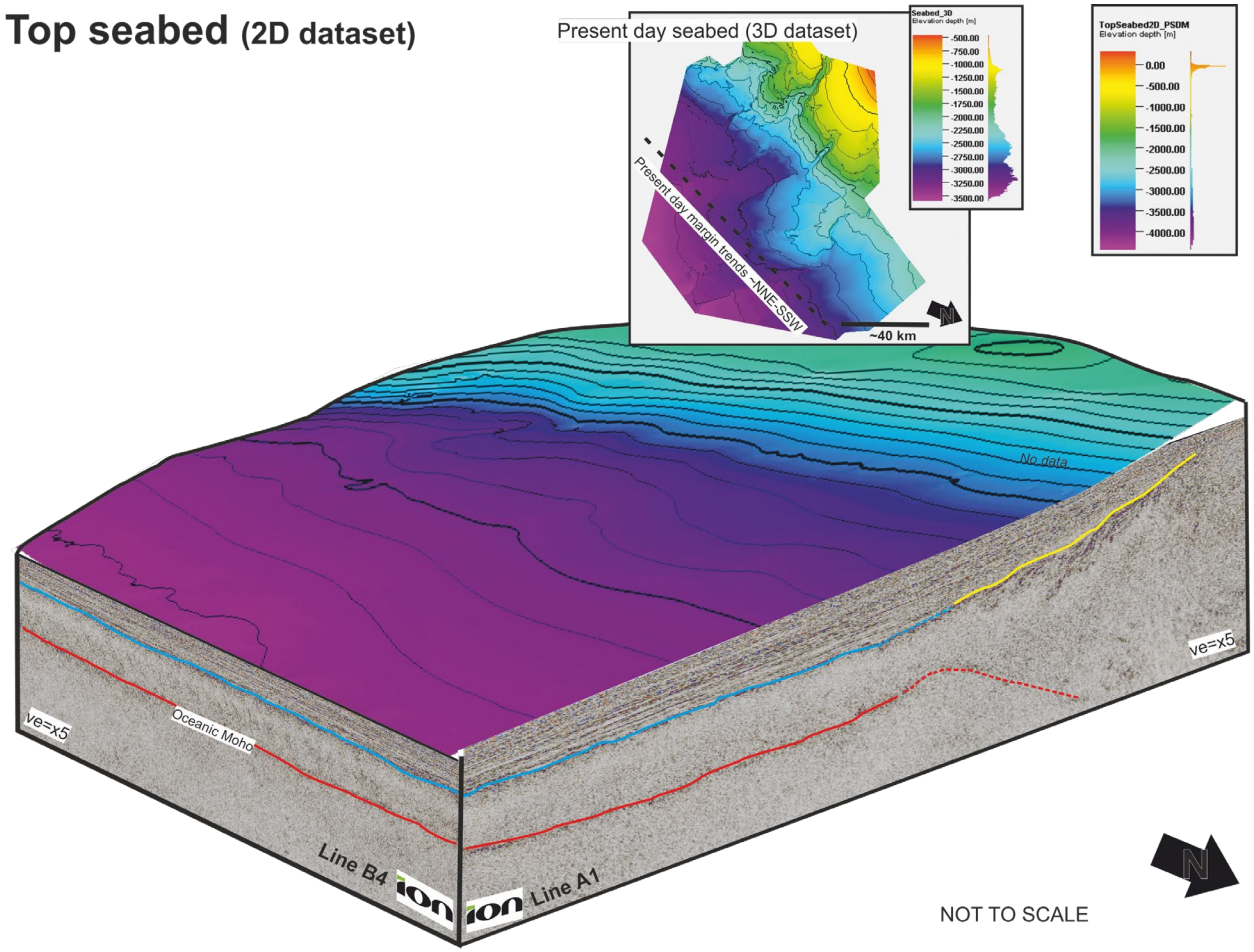

Figure 4.22: 3D view of the top seabed depth map across the 2D dataset with lines B4 and A1 of the ION SPAN dataset also shown. Inset map shows the top seabed depth surface for the 3D dataset. The 2D data only was used for the main surface, the 3D dataset has been used for the inset map.

4.6 Isopach maps (thickness maps)

Table 11 indicates the horizons used to produce thickness maps (TVT) (isopach maps) across the 2D region as well as the equivalent interval which is created. Isopach maps are useful in determining the distribution of an evolutionary interval across the basin, as they show changes in stratigraphic thickness in relation to a particular time interval.

Table 11: Isopachs created from mapped depth horizons of Moho, top crust, top syn-rift, top seabed.

Isopach	**Interval equivalent**	**Figure no.**
Top Moho to top crust	Crustal thickness (without syn-rift or post-rift deposits)	Figure 4.23
Top crust to top syn-rift	Syn-rift thickness (includes sediments and volcanics)	Figure 4 24
Top syn-rift to top seabed	Post-rift sediment thickness (present day)	Figure 4.25
Isopach: Top crust to top present day seabed	Crustal thickness with post-rift sediments (present day)	Figure 4.26

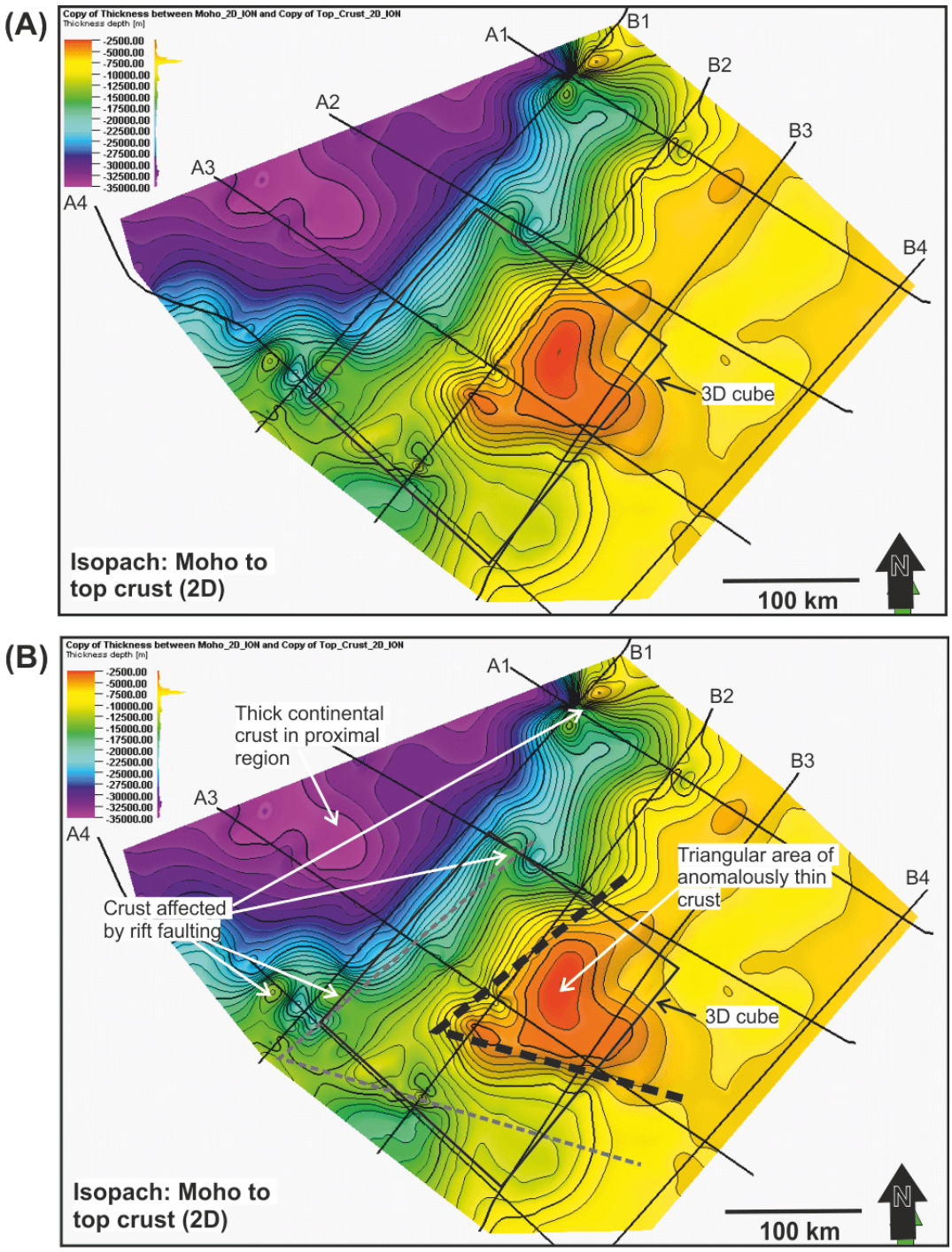

Figure 4.23: (A) Uninterpreted Isopach map showing the interval from the Moho to the top crust, this is a proxy for the crustal thickness across the region. (B) Interpreted section, note the triangular region (within dashed black lines) of significantly thinned crust through the area covered by the 3D dataset and an expected, thick region of crust in the proximal part of the margin, due to the craton and continental crust.

Figure 4.23 (A) shows an uninterpreted isopach map for the interval between the Moho and the top crust, (B) shows this map with interpretation, including a notably thicker region of crust (dark blue and purple) in the proximal region, corresponding

with the location of the craton and surrounding continental crust and best observed on the strike line B1 of the ION SPAN dataset. There are also significant anomalous areas surrounding the craton and correlating with the large half-graben extensional rift faults that have been identified on the continental shoulder in particular. Most striking, is the triangular area of thinned crust which is present through the lower central section of the 2D dataset and into the area covered by the 3D data. This has a distinct triangular or 'funnel-shaped' morphology and is generally trending E-W, with the point of the triangle towards the continent. This area of anomalously thinned crust is observed on the 2D dataset across lines B2 and B3 in particular. Figure 4.24 (A) shows an uninterpreted isopach map for the interval from the top crust horizon to the top syn-rift horizon. Section (B) of figure 4.24 shows an interpretation of (A), indicating areas of increased thickness during the syn-rift period. Areas of increased syn-rift sediment infill are present in the stretched continental region in half-graben rift faults around the edges of the continental craton. There is also a small area of increased syn-rift thickness in the central to south-east region of the 3D dataset. This map shows the distribution of the combined crustal thickness and sediment/volcanic deposits of the syn-rift period. This is shown only from the 2D dataset, which has meant that the details of the triangular depression covered by the 3D dataset are much less apparent. Figure 4.25 shows the overall thickness of post-rift deposits by calculating the thickness between the top syn-rift horizon and the present-day seabed across the margin (from the 2D and 3D dataset). This shows that the earlier triangular depocentre, associated with the thinned area of crust has left some evidence in the form of increased areas of thicker sediments, however the increased resolution of the data in the area from the 3D dataset may also have contributed to this apparent enhancement. Figure 4.26 shows the isopach

between the top crust horizon and top present day seabed (2D data only). Note the increased thickness in the syn-rift half graben around the edge of the craton and within stretched continental crust, however, this map is less well constrained as there has been the removal of the pre-rift crust in the 3D data area.

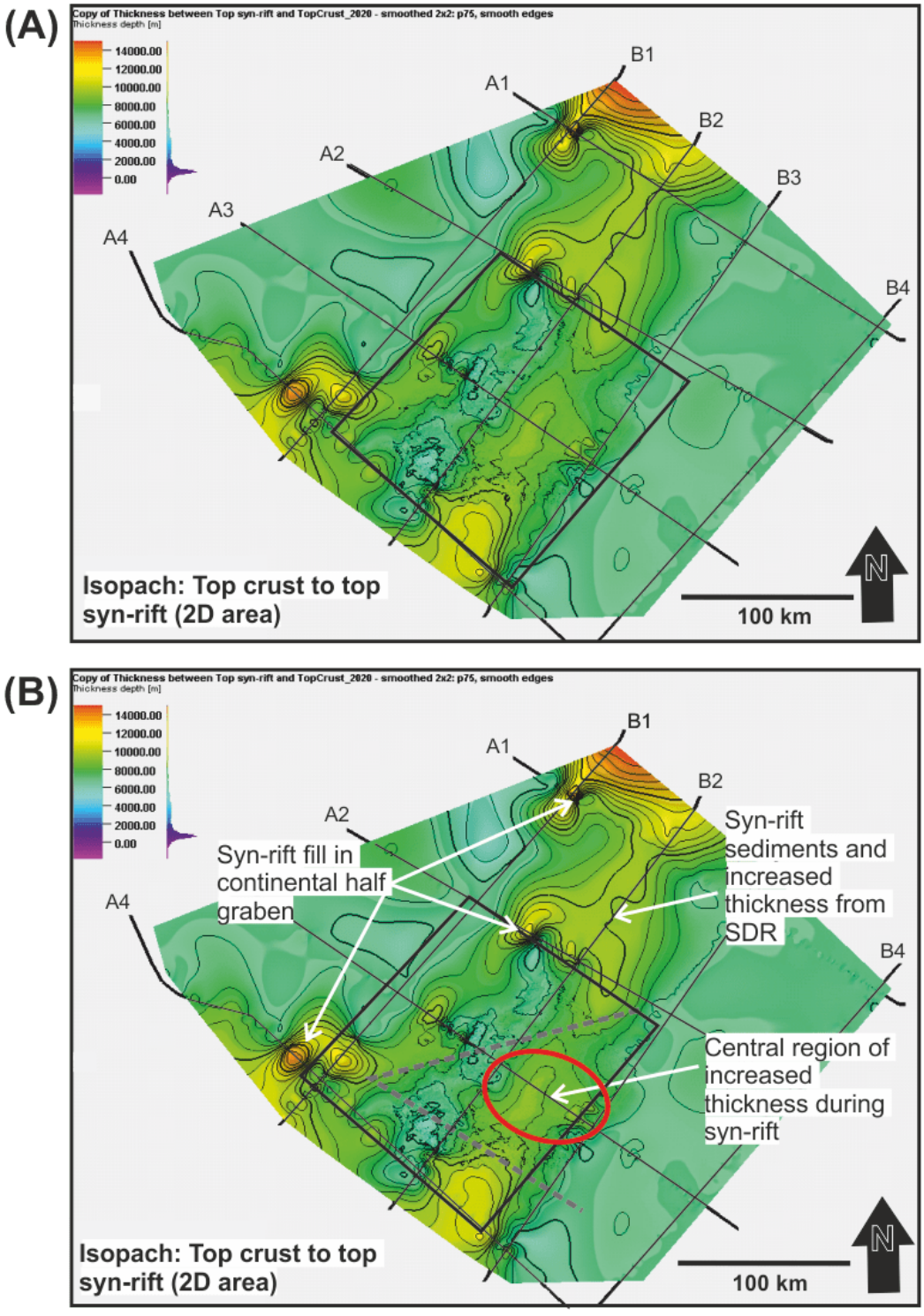

Figure 4.24: (A) Uninterpreted isopach map for the interval from the top crust horizon to the top syn-rift horizon. (B) Interpretation of (A) with areas of increased thickness during the syn-rift period. (2D and 3D data used).

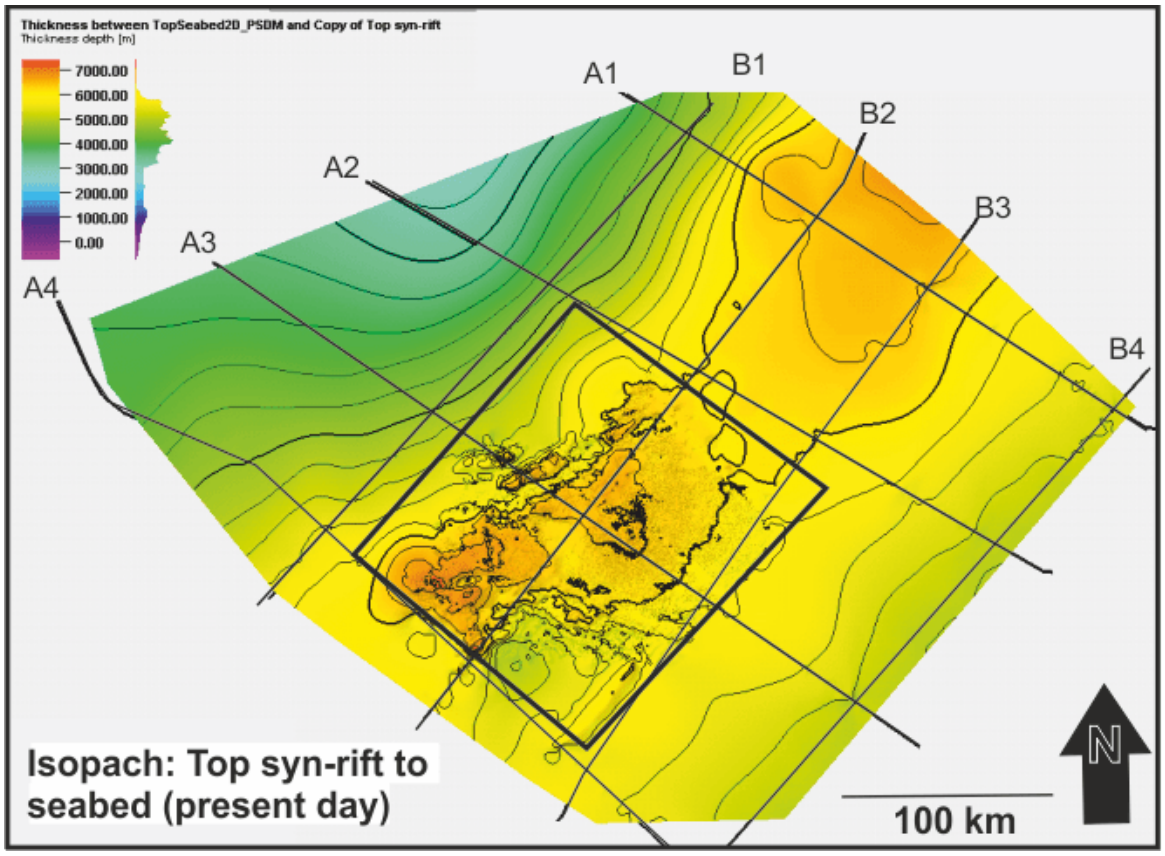

Figure 4.25: Isopach created from the top syn-rift horizon to the top seabed, using both the 3D and 2D datasets. This is a proxy for the overall post-rift sediment thickness across the margin. Note: due to increased resolution in the 3D dataset, this may be artificially highlighting the sediment thickness across the 3D data region. (2D and 3D data used).

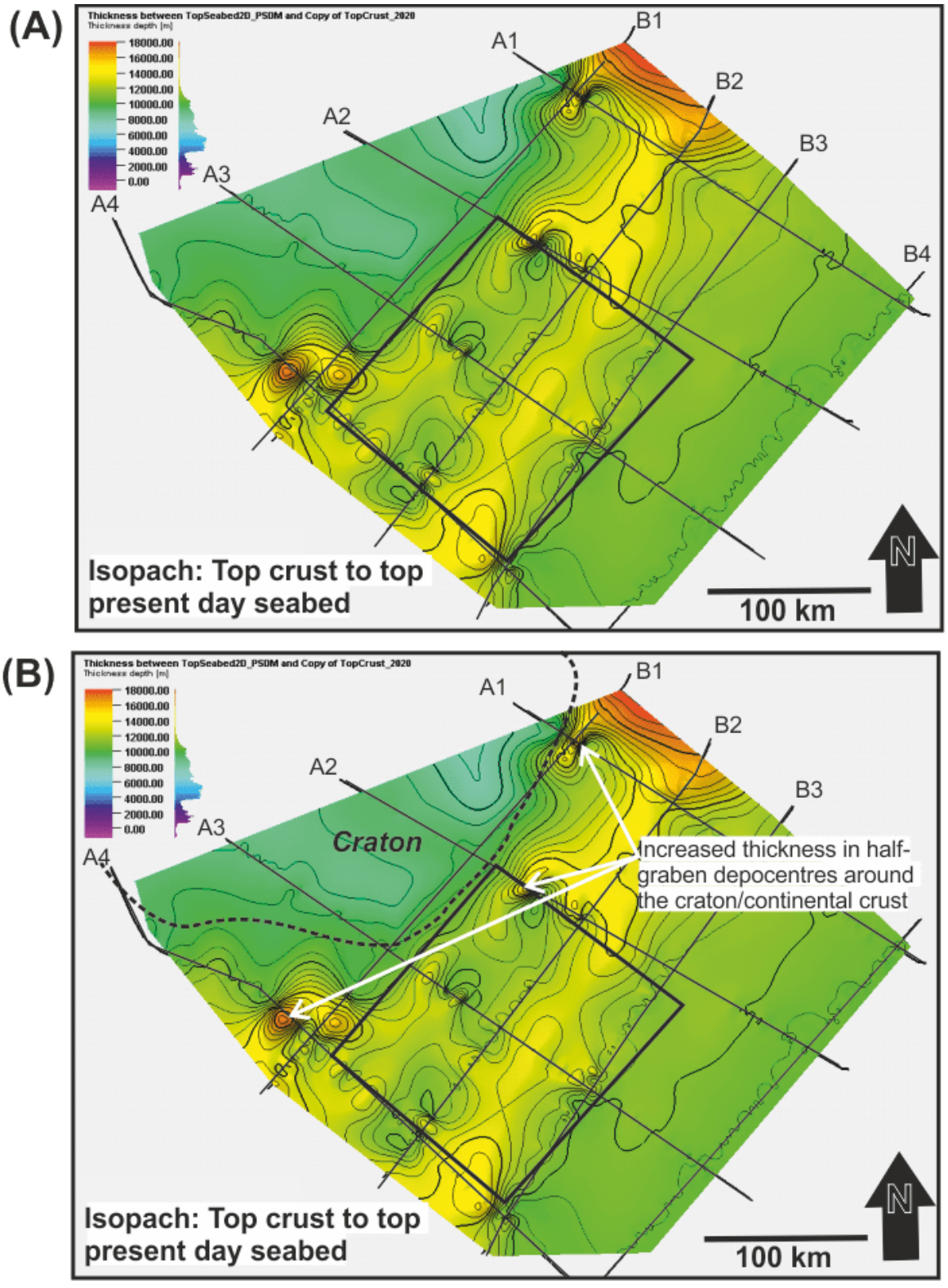

Figure 4.26: Isopach between the top crust horizon and top present day seabed (2D data only). Note the increased thickness in the syn-rift half graben around the edge of the craton and within stretched continental crust.

4.7 The evolution of the margin

4.7.1 Pre-rift distribution and the onshore continuation of lineaments

Pre-rift fabrics are evident around the southern section of the craton with fault-bound blocks of un-deformed pre-rift stratigraphy, interpreted as fault domain 2 (figure 4.6). On the eastern boundary of the craton, the pre-rift is found in fault domain 5 (figure 4.8) underlying divergent reflections of syn-rift half-graben structures and comprising the majority of the continental and cratonic crust. It can also be seen as resistant, flat-topped horsts, flanking the graben features (Figure 4.8). This domain is also evident in the 3D dataset and is explored in greater detail in Chapter 5. As noted in the following section 5 of this chapter, ‘depth mapping’ - the early attempts at mapping the 2D data ‘top pre-rift’ as a continuous horizon were hampered by the later identification of the removal of pre-rift and subsequent insertion of voluminous syn-rift volcanics. This resulted in the replacement of continental pre-rift by magmatic crust across the v-shaped region covered by the 3D data cube. As such, the distribution of the pre-rift remains almost entirely confined to the proximal region and continental shoulder, the feather edge of which is covered by the 3D dataset (and covered further in Chapter 5). Stretched continental crust in the 3D dataset in particular, has remnant horsts of pre-rift material which are proposed to be the same Palaeozoic sediments that have been drilled by the Gaviotín well, and may be correlated with units of the onshore, Norté (Paraná) Basin (Veroslavsky, 2003). There may also be allochthonous blocks of continental pre-rift ‘rafted’ by detachment faulting onto the upper mantle (see chapter 5). Figure 4.27 shows an uninterpreted large-scale view of vertical gravity gradient data on the offshore Uruguayan margin that is continuous and un-divided by crustal domain. The outline of the present day Uruguay and Argentinian coastline has been added for reference. Figure 4.28

shows an overlay of the major structural features which have been determined through data analysis in this chapter. The continuation of extensional faulting observed around the southern edge of the RdP craton is proposed to either, track up the Rio de la Plata estuary with the ‘Martin Garcia lineament’, proposed by Zambrano and Urien, (1970) and Urien and Zambrano, (1973) and Carlos Urien (personal communication, 2015) or, along the border of the Martin Garcia High in northern Argentina (figure 4.28). The Salado Basin has been interpreted as an episutural basin, focused around a 2.1-2.0 Ga suture, within the Rio de la Plata craton (Páengaro and Ramos, 2012) which may also correlate with MEF-2. In distal regions, the major extensional faults may also be linked, either directly (or indirectly) to the oceanic Meteor Fracture zone (figure 4.28) as suggested by Hernández-Molina et al., (2016).

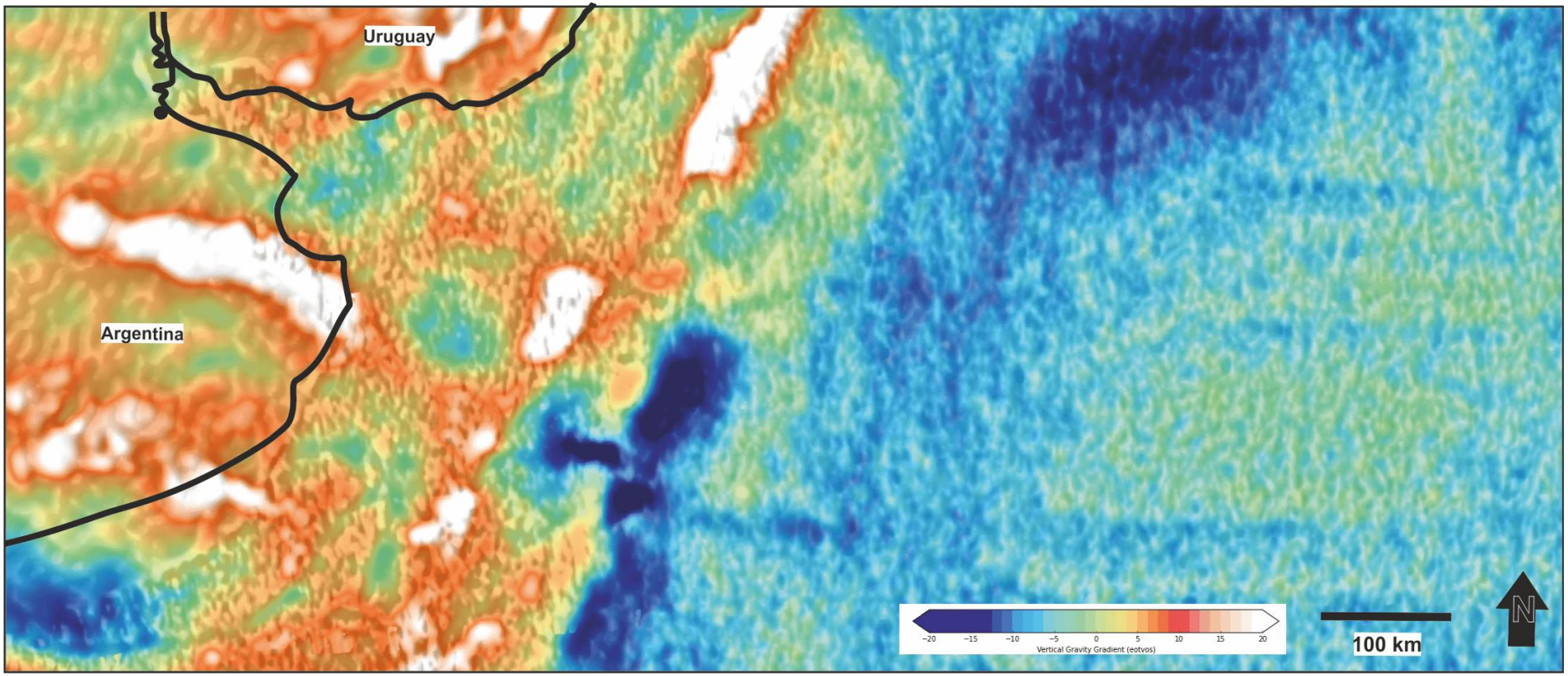

Figure 4.27: Uninterpreted, vertical gravity gradient map of the offshore Uruguayan margin (data from Cesium, GPlates online portal with data from Sandwell et al., (2014).

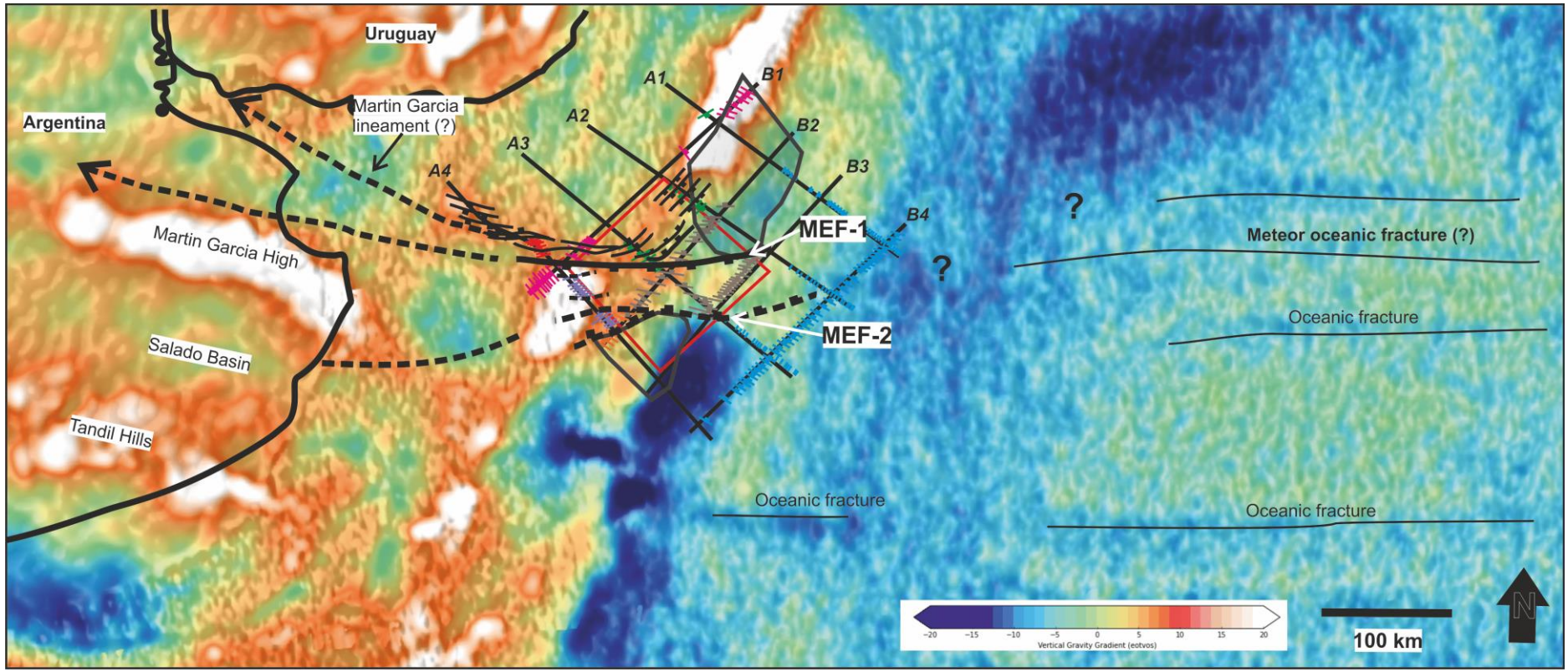

Figure 4.28: Interpreted vertical gravity gradient map of the offshore Uruguayan margin with an overlay of structural data and major structures from this study (Background data from Cesium, GPlates online portal with data from Sandwell et al., (2014).

4.7.2 The Rio de la Plata craton: An enduring tectonic buttress

Cratons have acted as buttresses to tectonics all along the South American Atlantic margin (Páengaro and Ramos, 2012) and have been dated to the Ediacaran and Neoproterozoic (Oyhantçabal et al., 2011). A major regional feature identified in the offshore region is the Rio de la Plata craton (RdP). During the late Palaeozoic, the collision of allochthonous terranes to the south of the study area in Argentina, resulted in the Ventania-Cape Fold Belt, which has been mapped to extend out to 600 km offshore Argentina (Páengaro and Ramos, 2012). The gravity and Emag data in this study suggest that a similar extension of structural fabrics has, at one time, extended into the offshore region of Uruguay. Structural data from this study confirms extensional faults all around the RdP craton which adds to evidence in the study by Rapela et al., (2011) that the RdP craton was surrounded by transcurrent faulting.

4.7.3 Palaeozoic fold belts and the Marmora back-arc basin

The cratons in Argentina and South Africa diverted the Palaeozoic, Ventania-Cape fold belt, forming the Colorado Syntaxis and creating the corresponding Cape Syntaxis of South Africa (Páengaro and Ramos, 2012).

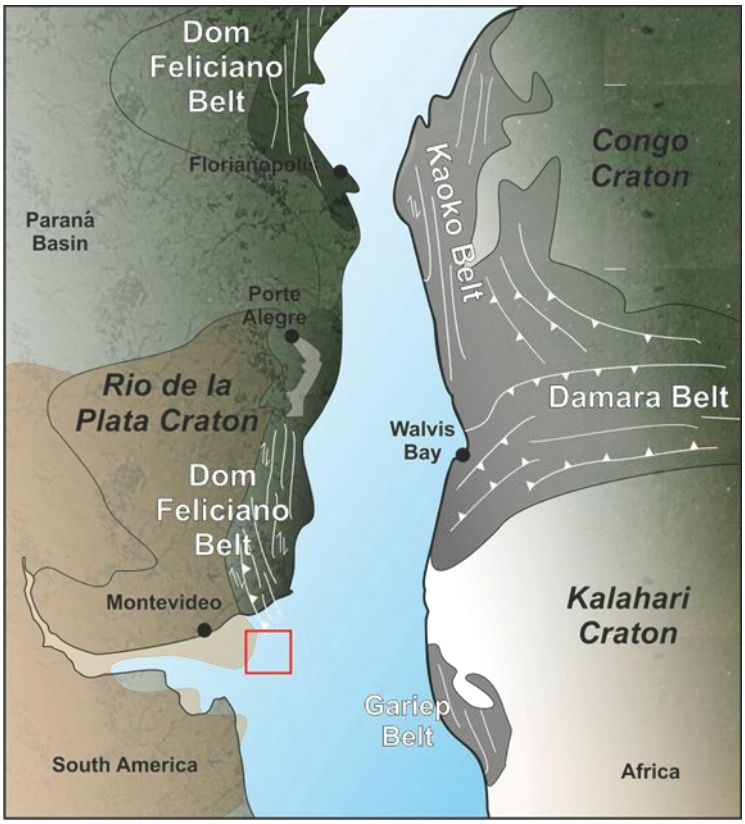

Figure 4.29: Brasiliano and Pan-African orogens showing the regional position of major fold belts on both the South American and African margins, modified from Oyhantçabal et al., (2009). Red box denotes the approximate location of the study area.

Figure 4.30 shows the proposed arrangement of major cratons and the regionally significant Dom Feliciano belt in the offshore Uruguay region. Figure 4.31 shows a central region within the cratonic crust (dark pink). This is observed on line B1 of the ION seismic reflection dataset and is interpreted to be the Aigua Batholith, one of three found within the Granite belt of the Dom Feliciano belt (Oyhantçabal et al., 2009) (figure 4.29). The Granite belt is the most eastern of three geotectonic units defined within the Dom Feliciano Belt (Basei et al., 2000) which runs ~N-S down the eastern edge of the present day Uruguay coastline, with the Gariep Belt being the South African equivalent (figure 4.29). Some authors have suggested that these batholiths are the roots of a magmatic arc (Basei et al., 2000; Oyhantçabal et al., 2009). This is proposed as the same magmatic arc, the ‘Cuchilla Dionisio-Pelotas Arc’ (noted in chapter 1B) which created the Marmora back-arc basin from 650-580

Ma. The axis of this Neoproterozoic, Marmora back-arc basin is the inherent weak zone that becomes the future opening of the Cretaceous South Atlantic (Will and Frimmel, 2018) (figure 4.30).

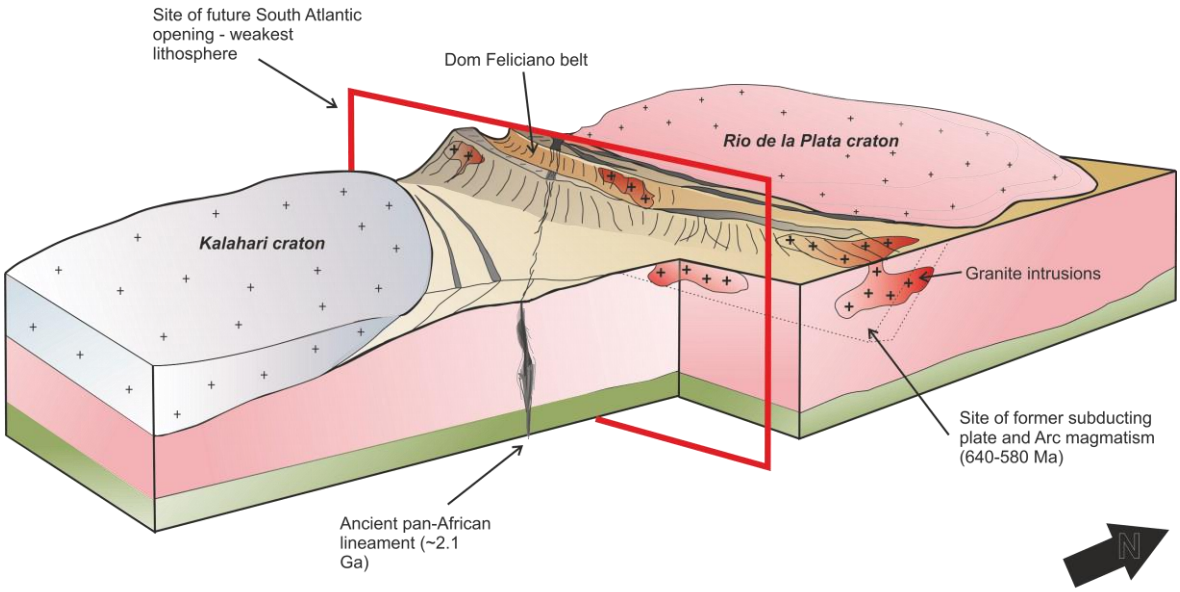

Figure 4.30: Model showing the proposed arrangement of major cratons and the regionally significant Dom Feliciano belt in the offshore Uruguay region. Note also the presence of a large pan-African lineament (2.1 Ga) identified by Rapela et al., (2011) that becomes the nucleus for the Mesozoic Salado Basin. Also, in red, the site of the future South Atlantic rift based upon Will and Frimmel, (2016) and the formed subducting plate and Arc magmatism of 640-580 Ma. Modified from Oyhantçabal et al., (2009) and Rapela et al., (2011).

Figure 4.30 is modified from Oyhantçabal et al., (2009) and Rapela et al., (2011) and shows the large-scale positioning of the 2.1 Ga lineament (of the future, Mesozoic Salado Basin) and Pan-African orogen. Figure 4.30 also shows the Dom Feliciano Belt, oriented approximately north-south along the eastern edge of the Rio de la Plata craton. This is proposed as the underlying fabric/structural weakness for the nucleation of early cretaceous, syn-rift half-graben faults in domains 5 and 7 which trend ~N-S along the present day margin (figures 4.29, 4.30). Faulting around the southern edge of the RdP craton in domains 1 and 2 and oriented WNW-ESE (figure 4.31) is inferred as relating to the northern edge of the Salado Basin and may be traced to the long-lived, 2.1 Ga lineament upon which the nascent, Mesozoic

Salado Basin was later sited. The arrangement of fold belts in this era, along with the orientation and pattern of faulting observed in the 2D dataset, leads to the proposal of a linkage between the 2.1 Ga lineament of the Salado Basin and the African, Damara belt through the landmass connection, prior to break-up, and the N-S trending Dom Feliciano fabric as proposed by Macdonald et al., (2003) and Páengaro and Ramos, (2012) (figure 4.31).

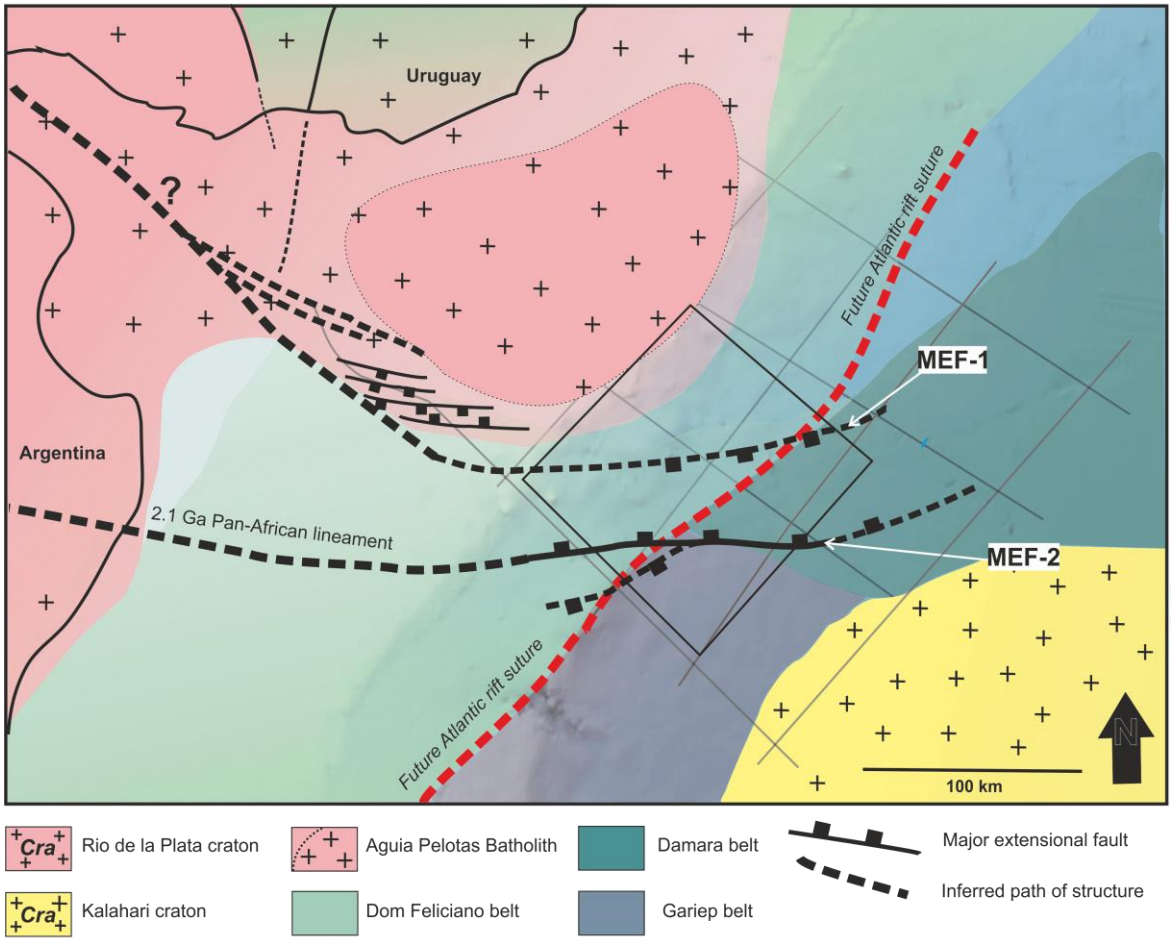

Figure 4.31: Major structures of the Palaeozoic offshore Uruguay region, mapped in this study, with the Dom Feliciano Belt and Damara Belt locations super-imposed. Also shown are the RdP craton in the north-west with the internal Aiguà-Pelotas Batholith and the Kalahari craton to the south-east (yellow). A continental landmass connection is inferred between them during this time period.

Both the location of an extended, pan-African and intra-continental lineament (upon which the Salado Basin nucleated according to Páengaro and Ramos, (2012) and the juncture of the Dom Feliciano and Damara fold belts are possible factors in the

Palaeozoic, pre-weakening of the specific area of crust (covered by the 3D dataset) in the offshore Uruguay margin. This helps in part to explain the anomalous crustal thinning over a short wavelength which is observed in this study (figure 4.14, 4.15) which becomes the triangular depression of the Mesozoic, Punta del Esté Basin. Figure 4.32 shows the likely paleo-geographic arrangement of tectonic features (in the area later to become the offshore margin of Uruguay) in the Palaeozoic, prior to Atlantic rifting and with the inferred positioning of a major pan-African lineament through the Gondwanan land surface (feature 1), situated along the southern boundary of the resistant RdP craton (feature 2). Transcurrent/extensional faulting is proposed to have already been in existence around the edges of the craton (Rapela et al., 2011).

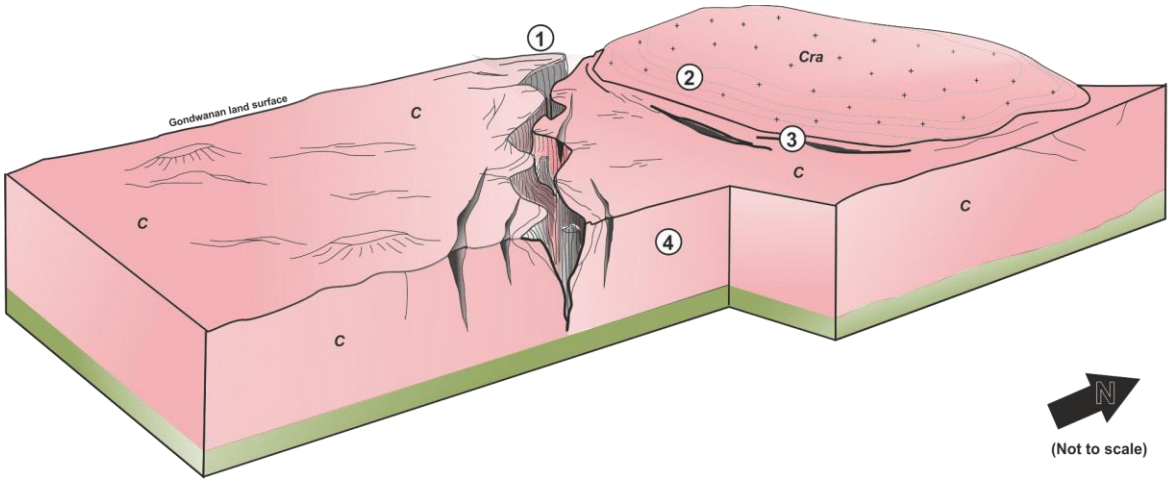

Figure 4.32: Proposed paleo-geography of the future offshore margin of Uruguay in the Palaeozoic with Kalahari craton not pictured (1) Proposed pre-rift major lineament through Gondwanan land surface (2) Rio de la Plata craton (3) Transcurrent faulting around the RdP craton (4) Thick continental crust.

Figure 4.33 presents a composite model of the arrangement of tectono-magmatic features in the syn-rift period of the offshore margin of Uruguay. A division has been made to highlight that the proximal region of the margin has predominantly pre-rift structures. An exception may be the southern side of the RdP craton where

extensional faulting within continental crust which has created fault-bound blocks of un-deformed pre-rift. Oceanward, there are the characteristic features of a syn-rift magmatic margin (i.e large SDR deposits in the north and south). Also notable is the complex region between the SDR of extensional faulting that has been labelled as new magmatic crust (see Chapter 5 for details). Stretched continental crust is found on the eastern continental shoulder in the form of extensional half-graben structures which are filled with syn-rift sediments. Also briefly noted is the occurrence of an anomalous region of exhumed mantle/proto-oceanic crust which is explored further in both chapters 5 and 6.

Composite model of tectono-magmatic features in the syn-rift offshore Uruguay margin

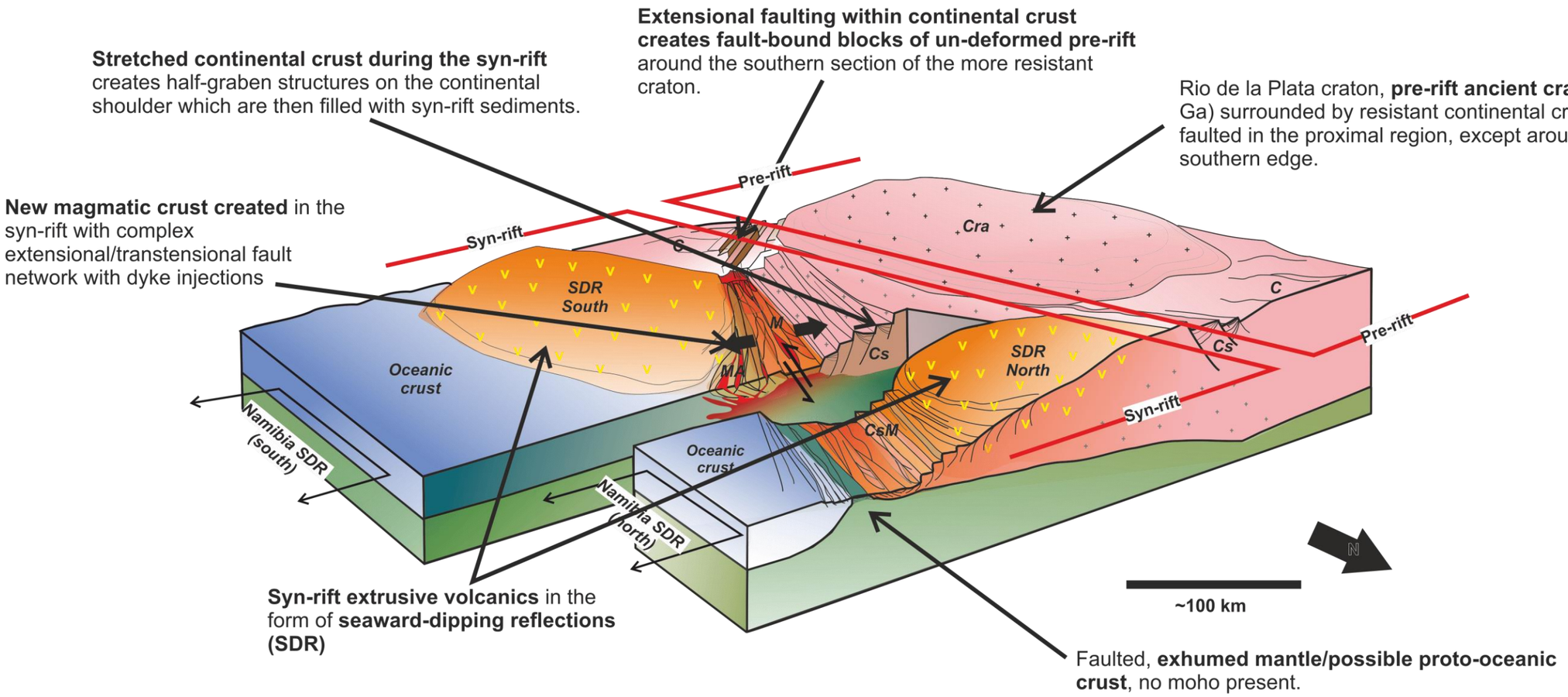

Figure 4.33: Composite model of tectono-magmatic features in the syn-rift period of offshore Uruguay.

4.8 Summary

This chapter has outlined the faulting which is observed from the ION SPAN dataset in the offshore Uruguay region. Major tectonic features have been identified, which include two major extensional faults (MEF-1 and MEF-2) which are regionally significant. Faulting has also been grouped into related domains, based upon fault trend, patterns of displacement and fault style. Anomalies in the fault domains were useful to determine the location of through-going features, although the wide line spacing of the dataset made this challenging. Fault orientations were adapted according to the presence of the regionally resistant RdP craton but were unable to be further constrained at this point, also due to line spacing. To understand the evolution of the margin from the pre-rift to the top syn-rift, depth mapping was undertaken in Petrel software of the ION SPAN PSDM reflection dataset to capture the top horizons of the Moho, top crust, top syn-rift and present day seabed. The intervals between these surfaces were also calculated as isopachs, determining the thickness and distribution of sediments (and volcanics) within different periods of the margins evolution. These showed that there is significant crustal thinning, identified by a raised Moho, in a v-shaped or triangular region of the margin which is also the area covered by the 3D dataset. Maps of the top crust horizon were created, showing there was a general NE-SW trending depocentre down the margin before rifting began. However, this is superseded in the area covered by the 3D dataset as much of this was later found to be syn-rift magmatic crust (therefore not time co-incident with the rest of the 2D top crustal map (see chapters 5 and 6). Syn-rift deposition infilled half-graben rift faults on the continental shoulder and has been affected by the creation of the triangular depocentre in the 3D data cube, which is consistent with the previously identified, Punta del Esté basin (Soto et al., 2011;

Hernández-Molina et al., 2016; Morales et al., 2017). Gravity and Emag data has been analysed and is useful in outlining structures which continue onshore and may also link to oceanic fracture zones. The major faults identified in the fault mapping are consistent with high-low boundaries within the gravity data and magnetic data which is unconstrained by crustal types. The large (~15 km) of post-rift deposits across the margin has meant that only a small increased thickness is visible to indicate the presence of the triangular Mesozoic depocentre of the Punta del Este Basin. This modern, present day margin also shows no evidence of earlier structures and the basement formation of the Punta del Esté Basin. Faulting across the 2D region is constrained to the syn-rift period, however the fault-bound blocks around the southern edge of the RdP craton may indicate the only area of pre-rift tectonics, although this is hard to date with this dataset. Other authors have suggested that this region may represent Jurassic aged faulting (Zambrano and Urien, 1970; Urien and Zambrano, 1973; Urien et al., 1981). The Rio de la Plata craton has played an enduring role throughout the region from the Neoproterozoic onwards. This is seen in both the localisation of tectonics around its boundaries (particularly the southern boundary) and with it acting as a buffer to northward-propagating Atlantic tectonics. This has essentially controlled the location of syn-rift deformation, channelling it into a funnel-shaped depocentre around the SE boundary of the craton, with the broader edge widening oceanward away from the eastern cratonic shoulder. Palaeozoic tectonics have played a role in the evolution of all similar geometry, South American Atlantic basins, such as the Colorado Basin, the Salado Basin and the San Jorge Basin - and it is likely this is also true here. They have enhanced zones of pre-existing weakness and crustal heterogeneities which date back to the Precambrian. Emag and Gravity data in this study suggests

that the tectonics of offshore Uruguay are also considerably related to those of northern Argentina. Firstly with the 2.1 Ga lineament that became the nucleating weakness for the Salado Basin, which may be the same as the MEF-2 lineament, adding further evidence that ancient, pre-rift weaknesses have set up the foundations of both the Mesozoic, Salado Basin and Punta del Esté Basin, likely along the same pan-African lineament. The following chapter will add significantly more information on the syn-rift evolution of the anomalously thinned crustal region that is highlighted in the 2D dataset. This will include much more on the ratio and relationship between magmatics and tectonics during early rifting.

Chapter 5: 3D dataset: New insights into a magmatic plumbing system on the continent-ocean boundary.

5.1 Introduction and rationale

In the previous chapter, the large-scale 2D crustal architecture of the margin was determined. It showed anomalous and unexpected, crustal thickness variations that were oblique to the margin. In this chapter this region of anomalous crust is investigated in greater detail using a 3D data cube, provided by ANCAP/Shell and located within the 2D data grid (figure 5.1). The 3D dataset captures the northern section of the SDR South, the southern section of the SDR North and the structural transfer region between them. The major regional structures interpreted as the MEF-1 and the MEF-2 have been highlighted by the 2D dataset in the previous chapter and run through the area covered by the 3D dataset. The 3D dataset is the first known 3D seismic reflection survey across a transfer zone. This chapter will provide a detailed view of complex, transtensional tectonics and syn-rift magmatics which are previously unrecognised in offshore Uruguay and likely, globally. A detailed study of the interactions between syn-rift magmatism and the transfer system give new insights into the early stages of SDR extrusion, faulting and a magmatic conduit system sourced from the upper mantle.

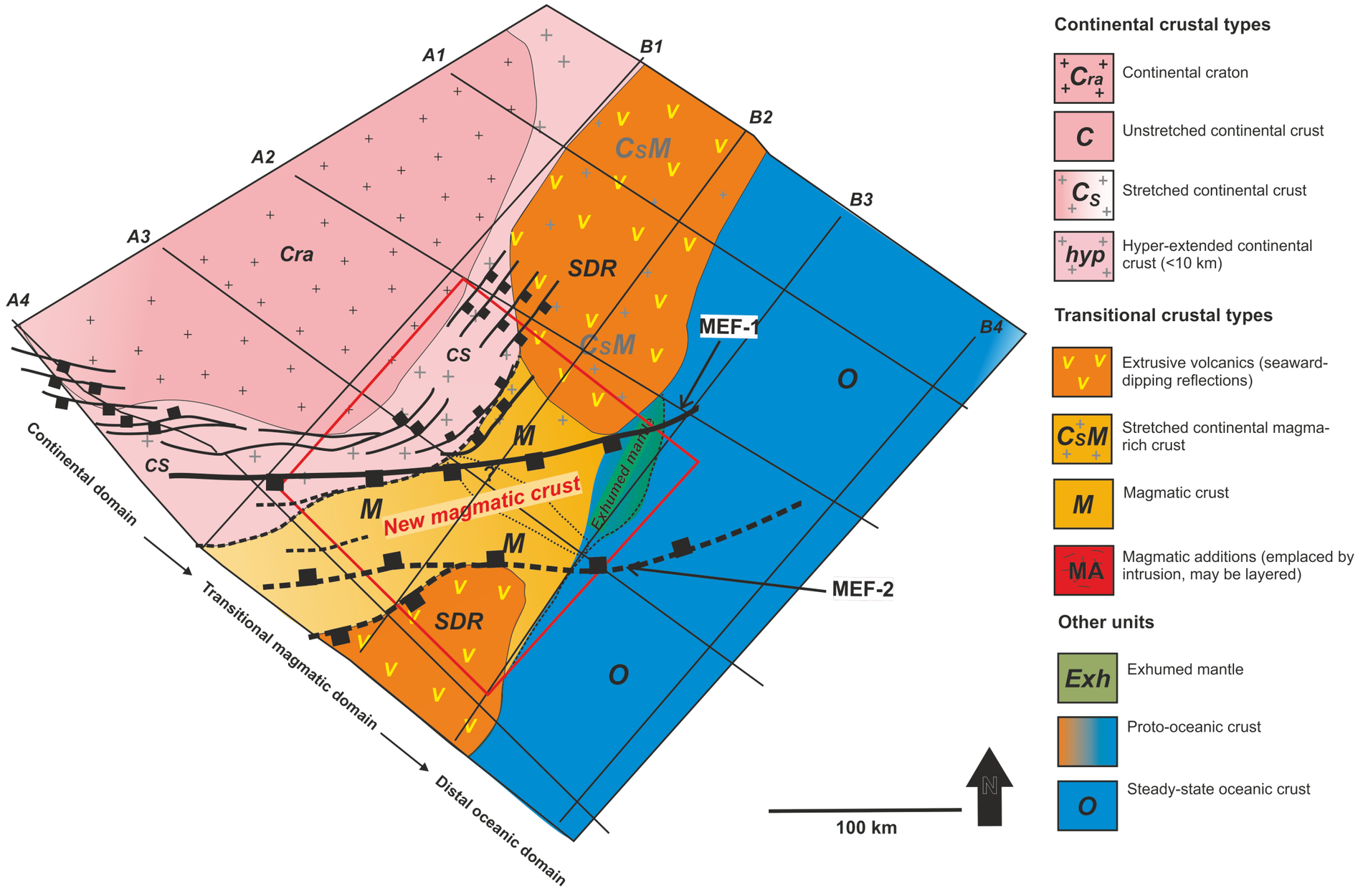

Figure 5.1: Map of the offshore Uruguay region showing crustal type distribution and major structural features recognised in the 2D dataset. Red outline denotes the 3D PSDM cube within a section of the 2D dataset, provided by ANCAP/Shell.

The data covers an area which has been previously identified as the Rio de la Plata transfer system by (Soto et al., 2011) which is shown in figure 5.2. The yellow dashed region (in figure 5.2), shows the uncertainty of the underlying crust type throughout the zone defined as the RPTS, due to a lack of data coverage in 2011. This study is the first to investigate the region utilising a high resolution 3D dataset. The 3D, PSDM seismic reflection dataset has been provided by ANCAP/Shell and was shot within the regional ION SPAN 2D dataset grid, to allow a detailed examination of the petroleum potential of the offshore margin. The previous chapter has built a regional picture of the architecture and evolution of the basement in the Uruguay offshore margin using a 2D dataset. This chapter expands upon our large-scale understanding of the margin by focusing upon a smaller region in greater detail. This is achieved through the use of a 3D data cube that helps to constrain the nature of the basement and to further investigations into the inter-relationship between tectonics and magmatism. The aims of this chapter are to address the following; to characterise the transitional zone across the offshore margin, to explore the relationship and transition between inherited continental crust and new, Penrose oceanic crust (one of the last major unsolved problems in plate tectonics) (Gillard et al., 2017). This chapter also seeks to determine the detailed characteristics of a complex, margin-oblique, transfer zone on a magmatic margin, the first known study to do so using a 3D dataset. The following chapter also aims to characterise the relationship of structures and magmatism in the syn-rift period and how this relates to the early formation of seaward-dipping reflections and transitional crust before the establishment of ‘steady-state’, oceanic crust.

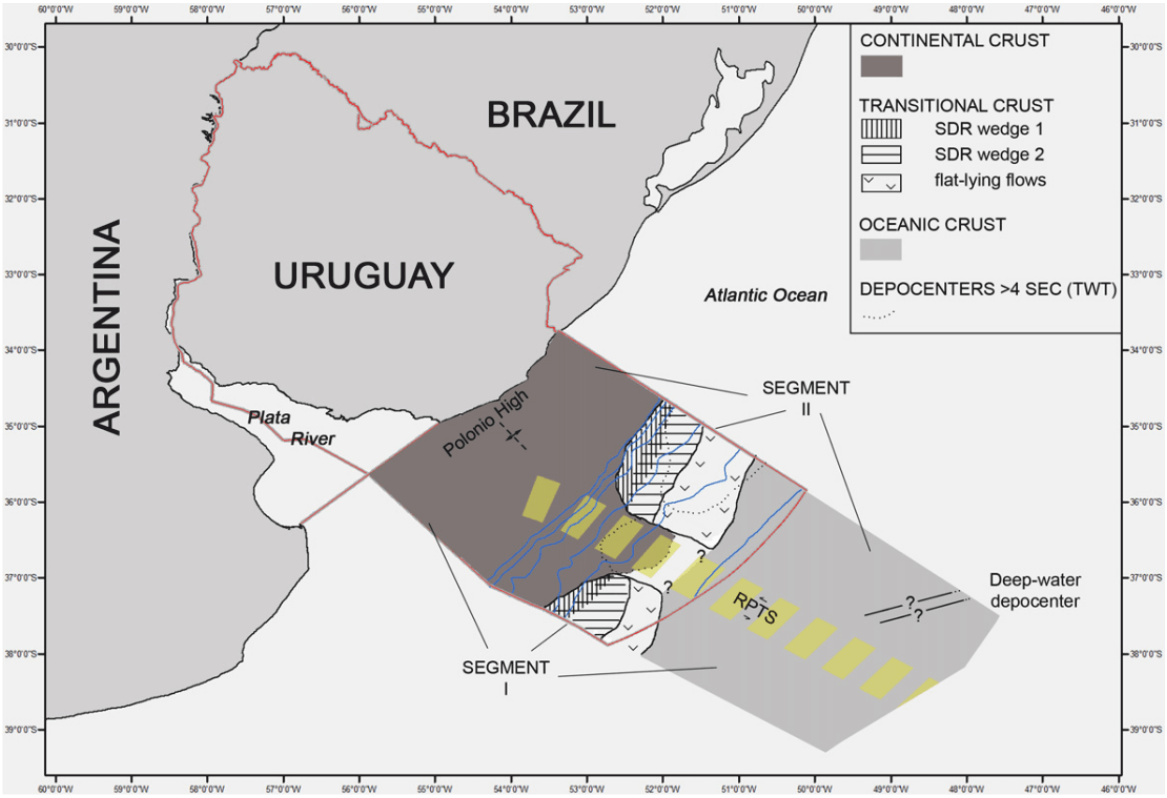

Figure 5.2: Map of crustal types and major features in the offshore region of Uruguay (Soto et al., 2011). Yellow zone and question marks reflect the uncertainty of the underlying crust in 2011, through the RPTS zone due to poor data coverage.

5.2 Data and methodology

The 3D dataset covers an area of 10,314^2 km and was shot to fit within the ION SPAN 2D dataset. It records to a depth of ~15 km whereby the data was provided with a base mute. It was shot in two parts in 2013-2014 by ANCAP and provided originally by BG Group (now Shell). Further details on the acquisition and processing parameters were not available. All Inline sections are presented SW-NE and all X-line sections are shown NW-SE. An uninterpreted example of a cross-line (X-line) is shown in figure 5.3 (A) from the 3D dataset, which is perpendicular to the present day margin (see inset map for detailed line location). Figure 5.4 presents an uninterpreted Inline section which runs parallel to the margin. Crustal types and horizons are those recognised in the 2D dataset (see key at the base of figures 5.4 and 5.5). Major features of the X-line section are a proximal structural high on the

left of the section of continental crust which transitions over ~15 km into very thin, transitional crust in the centre of the line. The edge of the continental crust has been interpreted as a sharp transition over < 1km and delineated by the end of the flat-topped horst (see figure 5.4 (C). Seaward-dipping reflections (SDR) are notable on the right of the section with their distinguishing, convex-up, high amplitude dipping reflections. Figure 5.4 (A) shows an example Inline section from the ANCAP/Shell 3D PSDM dataset (see inset map for line location). Figure 5.4 (B) shows an interpreted section of (A) showing the major crustal types and horizons. Major features are the SDR packages to the left of section that are vertically faulted, as well as an area of magmatic crust which covers the rest of the section, no Moho is observed due to the base mute of the data. Above the magmatic crust is a region of syn-rift lava flows and extrusive volcanics which are succeeded by a sequence of more stratified, syn-rift sediments. When interpreting the 3D dataset, the seismic facies recorded from the 2D dataset have been used. However, there are some differences and additional seismic facies which have been observed that are noted in Table 12.

Table 12: Additional key seismic facies noted from the 3D dataset.

Crustal type	Seismic facies	Key reflection relationships	Reflection characteristics	Seismic Facies Association
SDR	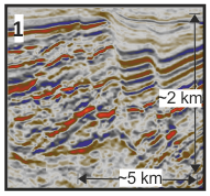	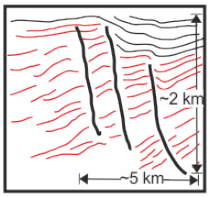	**1** High amplitude, discontinuous reflections, punctuated by extensional faults and overlain by mid-low amplitude reflections with a sag geometry.	Volcanic extrusive packages with extensional faults.
SDR	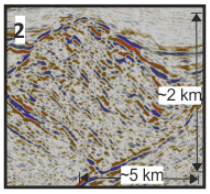	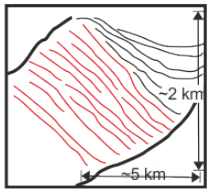	**2** Mid-high amplitude, partially continuous, parallel reflections in a package of a continuous thickness. Overlain by divergent mid-high amplitude reflections.	Volcanic extrusive packages rotated by a syn-rift extensional fault.
MA	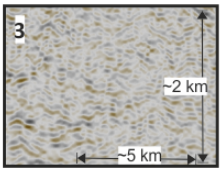	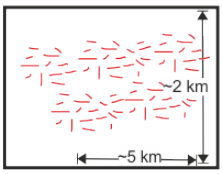	**3** Low amplitude, chaotic and discontinuous reflections with no internal structures, distinct and in contrast to surrounding reflections	Volcanic intrusives sitting adjacent to fault.
CSM MA	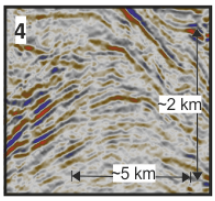	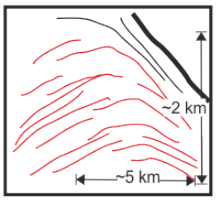	**4** Mid-high amplitude curved reflections forming a domed structure (at depth) only found directly adjacent to large extensional fault.	Magmatic addition/intrusives or inherited compressional fabric.
Volc	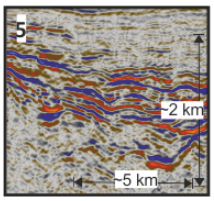	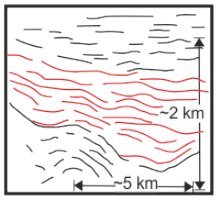	**5** High amplitude parallel reflections, partially continuous, lying in topographic lows or adjacent to pre-rift horst structures.	Syn-rift extrusive volcanics, infilling pre-rift topographic lows.
O	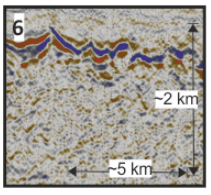	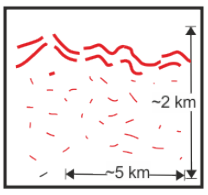	**6** High amplitude discontinuous reflections (1-3 reflections) with a base section of low amplitude, chaotic and discontinuous reflections.	Oceanic crust.

5.2.1 Horizon mapping

The discontinuous nature of basement reflections is an inherent challenge to interpretation on a magmatic margin. Horizon mapping was undertaken in Petrel software ©Schlumberger and included the horizons noted in Table 13. Manual picking was the only form of horizon interpretation which could be employed due to the highly discontinuous nature of the majority of the top reflections of seismic facies. The distinct changes between the internal nature of the seismic facies and the amplitude and continuity of reflections allowed for a higher degree of confidence in picking horizon boundaries than might otherwise be obtained when using a manual picking process. The more continuous nature of the top syn-rift reflection meant that the guided auto-tracking feature could be employed on this horizon, however, in places, this boundary was also indistinct due to the downlap of early post-rift turbidites/contourites. Initially, a ‘top pre-rift’ surface was the primary horizon mapping objective, however, the presence of the SDR also meant that any true, ‘top pre-rift’ surface would lie beneath these, obscured or erased by syn-rift extrusives - a common problem with magmatic margins. This made the picking of a true ‘top pre-rift’ at best, subjective. Also noted was that the true depth of the full SDR wedges was unlikely to be reached within the ~15 km depth of data, covered by the 3D cube. The Moho was identified through the 2D dataset as shallowing significantly in this region. High amplitude reflections at the very base of lines within the 3D dataset are identified as the Moho. This identification can be confirmed by the comparison of a 3D line against a similar positioned line from the 2D dataset (figure 5.3).

Table 13: Horizons mapped in the 3D dataset with defining criteria and characteristics.

Interpreted horizon	Colour	Defining criteria & characteristics	Interpretation	Crust type	Domain
Moho	Red	Lowest high amplitude reflections, sub-continuous, convex-up, below top magmatic crust.	Manual pick only	–	–
Top continental crust	Dark grey	Largely continous, high amplitude reflection/s, above continental seismic facies, below post-rift sediments. Often observed as a flat-topped horst directly abutting magmatic crust. May also be observed at the base of syn-rift half-graben structures.	Manual pick only	Continental crust	Proximal (stretched)
Top magmatic crust	Magenta	Discontinous, chaotic, mid-high amplitude reflection/s, above magmatic seismic facies, below syn-rift lava flows and syn-rift sediments. Highly irregular horizon, may be discernable by contrasting relationship to surrounding facies.	Manual pick only	Transitional crust	Transitional
Top SDR	Yellow	High amplitude, discontinous reflection/s, immediately above SDR seismic facies with convex-up, dipping reflections. May be highly irregular with variable heights due to faulting.	Manual pick only	Transitional crust	Transitional
Top lava flow (intra syn-rift)	Green (dashed)	High to very-high amplitude, sub-continous reflection/s, immediately above a package of high amplitude, continous reflections. Infills topographic low regions and onlaps magmatic crust but is discernable from it due to very high amplitude, continuous reflections. May have an atypical surface geometry ajacent to volcanic vents due to high viscosity at time of emplacement and subsequent movement of underlying magmatic features. (i.e may appear to bulge into upper syn-rift sediments above).	Manual pick only	Transitional crust	Transitional
Top syn-rift	Blue	Mid-amplitude, largely continuous reflection, onlaps continental crust or magmatic crust, above stratified syn-rift sediments and SDR packages. May be difficult to interpret in places due to reflection merges with early post-rift contourite features.	Guided auto-pick	Transitional crust	Transitional
Seabed	Black				

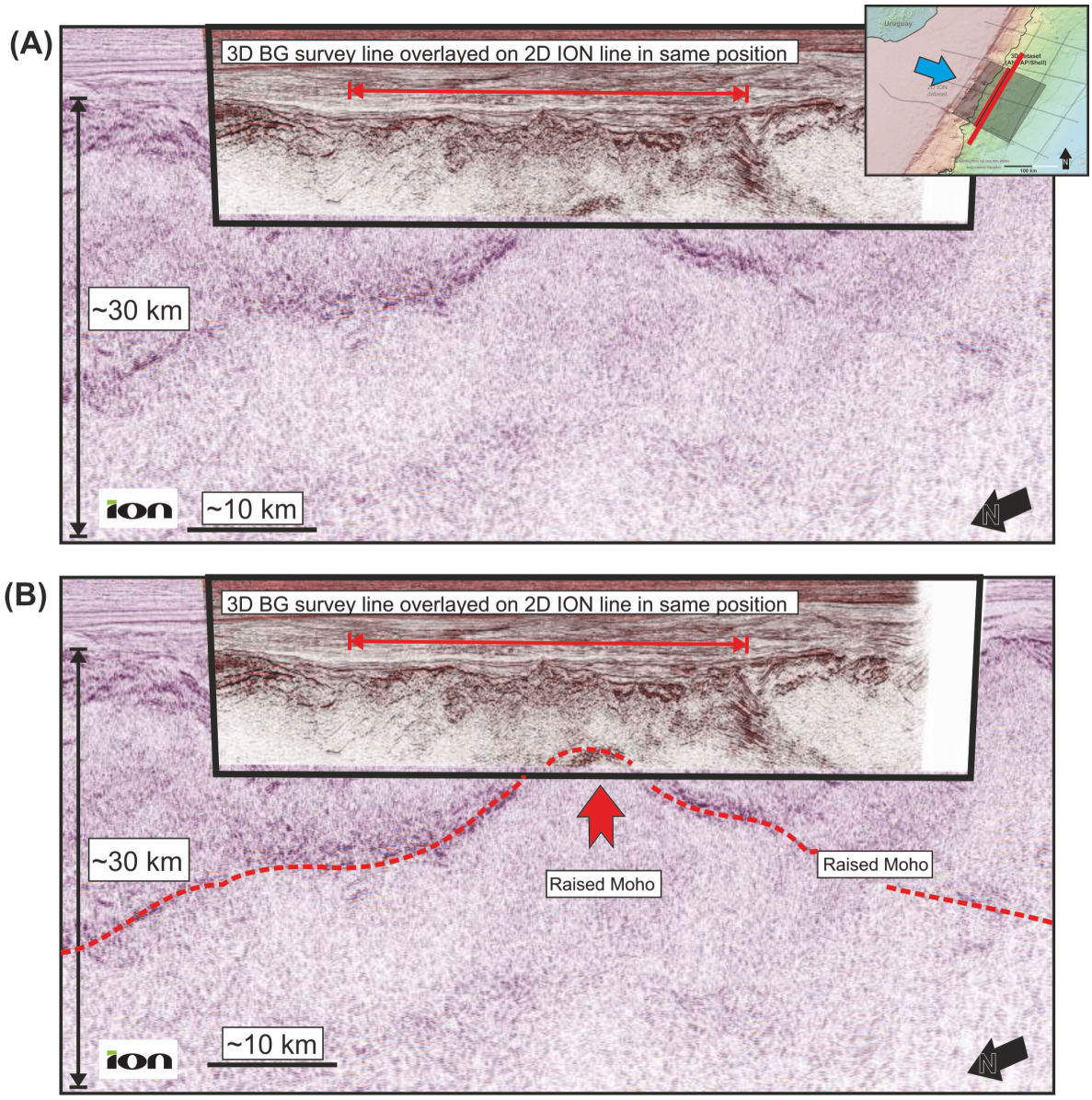

Figure 5.3: (A) 3D ANCAP/BG Group line overlain on the same position line within the 2D ION SPAN dataset. (B) Comparison of both the 3D line and 2D line show that the high amplitude reflections at the base of some of the 3D data profiles are likely to correspond to the Moho. Both lines are oriented SW-NE (see inset map).

Figure 5.4 and figure 5.5 show example X-line (figure 4) and Inline (figure 5.5) PSDM seismic reflection sections from the 3D data cube (ANCAP/Shell) at x3 vertical exaggeration. These are shown uninterpreted in (A), with the major horizons identified in (B) and the crustal types along with the key horizons in (C).

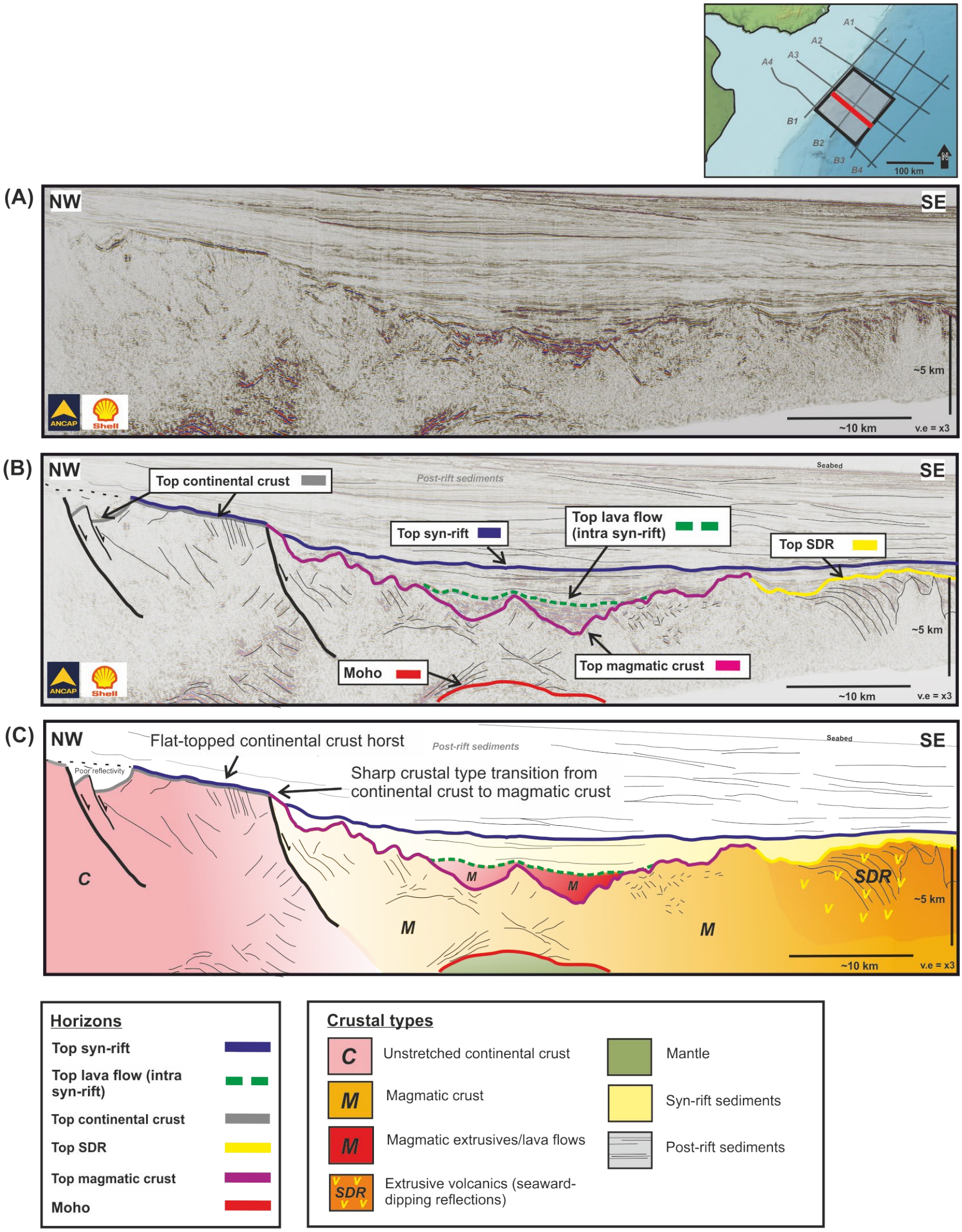

Figure 5.4: (A) Uninterpreted example X-line section from the BG/ANCAP 3D PSDM dataset (see inset map for line location) (B) Interpreted section of (A) showing the mapped horizons. (C) The key crustal types and major, mapped horizons of (A).

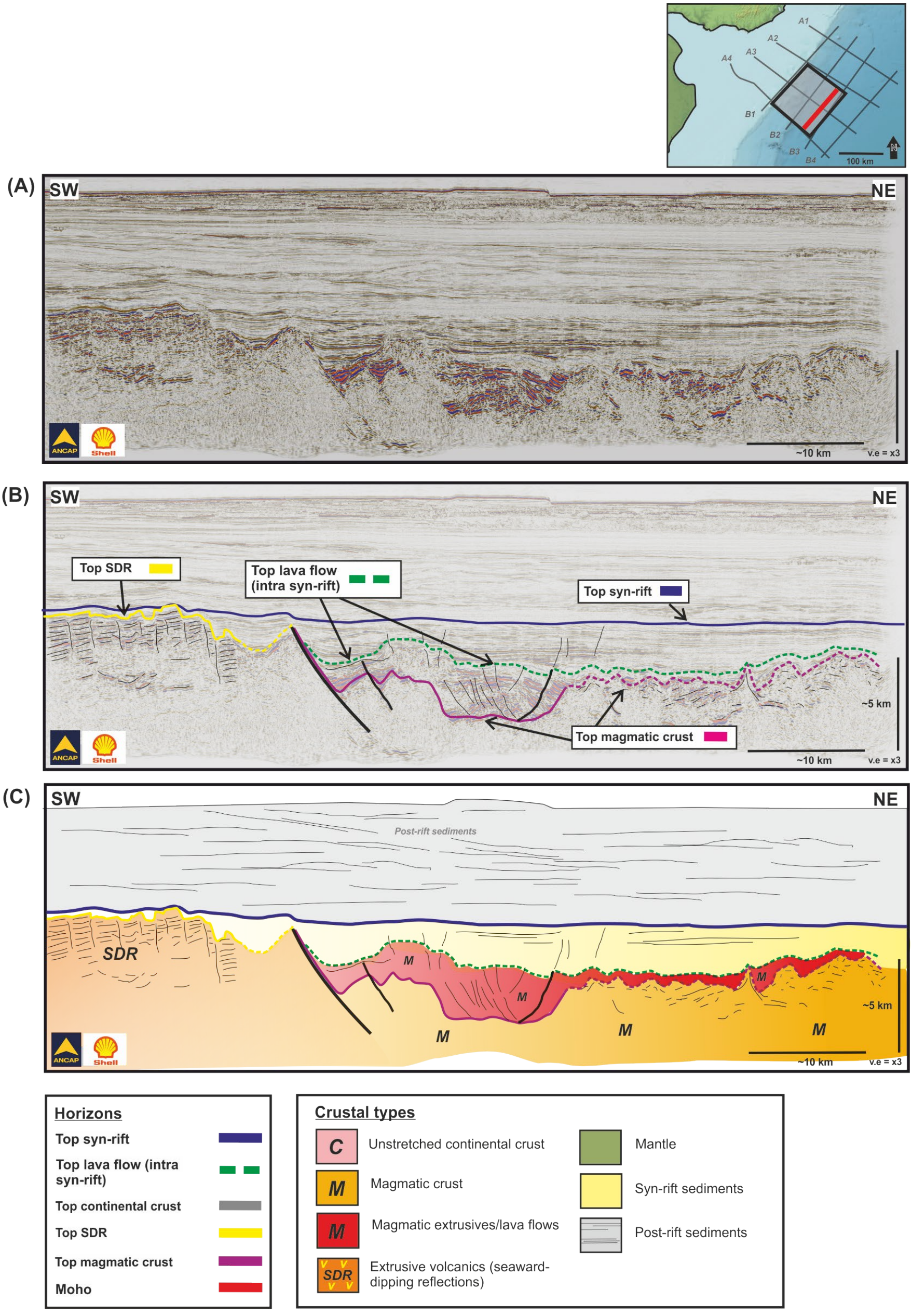

Figure 5.5: (A) Example Inline section from the BG/ANCAP 3D PSDM dataset (see inset map for line location) (B) Interpreted section of (A) showing the mapped horizons. (C) The key crustal types and major mapped horizons of (A).

5.2.2 Fault mapping

Figure 5.6 shows an enhanced view of the major faults that have been previously mapped in the 2D dataset, which run through the 3D dataset region. This includes the two major extensional faults, MEF-1 and MEF-2 as well as NE-SW trending extensional faults on the edge of the stretched continental crust and into the northern package of SDRs.

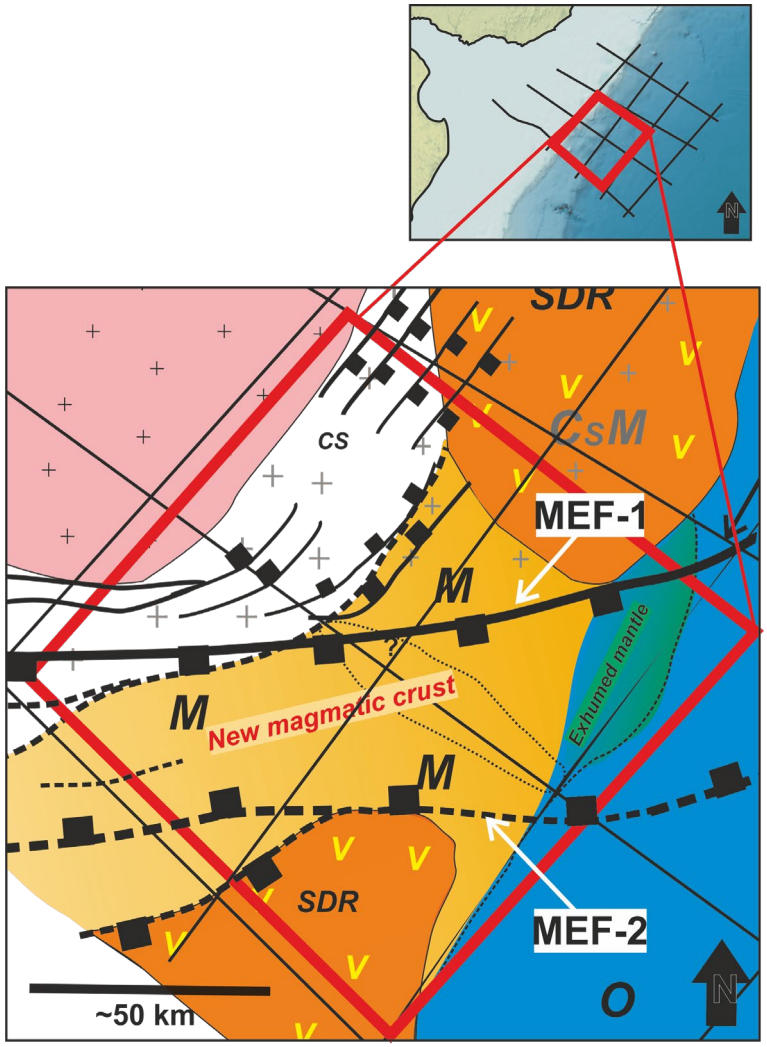

Figure 5.6: Enhanced view of the major structures mapped in the 2D dataset which are expected to be observed in the 3D dataset. These include the two major extensional faults MEF-1 and MEF-2 as well as NE-SW trending extensional faults on the edge of stretched continental crust and into SDR North.

The major through-going faults which were identified on the 2D dataset are less easily recognised on many of the Inline and X-line profiles of the 3D dataset. This is

partially due to the 3D data only capturing the top 15 km of the subsurface such that the whole-crustal nature of the faults cannot be seen and the complex and inter-related faulting, along with both intrusive and extrusive volcanics, has obscured the track of the major faults within highly volcanic intervals. However, when studying depth sections (Z-slices), these faults become more readily identified. Fault mapping was initially attempted using a traditional mapping approach of fault stick production, using Petrel software ©Schlumberger with a view to creating a fault model. However, connecting and tracing these faults quickly became difficult, especially within the confines of the software. Depth section mapping was instead used in order to capture the detail of the complex fault kinematics and their interactions with magmatism. The Petrel software is not designed to accommodate complex structures, which may show transtension, reidal shear and the switching of faults dips along singular fault planes. This complex fault system is also only present in a discreet interval at the lowest limit of the recorded data. Trace mapping of the intersection of fault planes with a depth sections (z-slices) was used at a variety of depths, within this interval. These were taken within a sequence of 438 m (figure 5.7) between depths of -10,020 metres and -10,458 metres. This allows for the visualisation of early syn-rift structures and volcanics before the overprint of the majority of late syn-rift sediments. Slices were taken depending on which best visually captured different sections in terms of; faulting, high-amplitude areas, transparent circular areas and through-going structures. The (unrelated) thick, post-rift sediment overburden is also omitted at this depth. Depth section mapping was then combined with detailed mapping of the volcanics, based upon seismic reflection characteristics and seismic facies.

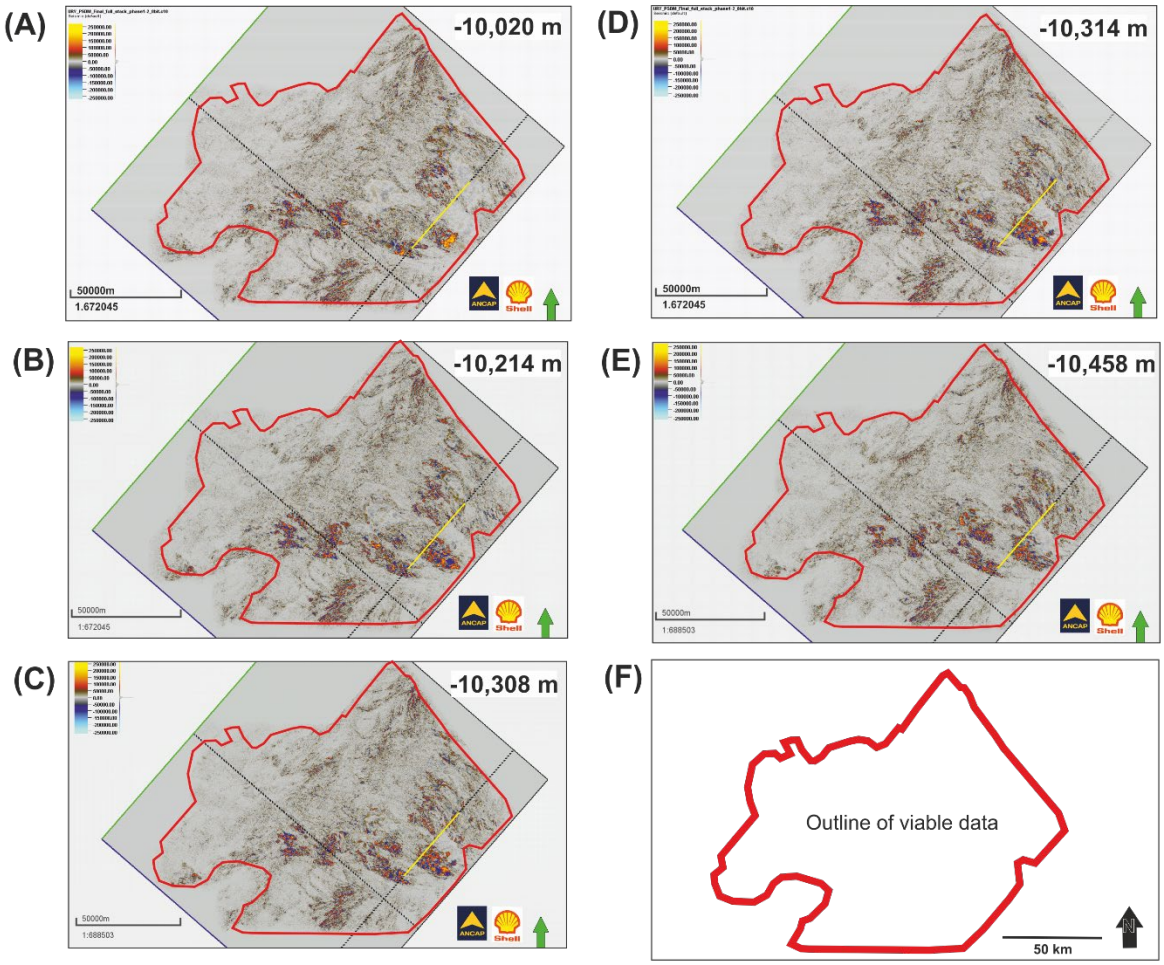

Figure 5.7: Depth-slice (Z) sections used in this chapter to capture the complex volcano-tectonic arrangement and major structures of the volcanic basement. (A) -10,020 m (B) -10,214 m (C) -10,308 m (D) -10,314 m (E) -10,458 m (F) Outline of viable/useable data across the 3D dataset.

Figure 8 shows a 3D view from above of a depth slice section at -10,458 m and its intersection with Inline and Cross-line seismic profiles. Also noted are some of the major features such as the two major extensional faults, MEF-1 and MEF-2 which are recognised as through-going structures from the 2D dataset.

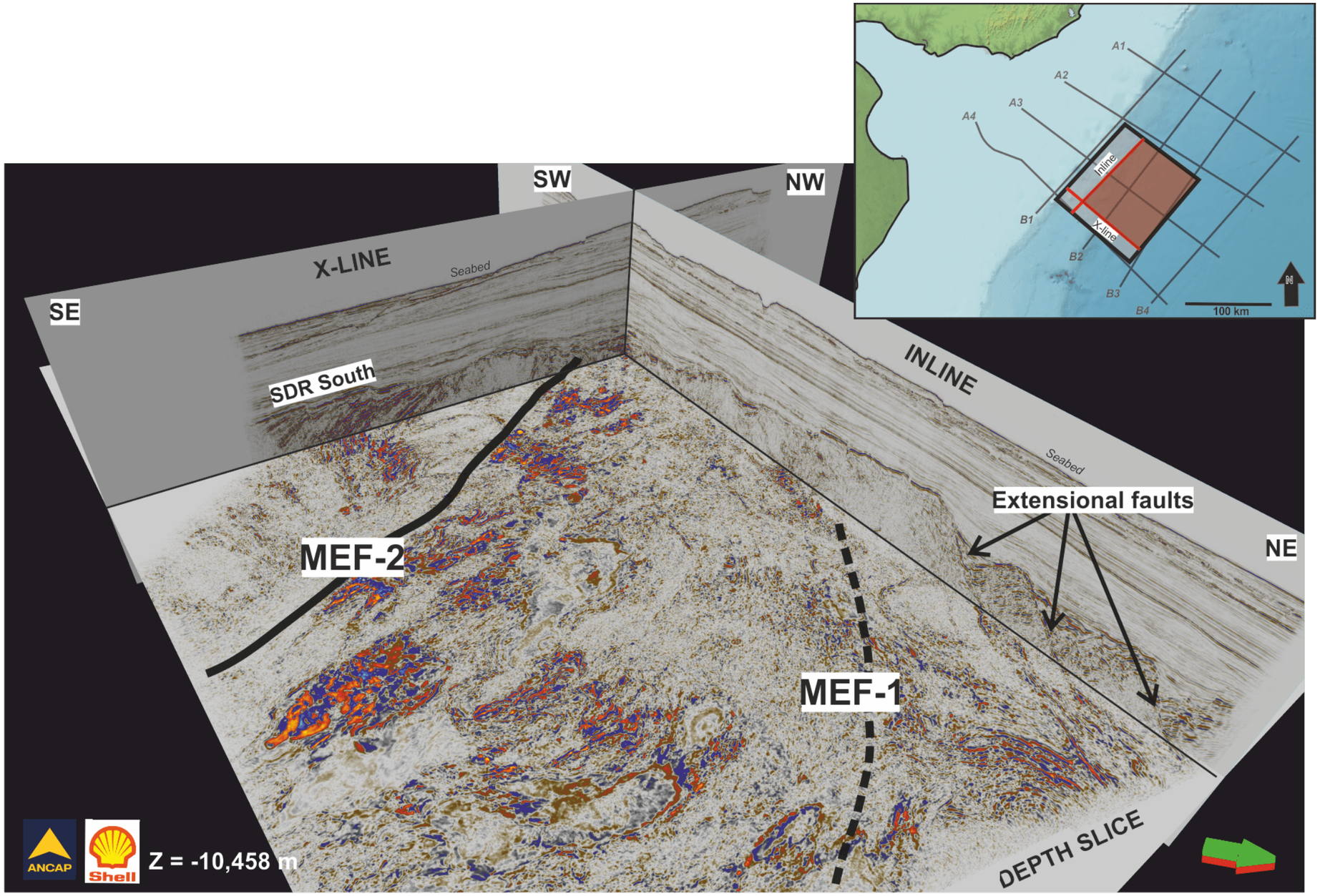

Figure 5.8: View from above of depth slice -10,458 metres and the intersection with X-line and Inline profiles of the 3D dataset. Also shown are the major extensional faults, MEF-1 and MEF-2, other extensional faults and the SDR South.

5.3 Data insights

5.3.1 Pre-rift strata in the 3D dataset

The majority of the proximal region of the 2D dataset has been shown to comprise ancient continental craton or continental crust. The 3D dataset allows further insight into the character of this region of the crust. Figure 5.9 (A) (i) shows to the left of the section, a resistant horst of pre-rift continental crust, onto which the top syn-rift horizon onlaps. In (A) (ii), the interpreted horizons are shown along with the abrupt transition from continental seismic facies into magmatic facies. This is characterised by a reversal in dip direction of internal reflections that is indicative of this boundary relationship. Figure 5.9 (B) (ii) shows another line section of a pre-rift continental crust with a flat-topped horst structure which is extensionally faulted. Figure 5.9 (C) shows a long wavelength fold structure at depth within the pre-rift. It is proposed that this structural compression has its origin in a Palaeozoic, Gondwanan fold and thrust belt, similar to those seen to the south in the Argentinian offshore.

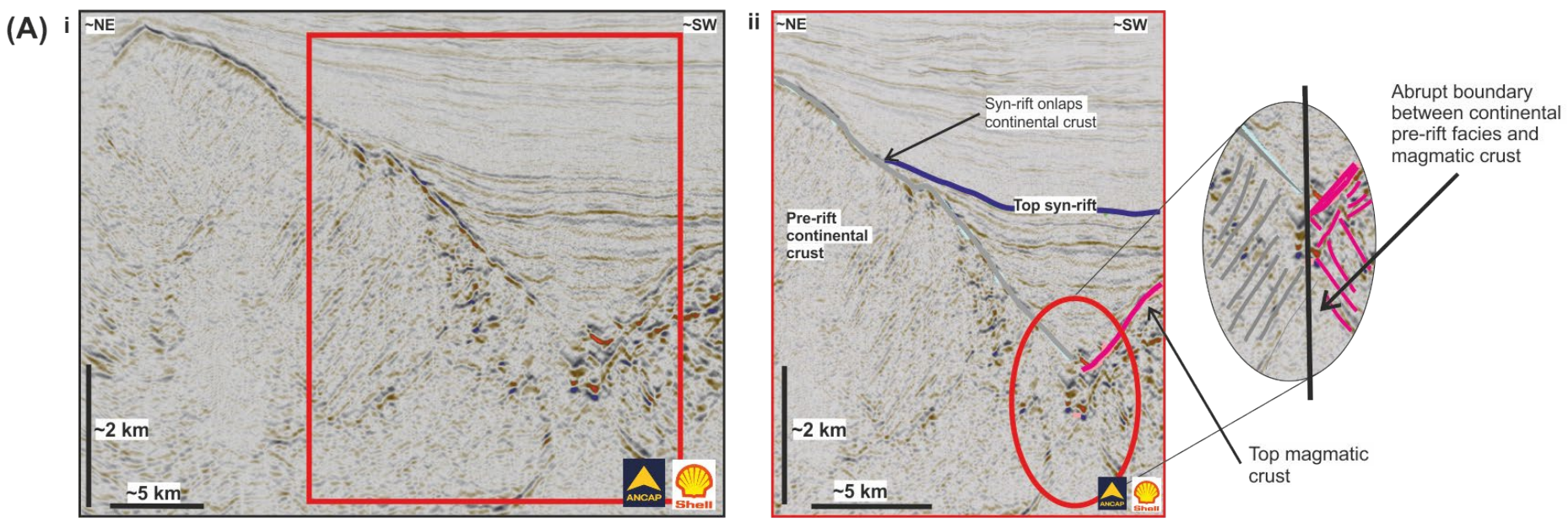

Figure 5.9: (A) (i) Pre-rift seismic facies within an uninterpreted section of a PSDM X-line of the 3D dataset (ANCAP/Shell) Red box denotes area of (ii). (A) (ii) Interpreted section of (Ai) showing a pre-rift horst of continental crust with onlapping syn-rift sediments. Note, abrupt boundary between continental seismic facies and magmatic facies. (B) (i) Section of an Inline showing a resistant horst of pre-rift continental crust. (ii) Interpretation of major features of (B (i). (C) Uninterpreted X-line section showing pre-rift compression at the base of continental crust.

5.4 Identification and mapping of a complex, transtensional fault system

The major structures of the 3D dataset were interpreted in plan-view using the identification of seismic reflection terminations and reflection morphology as well as variations in seismic reflection amplitudes. A combination approach of constraining major features with those observed on the 2D ION SPAN dataset was undertaken, as well as in Inline, X-line or depth section in the 3D dataset. The first task was to create a plan-view map of the major structural features of the region, for which a depth slice section was used. Figure 5.10 shows the division of the major crustal types across the 3D dataset, along with the major structures. There are two primary through-going faults that were recognised in the 2D dataset and have been labelled MEF-1 (Major Extensional Fault 1) and MEF-2 (Major Extensional Fault 2). The exact path of MEF-1 especially, is uncertain due to a high degree of over-printing from volcanic intrusions (figure 5.10, feature 3). The more detailed 3D dataset allows us to observe a zone of en-echelon segments between these faults, indicative of strike-slip or transtensional tectonics (figure 5.10, feature 10).

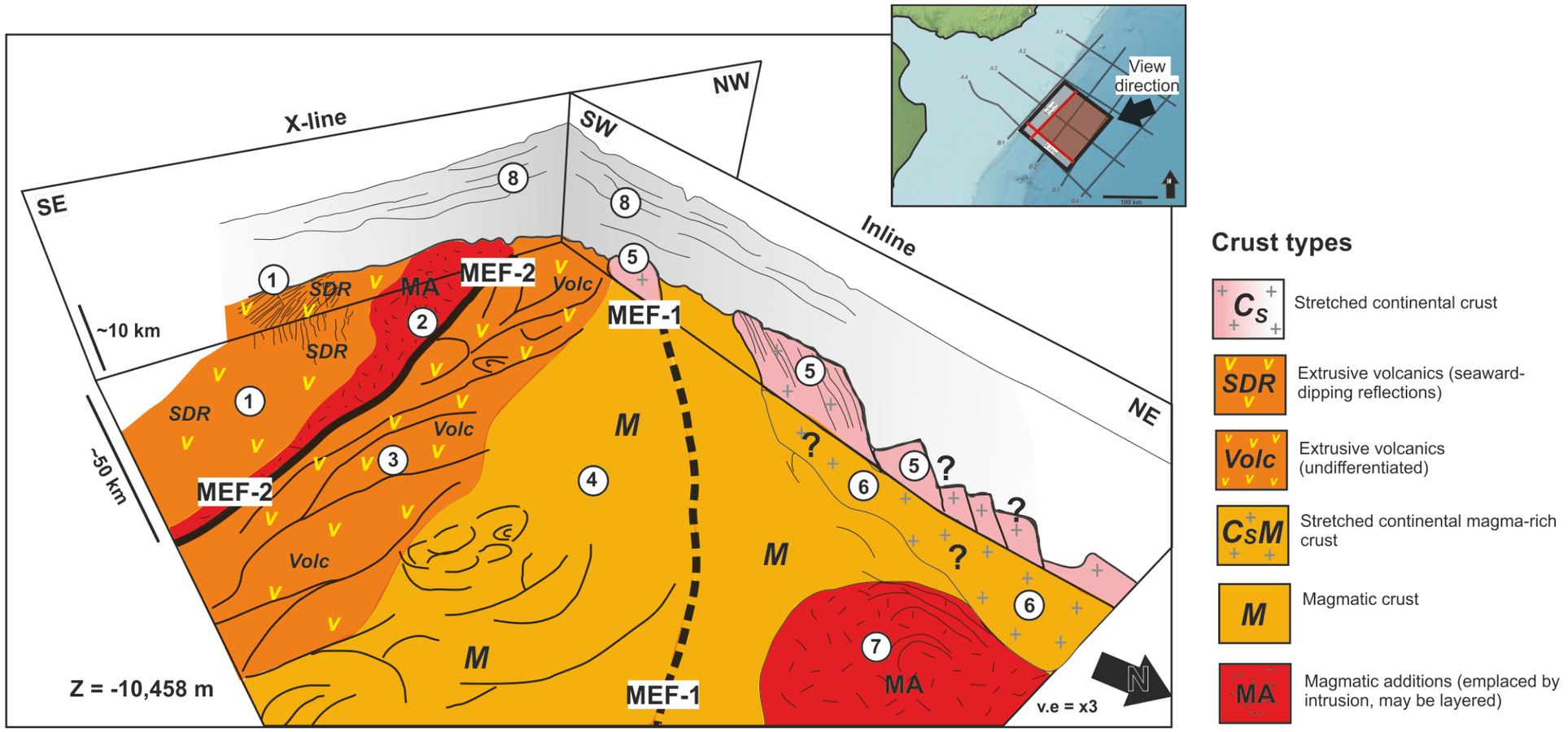

Figure 5.10: Map following from figure 8 of major volcano-tectonic domains identified in the 3D dataset (ANCAP/Shell) using Inline, X-line and depth sections (Z=-10,485 km). (1) SDR South packages, showing both typical convex-up, seaward-dipping reflections and horizontal striped reflections in depth section (2) Transparent reflection area interpreted as magmatic additions/intrusions (3) Area of high amplitudes in an en-echelon arrangement and fault-bound by curvilinear fault plane traces – transtensional faults? (4) Transitional, magmatic crust (5) Remnant blocks of pre-rift continental crust (6) Stretched and intruded magma-rich, continental crust, related to (5). (7) Circular area of volcanic intrusives (8) Post-rift passive margin sediments.

5.4.1 Faulting in the 3D dataset

Faulting in the 3D dataset is based upon the crust type and its rheological properties. Figure 5.11 shows an arbitrary line section from the 3D dataset from SSE to the NNW that illustrates the majority of faulting styles across the cube. Figure 5.11 (A) is an uninterpreted section, section (B) shows a brief interpretation of (A) with a table noting faulting characteristics according to crustal types. All faulting dips to the north on this line and shows, from the SSE, near vertical high-angle extensional faulting through the packages of the SDR South. Immediately to the north, the style of faulting changes into listric faults with a common basal decollément. This decollément becomes clearer towards the centre of the section and is interpreted as the Moho (this is due to basal high amplitude reflections that can be constrained against the position of the Moho in the 2D dataset). Listric detachment faulting continues throughout the magmatic crust until the substrate becomes more rigid within regions of stretched continental crust, whereby faulting becomes planar with ~60^{o} normal faulting. This continues into the horst block in the NNW which also has a 'striped' seismic reflection characteristic, diagnostic of the pre-rift continental crust. Faulting is almost entirely confined to the pre-rift and syn-rift sequences, the only exception being the infiltration of early post-rift sediments by some volcanic vents which remained active into this period (see figure 5.22, section 5.5.2).

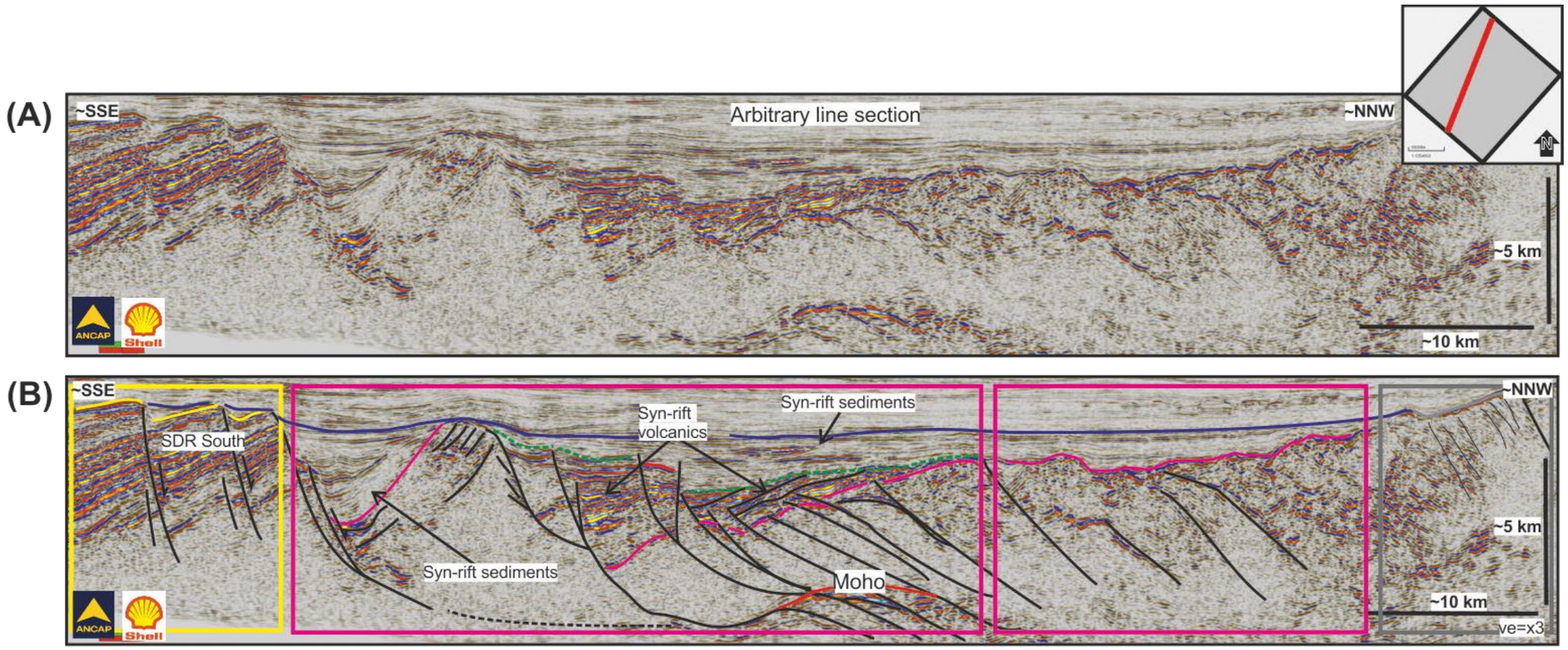

Faulted crust type	Faulted SDR	Faulted, thinned magmatic crust	Faulted stretched continental (?)/magma rich crust	Pre-rift continental crust
Fault characteristics	High-angle, near vertical, extensional faults	Detachment faulting with listric faults decolling onto the Moho/rheologically weaker boundary	Normal faulting without listric decollement	High angle extensional faulting with planar fault planes

Figure 5.11: (A) Uninterpreted, arbitrary line section ~SSE-~NNW (see inset map for location) (B) Interpreted section of (B) showing a variety of faulting styles across the 3D dataset. Below image: table showing the relationship of crustal types to the faulting characteristics.

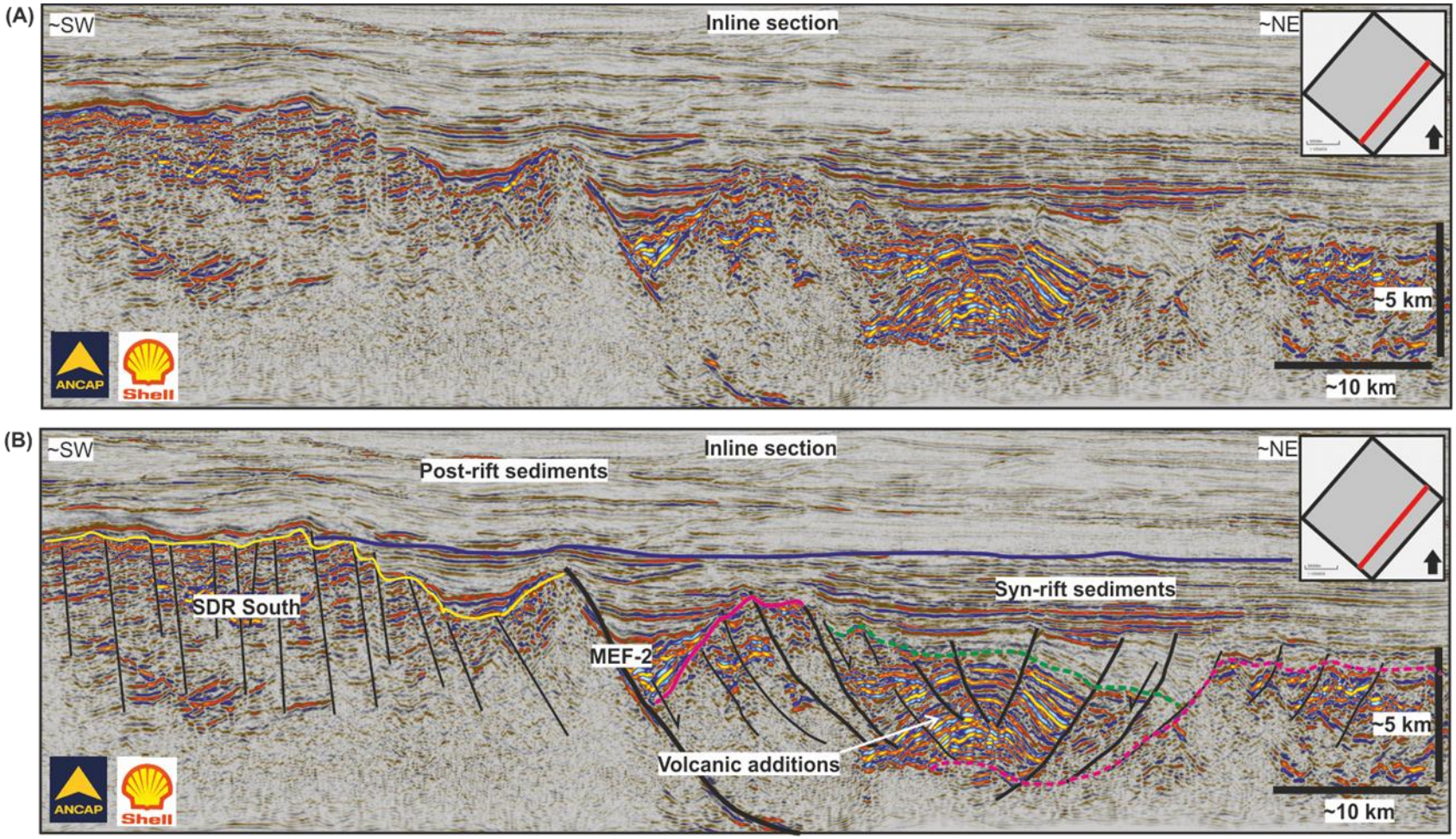

Figure 5.12: (A) Uninterpreted Inline seismic reflection profile from the 3D dataset. (B) Interpreted section of (A) showing the SDR South to the left of the section and a region of central faulting through high amplitude basement reflections.

5.4.2 Strike-slip and transtensional faulting

A Strike-slip element to the basement faulting was identified through Inline sections such as figure 5.12, which showed an apparent, ‘flower-structure’ of faulting through high amplitude reflections at the lowest basement depth. This was confirmed by depth section analysis which showed a variety of diagnostic features of strike-slip tectonics. These included, in map view, an extensional duplex and leading extensional imbricate fan (figure 5.13, A, B, C). Despite initial interpretation suggesting a compressive element (the positive flower structure on figure 5.12) this was later determined, through depth section analysis, to actually be primarily transtensional. The high amplitude reflections which were considered to be volcanic in nature are also bound by these transtensional faults, which proved complex to map due to their anastomosing geometries throughout the 3D dataset. This is why the depth sections were invaluable in discovering the complexity and style of faulting across the cube. Figure 5.14 shows two of the processes used, whereby various depth sections and an RMS Amplitude attribute map were both used to discern different areas of structure, with a simplified, final structure map shown in Figure 5.14, section F. Figure 5.15 identifies two orientations of faulting, highlighted using an RMS Amplitude attribute overlay on an early version of a top magmatic crust surface. Yellow highlights the trend of inherited structures, blue shows the transtension direction and red shows the post-SDR, N-S extension. Feature 1 highlights the curvilinear faulting that affects the southern section of the northern SDR. Feature 2 shows extremely curved faulting within the northern section of the pull-apart system. Feature 3 shows the Major Extensional Fault 2, (MEF-2) which is also subject to extreme curvature through the dataset. Figure 5.15 (C) Red,

highlights the high amplitudes which are interpreted to be intrusive volcanics, these primarily follow the inheritance structural trend and are contained within the en-echelon fault-bound segments of the transtensional pull-apart system. Figure 5.16 shows another style of faulting, which is present through the central area of an arbitrary line trending SSW-NNE. This extensional, ‘domino-style’, or rotational block faulting, is indicative of upper-lithospheric extension through more brittle regions of crust. This style may also be linked to the ascension of more ductile lower crust. It is often seen at metamorphic core complexes and can occur on both continental and oceanic crust (Whitney et al., 2013).

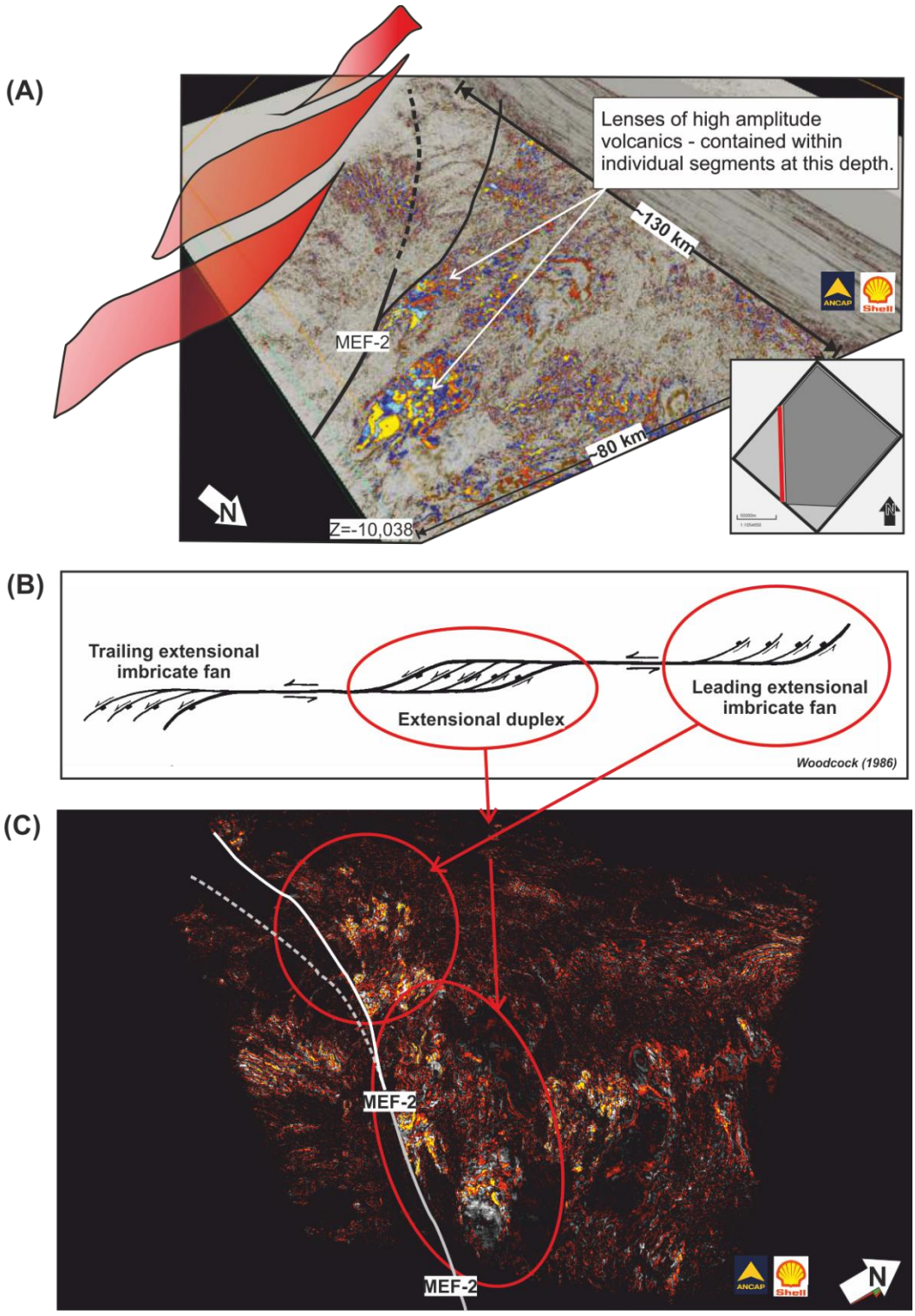

Figure 5.13: (A) A high-angle view of depth slice Z=-10,038 m showing lenses of high amplitude reflections, contained within individual, fault-bound segments. (B) Diagram of the features of strike-slip tectonics in map-view interpretations, note, extensional duplex and leading extensional imbricate fan which are recognised in (C). (C) Plan view of RMS Amplitude attribute in Petrel across a depth slice -10,038 m which has also been additionally edited for contrast to show more detailed faulting.

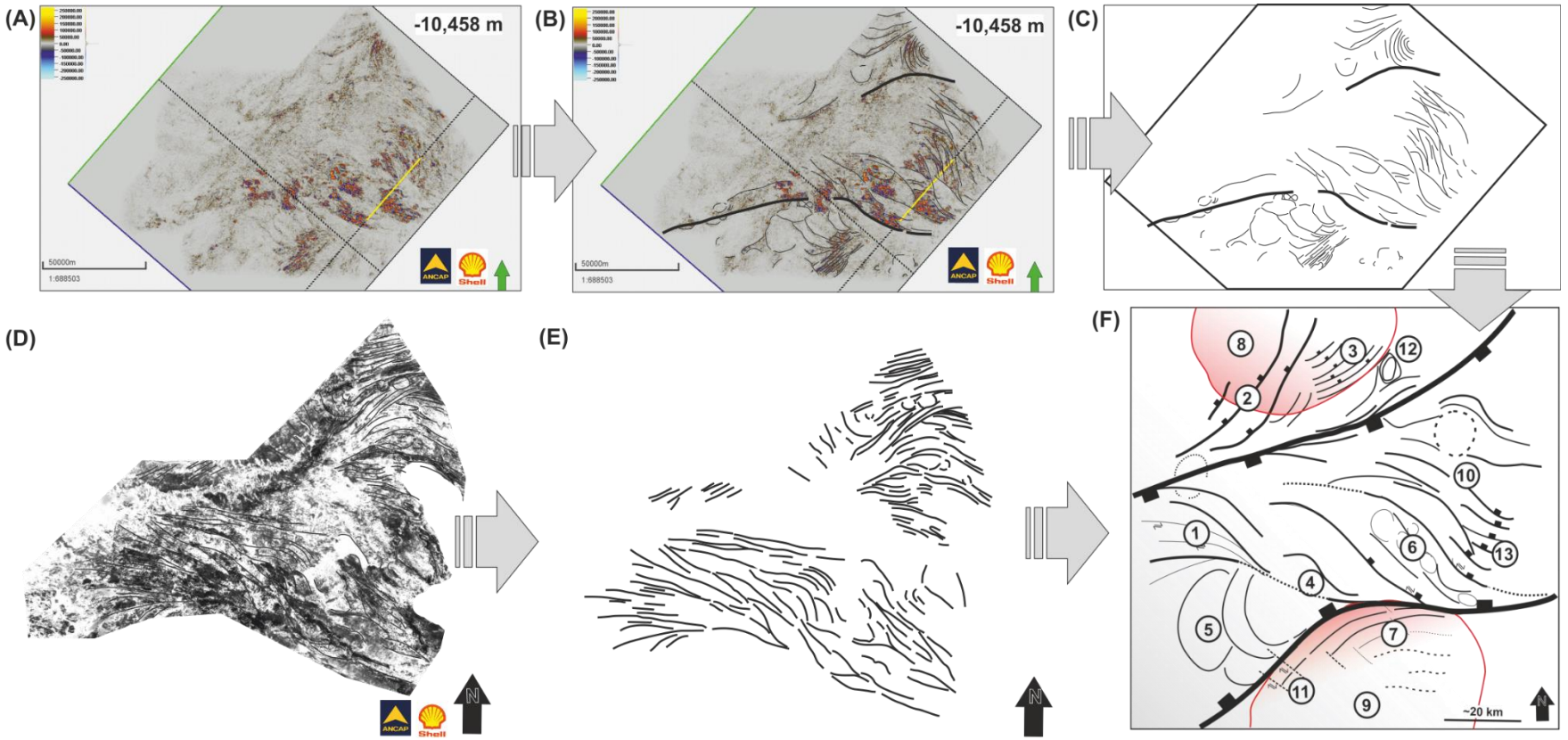

Figure 5.14: (A) Uninterpreted depth section, -10,458 m. (B) The start of fault trace interpretation on depth section, -10,458 m (C) Simple line interpretation of structures in (B) with the depth map removed for clarity. (D) RMS Amplitude attribute map across the same area as (A). This is used to help discern more detailed areas of faulting. (E) Line interpretation of structures with the amplitude map in A removed for clarity. (E) Composite line diagram of structures from using both the RMS Amplitude map (D) and Depth map (A).

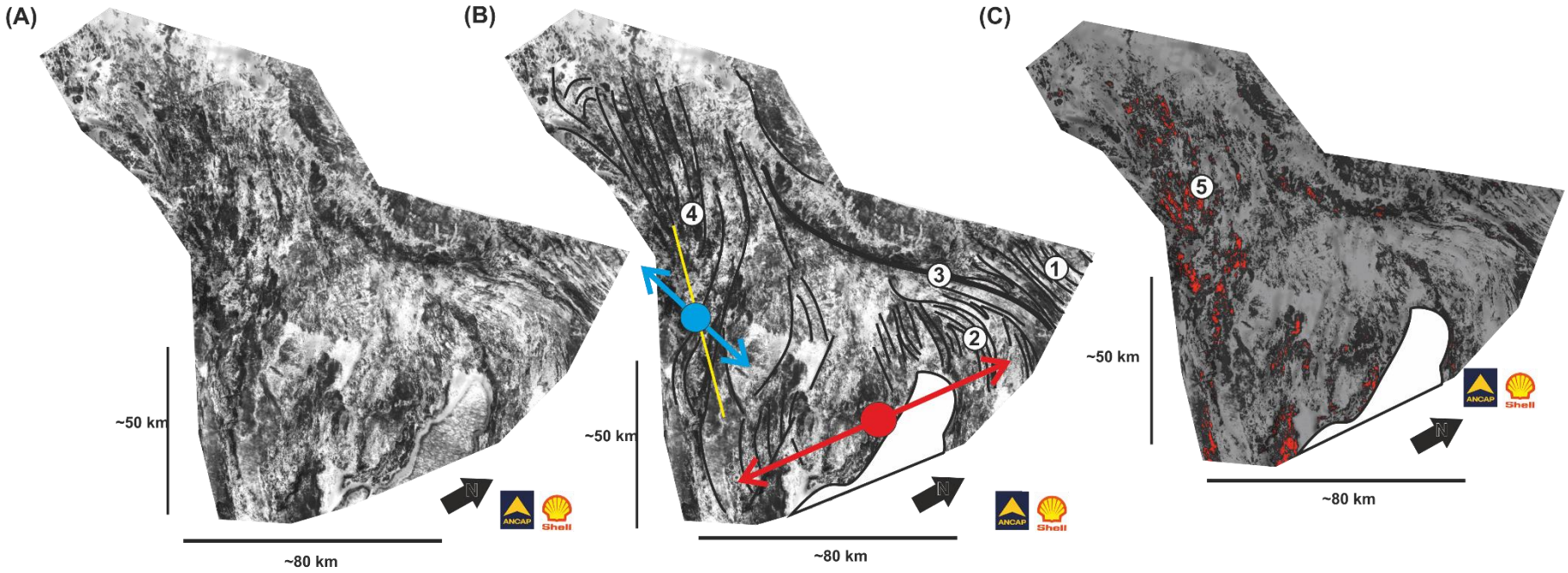

Figure 5.15: (A) RMS Amplitude overlay on an early version of a top magmatic crust surface. (B) Yellow highlights the trend of inherited structures, blue shows the transtension direction and red shows the post-SDR, N-S extension. Feature 1 highlights the curved faulting that affects the southern section of the Northern SDR. Feature 2 shows extremely curved faulting within the northern section of the pull-apart system. Feature 3 shows the Major extensional fault 2, (MEF-2) which is also subject to extreme curvature through the dataset. (C) Red areas highlight the high amplitudes which are interpreted to be intrusive volcanics, these primarily follow the inheritance structural trend and are contained within the en-echelon fault-bound segments of the transtensional pull-apart system.

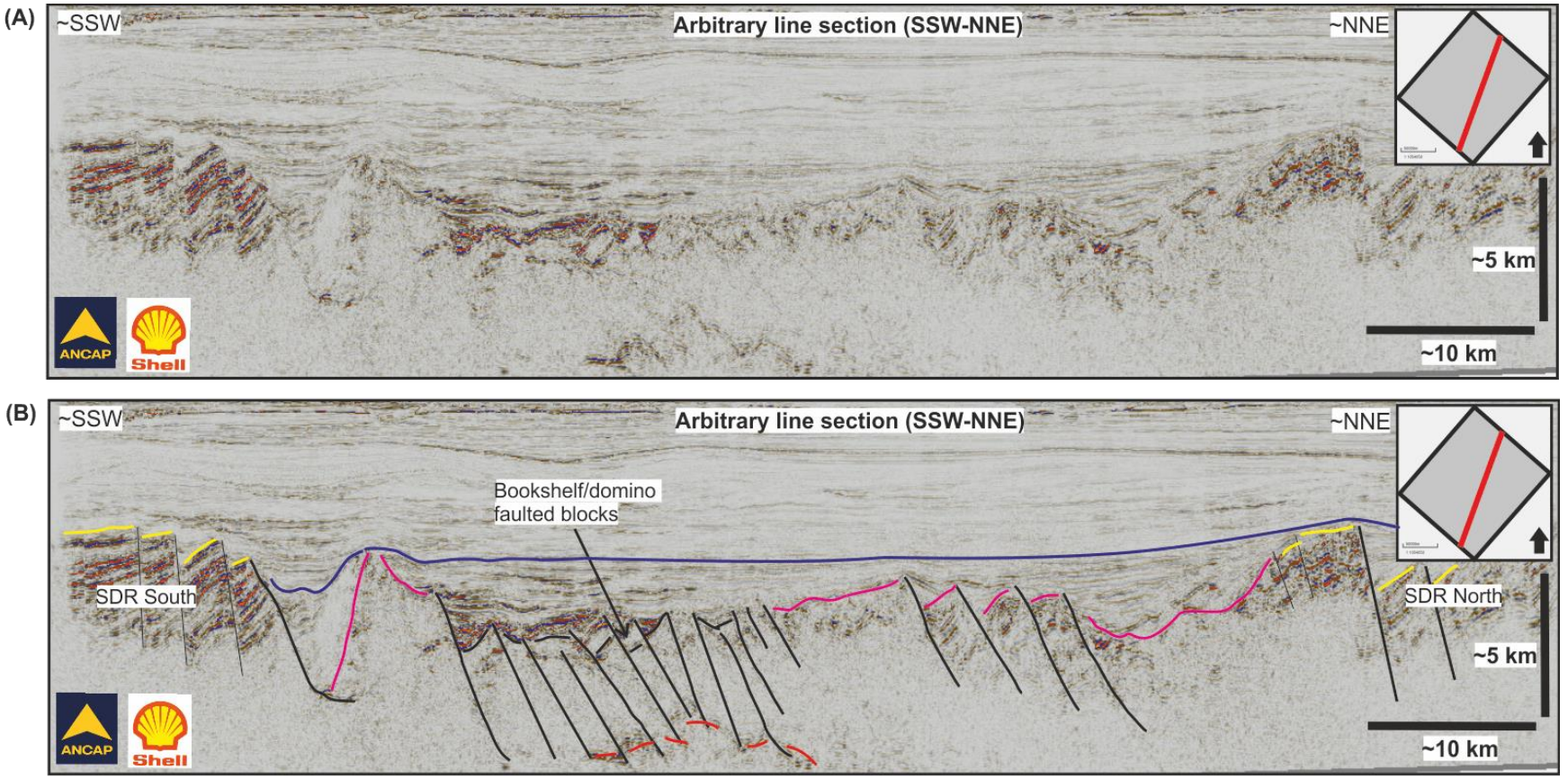

Figure 5.16: (A) Uninterpreted seismic reflection profile in an arbitrary line section trending SSW-NNE (See inset map for line location (B) Interpreted section of (A) showing the SDR South to the left of the section and a central region of rotational block faulting.

Figure 5.17 (A) shows an uninterpreted section of a SW-NE trending Inline with the ‘box probe’ visualisation feature of Petrel (c) Schlumberger software. This is taken at the lowest portion of the basement in the dataset and helps to highlight the complex 3D elements of transtensional faulting. Figure 5.17, section (B) shows an interpreted section of (A) with highlighted fault planes, both through the SDR South and the zone of transtensional faulting. This is to show the difference in these two styles of faulting over a short lateral distance within the dataset and divided by the MEF-2 and MEF-2 splay. The early syn-rift sediment deposits are also highlighted, starting to infill topographic lows. An added challenge to mapping the path of the transtensional faults, including the major extensional fault 2 (MEF-2) is the presence of local intrusives which have obscured the trace of many of the faults, especially in the south and south-west region. To visually confirm the track of these faults, especially MEF-2, it was often necessary to scan through multiple depth-slice sections in Petrel, at which point it also became clear that the intrusive volcanics appeared to be locally multi-levelled, with the MEF-2 also being splayed and with the splay at some level, being obscured by magmatism.

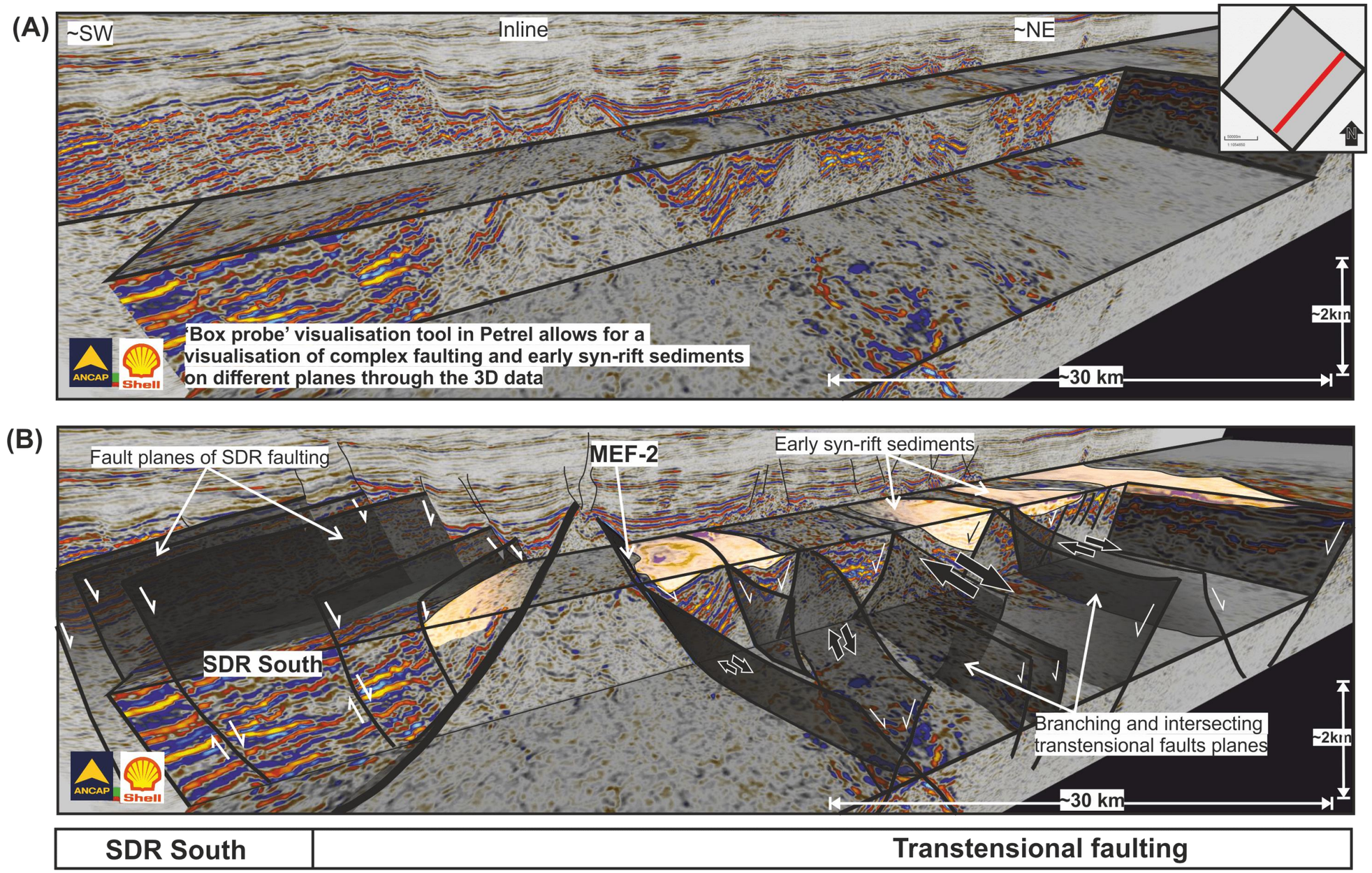

Figure 5.17: (A) Uninterpreted section of a SW-NE trending Inline with the 'box probe' visualisation feature of Petrel software, used to show different 3D elements of complex faulting (B) Interpreted section of (B) with highlighted fault planes both through the SDR South and the zone of transtensional faulting to show the difference in these two styles of faulting over a short lateral distance.

5.5 The nature of the crust in the 3D dataset

5.5.1 Magmatic crust

The top of magmatic crust is characterised by highly irregular, discontinuous mid-high amplitude reflections (figure 5.18) which are often faulted and vertically displaced. Distinction of the top magmatic crust horizon is also based upon the change in seismic character to the overlying syn-rift sediments. A chaotic internal reflection geometry is characteristic of magmatic crust with the transition to the overlying, stratified, syn-rift sediments being diagnostic of the top magmatic crust boundary. Challenging areas to interpret are those where there is very low reflectivity (figure 5.19) with an amorphous outline. This is often directly adjacent to high amplitude, parallel reflections, initially assumed to be stratified volcanics, infilling topographic lows. These are difficult to determine whether; 1) they are part of the magmatic crust itself or, 2) are a distinct volcanic phase of intrusive/injected magmatism, the latter being the favoured explanation. These anomalous areas have an intrinsic relationship to the complex faulting throughout the central region of the 3D cube. This is discussed in greater detail in section 5.6 of this chapter when fault-magma relationships are further investigated. Figure 5.20 (A) shows the top mapped surface of the magmatic crust. The major extensional fault 2 (MEF-2) is relatively easily defined along the lower section, but appears to splay towards the west, however the track of the northern MEF-1 is much harder to determine. To the north-west are several volcanic ridges which are prominent and have volcanic vent structures on top of them. To the central-southern part of the magmatic crust, there are 5-6 unusual depressions which stand out along the north-eastern edge of the MEF-2. Each is broadly circular or semi-circular and distinct from one another,

separated by fault segments, which are inferred here to be part of a wider, connective fault system. However, by the end of the syn-rift period, indicated by (B) the top syn-rift surface, these depressions have disappeared, replaced by a more central zone with an expected, syn-rift basin depocentre.

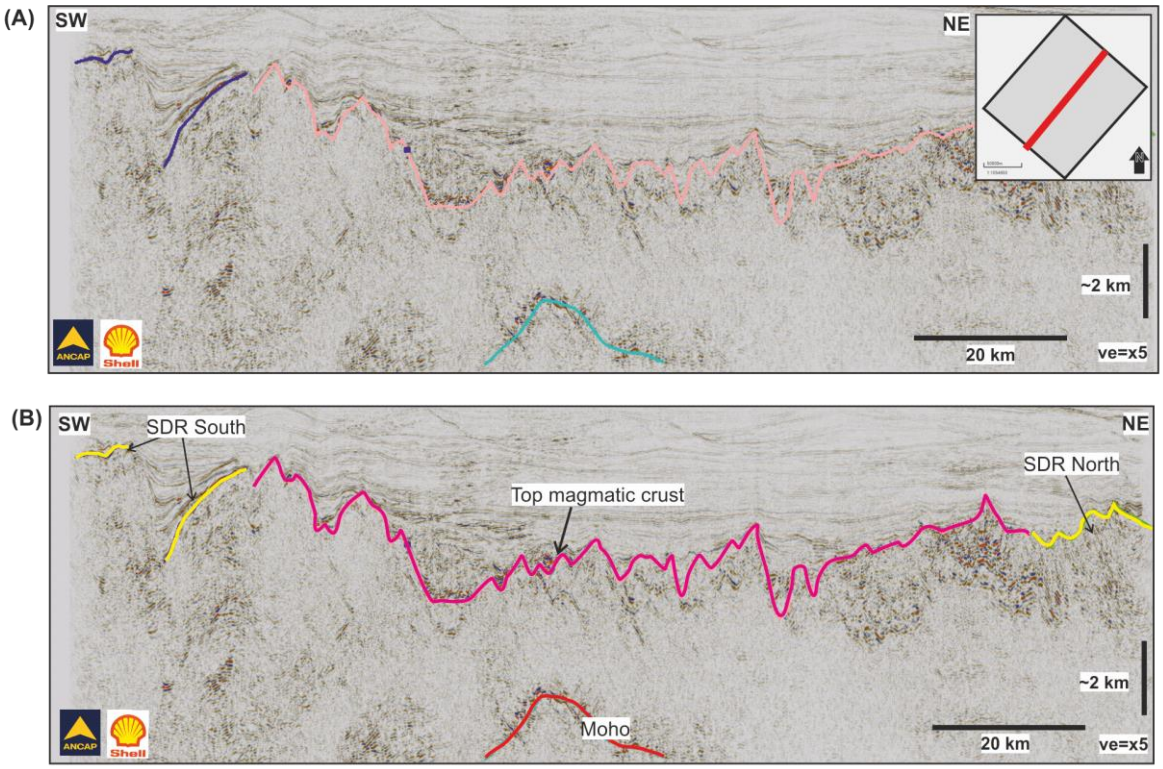

Figure 5.18: (A) PSDM Inline seismic reflection profile through the central region of the 3D dataset. Horizons as mapped in Petrel software. (B) Interpreted section of (A) showing highly irregular top surface of magmatic crust.

Figure 5.20 (C) shows an isopach (total vertical thickness (TVT) between the base surface (top magmatic crust) and the top surface (top syn-rift). This determines the specific areas of deposition across the central region of the 3D cube. If the region was amagmatic - these would represent the regions of the greatest thickness of syn-rift sediments in the 5-6 areas identified in the top magmatic surface. However, due to the highly magmatic nature of this region, these are more accurately termed, fault-bound, isolated (though broadly related) magmatically intruded syn-rift fill, following

an E-W trend. They lie to the north of the MEF-2 but lie primarily in the south-west corner of the magmatic crust. These features are confined to the syn-rift period as they have disappeared by the deposition of the top syn-rift sediments, indicated by figure 5.20 (B), which have begun to blanket the area and produce a more centralised, depocentre. Analysis of the Inline and X-line sections that best show the relationship of the syn-rift packages is now undertaken to further determine the nature and timing of these features.

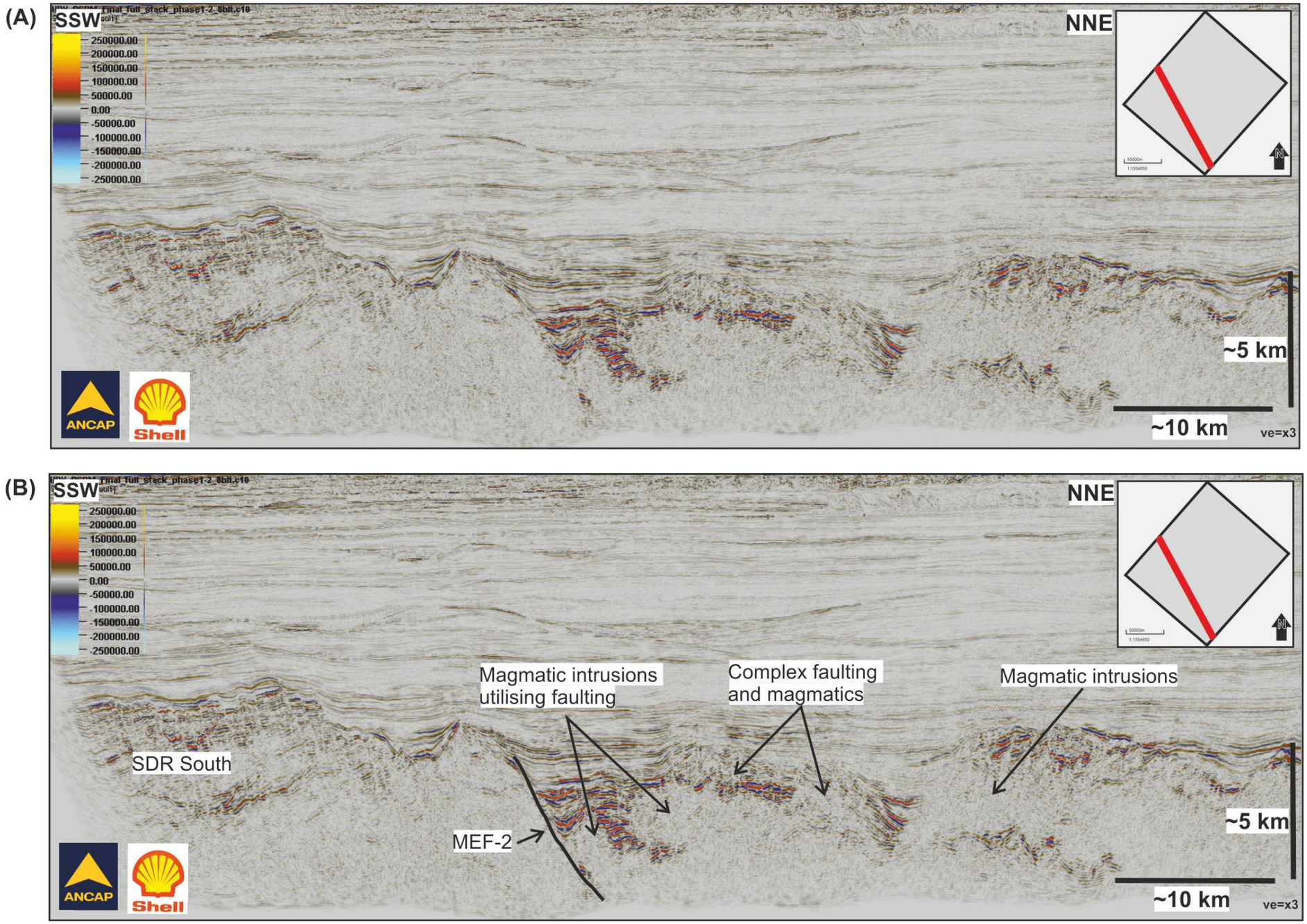

Figure 5.19: (A) PSDM uninterpreted seismic reflection profile across an arbitrary line through the 3D cube ~SSW-NNE (see inset map for line location) (B) An interpreted section of (A) showing SDR South and a central zone of low reflectivity interpreted as intrusive volcanics.

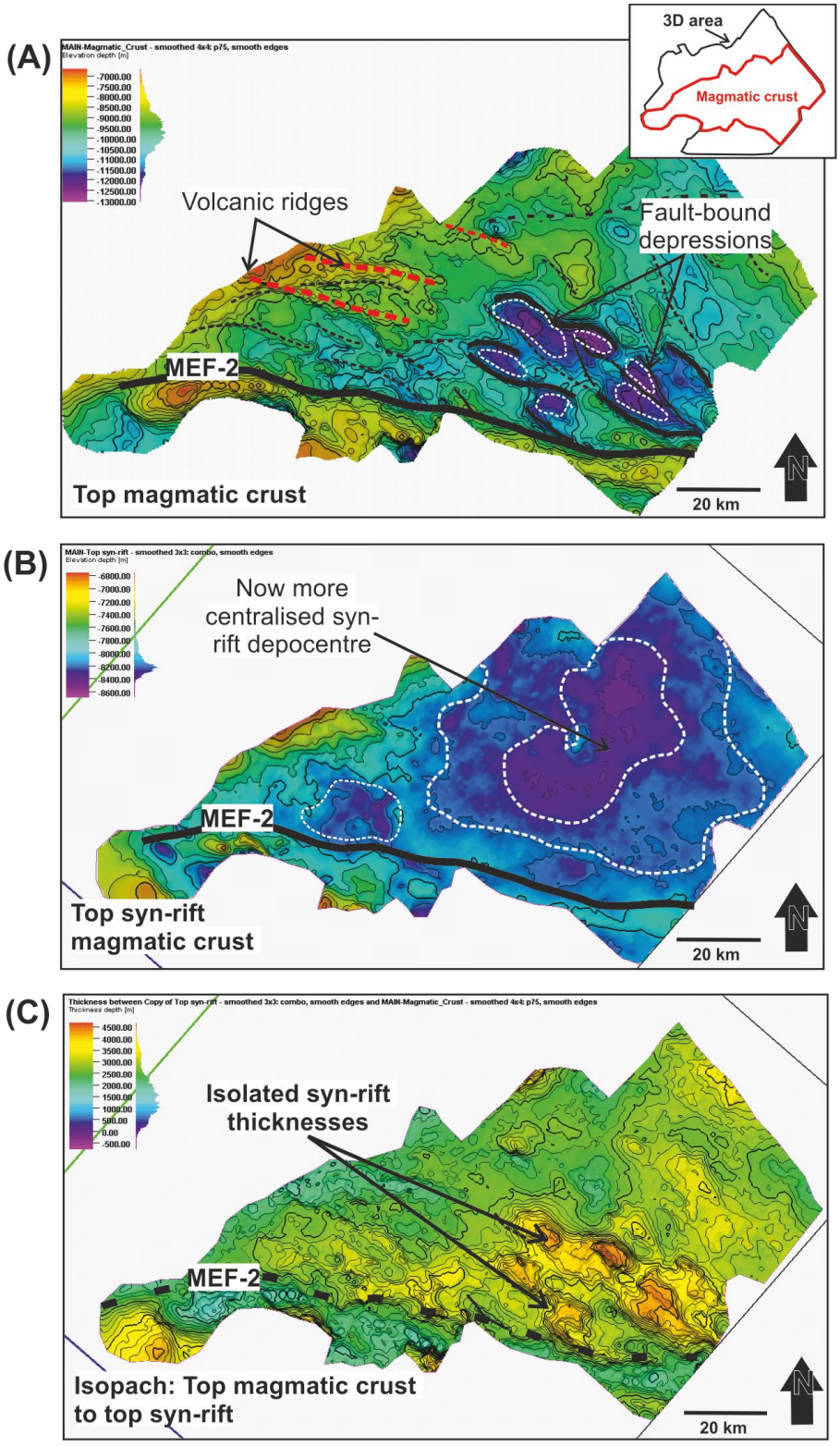

Figure 5.20: (A) Depth map of the top magmatic crust across the 3D data region (see inset map, the surface is of the magmatic crust across a sub-section of the 3D data cube. '3D area' in inset map denotes useable data area of the 3D cube. (B) Depth map of the top syn-rift across the magmatic crust area (C) Isopach map between top magmatic crust and top syn-rift.

5.5.2 Syn-rift sediment relationships

The syn-rift is most easily recognised in the north-west region (figure 5.21), where divergent packages of sediment are overlying the SDR North. The syn-rift packages may also have a higher amplitude reflectivity than the overlying post-rift and in this region in particular, they show the expected divergence of reflections into the footwall of syn-rift faults, affecting the SDR (figure 5.21, B). The top syn-rift horizon is of mid-high amplitude and is a broadly continuous refection that onlaps areas of resistant pre-rift, continental crust topography (figure 5.21). By using a combination of markers which include reflection terminations, seismic facies changes and amplitude changes, this boundary can be mapped across the 3D dataset with a relatively high degree of confidence. Challenges arise where there has been contourite development in the early post-rift that has scoured down, eroding into the top syn-rift horizon and producing a cross-cutting reflection (figure 5.22) (although this is a localised effect). The base of the syn-rift/top magmatic crust is best defined by the transition from broadly continuous reflections into chaotic, discontinuous mid-high amplitudes, often with a highly irregular upper surface (figure 5.22). Volcanic vents of various sizes are prolific across the magmatic crust, some of which appear to have remained active into the early post-rift (figure 5.22). Figure 5.23 shows a full uninterpreted Inline section across the whole of the 3D cube, the red box numbered (i) refers to figure 5.25 which is a more detailed look at this sub-section and the (ii) refers to the sub-section in figure 5.21.

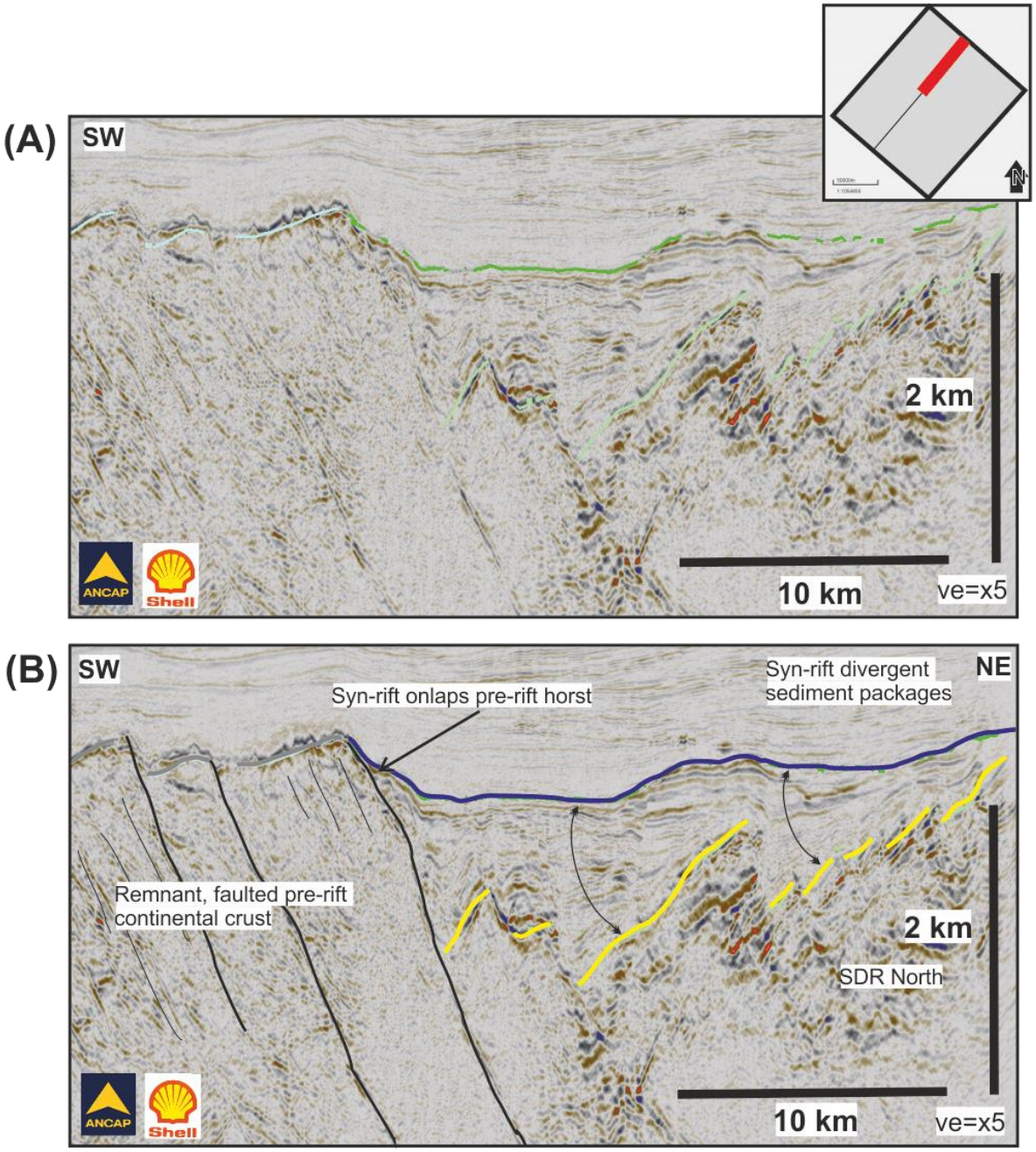

Figure 5.21: (A) Uninterpreted, north-east section of a PSDM seismic reflection Inline from the 3D dataset, showing pre-rift continental crust, SDR and syn-rift sedimentation (B) Interpretation of (A) showing top continental crust, top syn-rift and top SDR horizons. Note, divergent syn-rift sediment above faulted SDR packages.

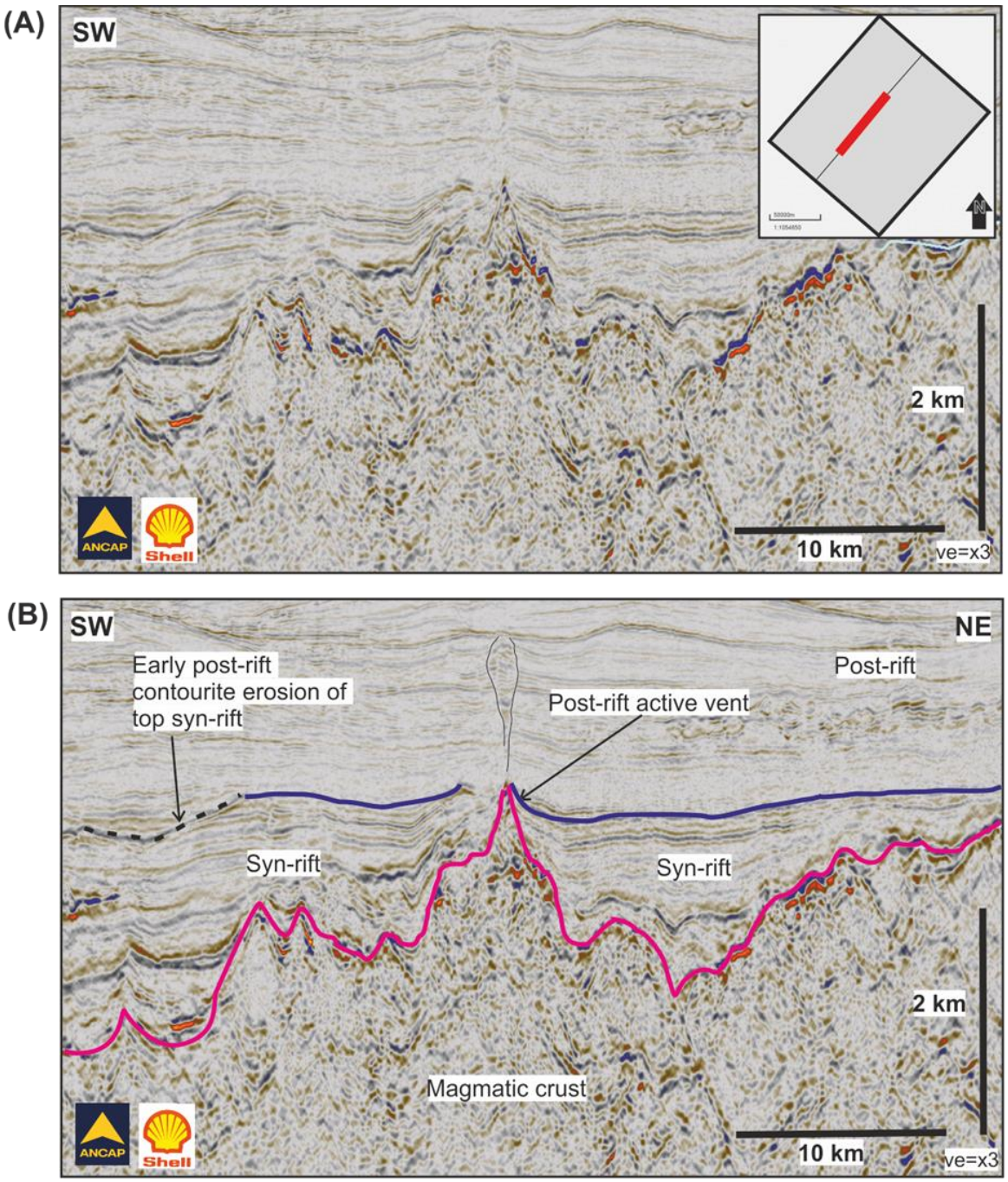

Figure 5.22: (A) Uninterpreted central section of a PSDM Inline from the 3D dataset (see inset map for line location) (B) Interpreted section of (A) showing parallel continuous reflections of the syn-rift on either side of a major volcanic vent, sourced from the magmatic crust and remaining active into the post-rift. Note the difference in seismic reflections character from the magmatic crust into the syn-rift.

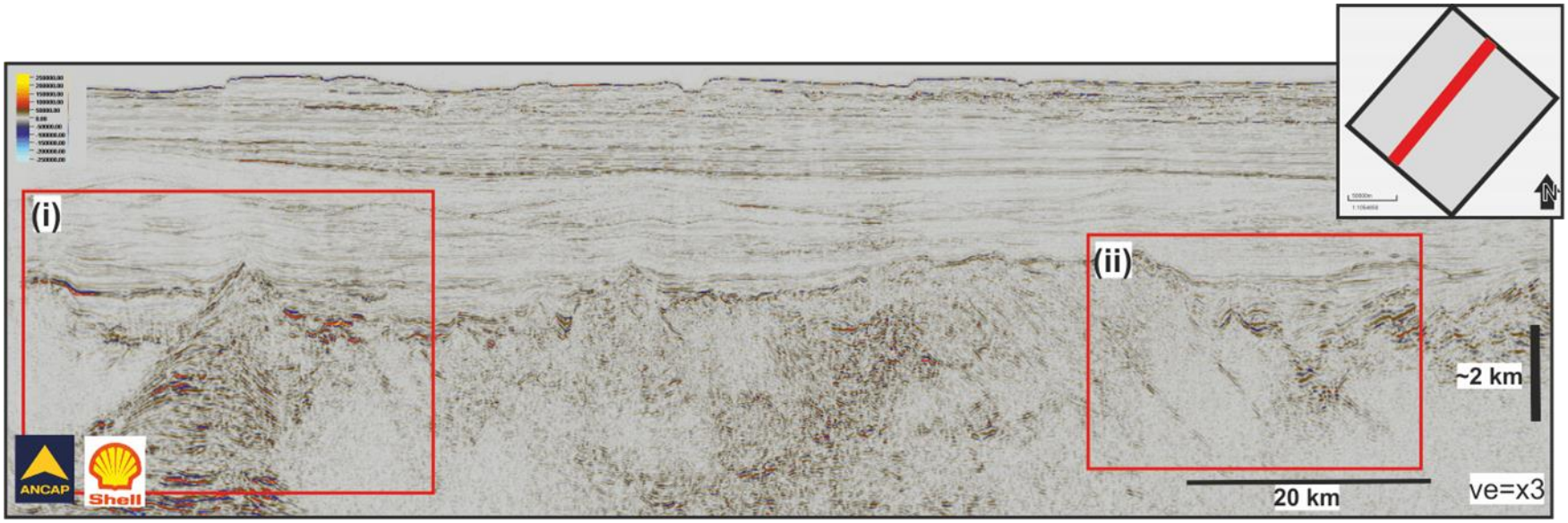

Figure 5.23: Uninterpreted full Inline seismic reflection profile from the 3D dataset (see inset map for line location). (i) See figure 5.25 (ii) See figure 5.21.

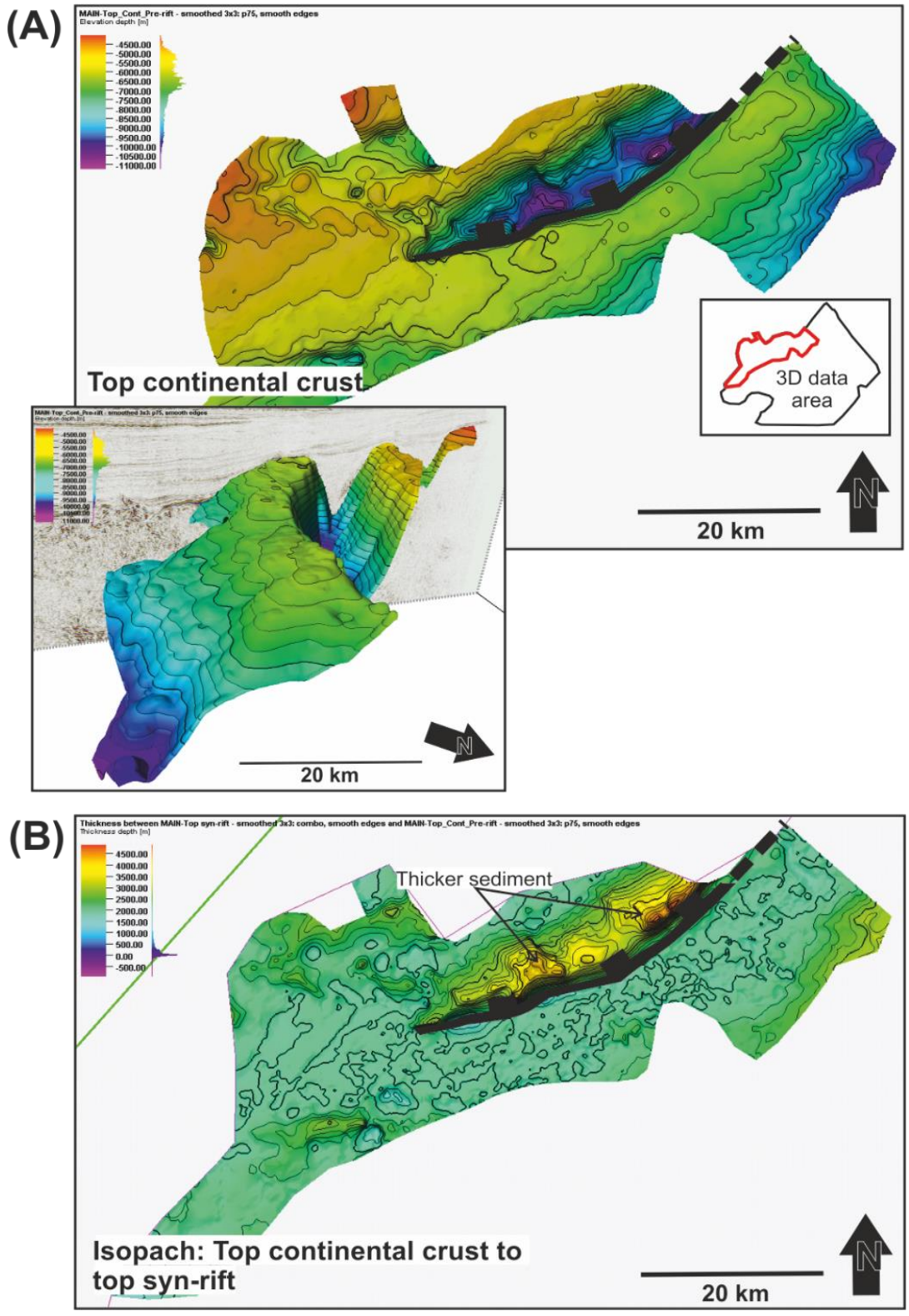

Figure 5.24: (A) Top stretched continental crust surface within the 3D dataset and large continental extensional fault trending NE-SW. See inset map for location of the surface as a sub-section of the useable data region of the 3D data cube. '3D area' in inset map denotes the whole useable data area of the 3D cube. (B) Isopach map between the top continental crust and the top syn-rift.

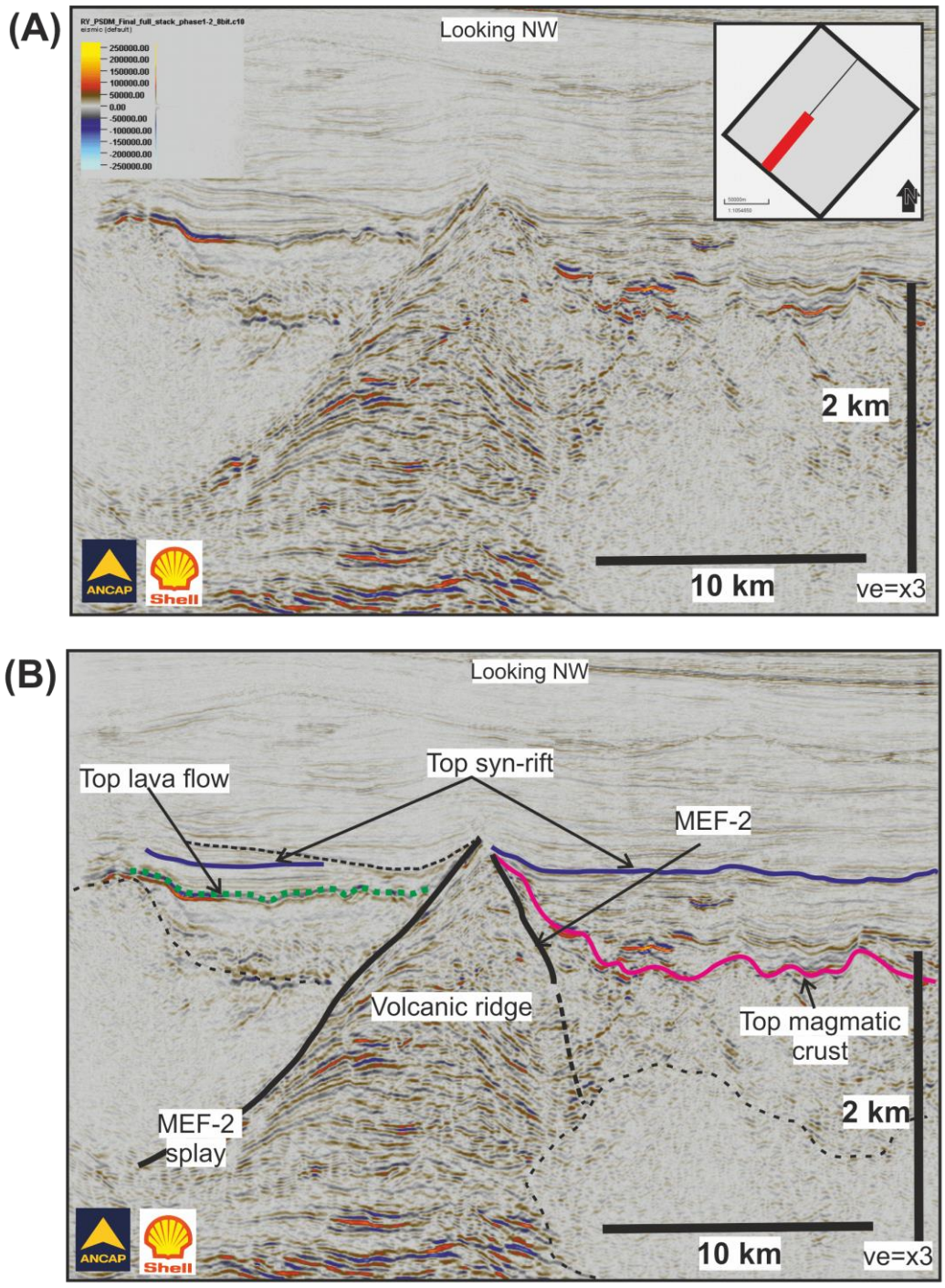

Figure 5.25: Uninterpreted section of the Inline shown in figure 16 (i) (B) Interpreted section of (A) showing a volcanic ridge, top magmatic crust and top syn-rift, as well as a top intra-syn-rift/lava flow horizon.

Figure 5.24 (A) shows a depth map of the top continental crust area of the 3D dataset. A large extensional fault is shown trending NE-SW which is marked through the isopach map in image (B) which has considerable syn-rift sediment infill. Figure

5.25 shows the top syn-rift horizon, however in this section of the data there is also recognised, an intra-syn-rift horizon, which is the top of an extrusive lava flow (which is investigated in detail in section 5.6.1). This was recognised in the mapping process due to changes in the seismic reflection character of these packages to the overlying stratified syn-rift, as well as their geometric relationship to adjacent magmatic features. This intra-syn-rift horizon is also confined by the large volcanic ridge to the south and the MEF-2 fault which lies to the north of this feature. Figure 5.26 (A) shows the top surface of the SDR North packages with image (B) showing the isopach map between the top SDR North and the top syn-rift. The thickest syn-rift sediments are found on the north-western side of the NE-SW trending faults which are prolific throughout the SDR packages. Figure 5.26 (C) shows the top surface of the SDR South and (D) shows the isopach created between the top SDR South and the top syn-rift. In contrast to the SDR North, syn-rift sediments are not of any notable thickness in the SDR South and faulting trends primarily, NE-SW.

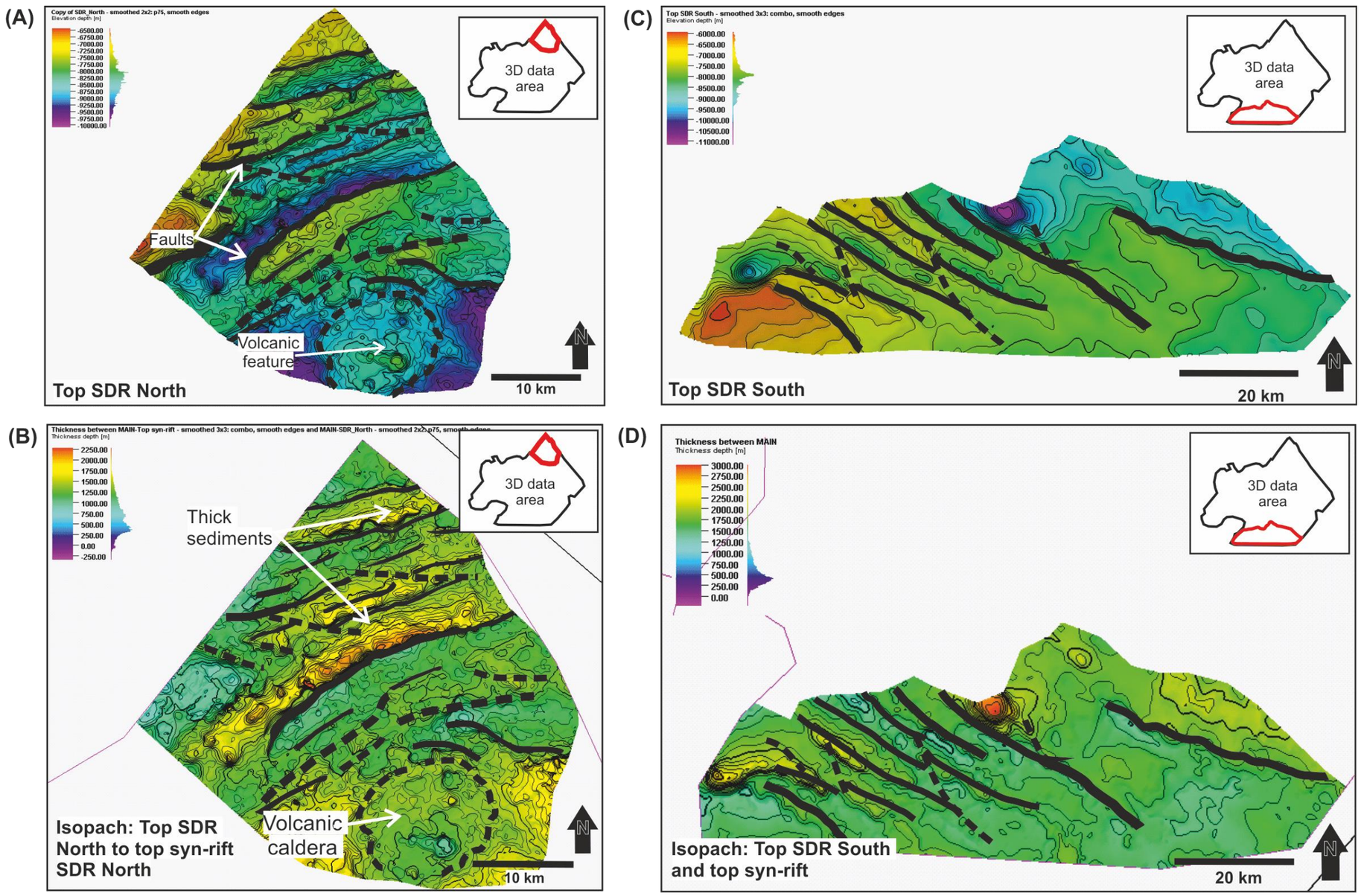

Figure 5.26: (A) Top SDR North surface with NE-SW faulting (B) Isopach created from the top SDR north to the top syn-rift surface (C) Top SDR South depth surface (D) Isopach map between the top SDR South and the top syn-rift.

5.6 3D imaging of a syn-rift magmatic plumbing system

5.6.1 Introduction

The 3D dataset provides a unique and detailed window into smaller scale tectono-magmatic relationships. In particular this includes the identification of a large magma chamber and the direct linkage of adjacent lava flows to this chamber. These new observations on this margin will be combined with what is already known about the complex transtensional fault system (through the magmatic crust) and lead to the development of a 3D model which provides a detailed understanding of the tectono-magmatic relationships across the 3D cube.

5.6.2 Preservation of a magma chamber

Figure 5.27 shows a depth slice at -10,458 m with the outline and top surface of a mapped magma chamber (red box). This magma chamber was identified on several arbitrary line sections, running E-W and also NNW-SSE. Figure 5.28 (A) presents an uninterpreted section of an E-W line showing clearly an area of very low reflectivity with distinct boundaries and a chimney-like section towards the top. Section (B) highlights the major features in this profile. Figure 5.28 section (C) shows an uninterpreted section of the line (red box in (A) and section (D), includes two large areas adjacent to the magma chamber that are directly derived from it.

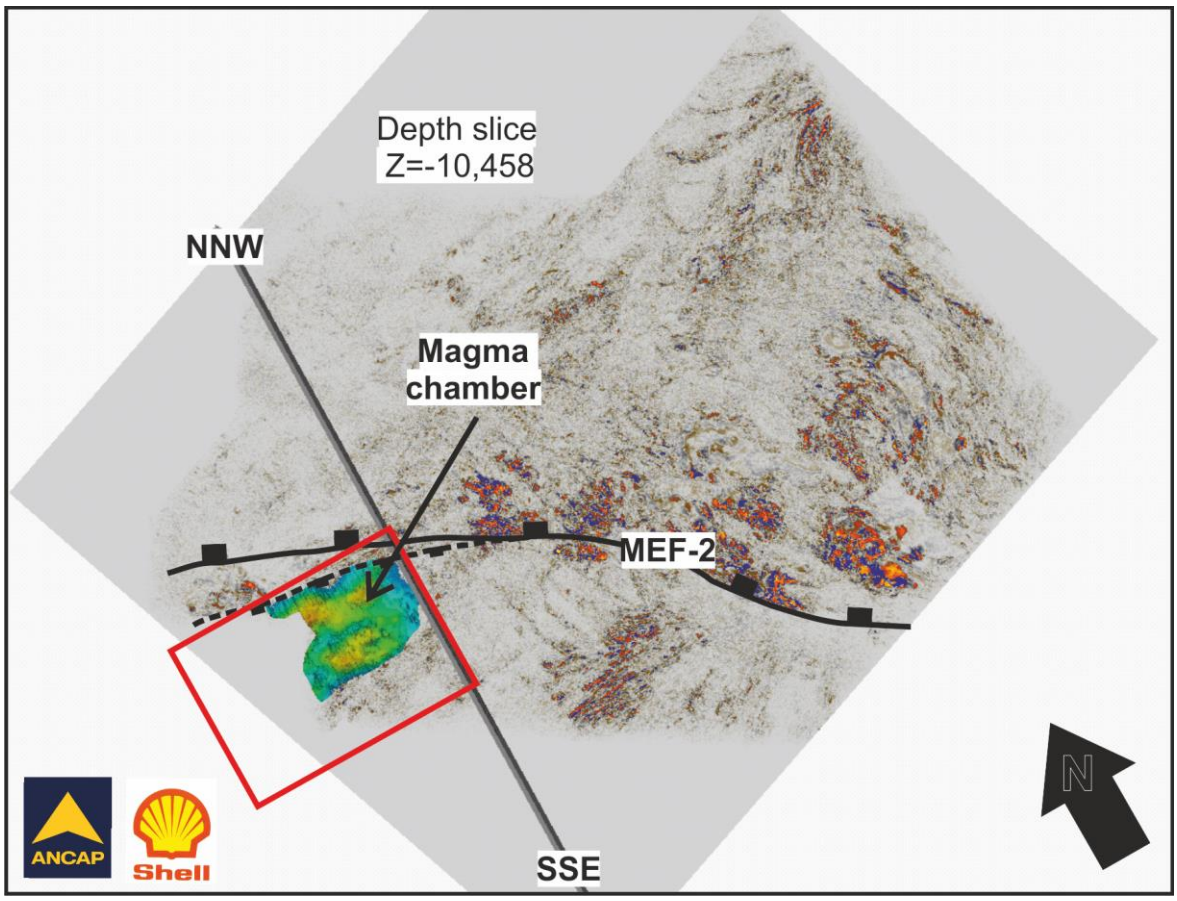

Figure 5.27: Depth slice Z=-10,458 m showing location of Arbitrary line NNW-SSE and the top depth surface of the magma chamber, positioned adjacent and immediately south of a splay fault from MEF-2.

The anomalous, extremely low reflectivity circular areas which have been previously noted on the depth sections in this region of the cube can now be definitively linked to the development of magma chambers. This is illustrated in figure 5.29 which shows a box-probe cut-out section to illustrate that the depth section, low reflectivity is the same feature as that seen in profile sections of the magma chamber.

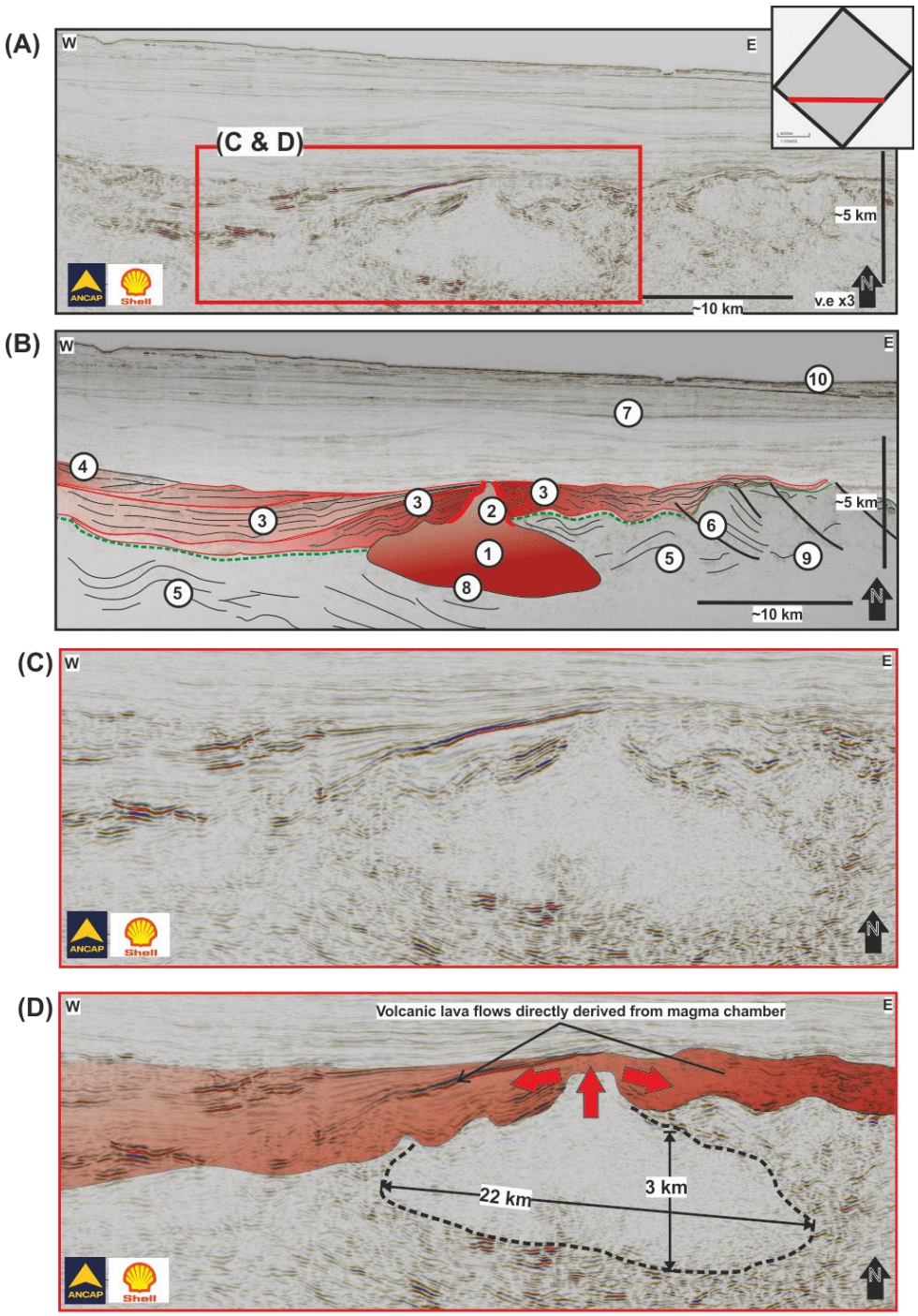

Figure 5.28: (A) Uninterpreted arbitrary line section trending W-E (see inset map for line location) showing an anomalous area of very low reflectivity with an upper chimney section. (B) Interpreted line (A) with major features mapped which include; 1) Transparent area of very low reflectivity 2) magma chamber with chimney/volcanic vent, 3) High amplitude reflections, volcanic flows with origin from (1), 4) High amplitude reflections, volcanic flows with origin from unseen vent off to the left of section, 5) Compression evident in the underlying basement/pre-rift, 6) Low angle large faults, 7) Post rift passive margin sediments, 8) Base of pond follows reflections/fabric beneath 9) Volcanic intrusions/sills, 10) Seabed.

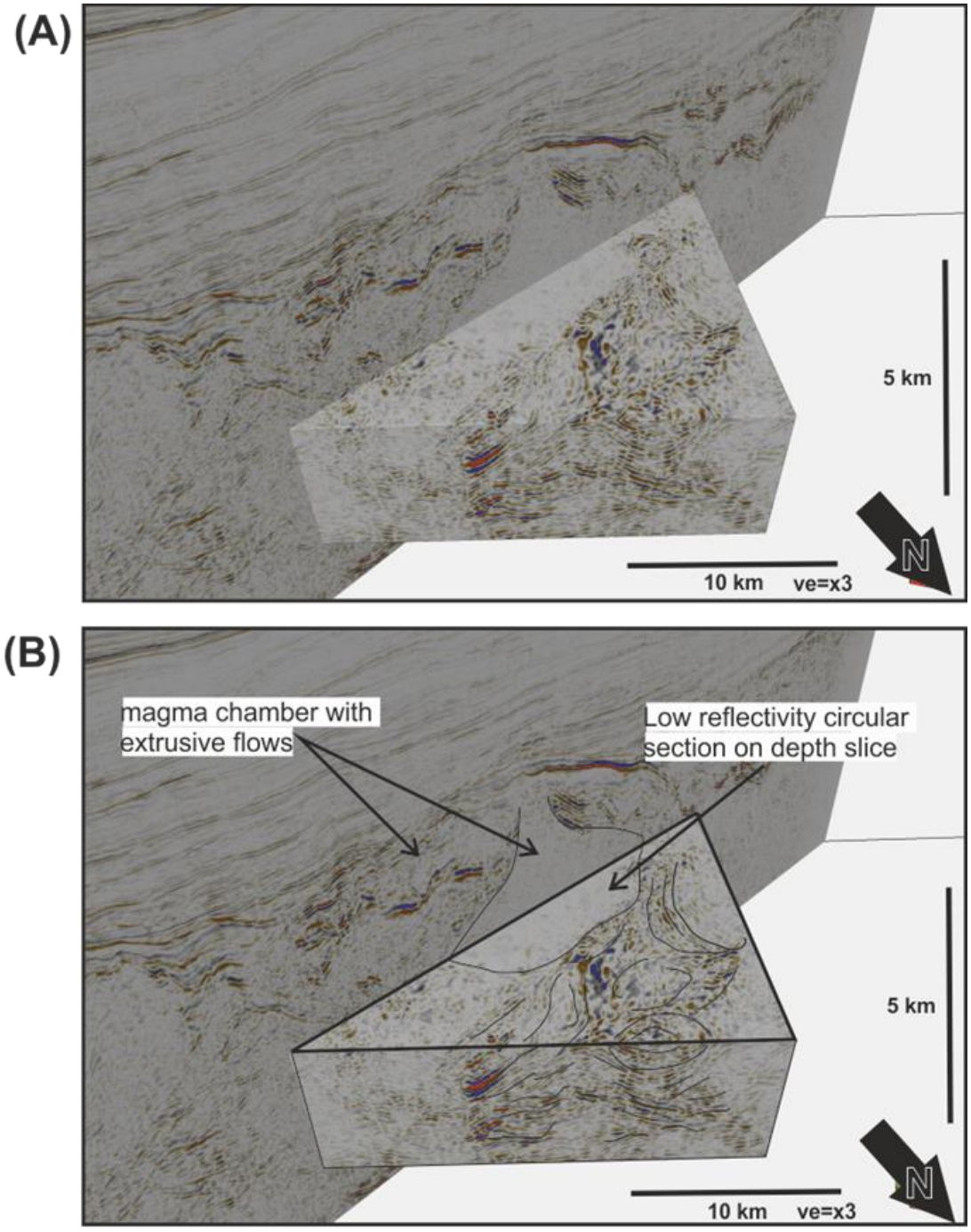

Figure 5.29: (A) Uninterpreted section of an Inline section showing the magma chamber, also shown, box probe cut-out section of the 3D cube. (B) Box-probe section shows that the low reflectivity in circular patterns on depth sections are the same feature as the magma chamber. Data from 3D cube ANCAP/BG Group/Shell.

5.6.3 The relationship between MEF-2, MEF-2 splay and the magma chamber

Major extensional fault 2 (MEF-2) runs broadly from the west to the east on the southern section of the 3D cube. Figure 5.30 shows the intersection of two arbitrary profile lines that both show a different view of the magma chamber. In a SW-NE line orientation, the magma chamber is completely bound by a southward-dipping fault that is considered to be a major splay of the MEF-2. This confines the magma chamber, with it not appearing on the northern side of the high amplitude volcanic feature, which is interpreted as a volcanic ridge related to MEF-2 and its major splay fault. Also of note is that there are now two chimneys visible along with extrusive lava flows from the magma chamber that are confined to the southern side of the volcanic ridge, associated with the splay from MEF-2. This speaks to the importance of the MEF-2 as a controlling early syn-rift structure and may also suggest that the magma chamber is sourced via dyke intrusion, facilitated by the splay from MEF-2. Figure 5.31 shows two lines in the same general location, one is the 2D ION SPAN line A4 that shows the convex-up, high amplitude packages of the SDR South in close proximity to the magma chamber and the other is from the 3D dataset. A chimney feature is evident at the top of the chamber and the MEF-2 splay provides a hard boundary to the north of the chamber. Figure 5.32 shows a true scale, 1:1 line intersection of the magma chamber, this figure also shows that there are multiple chimneys from the top of the chamber. Due to the well-defined boundaries of the magma chamber based upon the stark contrast in seismic reflection characteristics with the adjacent crust, both a top and bottom, depth surface of the magma chamber were able to be mapped. These are shown in figure 5.33.

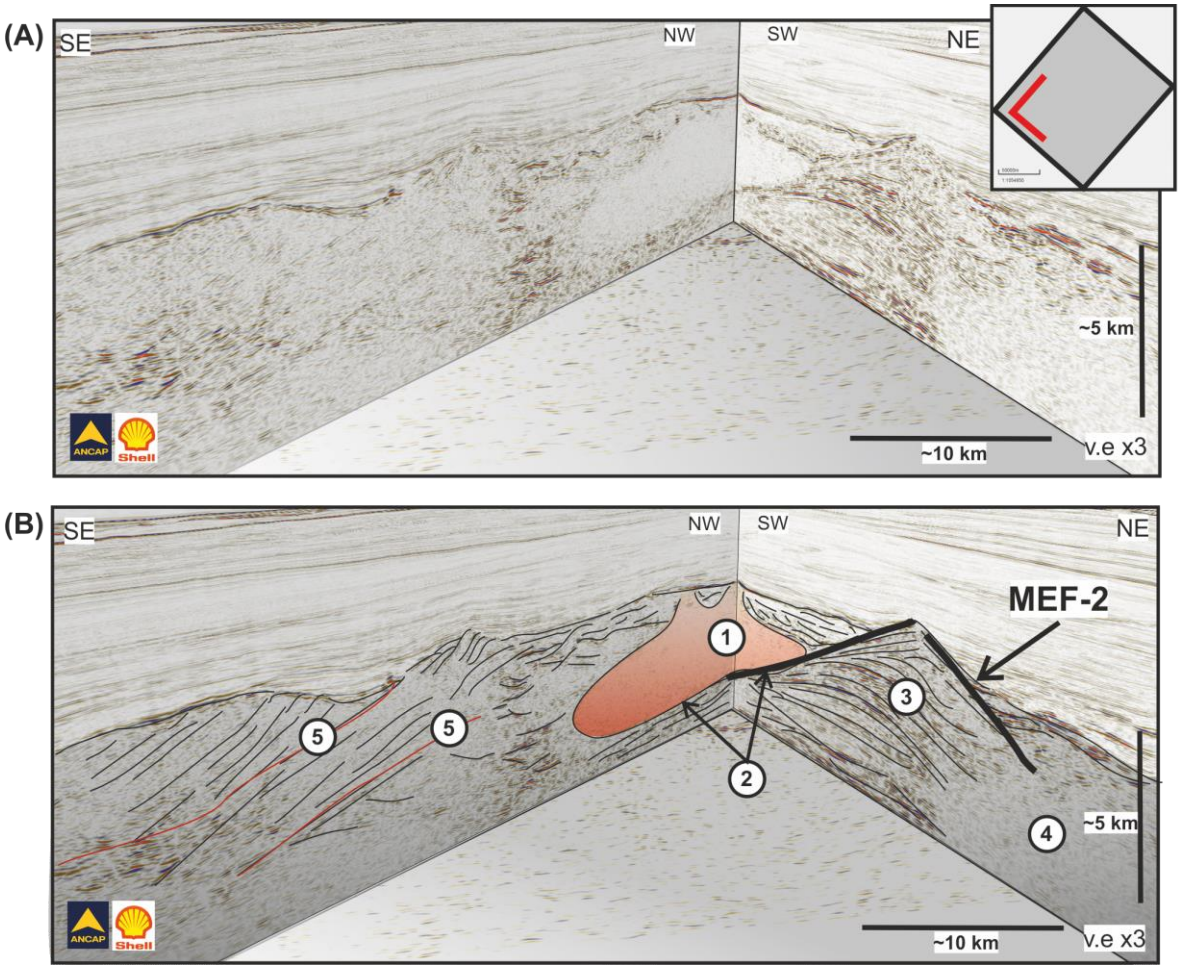

Figure 5.30: (A) Uninterpreted intersection of two arbitrary profiles trending SE-NW and SW-NE (B) Interpreted section of (A) showing the magma chamber directly abutting the MEF-2 fault splay and associated volcanic ridge feature. Major features are; (1) Magma chamber (2) Confining fault plane of MEF-2 splay (3) Volcanic feature associated with MEF-2 and splay (4) Possible second magma chamber (5) Low angle fault planes.

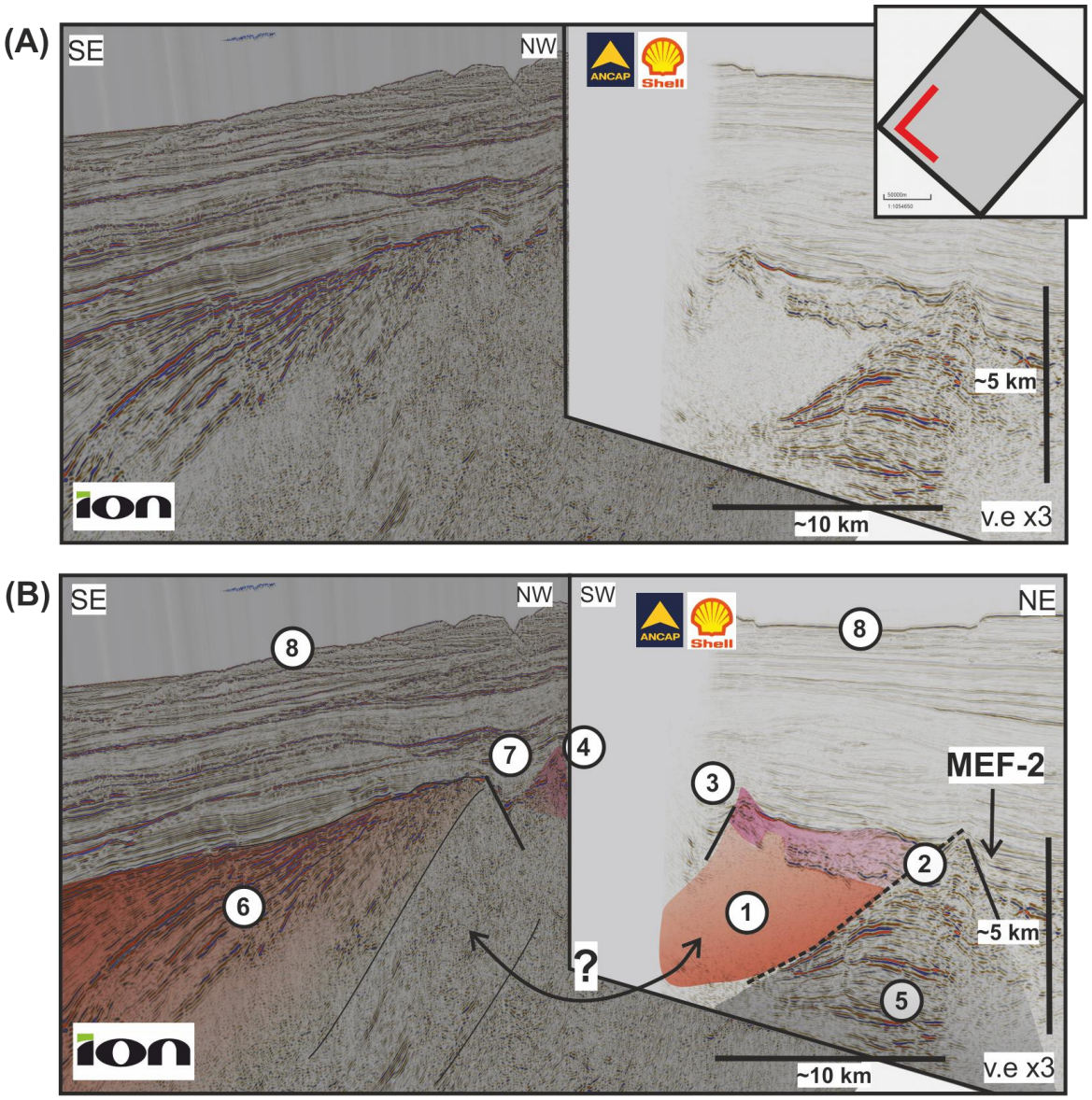

Figure 5.31: (A) (left) ION SPAN line A4 showing convex-up high amplitude reflections of the SDR South packages (B) Interpreted section of (A) with major features (1) Magma chamber (2) MEF-2 splay (3) Extrusive lava flows (4) Prominent area of extrusive lava flows (5) High amplitude volcanic feature associated with the splay from MEF-2 (6) SDR South (7) Down-cutting, post-rift contourite deposits (8) Seabed.

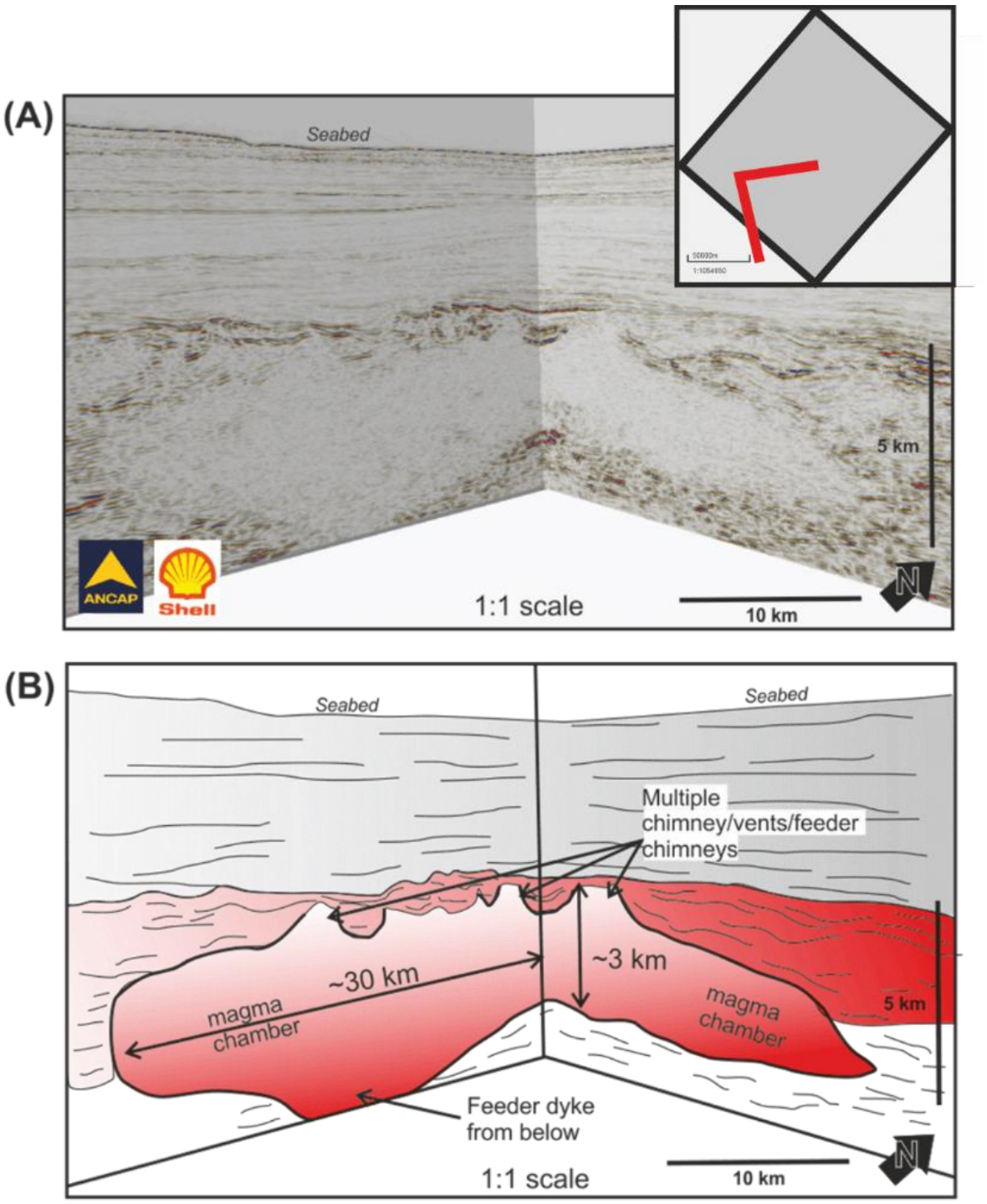

Figure 5.32: (A) Uninterpreted line intersections in true scale (1:1) (B) Interpreted (A) with multiple chimney structures shown from the top of the magma chamber as well as lava flows from it and surrounding the structure. Also present at the base of this feature is an apparent lower feeder dyke from which the magma-chamber appear to be fed from below.

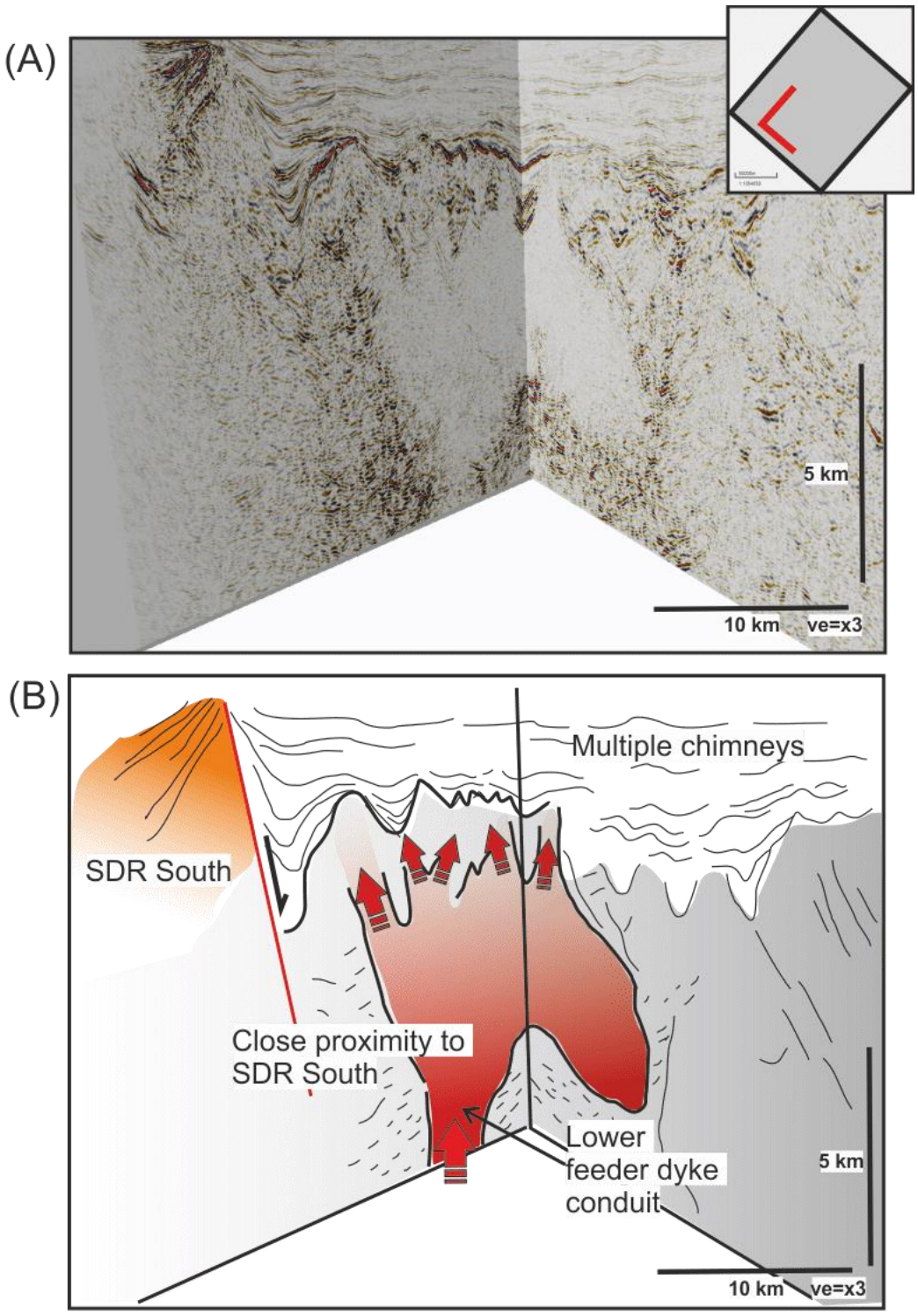

Figure 5.33: (A) Uninterpreted intersection of seismic profile lines showing the magma chamber and SDR South (B) Interpretation of (A) with the major magma chamber and associated multiple top chimneys and also lower, feeder dyke conduit. Data from 3D data cube, ANCAP/BG Group/Shell.

5.6.4 Surface mapping of the magma chamber

Figure 5.34 shows the top depth map of the magma chamber identified in figure 5.28. This is shown with x3 vertical exaggeration so that the main features are highlighted. Red areas are shallower areas which are interpreted as volcanic vents/chimneys similar to those shown in figure 5.28 which have fed lava flows to the surrounding area, as observed in feature 3, section B, figure 5.28.

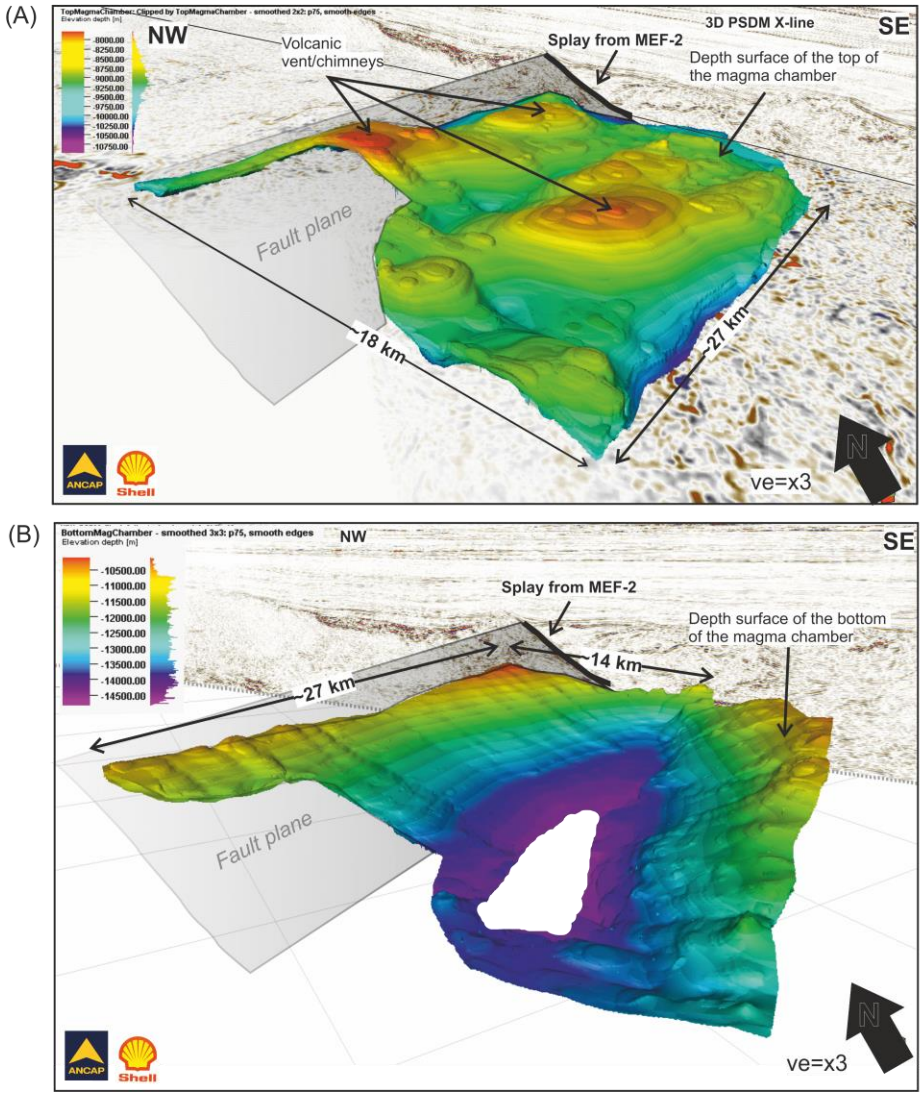

Figure 5.34: (A) Top depth map of the magma chamber identified in figure 5.28. Red areas are shallower areas which are interpreted as volcanic vents/chimneys similar to that shown in figure 5.28 which fed lava flows to the surrounding area. Note: position directly adjacent to the fault plane of MEF-2 splay. (B) Lower surface of the magma chamber with open bottom section.

In consideration with the depth section shown in figure 5.27, there is a relationship between the MEF-2 fault splay and the magma chamber. This relationship is further strengthened when the lower surface of the magma chamber is mapped (figure 5.30, B). The lower surface was mapped with the bottom section appearing to be absent. When considering the relative position of the magma chamber and the nature and interaction of the adjacent areas of low reflectivity, it is reasonable to suggest that the magma chamber did not exist in isolation and was instead, connected to a wider magmatic system of multi-depth, multiple magma chambers. This is also suggested by depth sections (figure 5.35).

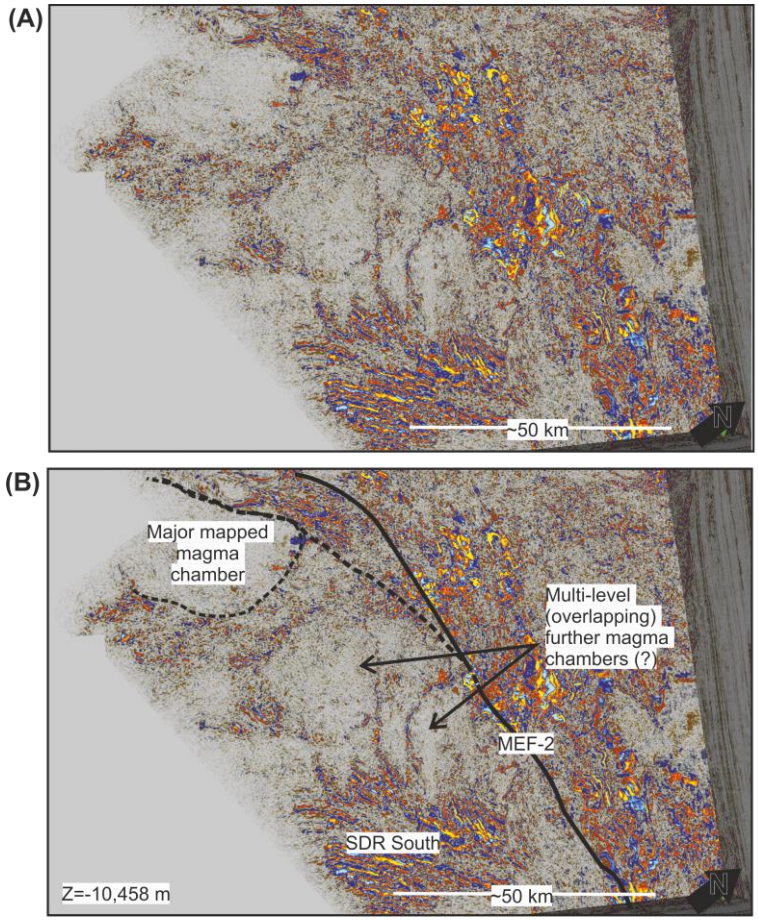

Figure 5.35: (A) Uninterpreted SW section of depth slice Z=-10,458 m (B) Interpretation of (A) showing major mapped magma chamber and other possible magma chambers in the vicinity which are not as clearly imaged. Data from 3D cube, ANCAP/BG Group/Shell.

It is also proposed that the magma chamber would have been fed from a feeder dyke/conduit below, which is observed in both figure 5.32 and figure 5.33. This would link the chamber to a wider magmatic plumbing system and allow for the chamber to be filled and produce the related extrusive lavas.

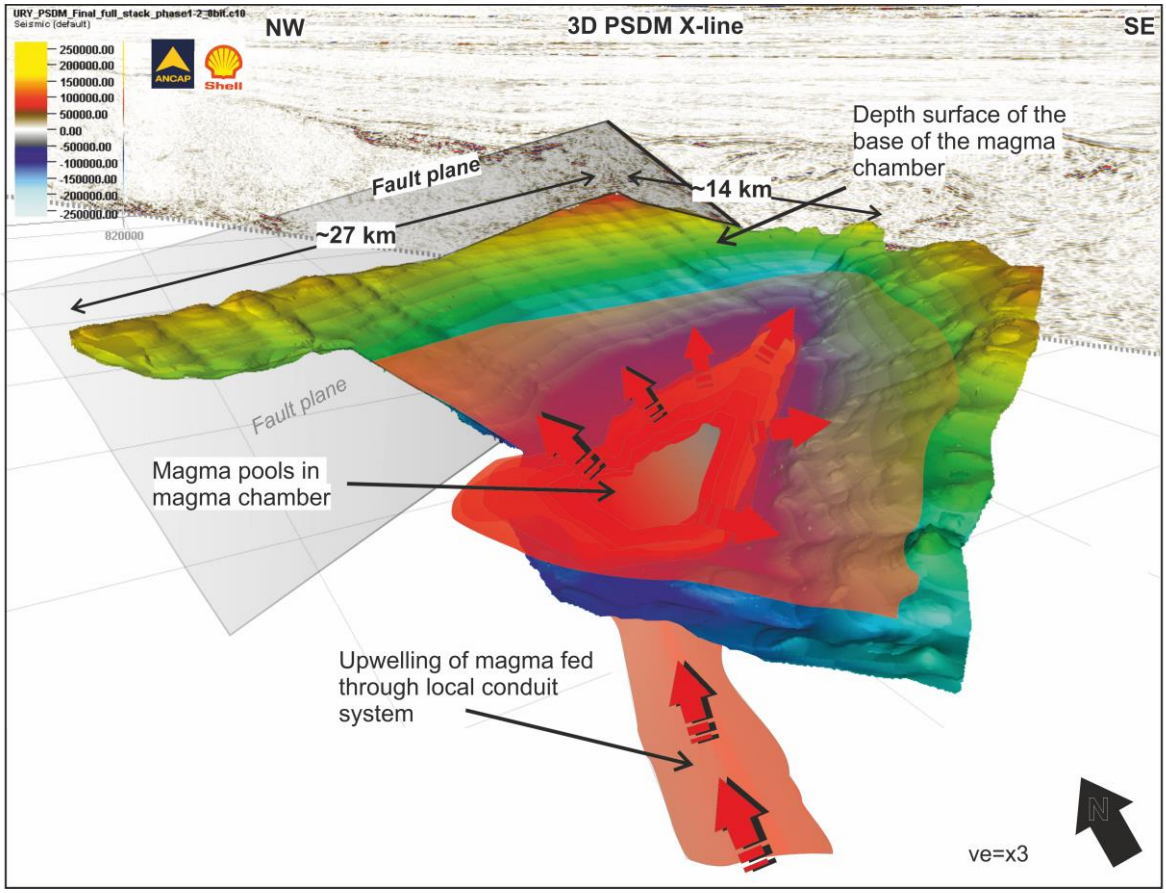

Figure 5.36: Lower depth surface map of the magma chamber and its close relationship with the MEF-2 splay. Also shown is a proposed local conduit system which would have fed the chamber with magma from below as an element of an interconnected, volcanic plumbing system.

Figure 5.37 is a 3D conceptual diagram of the combined and mapped elements of the magma system at the time the lava flows around it were extruded. This includes the shallow sections at the top of the magma chamber being volcanic vents/chimneys which allowed the movement of magma from the chamber into the surrounding areas, creating much of the early syn-rift packages observed in this region of the data cube.

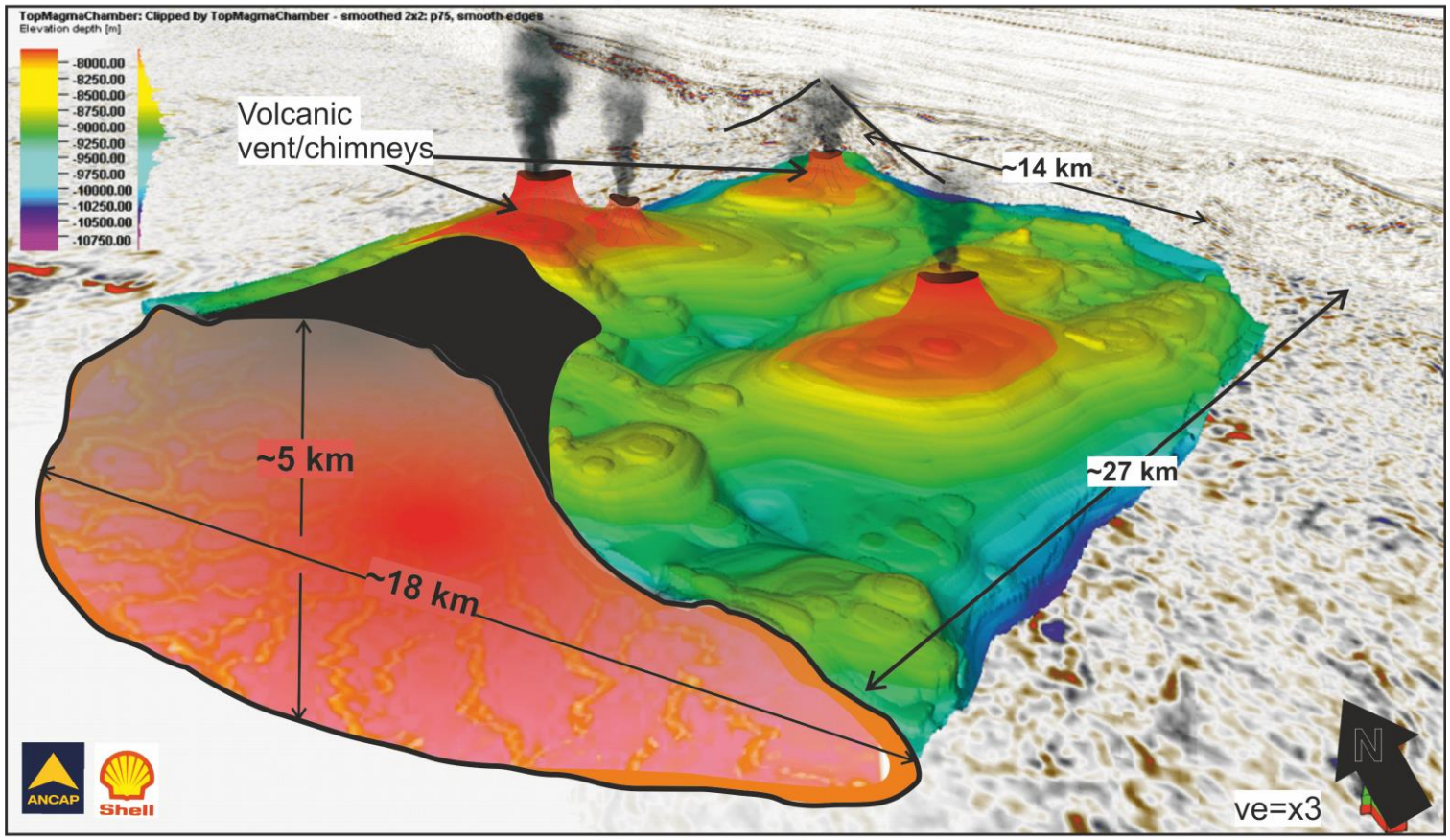

Figure 5.37: Conceptual diagram of the magma chamber at the time of extrusion of adjacent lava flow packages from shallow regions interpreted as volcanic vents/chimneys through which magma was extruded.

5.7 Relationship of the magma chamber to the SDR South

Figure 5.38 shows a colour inverted intersection of two lines to show the contrast between the magma chamber and surrounding high amplitude reflections, including the packages of the SDR South. Feeder conduits which have produced the overlying extrusive deposits above the magma chamber are also present and appear to feed into the early SDR packages. This suggests both a similar creation process and possible temporal link.

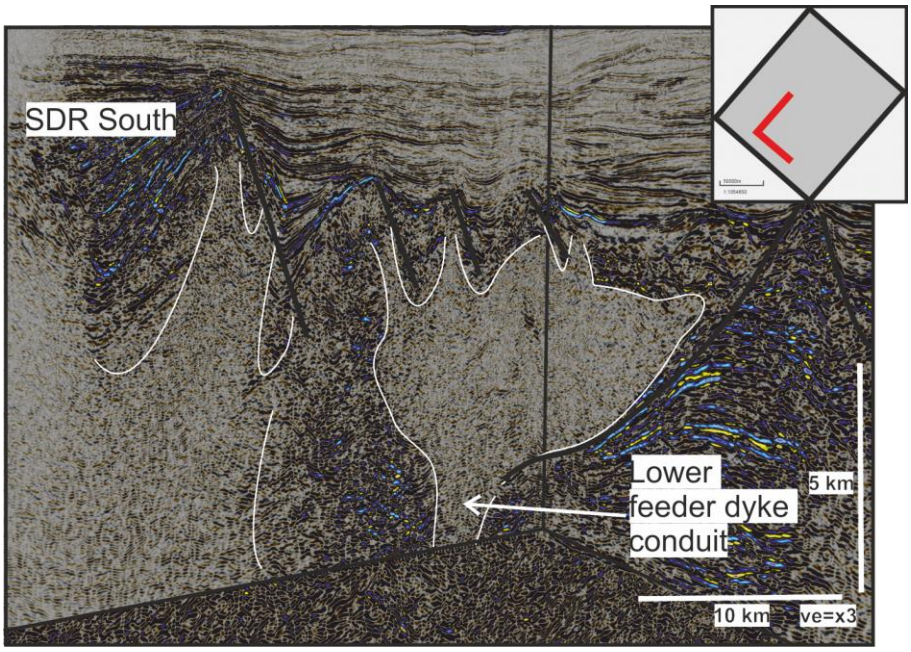

Figure 5.38: Colour inverted and contrast enhanced intersection of lines from the 3D data showing the relationship of the major magma chamber to the SDR South in term of similar feeder systems. Data from 3D cube, ANCAP/BG Group/Shell.

Figure 5.39 shows an uninterpreted section of an Inline (see inset map for location) showing initial SDR packages with oblique reflections at the base which continue to various internal points in the dipping reflectors sequence. These are proposed as early feeder dykes, contributing to the early SDR packages. Figure 5.40 shows a 3D model of the transtensional fault system, with implied intrusions at depth and interconnected magma chambers, along with the relationship to the SDR packages.

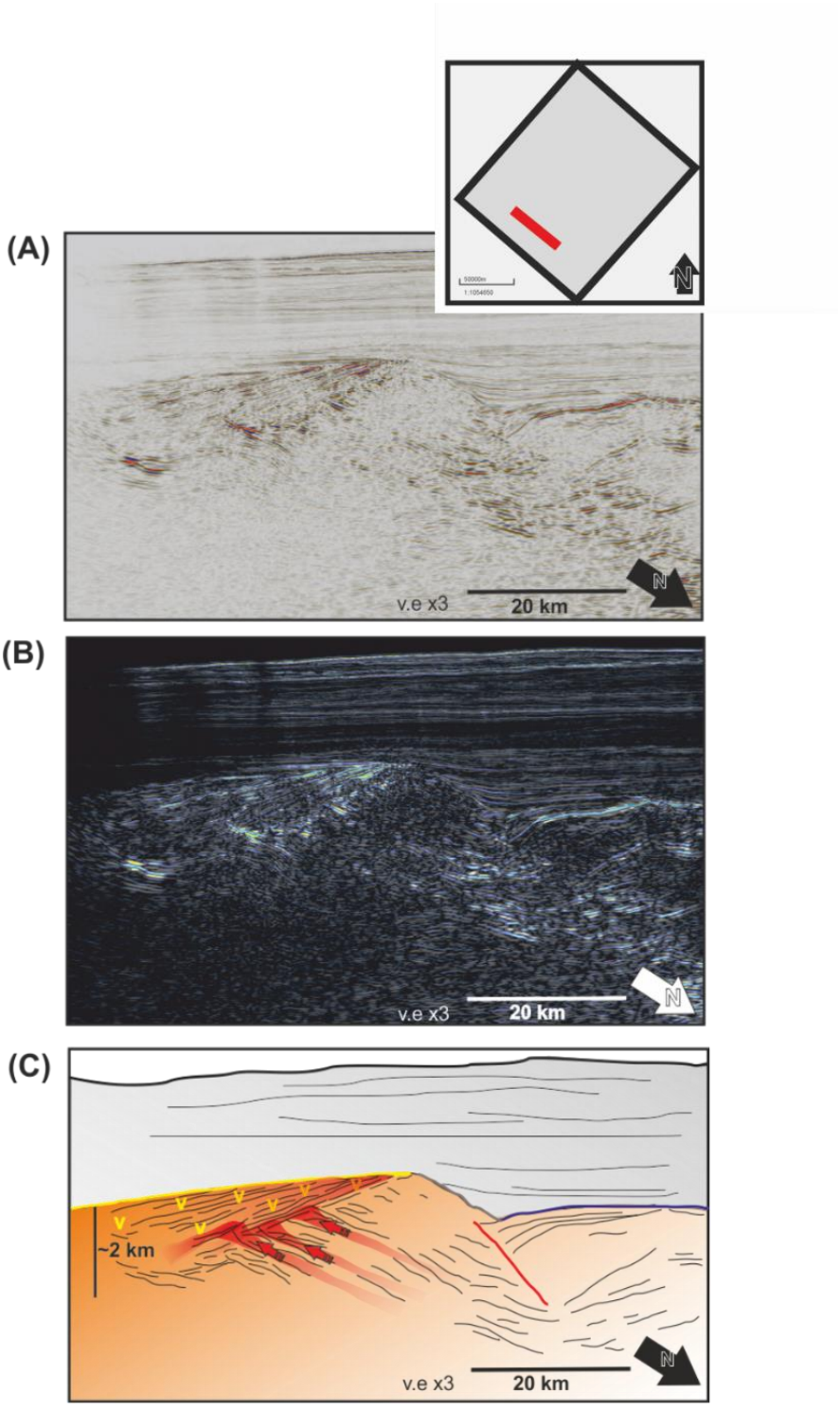

Figure 5.39: (A) Uninterpreted section of an Inline (see inset map for location) showing initial SDR packages with oblique reflections at the base which continue to various internal points in the dipping reflectors sequence. These are proposed as early feeder dykes. (B) Colour inverted section of A to highlight reflections (C) Interpreted section of (A) showing magmatic feeder dykes penetrating the lower levels of the SDR packages. Data from 3D cube, ANCAP/BG Group/Shell.

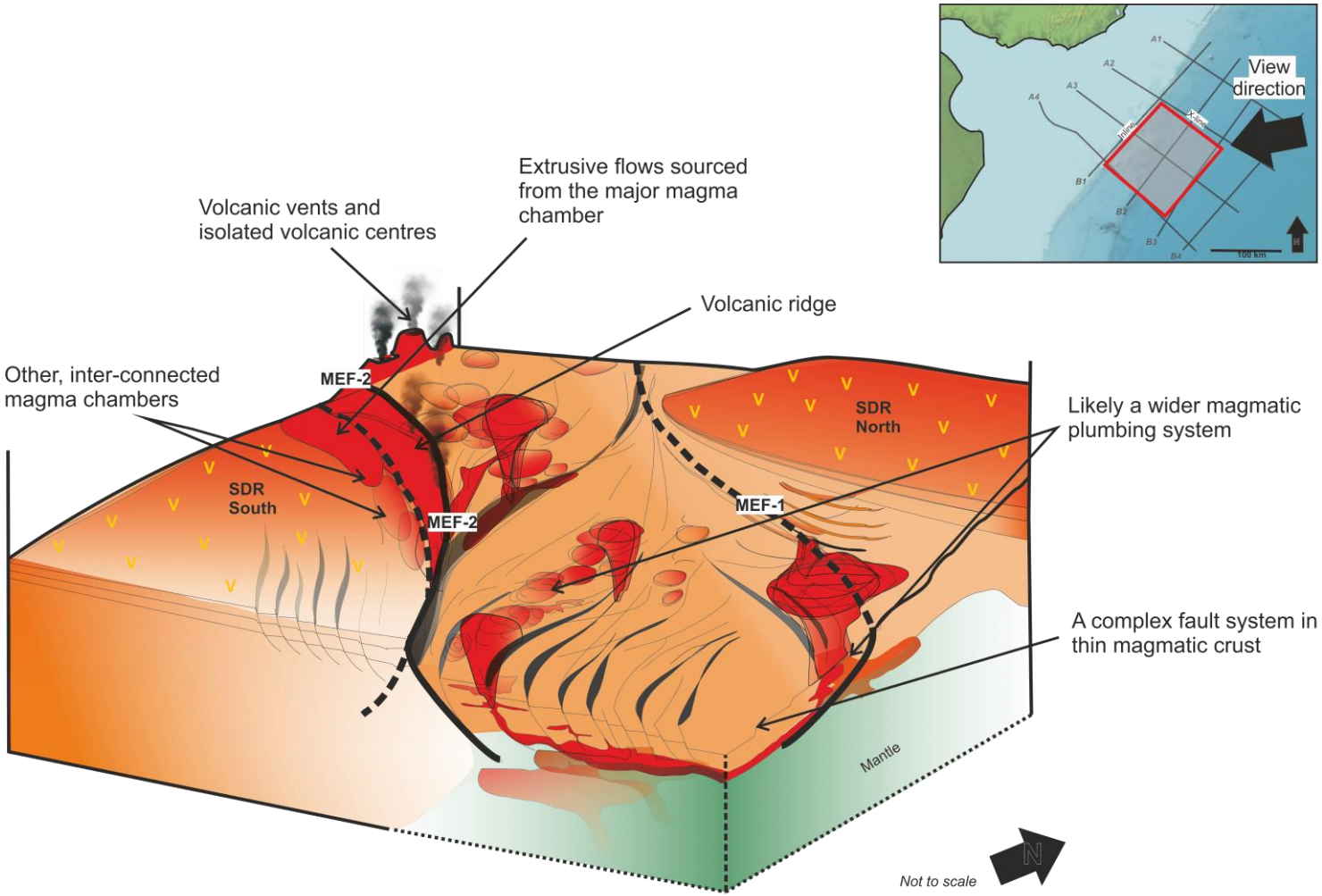

Figure 5.40: 3D model of the 3D data cube transtensional fault system with implied intrusions at depth and interconnected.

5.8 Synthesis

New insights are provided by the 3D dataset into a complex tectono-magmatic region on the continental-oceanic boundary, giving a window into a range of complex geometries which were active in the syn-rift but shut off completely by the early post-rift period. This chapter also shows the varied nature of the faulting across the 3D dataset and how this is related to the strength of the affected crust. The traces of faults have been mapped using depth slice sections at a basement level. This has captured a previously unknown system of complex, anastomosing, transtensional faults and significant intrusive magmatism. A previously unrecognised magmatic plumbing system has been shown with an intrinsic relationship to the syn-rift fault system and the MEF-2. A large preserved magma chamber was identified and both upper and lower surfaces of this feature were mapped. In conjunction with observations across the region in a series of intersecting profiles, multiple chimneys at the top of the magma chamber were observed, as well as a feeder dyke system below, which is likely facilitated by the presence of the MEF-2 that has acted as a volcanic conduit. The 3D data through this complex volcano-tectonic region may have both local and regional implications to similar areas of other magmatic margins which may be unrecognised.

Chapter 6: Discussion

6.1 Introduction

The aims of this thesis were to investigate the influence of basement structure and volcanics on the evolution of the offshore Uruguay margin. Also, to propose mechanisms and suggest models to explain the development of the observed features. This has included a focus on the role of magmatism and its interaction with tectonics. Defining crustal architecture in deep-waters along the petroleum-rich South Atlantic frontiers has proved challenging (Rosendahl, 1987; Mohriak et al., 2002). This study has used high resolution, 2D and 3D PSDM seismic reflection datasets as well as Emag and Gravity data to uncover new evidence of the tectono-magmatic evolution of the offshore Uruguay margin. The work significantly adds to our understanding of the basement evolution of a relatively frontier region. It also provides new evidence about the nature of the continent-ocean boundary, complex faulting within magmatic crust/proto-oceanic crust and a newly identified, magmatic plumbing system.

6.2 The role of structural inheritance in margin evolution

6.2.1 The Punta del Esté Basin – an aulacogenic, volcanic rift basement

The Punta del Esté Basin is recognised as a region of ~50,000 km^2 of offshore Uruguay and has previously been suggested to be a ‘funnel-shaped’ aulacogen overlying continental crust (Soto et al., 2011). Stoakes and Campbell, (1991) suggested it was the northernmost aulacogenic embayment of the south Atlantic region, however, until this study, little has been known about the nature of the basement (Stoakes and Campbell, 1991; Pángaro et al., 2016) and the true volcano-tectonic genesis of the offshore region, has remained poorly defined. This study firstly examined the role of structural inheritance on the development of the margin.

Recent studies have questioned the influence of structural inheritance in relation to both the segmentation of margins, oceanic transform fault development and the localisation of continental break-up itself (Lundin and Dore, 2011; Tugend et al., 2015). Cross-cutting of inherited structures is observed by major fracture zones in the Colorado Basin (Autin et al., 2013) and the initiation of extension and/or transtension is by no means always linked to an existing crustal heterogeneity. Transtension is observed in this study characterised by en-echelon magmatic segments seen in the depth sections of the 3D dataset. Transtension and large-scale shearing has been previously identified on crustal scale faults in the region, back to the Jurassic and earlier (Zambrano and Urien, 1970). It is also known that inherited weaknesses from plate reorganisation can be re-activated by the rifting process (Ziegler and Cloetingh, 2004; Brune et al., 2012). Within the Salado Basin to the south, the late Jurassic faults are responsible for the localisation of strain and have experienced multiple reactivations (Zambrano and Urien, 1970). Precedent has been set with authors noting a link between this early phase of extension and the creation of pull-apart basins (Keeley and Light, 1993; Tankard et al., 1995; Franke et al., 2006; Loegering et al., 2013) which are recognised in onshore areas, as far as Cape Horn on the African conjugate (Ghiglione et al., 2010). In the South Atlantic, crustal-scale faults and cratonic boundaries have been identified along both conjugate margins and can be traced to Gondwanan lineaments (Nürnberg and Müller, 1991; Rabassa, 2010; Moulin et al., 2010). Gondwanan rifting has reactivated predominantly Pan-African-aged mobile belts, accounting for the preferential reactivation of margin-oblique structures first, in the rifting process (Janssen et al., 1995; Ziegler and Cloetingh, 2004). In areas such as Afar and the Main Ethiopian rift we see similar utilisation of preferentially aligned, pre-existing basement faults that aid early extension (Ebinger and Casey, 2001; Wright et al.,

2006; Keir et al., 2015). Many rifts are abandoned at an early stage of extension, often leaving a failed rift arm (aulacogen) of a tri-axial system. The margin-oblique rift sections of the South Atlantic are proposed to be remnants from this process, with a suite of rifts during the late Triassic to early Jurassic through the lower South American peninsular that are likely contemporaneous with this early stage of basin formation and faulting (Tankard et al., 1995). In offshore Uruguay, this study finds evidence of pre-rift faulting around the southern edge of the RdP craton (figure 4.6, chapter 4). It has been proposed that the continuation of the Martin Garcia lineament (Jacques, 2003) occurs through the Rio de la Plata embayment (Carlos Urien, personal communication, 2016) before it swings to a more north-easterly direction onshore. This study now agrees with Jacques, (2003) in that this lineaments offshore continuation, is represented by one of the major extensional faults now recognised in this work (most likely MEF-1) (figure 6.1). Another primary lineament, MEF-2 can be correlated with the northern Salado basin which can be traced back to a 2.1 Ga suture (Páengaro and Ramos, 2012) (figure 6.1). This fault geometry is consistently seen in continental rift settings (Van Wijk and Blackman, 2005). This lineament likely began as a diffuse cluster of early fractures within the Gondwanan landscape (figure 4.32, Chapter 4) and may be laterally continuous with the Damara Belt on the conjugate African margin (figure 6.1). From this work, it is suggested that the MEF-2 fault represents the offshore continuation of this structure, linking the epi-sutural genesis of the Punta del Esté Basin with that of the Salado Basin for the first time. These major structures are likely to have had a ‘flip-flop’ tectonic evolution, related to changes in polarity and various mantle melting events (Sauter et al., 2013; Geoffroy et al., 2014). This is also observed with large faults at nascent spreading centres like SE Afar (Geoffroy et al., 2014). This study also suggests that these two lineaments are both Gondwanan age sutures and likely have a genetic link, created

by regional scale extension/transtension within an intra-continental shear zone (figure 4.32, Chapter 4). Remnant faulting related to this may correlate with that which is observed around the southern edge of the Rio de la Plata craton (RdP) craton (figure 6.1). Similar massive shear zones were known to be utilised to accommodate fault block rotation along regions of dextral shear during early Atlantic opening (Tankard et al., 1995).

6.2.2 Routes for magmatism and the siting of a nascent rift centre

If early movement along the transfer faults/the fracture zones was trans-tensile (as is likely), the influence of inherited structures in the continental crust during early rifting would cause a ‘leaky’ transform zone to be created, and provide a route for magmatism (Wilson et al., 2003). This study supports this idea and provides evidence of the facilitation of magmatism by faulting, especially notable with the presence of a major magma chamber directly adjacent to MEF-2. Similar, large-scale, deep detachment faults are also present within the Colorado Basin to the south and have created similar, asymmetrical rift basins during an early phase of deformation (Páengaro and Ramos, 2012; Autin et al., 2013). These structures controlled the siting of nascent rift depocentres, helping to develop the basin structure we now observe. Key factors in nucleating a rift are the inherited crustal strength of the pre-existing fabric as well as the presence of upper mantle convection. Recent studies have supported the idea that rift migration and failure is a part of rift evolution with rifts often either failing completely or becoming ‘offset’ from the initiating rift (Franke et al., 2002; Chenin and Beaumont, 2013). Crustal strength influences the path of reactivated or offset rifts with stiff layers preferentially reactivated over more ductile zones which may be bypassed completely (Chenin and Beaumont, 2013). However, zones of ‘soft’ lithosphere have been shown to

localise convection in the upper Mantle, controlling the segmentation of margins and rift processes (Corti, 2012). The Gabon Basin provides an analogue as it developed as a double-rift system, between two ancient cratonic lineaments, with the ultimate failure of one rift arm (Dupré et al., 2011). Dupré, Cloetingh and Bertotti, (2011) also note that the syn-rift of the Gabon Basin is associated with thin crust, which is also observed in this study beneath the syn-rift sediments. Four fracture zones with steps in the Moho (which are observed on the major structures in this study) are also observed on the Rio Muni transform margin of Equatorial Guinea (Wilson et al., 2003), these split an area of proto-oceanic crust. Wilson, Turner and Westbrook, (2003) conducted gravity modelling that suggested this area is a combination of two parts serpentinized peridotite with oceanic crust between. An important finding that may also be applicable to the basement of the Punta del Esté Basin in this work. Another example of the abandonment of early rifting is the Reconcavo-Tuscano-Jatoba rift of north-east Brazil. This is an abandoned intra-continental rift that is characterised by transfer faults (Milani et al., 1988; Milani and Davison, 1988). It also shows crustal thinning of up to 45% and localised mantle up-warping similar to that which we observe during the syn-rift over the magmatic crust underlying the Punta del Esté Basin (figures 4.23, 4.24 Chapter 4). The unusual geometry of the Reconcavo depression appears to be a consequence of not just a transform zone, but the interaction of a variety of inherited and super-imposed tectono-morphological events (Milani and Davison, 1988; Milani et al., 1988), similar to the evidence now presented in offshore Uruguay. Globally, early oblique rifting is also seen in the equatorial Atlantic, Gulf of California, Ethiopian rift and the Dead Sea Transform fault (Brune et al., 2012). The age of early rift initiation on the conjugate African margin, has been suggested to be linked to extension coincident with the Karoo-Ferrar large igneous province (LIP) at 183 Ma (Encarnación et al., 1996; Páengaro

and Ramos, 2012). The Namib rift as an example on the conjugate African margin, is proposed as an early rift phase (Clemson et al., 1999). Inheritance is increasingly recognised as involving both compositional and thermal elements, not only structural ones (Manatschal et al., 2015). Manatschal, Lavier and Chenin, (2015) suggest that acquired physical processes, such as serpentinisation and decompression melting also play an often under-appreciated role in rift evolution, applicable to both magma-rich and magma-poor margins.

6.2.3 Why was rifting abandoned?

Ultimately, the degree of importance inheritance plays on rift evolution of both end member margins is likely a diminishing role as rifting evolves (Manatschal et al., 2015). This is in agreement with the finding that oblique rifting was abandoned in offshore Uruguay, along the axis of the Punta del Esté Basin (and epi-sutural, margin-oblique, pan-african lineaments) in favour of ~E-W oriented, Atlantic spreading. This orientation became thermo-mechanically more favourable due to rheological pre-weakening of the crust along the long axis of former back-arc basins from the Ediacaran and early Mesozoic, such as the Neoproterozoic, Marmora back-arc Basin (Will and Frimmel, 2016) (see also section 7.3 and figure 5.30). The evidence shown in this study indicates inheritance and pre-Mesozoic tectonics have played a major role in the early development of the offshore Uruguay margin. This is illustrated by the through-going structures of the MEF-1 and MEF-2, as well as faulting around the southern edge of the RdP craton and the alignment of these features with Gondwanan, pan-African-aged lineaments, upon which early Mesozoic rifting was centred. Gravity and Emag data has been useful in mapping the linkage of these structures to the onshore region (figure 4.28, Chapter 4 and section 7.2) as these data are not constrained by continent-ocean crustal divisions. The Argentinian, Colorado Basin to the south is another basin highly influenced by

pre-Mesozoic structural inheritance (Urien and Zambrano, 1973; Franke et al., 2006; Autin, 2010; Páengaro and Ramos, 2012; Autin et al., 2013). SDR are dominant features of the offshore South American margin, their formation associated with a sub-aerial environment (Talwani et al., 1976; Mutter et al., 1982; Paton et al., 2017; Norcliffe et al., 2018). However the magmatic crust we observe between the SDR has a hummocky appearance, seen more in sub-marine spreading environments (Sauter et al., 2013) and only 2% of the global mid-oceanic ridge spreading system currently is sub-aerial (Wright et al., 2012) (Iceland and Afar). It may be that the region of replaced magmatic crust was isostatically depressed for a period during early rifting, especially in relation to the surrounding continental and cratonic crust. This is supported by evidence of a general, triangular depression of the top syn-rift horizon (figure 4.17, chapter 4). However, there is also evidence of localised magmatic uplift/prominent volcanics that are likely to have been sub-aerial and the depression may be as a result of later isostatic adjustment when rifting was abandoned.

6.2.4 The role of the Rio de la Plata (RdP) craton

The presence of the resistant, Rio de la Plata craton in southern Uruguay has acted as a long-lived, deflecting and rooted structure for all tectonics since the Palaeo-proterozoic era (Frimmel et al., 2011; Rapela et al., 2011; Will and Frimmel, 2016). Elsewhere on southern Atlantic margins, the late Palaeozoic tectonics responsible for the Ventania-Cape fold belt and the Cape Syntaxis in South Africa (Páengaro and Ramos, 2012; Paton et al., 2016) have been similarly affected by the ‘buttress effect’ of ancient cratons. The RdP craton has funnelled Mesozoic tectonics to the unstable, weakened crust around the borders of the craton (Rapela et al., 2011). In Chapter 3 of this thesis, the eastern offshore extent of the RdP craton was mapped for the first time using long-offset seismic reflection data. Analysis of 1:1 scale strike

line sections have provided new information on the internal structure and seismic make-up of the cratonic block to depths of ~30 km. The tectonic system which underlies the Punta del Esté Basin exhibits a triangular shape as it has been able to widen oceanwards, away from the effects of the RdP cratonic buttress.

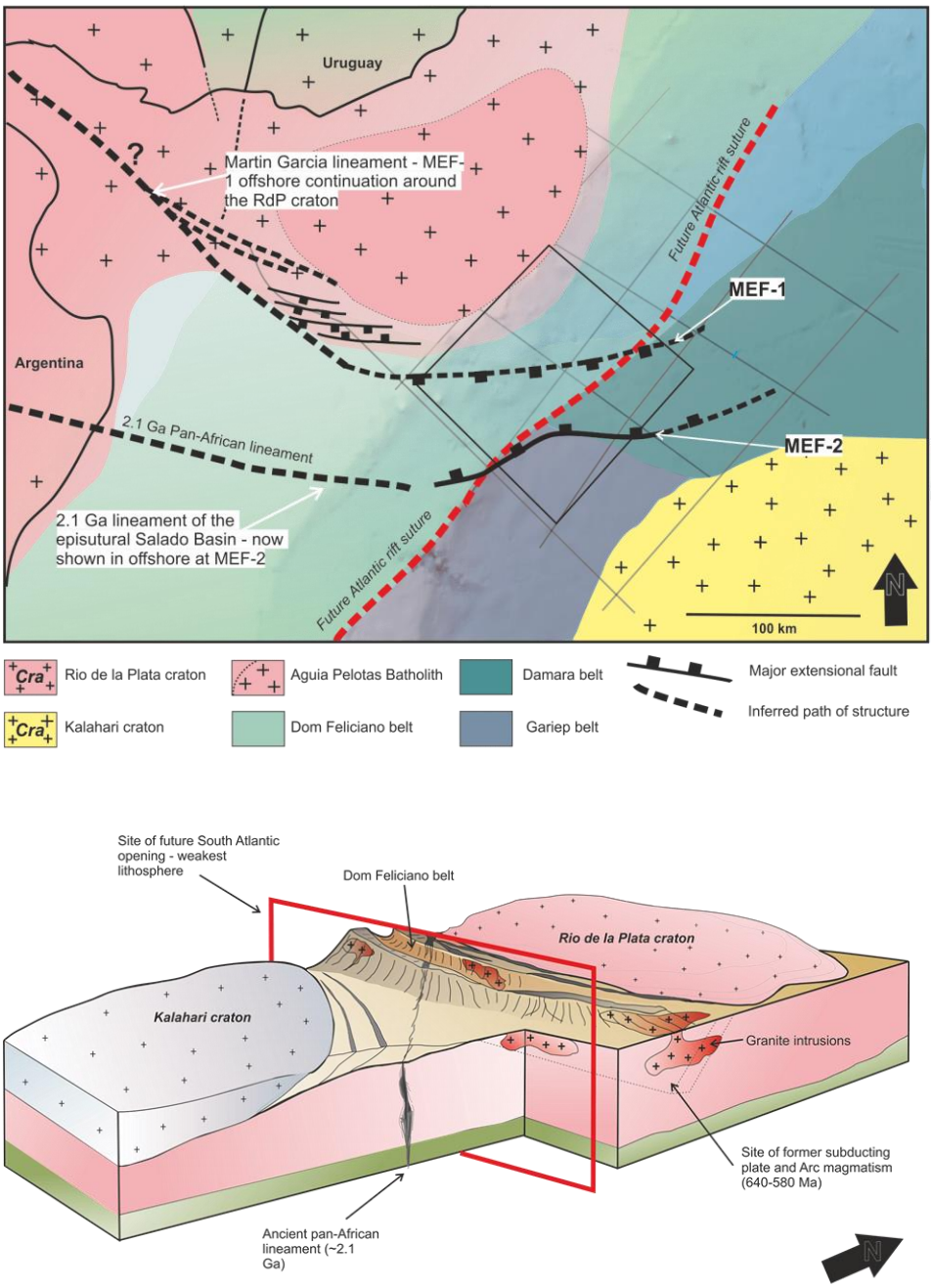

Figure 6.1: (Top**)** Major structures of the Palaeozoic offshore Uruguay margin from this study, overlain with the Dom Feliciano belt and Damara Belt locations super-imposed. Also shown are the Rio de la Plata craton (RdP) in the north-west with the internal Aiguả-Pelotas Batholith and the Kalahari craton to the south-east (Yellow). A continental landmass connection is inferred between them during this time period. (Bottom) Model showing the proposed arrangement of major cratons and the regionally significant Dom Feliciano belt in the offshore Uruguay region. Note also the presence of a large pan-African lineament (2.1 Ga) identified by Rapela et al., (2011) that becomes the nucleus for the Mesozoic Salado Basin. Also, in red, the site of the future South Atlantic rift based upon Will and Frimmel, (2016) and the formed subducting plate and Arc magmatism of 640-580 Ma. Modified from Oyhantçabal et al., (2009) and Rapela et al., (2011).

6.3 Does Uruguay conform to a typical magmatic margin?

This study has revealed both typical, and atypical, elements of the regional crustal geometry of a magmatic rifted margin. Expected features such as a thick, proximal zone of pre-rift continental crust is observed and in agreement with other parts of the margin, in particular, the Argentinian margin (Franke et al., 2002; Franke et al., 2006; Blaich et al., 2009; Becker et al., 2012; Loegering et al., 2013). Also present are syn-rift extensional half-graben structures on the continental shoulder and wide, voluminous extrusive wedges of SDRs with typical convex-up, dipping reflections. Oceanic crust, of a typical and expected thickness, is also recognised in the distal domain. However, through a broadly E-W section of the middle of the 2D dataset, there is a zone of hyper-thinned crust. In this study it is found to be thinned to <~3 km in some areas. This and the seismic reflection characteristics, lead to the interpretation that the region is comprised of magmatic crust (additive magma). This finding is strengthened by the location of this zone in a region of transition from the continental to oceanic domains and the disappearance of pre-tectonic sedimentary units, along with the deposition of younger units directly over basement. This suggests the creation of ‘new’ basement, as observed in the Australian-Antarctic margin (Gillard, Manatschal, et al., 2016). Gillard, Manatschal, et al., (2016), suggest that this may either be due to magma-accretion (oceanic crust) or exhumation due to extensional detachment faulting. It should be noted that the relationships between faults, sediments and magma is the only way to propose a relative age for faults and also the creation of ‘new basement’ in areas like the distal Australian-Antarctic margin (Gillard, Autin, et al., 2016). In recent work, predominantly focused upon magma-poor margins, authors have broken down the nature of the basement into different sub-domains, resulting from processes such as magmatic accretion and exhumation (Gillard et al., 2015). This study provides

evidence for both processes having played a major role in the evolution of the basement. It also provides new, significantly greater detail on the nature of the structural region termed the “Rio de la Plata transfer system (RPTS)” identified in previous work by Soto et al., (2011) and Morales et al., (2017) and now reveals complex tectono-magmatic interactions.

6.3.1 Atypical crustal structure for a magma-rich margin

The study has exposed an atypical crustal structure for a magmatic margin, yet agrees with previous work suggesting an aulacogenic rift (failed rift arm) origin for the Punta del Esté Basin (Ancap, 2011; Soto et al., 2011; Morales et al., 2017; Rossello et al., 2018). This also fits into the origin of the majority of the margin-oblique, South American, Mesozoic basins (see section 6.2). Recent work by authors predominantly focused upon magma-poor regions, have begun to address one of the last major unsolved problems of plate tectonics - the transition between inherited continental crust and newly-created oceanic crust (Lavier and Manatschal, 2006; Péron-Pinvidic and Manatschal, 2009; Cannat et al., 2009; Unternehr et al., 2010; Gillard et al., 2015; Manatschal et al., 2015; Gillard, Autin, et al., 2016; Gillard et al., 2017; Tugend et al., 2018; Decarlis et al., 2018). A ‘Proto-oceanic’ domain is identified by several authors and is increasingly used to describe the transition from rifting to steady-state, Penrose-type oceanic crust (Gillard et al., 2017; Keen et al., 2018; Decarlis et al., 2018). There are still many questions about the role and importance of magmatic versus tectonic processes associated with this transitional region from exhumed Mantle and gradual or abrupt changes into oceanic crust (Gillard et al., 2015). This region on magmatic margins is *even less* well defined, especially as it is often obscured by voluminous syn-rift magmatism (Blaich et al., 2009) and distinctions between intruded continental crust, under-plated continental crust and oceanic crust may become blurred (Ebinger and Casey, 2001; Blaich et

al., 2009). There is also still a lack of evidence of the nature of this transition and the nascent processes associated with embryonic spreading centres (Gillard et al., 2017). Some evidence can be gathered from fossilised systems which may once have been proto-oceanic domains, such as the Chenaillet Ophiolites in the French/Italian Alps, part of the Alpine-Tethys margins (Manatschal et al., 2011) and the Newfoundland margin, (ODP Site 1277) (Péron-Pinvidic et al., 2007). However, this study provides additional, detailed evidence of magma-tectonic interactions along this poorly understood boundary of continental to oceanic domains. Additional mechanisms which affect rift evolution may also emerge due to the three-dimensionality of an extensional system (Brune et al., 2012) which is not always considered and may be under-recognised. In the offshore Uruguay oceanic crust (line B4), dipping reflections are suggestive of the formation of this crust in a fast spreading environment, based up similar structures in Pacific transects (Eittreim et al., 1994; Ranero et al., 1997; Bécel et al., 2015). These have a notable change in dip direction in line with the distal continuance of the region of oblique-spreading along the axis of the Punta del Esté Basin. These have been imaged in other studies in the Atlantic (McCarthy et al., 1988) and in the Pacific (Ranero et al., 1997; Reston et al., 1999). Several authors suggest that these dip towards a palaeo-spreading centre (Ranero et al., 1997; Bécel et al., 2015).

6.3.2 Margin oblique spreading creates the Punta del Esté aulacogen

The change in dip of intra-oceanic crustal reflectivity also suggests that spreading was transiently attempted, oblique to the margin, along the epi-sutural axis of the Punta del Esté Basin but was ‘quickly’ aborted. This was abandoned as a result of a (regional) pole of rotation change that made ~E-W Atlantic opening geometrically more favourable, along the suture line of Palaeozoic back-arc basins. This agrees

with the formation of lower crustal shears in the oceanic crust as it requires differential motion at the base of the crust which may be produced by localised plate reorganisations, as is seen with the Kula-Pacific-Farallon triple junction (Bécel et al., 2015). This produces a focused, very local area of mantle upwelling (asthenospheric bulge) (which we observe, figure 4.24, chapter 4) causing differential shear at the base of the crust (Bécel et al., 2015) and re-localising deformation (Gillard, Manatschal, et al., 2016). The location of a hotspot associated with the Paraná-Etendeka LIP may also have associations with early magmatism and rifting, although this study does not provide specific evidence of an increased thermal regime under the offshore region, a raised mantle is observed and this cannot be ruled out as another factor contributing to the magmatism associated with early oblique rifting. A melt lens is also commonly observed in seismic reflection datasets associated with fast spreading oceanic centres and in oriented melt pockets near to volcanic centres in Afar (Keir et al., 2011; Combier et al., 2015). This may be illustrated by the magma chamber investigated in the next section (see section 6.4).

6.3.3 The East African Rift System, a modern analogue

The East African Rift System (EAR) has provided the ideal modern analogy of early stage of continental rifting (Mortimer et al., 2007). It remains a dynamic and evolving tectono-magmatic system, providing an opportunity in the present to study and understand similar early rifting scenarios and as such, it has been widely studied (Rosendahl, 1987; Morley et al., 1990; Ring, 1994; Ebinger and Casey, 2001; Keranen et al., 2004; Wright et al., 2006; Corti et al., 2007; Beutel et al., 2010; Rooney et al., 2011; Corti, 2012; Corti et al., 2015; Muirhead and Kattenhorn, 2018; Corti, Molin, et al., 2018). The early stages of the SE Afar rift were syn-magmatic (8-9 Ma or earlier) (Geoffroy et al., 2014) and had comparable features to what this region of offshore Uruguay may have experienced in early rifting - that being,

primarily - strong, localised, lithospheric thinning and extension, coeval with mantle melting (Geoffroy et al., 2014). In Afar, crustal thinning was locally accommodated by mafic magma accumulation at varied depths, rather than faulting, leading to the creation of transitional crust (Keir et al., 2011; Wright et al., 2012; Paton et al., 2017). The Neogene Stratoid Volcanic series is a depressed area with a Basaltic floor that has an active, en-echelon, tectono-magmatic axis (Geoffroy et al., 2014) similar to what is observed in this study in the Punta del Esté Basin basement (Rhomboidal magmatic segments in depth slice sections). This study has revealed that the Punta del Esté basement is comprised of magmatic crust which was likely to have acted as a proto-ridge axis for seafloor spreading prior to Atlantic rifting proper.

6.3.4 Exhumed mantle on a magma-rich margin

This study also found an area of exhumed mantle (line B3) an unusual finding for a magmatic margin. The seismic reflection architecture of this region has led me to believe it is exhumed mantle (sensu Gillard et al., (2015). Examples of this type of reflectivity are observed on seismic sections of the Australian margin (Gillard et al., 2015) along with the associated detachment faulting that is also seen in this study. Wilson, Turner and Westbrook, (2003) state that the Moho is absent in areas of serpentinized peridotite where the amount of seawater decreases with depth, therefore producing a diffuse boundary between the serpentinized peridotite and un-serpentinized upper-mantle, which explains the lack of Moho reflections. Dean, Sawyer and Morgan, (2015) also note that serpentinized mantle can show no coherent, internal seismic structure. It is not unusual to find serpentinized peridotite at the onset of seafloor spreading on magma-poor margins (Whitmarsh et al., 1990; Whitmarsh et al., 2001; Henning et al., 2004; Dean et al., 2015), however this finding on a classically magma-rich margin, does pose further questions regarding the margins evolution. The rugose, often curvi-linear morphology of the top boundary of

the exhumed mantle observed (in this study) is a typical finding at the zone of exhumed continental mantle, (ZECM) on magma-poor margins. The magma-poor north Atlantic margin and Labrador Sea rifted margins have similarly sized, ~50-100 km wide sections of exhumed and partially serpentinized mantle that similarly exist between the feather-edge of the continental crust and oceanic crust (Lundin and Dore, 2011). Other examples include the Labrador Sea margin (Chian et al., 1995) and tectonically emplaced, highly serpentinized mantle rocks along the Ghana Transform margin where oceanic crust is <4.4 km thick (Edwards et al., 1997; Wilson et al., 2003). A peridotite ridge along the Iberian continental margin (Pickup et al., 1996; Dean et al., 2000; Wilson et al., 2003) may be comparable to the volcanic ridge which accompanies and is adjacent to, the MEF-2 structure. However it may also represent a section of exhumed continental mantle which accompanies peridotite ridge formation, transitioning to episodic volcanism and locally thinned Basaltic crust (Dean et al., 2015). As such, some locally prominent regions of crust within the borders of the magmatic system may represent allochthonous rider blocks of crust with a higher felsic composition, or may just be resistant areas of exhumed upper-mantle. Work by Lundin and Dore, (2011) considered the existence of mantle exhumation on a magma-rich margin by proposing an earlier stage of hyper-extension which has pre-weakened the crust. This is supported by early work from Brun and Beslier, (1996) who propose a model which actually negates the need for a higher local geo-therm and allows for short-wavelength mantle exhumation. This study suggests that the region underlying the Punta del Esté Basin most likely represents a ‘Hybrid crust’ as suggested by Gillard et al., (2017) of exhumed mantle and magmatic rocks, which is also seen in the Gulf of Guinea at oceanic spreading onset (Gillard et al., 2017). Also recognised in this work, is that exhumed mantle has been found to be subject to magmatism and internal detachment and normal faulting

(line B3), similar to the Gulf of Guinea (Gillard et al., 2015; Gillard, Manatschal, et al., 2016; Gillard et al., 2017). The section of exhumed mantle on line B3 is highly faulted with different generations of faulting evident, however it appears confined between the rift border faults of the MEF-1 an MEF-2. Similar, large scale ‘flip-flop’ detachment fault systems (Sauter et al., 2013) can accommodate extension when a lower amount of magma is present (i.e early rift) (Gillard, Manatschal, et al., 2016) and have smaller-scale, cross-cutting detachment faults with alternating dips. The Australian-Antarctic margin and the Iberian margin both show similar detachment fault systems (Reston and McDermott, 2011; Gillard et al., 2015; Gillard, Manatschal, et al., 2016).

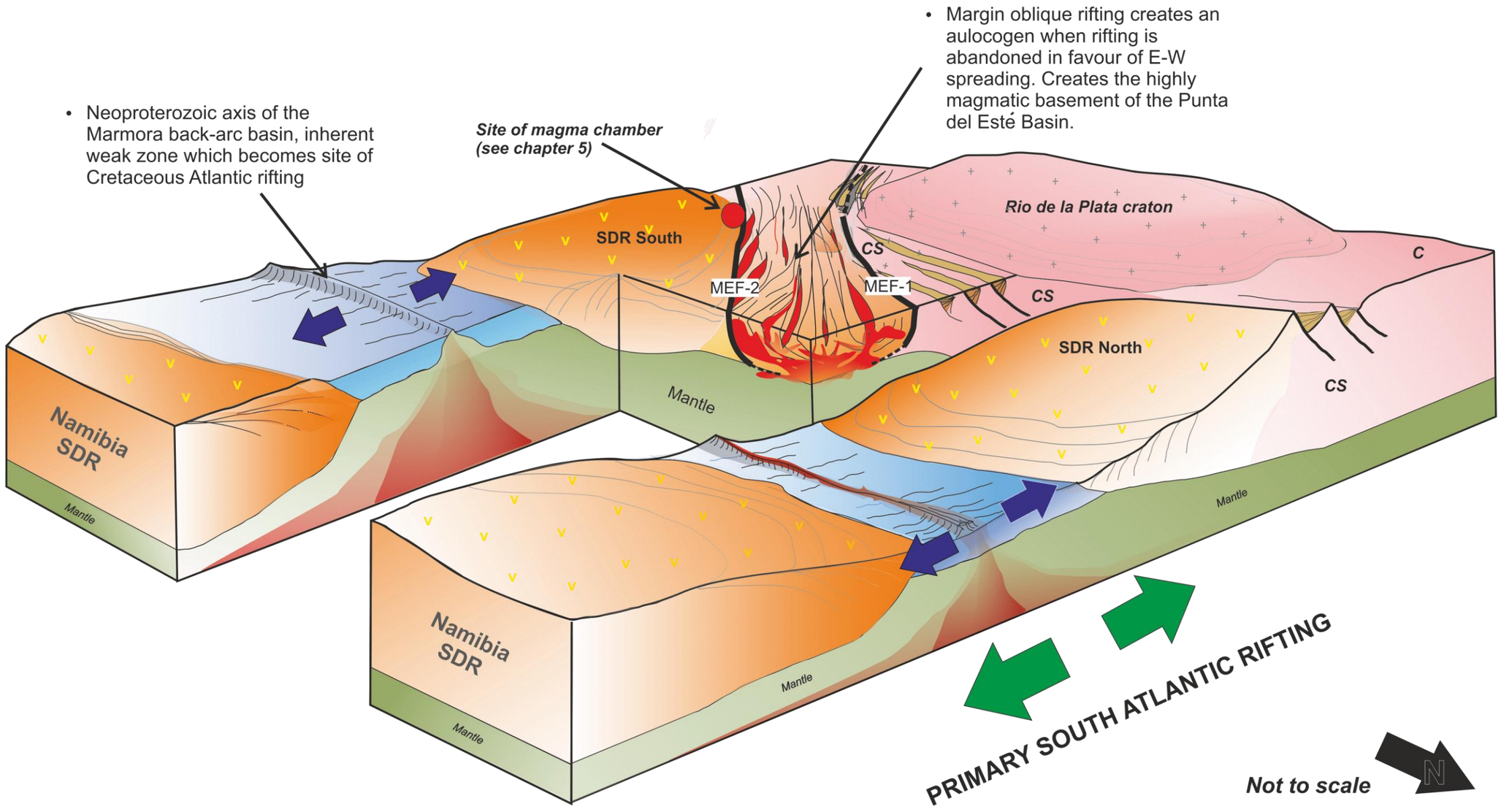

Figure 6.2: Composite 3D model of the tectono-magmatic features in the syn-rift period of the offshore Uruguay margin.

6.4 Insights into the 3D evolution of magmatic plumbing systems

6.4.1 A rare fossilised magma chamber

The acquisition of recent 3D seismic reflection data for the petroleum industry has provided insights into sub-volcanic, magmatic plumbing systems such as the Palaeogene, Faroe-Shetland Sill complex, (Schofield et al., 2017), the NE Atlantic margin (Davies et al., 2002) and the Rockall Trough of NW Scotland (Thomson and Hutton, 2004). There however remains sparse geophysical evidence of magma chambers, with direct ponding of magma at the Moho only observed in very few locations (Thybo and Artemieva, 2013). This study provides a clear and detailed example of a fossilised magma chamber that gives significant 3D insights into the initiation of early margin-oblique rifting in the South Atlantic and smaller-scale tectono-magmatic relationships. The upper and lower surfaces of the magma chamber were mapped using prominent changes in seismic reflection character, the chamber itself being of very low seismic reflectivity in comparison to surrounding seismic facies. This internal homogeneity of seismic character is observed with slow-cooling, large igneous bodies, creating smooth variations in properties which may be reflection-free at seismic frequencies (Thybo and Artemieva, 2013). This contrast has allowed for accurate mapping of the boundaries of the magma chamber in this study. The 3D geometry of the chamber was expanded in Chapter 5. In agreement with most chambers that exist for any length of time, it favours an elongated spheroid as the most thermo-mechanically stable geometry (Gudmundsson, 2012). Similar, crustal melt lenses are ubiquitous with fast spreading centres (Combier et al., 2015) giving further evidence in support of fast, early, oblique rifting along the Punta del Esté (PdE) Basin axis.

6.4.2 A wider magmatic plumbing system

Magmatic conduits are evident from both the upper section (extrusion/eruption conduit) and lower section (injection conduit) of the chamber. Many magma chambers are subject to recurrent injections of hot, primitive magma from below which provides a replenishment system and feeds surface eruptions (Huppert and Sparks, 1980; Gudmundsson, 2012; Huber et al., 2019). These cyclic, recharging systems are present at various volcanic environments including mid-oceanic ridges (Sparks et al., 1980), island arc volcanoes and silicic centres (Huppert and Sparks, 1980). The base of the magma chamber outlined in this study has a downward conduit section of low reflectivity which is likely to represent the entry point of the feeder dyke that has provided magma to the chamber from a magma supply network below, and/or a source zone of partial melt (Magee et al., 2018). Extrusive flows along the roof of the chamber make up some of the early syn-rift deposits in the seismic reflection sequence and can be directly traced back to ejection/extrusion conduits on top of the magmatic body itself. This suggests that there must have been a relatively high degree of liquid melt within the magma chamber for eruptions to occur, rather than a crystal mush which often makes up most of a chamber and generally can’t be erupted (Magee et al., 2018).

6.4.3 What controls the position of the magma chamber?

Neutral buoyancy or rheological transitions are the most favourable points at which magma accumulates and forms chambers (Huber et al., 2019). This suggests that despite the position of the chamber against the MEF-2, it is likely to be not only tectonically controlled, but depth controlled by a rheological transition (i.e the Moho).

Most magmas are likely to first accumulate here (Huber et al., 2019). This fits with the location of the chamber sitting in isostatic equilibrium in a region of ductile, lower magmatic crust on, or just above, the Moho. To sustain an eruption from a chamber, the pressure must have been within a narrow range (~2 kbar (+ or - 0.5 bar) with the high viscosity of the crust creating an over pressurization for eruption (Huber et al., 2019). The presence of broadly circular zones of low reflectivity, ringed by higher amplitudes are observed on depth slice sections in this study and in time-slice sections from the north Rockall Trough. They are interpreted as concentric dyking, approximately 2-4 km wide (Thomson and Hutton, 2004). This study illustrates that the larger of these features, (~10-20+ km length) that are similar in size to the chamber in this study, may be magma chambers at the terminal end of feeder dykes and inter-connected conduits, unrecognised on other margins. Both in the Rockall Trough and this study, the features overlap, suggesting a complex, multi-level system of sills and/or magma chambers. In this study, these are situated along the northern border of the SDR South, corresponding with the magma chamber and along the southern boundary of a major through-going lineament (MEF-2), as such, these are highly likely to be facilitated by syn-rift, extensional faulting. Although not individually mapped in this study, further evidence for the existence of extended magma chambers and a wider plumbing system is indicated by the presence of additional concentric reflectivity (along the MEF-2 boundary with the SDR South and the inner segment of magmatic crust) and is likely part of a ‘stepped’ series, facilitated by the syn-rift extension of MEF-2 and the evolution of smaller-scale

extensional faulting within the magmatic crust. Trans-lithospheric faults similar to MEF-2 have also been linked to magma chamber growth (Yu et al., 2015).

6.4.4 Magma plumbing systems analogues

In the Faroe-Shetland sill complex, interconnected sills form a unique type of magma chamber where there is a complex interconnected magmatic body which essentially acts as a singular magma chamber (Schofield et al., 2017). A shallow series of magma chambers (~10 km depth) are also part of a complex plumbing system in Deception Island (South Shetland Islands) (Geyer et al., 2019). Deception Island chambers are fed directly from the mantle or an 'accumulation zone' located at ~15-20 km depth. In this study, rhomboidal magmatic lenses were observed on depth sections of the magmatic basement in an en-echelon arrangement, in agreement with oblique segments of rifts such as in Afar, and the oceanic ridges, the Mohns and Reykjanes (Corti et al., 2001; Corti, Sani, et al., 2018). Magmatic underplating and the intrusion of magma into the crust and upper-mantle are key processes in crustal formation, providing a way to facilitate crustal thickening by magma addition, independent of tectonics (Thybo and Artemieva, 2013). Axial melt lenses between oceanic crust and sheeted dyke sequences are also a major contribution to oceanic crust accretion at fast-spreading mid-ocean ridges (Zhang et al., 2015). Suggesting a more precise timing for magma emplacement is challenging (Tugend et al., 2018). Magmatic lenses such as those in this study and those observed in Afar, may indicate that the chamber formed contemporaneously with Atlantic rifting (but obliquely, along the PdE Basin axis). However, studies have also linked the growth of basaltic magma chambers to flood basalts (Yu et al., 2015) which does not rule out their creation during an early rift phase, synchronous with the Paraná-Etendeka LIP. Faulting can provide a nucleating crustal weakness to be exploited by upwelling magma, however, normal faulting can itself, be induced and

enhanced by dyke emplacement, a common example being Krafla on Iceland (Rubin, 1992; Combier et al., 2015). It is likely that both mechanisms have played a synergistic role in the evolution of this funnel-shaped region of the Uruguay margin basement (figure 6.3).

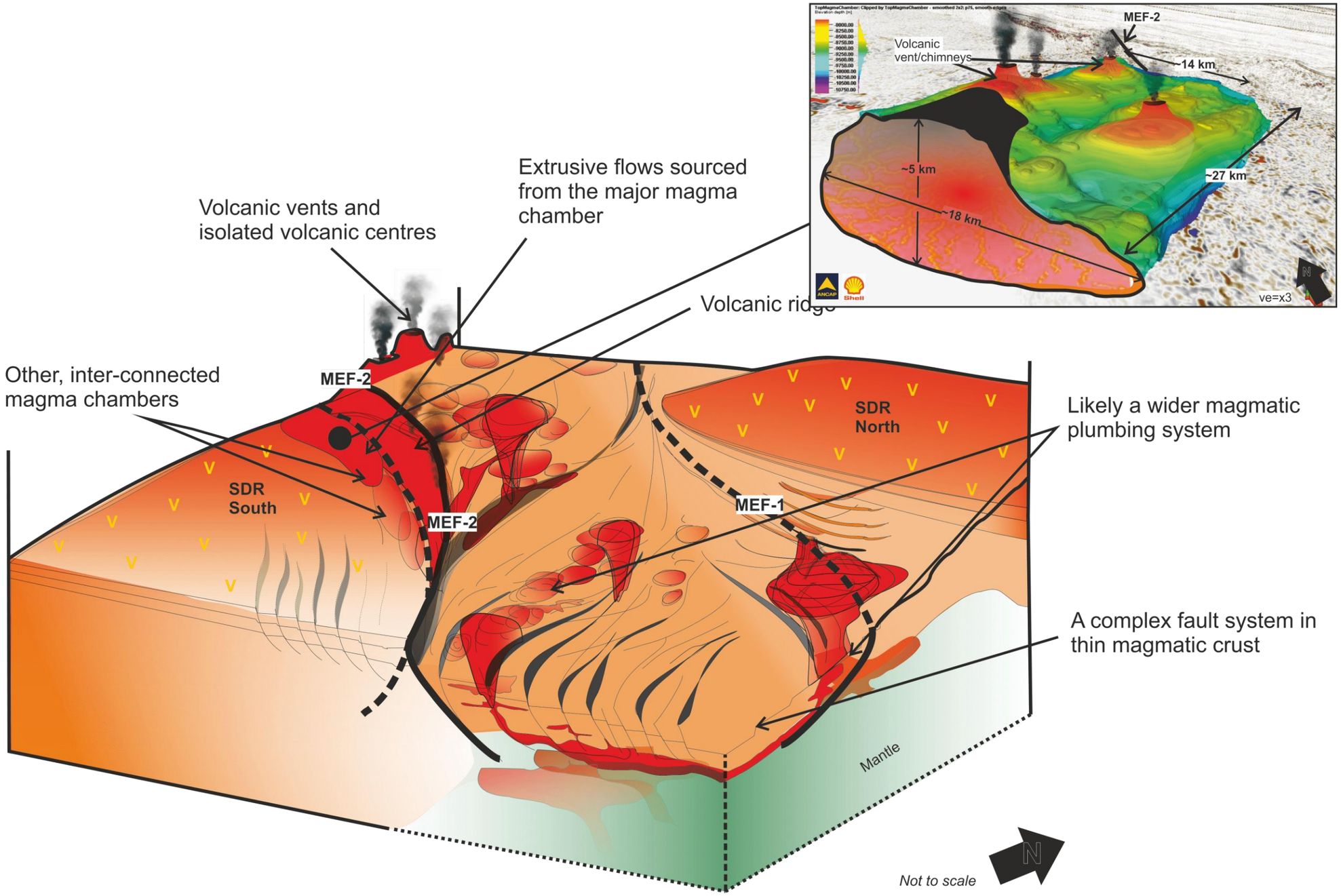

Figure 6.3: 3D model of the 3D data cube with complex fault system (mapped from depth slice Z=-10,214 m) and implied interconnected magma plumbing system.

6.5 Implications and recommendations for further work

Detailed analysis of a high resolution PSDM 3D dataset has revealed both the existence of magmatic crust as the predominant basement to the Punta del Esté Basin and a complex interplay of magma and tectonics. This has included a well-preserved, fossilised magma chamber along the continent-ocean boundary that has provided a unique window into the early syn-rift magmatism of the offshore Uruguay margin and a previously unrecognised, magmatic plumbing system. Generic rift models are increasingly inadequate to explain the diversity of continental margins observed (Zastrozhnov et al., 2020). The recent advent of high resolution 3D seismic reflection datasets, primarily for petroleum exploration has, as a bi-product, provided a detailed window into complex, tectono-magmatic processes of the under-studied seismic basement of a magma-rich margin. The recognition of a highly magmatic, early rift system in offshore Uruguay might otherwise have remained unrecognised. This has wider implications to margins globally, as under-representation of volcanics in syn-rift systems may affect paleo-heatflow into potentially source-bearing, sediment overburdens and alter the thermal evolution of a margin. For future work, combining the geophysical observations of this study with petrological and geochemical data would ideally provide greater insights into the nature of the atypical volcanic basement. Additionally, methods such as gravimetry and electromagnetics may be remotely employed to delineate additional magma chambers and melt reservoirs (Magee et al., 2018). 3D tomography and creating a velocity model from ocean-bottom seismometer measurements would provide a 3D geometry of the magma chamber, as used in work by Combier et al., (2015) on the Lucky Strike volcano of the Mid-Atlantic ridge. Creating a velocity dataset from the

3D cube would provide an additional methodology for differentiating the magma chamber from host rock, based upon velocity contrasts, although the high resolution 3D PDSM data in this study has done this remarkably well. Gravity inversion techniques would help to determine more precisely, the amount of magmatic additions within the continent-ocean boundary (Kusznir et al., 2018). The benefits of integrating methodologies is also championed for investigating complex magmatic plumbing systems, such as those now identified in this thesis, but the challenges of scale and the restraints of physical settings, remains (Magee et al., 2018).

Chapter 7: Conclusions

The aims of this project were to provide a 2D regional framework in order to understand the regional development of the volcanic basement of offshore Uruguay. Also, to investigate for the first time a rift system using 3D data across the region identified as the Rio de la Plata Transfer System (RPTS) and to discuss and propose a model to explain these morphologies. This has been achieved using a combination of 2D and 3D seismic reflection datasets and gravity and magnetic data. The findings of this study are:

- Structural inheritance has played a key role in the evolution of the margin by creating crustal heterogeneities and providing pre-existing zones of weakness that have been exploited by early Cretaceous Atlantic rifting. Pan-African lineaments have provided nucleating structures for margin-oblique weaknesses and the axis of Palaeozoic back-arc basins has been fundamental to locating Atlantic rifting proper.
- On a regional scale, the offshore Uruguay margin broadly conforms to the features typical of a magmatic margin. This is evidenced through voluminous syn-rift deposits in the form of two SDR wedges and conformable 2D dip-line crustal architecture. However, there is considerable variability exhibited in syn-rift magmatism, especially in regions affected by margin-oblique rifting. This is observed in atypical 2D crustal architectures both in dip line and strike line profiles with considerable unexpected crustal thinning.
- A local scale analysis of the interaction between structure and magmatism has revealed a previously unidentified magmatic plumbing system in the magmatic, transitional crust of the offshore Uruguay margin. Observed is a fossilised magma chamber approximately measuring 18 km by 5 km that has

been identified in the 3D PSDM dataset, through significant changes in seismic reflection character between the chamber and the adjacent volcanics/volcani-sediments. The seismic reflection facies of the internal chamber is of very low amplitude, chaotic and discontinuous reflectivity. This internal homogeneity of seismic character is observed with slow-cooling, large igneous bodies, creating smooth variations in properties which may be reflection-free at seismic frequencies (Thybo and Artemieva, 2013). The high resolution of the dataset at ~10-15 km depth on the offshore margin has allowed the mapping of this volcanic feature using the contrast in seismic amplitude and changes in seismic reflection characteristics of the internal chamber to surrounding reflectivity. This is a rare achievement in a deep region of a highly magmatic margin, where voluminous magmatism more commonly obscures the seismic signal produced from structures and individual volcanic features.

- Mapping of the magma chamber has been possible within Petrel software in three dimensions, including both the top and bottom surfaces of the spheroid chamber and giving a chamber volume of approximately 2,430 km^3. This has been achieved with a high degree of confidence and subsequently, a 3D model has been created. Additionally, superior 3D PSDM dataset resolution allows the clear identification of volcanic conduits and dyking features both from the upper and lower surfaces of the magma chamber. These suggest that the chamber was fed/charged from below and that it is connected to a wider, previously unknown, magmatic plumbing system.
- Vent/conduit features are also identified protruding from the upper surface of the magma chamber and can be directly associated with high amplitude

continuous reflectivity representing extrusive volcanics, above the chamber and leading away from conduits. This indicates the layered extrusive deposits are directly sourced from volcanic material within the magma chamber. This also gives further information on the viscosity and relative pressure within the chamber at the time of magmatic extrusion. The magma chambers upper conduits are also linked with the creation of some of the early packages of SDRs and extensional faulting which may be associated with SDR evolution.

- The local-scale structural relationships with magmatism vary - from acting as an apparent baffle or confining structure (MEF-2 splay) to likely helping facilitate the movement of magma through the wider plumbing system.
- Identification of the magma chamber as well as new evidence to suggest it is part of a wider previously unidentified, magmatic plumbing system (mapped in 3D PSDM seismic reflection data), are novel findings for an offshore highly magmatic region, as well as for this particular part of the South American Atlantic margin and as such, provide ample material for subsequent publication.

References

Abdelmalak, M.M., Meyer, R., Planke, S., Faleide, J.I., Gernigon, L., Frieling, J., Sluijs, A., Reichart, G.-J., Zastrozhnov, D., Theissen-Krah, S., Said, A. and Myklebust, R. 2016. Pre-breakup magmatism on the Vøring Margin: Insight from new sub-basalt imaging and results from Ocean Drilling Program Hole 642E. *Tectonophysics*. **675**, pp.258-274.

Alves, T.M., Moita, C., Cunha, T., Ullnaess, M., Myklebust, R., Monteiro, J.H. and Manuppella, G. 2009. Diachronous evolution of late jurassic-cretaceous continental rifting in the northeast atlantic (west iberian margin). *Tectonics*. **28**, (4), pp.1-32.

Ancap (2011) *Regional Geology: Offshore Uruguayan basins*.

Aslanian, D. and Moulin, M. 2010. Comment on 'A new scheme for the opening of the South Atlantic Ocean and the dissection of an Aptian salt basin' by Trond H. Torsvik, Sonia Rousse, Cinthia Labails and Mark A. Smethurst. *Geophysical Journal International*. **183**, (1), pp.20–28.

Autin, J. 2010. Colorado Basin structure and rifting, Argentine passive margin. *EGU General* **12**, (1997), pp.8706.

Autin, J., Bellahsen, N., Leroy, S., Husson, L., Beslier, M.O. and D'Acremont, E. 2013. The role of structural inheritance in oblique rifting: Insights from analogue models and application to the Gulf of Aden. *Tectonophysics*. **607**, pp.51–64.

Autin, J., Scheck-Wenderoth, M., Loegering, M.J., Anka, Z., Vallejo, E., Rodriguez, J.F., Dominguez, F., Marchal, D., Reichert, C., di Primio, R. and Götze, H.J. 2013. Colorado Basin 3D structure and evolution, Argentine passive margin. *Tectonophysics*. **604**, pp.264–279.

Basei, M. Â. S. *et al.* (2000) 'The Dom Feliciano Belt and the Rio de la Plata Craton: tectonic evolution and correlation with similar provinces of southwestern Africa', in *Tectonic evolution of South America, 31st International Geological Congress, Rio de Janeiro*.

Basei, M.A.S., Frimmel, H.E., Nutman, A.P., Preciozzi, F. and Jacob, J. 2005. A connection between the Neoproterozoic Dom Feliciano (Brazil/Uruguay) and Gariep (Namibia/South Africa) orogenic belts - Evidence from a reconnaissance provenance study. *Precambrian Research*. **139**, (3–4), pp.195–221.

Bécel, A., Shillington, D.J., Nedimović, M.R., Webb, S.C. and Kuehn, H. 2015. Origin of dipping structures in fast-spreading oceanic lower crust offshore Alaska imaged by multichannel seismic data. *Earth and Planetary Science Letters*. **424**, pp.26–37.

Becker, K., Franke, D., Schnabel, M., Schreckenberger, B., Heyde, I. and Krawczyk, C.M. 2012. The crustal structure of the southern Argentine margin. *Geophysical Journal International*. **189**, (3), pp.1483–1504.

Beutel, E., van Wijk, J., Ebinger, C., Keir, D. and Agostini, A. 2010. Formation and stability of magmatic segments in the Main Ethiopian and Afar rifts. *Earth and Planetary Science Letters*. **293**, (3–4) pp.225–235.

Blaich, O. a., Faleide, J.I., Tsikalas, F., Franke, D. and León, E. 2009. Crustal-scale architecture and segmentation of the Argentine margin and its conjugate off South Africa. *Geophysical Journal International*. **178**, (1), pp.85–105.

Blaich, O. a., Faleide, J.I. and Tsikalas, F. 2011. Crustal breakup and continent-ocean transition at South Atlantic conjugate margins. *Journal of Geophysical Research*. **116**, (1), pp.1-38.

Blaich, O., Faleide, J.I., Tsikalas, F., Gordon, a. C. and Mohriak, W. 2013. Crustal-scale architecture and segmentation of the South Atlantic volcanic margin. *Geological Society, London, Special Publications*. **369**, (1), pp.167–183.

Boillot, G., Grimaud, S., Mauffret, A., Mougenot, D., Kornprobst, J., Mergoil-Daniel, J. and Torrent, G. 1980. Ocean-continent boundary off the Iberian margin: A serpentinite diapir west of the Galicia Bank. *Earth and Planetary Science Letters*. **48**, (1), pp.23–34.

Boillot, G., Recq, M., Winterer, E.L., Meyer, A.W., Applegate, J., Baltuck, M., Bergen, J.A., Comas, M.C., Davies, T.A., Dunham, K., Evans, C.A., Girardeau, J., Goldberg, G., Haggerty, J., Jansa, L.F., Johnson, J.A., Kasahara, J., Loreau, J.P., Luna-Sierra, E., Moullade, M., Ogg, J., Sarti, M., Thurow, J. and Williamson, M. 1987. Tectonic denudation of the upper mantle along passive margins: a model based on drilling results (ODP leg 103, western Galicia margin, Spain). *Tectonophysics*. **132**, (4) pp.335–342.

Bronner, A., Sauter, D., Manatschal, G., Péron-pinvidic, G. and Munschy, M. 2009. Magmatic breakup as an explanation for magnetic anomalies at magma-poor rifted margins. *Nature Physics*. **5**, (2) pp.85–85.

Bronner, A., Sauter, D., Manatschal, G., Péron-Pinvidic, G. and Munschy, M. 2011. Magmatic breakup as an explanation for magnetic anomalies at magma-poor rifted margins. *Nature Geoscience*. **4**, (8) pp.549–553.

Bronner, A., Sauter, D., Munschy, M., Carlut, J., Searle, R., Cannat, M. and Manatschal, G. 2014. Magnetic signature of large exhumed mantle domains of the Southwest Indian Ridge – Results from a deep-tow geophysical survey over 0 to 11 Ma old seafloor. *Solid Earth*. **5**, (1) pp.339–354.

Brune, S., Popov, A.A. and Sobolev, S. V. 2012. Modeling suggests that oblique extension facilitates rifting and continental break-up. *Journal of Geophysical Research: Solid Earth*. **117**, (8) pp.1–16.

Brune, S., Heine, C., Pérez-Gussinyé, M. and Sobolev, S. V 2014. Rift migration explains continental margin asymmetry and crustal hyper-extension. *Nature communications*. **5**, pp.4014.

Brun, J.P. and Beslier, M.O. 1996. Mantle exhumation at passive margins. *Earth and Planetary Science Letters*. **142**, (1–2) pp.161–173.

Brun, J.P., Sokoutis, D., Tirel, C., Gueydan, F., Van Den Driessche, J. and Beslier. 2018. Crustal versus mantle core complexes. *Tectonophysics*. **746**, (September 2017) pp.22–45.

Brune, S., Heine, C., Clift, P.D. and Pérez-Gussinyé, M. 2017. Rifted margin architecture and crustal rheology: Reviewing Iberia-Newfoundland, Central South Atlantic, and South China Sea. *Marine and Petroleum Geology*. **79**, pp.257–281.

Buck, W.R. 1988. Flexural Rotation of Normal Faults. *Tectonics*. **7**, (5) pp.959–973.

Callot, J.P., Geoffroy, L. and Brun, J.P. 2002. Development of volcanic passive margins: Three-dimensional laboratory models. *Tectonics*. **21**, (6) pp.2-1-2–13.

Calvès, G., Schwab, A.M., Huuse, M., Clift, P.D., Gaina, C., Jolley, D., Tabrez, A.R. and Inam, A. 2011. Seismic volcanostratigraphy of the western Indian rifted margin: The pre-Deccan igneous province. *Journal of Geophysical Research: Solid Earth*. **116**, (1).

Cannat, M., Manatschal, G., Sauter, D. and Péron-Pinvidic, G. 2009. Assessing the conditions of continental breakup at magma-poor rifted margins: What can we learn from slow spreading mid-ocean ridges? *Comptes Rendus - Geoscience*. **341**, (5) pp.406–427.

Casquet, C., Rapela, C.W., Pankhurst, R.J., Baldo, E.G., Galindo, C., Fanning, C.M., Dahlquist, J. a. and Saavedra, J. 2012. A history of Proterozoic terranes in southern South America: From Rodinia to Gondwana. *Geoscience Frontiers*. **3**, (2) pp.137–145.

Chenin, P. and Beaumont, C. 2013. Influence of offset weak zones on the development of rift basins: Activation and abandonment during continental extension and breakup. *Journal of Geophysical Research: Solid Earth*. **118**, (4), pp.1698–1720.

Chian, D., Louden, K.E. and Reid, I. 1995. Crustal structure of the Labrador Sea conjugate margin and implications for the formation of nonvolcanic continental margins. *Journal of Geophysical Research*. **100**, (B12).

Chorowicz, J. 1989. Transfer and transform fault zones in continental rifts: examples in the Afro-Arabian Rift System. Implications of crust breaking. *Journal of African Earth Sciences*. **8**, (2–4) pp.203–214.

Clemson, J., Cartwright, J. and Swart, R. 1999. The Namib Rift: a rift system of possible Karoo age, offshore Namibia. *Geological Society, London, Special Publications*. **153**, pp.381–402.

Cochran, J.R. and Karner, G.D. 2007. Constraints on the deformation and rupturing of continental lithosphere of the Red Sea: the transition from rifting to drifting. *Geological Society, London, Special Publications*. **282**, (1), pp.265–289.

Combier, V., Seher, T., Singh, S.C., Crawford, W.C., Cannat, M., Escartín, J. and Dusunur, D. 2015. Three-dimensional geometry of axial magma chamber roof and faults at Lucky Strike volcano on the Mid-Atlantic Ridge. *Journal of Geophysical Research: Solid Earth*. **120**, (8), pp.5379–5400.

Contrucci, I., Matias, L., Moulin, M., Géli, L., Klingelhofer, F., Nouzé, H., Aslanian, D., Olivet, J.-L., Réhault, J.-P. and Sibuet, J.C. 2004. Deep structure of the West African continental margin (Congo, Zaïre, Angola), between 5°S and 8°S,

from reflection/refraction seismics and gravity data. *Geophysical Journal International*. **158**, (2) pp.529–553.

Co-operative Institute for Research in Environmental Sciences (CIRES) 2015. EMAG2: Earth magnetic anomaly grid (2-Arc-minute resolution). Accessed 16th February, 2021. Available from: https://geomag.colorado.edu/emag2-earth-magnetic-anomaly-grid-2-arc-minute-resolution.html

Corti, G., Bonini, M., Innocenti, F., Manetti, P. and Mulugeta, G. 2001. Centrifuge models simulating magma emplacement during oblique rifting. *Journal of Geodynamics*. **31**, (October 2015) pp.557–576.

Corti, G., van Wijk, J., Cloetingh, S. and Morley, C.K. 2007. Tectonic inheritance and continental rift architecture: Numerical and analogue models of the East African Rift system. *Tectonics*. **26**, (July) pp.1–13.

Corti, G. 2012. Evolution and characteristics of continental rifting: Analog modeling-inspired view and comparison with examples from the East African Rift System. *Tectonophysics*. **522**–**523**, pp.1–33.

Corti, G., Agostini, a., Keir, D., Van Wijk, J., Bastow, I.D. and Ranalli, G. 2015. Magma-induced axial subsidence during final-stage rifting: Implications for the development of seaward-dipping reflectors. *Geosphere*. (3) pp.563–571.

Corti, G., Molin, P., Sembroni, A., Bastow, I.D. and Keir, D. 2018. Control of Pre-rift Lithospheric Structure on the Architecture and Evolution of Continental Rifts: Insights From the Main Ethiopian Rift, East Africa. *Tectonics*. **37**, (2) pp.477–496.

Corti, G., Sani, F., Agostini, S., Philippon, M., Sokoutis, D. and Willingshofer, E. 2018. Tectonophysics off -axis volcano-tectonic activity during continental rifting: Insights from the transversal Goba-Bonga lineament , Main Ethiopian Rift (East Africa). *Tectonophysics*. **728**–**729**, (February), pp.75–91.

Creaser, A., Hernández-Molina, F.J., Badalini, G., Thompson, P., Walker, R., Soto, M. and Conti, B. 2017. A Late Cretaceous mixed (turbidite-contourite) system along the Uruguayan Margin: Sedimentary and palaeoceanographic implications. *Marine Geology*. **390**, (February), pp.234–253.

Davies, R., Bell, B.R., Cartwright, J.A. and Shoulders, S. 2002. Three-dimensional seismic imaging of Paleogene dike-fed submarine volcanoes from the northeast Atlantic margin. *Geology*. **30**, (3) pp.223–226.

Davis, J.K. and Lavier, L.L. 2017. Influences on the development of volcanic and magma-poor morphologies during passive continental rifting. *Geosphere*. **13**, (5), pp.1524–1540.

Davy,R.G; Minshull,TA; Bayrakci,G; Bull,J.M; Klaeschen, D. 2016. Continental hyperextension, mantle exhumation and thin oceanic crust at the continent-ocean transition, West Iberia: New insights from wide-angle seismic. *Journal of Geophysical Research : Solid Earth*. **121**, (5), pp.3177–3199.

Dean, S.M., Minshull, T.A., Whitmarsh, R.B. and Louden, K.E. 2000. Deep structure of the ocean-continent transition in the southern Iberia Abyssal Plain from seismic refraction profiles: The IAM-9 transect at 40°20′N. *Journal of*

Geophysical Research: Solid Earth. **105**, (B3) pp.5859–5885.

Dean, S.L., Sawyer, D.S. and Morgan, J.K. 2015. Galicia Bank ocean-continent transition zone: New seismic reflection constraints. *Earth and Planetary Science Letters*. **413**.

Decarlis, A., Gillard, M., Tribuzio, R., Epin, M.E. and Manatschal, G. 2018. Breaking up continents at magma-poor rifted margins: a seismic v. outcrop perspective. *Journal of the Geological Society*. **175**, (6), pp.875-882.

DiFrancesco, D., Meyer, T., Christensen, A. and FitzGerald, D. 2009. Gravity Gradiometry – Today and Tomorrow *In*: *SAGA Biennial Technical meeting and Exhibition Swaziland*., pp.80–83.

Direen, N.G., Borissova, I., Stagg, H.M.J., Colwell, J.B. and Symonds, P.A. 2007. Nature of the continent–ocean transition zone along the southern Australian continental margin: a comparison of the Naturaliste Plateau, SW Australia, and the central Great Australian Bight sectors. *Geological Society, London, Special Publications*. **282**, (1), pp.239–263.

Doré, T. and Lundin, E. 2015. Hyperextended continental margins - Knowns and unknowns. *Geology*. **43**, (1), pp.95–96.

Dupré, S., Cloetingh, S. and Bertotti, G. 2011. Structure of the Gabon Margin from integrated seismic reflection and gravity data. *Tectonophysics*. **506**, (1–4) pp.31–45.

Eagles, G. 2007. New angles on South Atlantic opening. *Geophysical Journal International*. **168**, (1), pp.353–361.

Eagles, G., Pérez-Díaz, L. and Scarselli, N. 2015. Getting over continent ocean boundaries. *Earth-Science Reviews*. **151**, pp.244–265.

Ebinger, C.J. and Casey, M. 2001. Continental breakup in magmatic provinces: An Ethiopian example. *Geology*. **29**, (6) pp.527–530.

Edwards, R.A., Whitmarsh, R.B. and Scrutton, R.A. 1997. The crustal structure across the transform continental margin off Ghana, eastern equatorial Atlantic. *Journal of Geophysical Research: Solid Earth*. **102**, (B1) pp.747–772.

Eittreim, L., Survey, U.S.G. and Park, M. 1994. Transition from continental to oceanic crust on the Wilkes-Adelie margin of Antarctica **99**, (94) pp.24,89-24,205.

Eldholm, O. and Grue, K. 1994. North Atlantic volcanic margins: Dimensions and production rates. *Journal of Geophysical Research*. **99**, (B2), pp.2955–2968.

Eldholm, O., Gladczenko, T.P., Skogseid, J. and Planke, S. 2000. Atlantic volcanic margins: a comparative study. *Geological Society, London, Special Publications*. **167**, (1), pp.411–428.

Encarnación, J., Fleming, T.H., Elliot, D.H. and Eales, H. V. 1996. Synchronous emplacement of Ferrar and Karoo dolerites and the early breakup of Gondwana. *Geology*. **24**, (6), p.535.

Florineth, D. and Froitzheim, N. 1994. Transition from continental to oceanic basement in the Tasna nappe (Engadine window, Graubunden, Switzerland):

evidence for early Cretaceous opening of the Valais Ocean. *Schweizerische Mineralogische und Petrographische Mitteilungen*. **74**, (3), pp.437–448.

Franke, D., Neben, S. and Hinz, K. 2002. Deep crustal structure of the Argentine continental margin from seismic wide-angle and multichannel reflection seismic data *In*: *Habitat of Volcanic Rifted Passive Margins*., pp.1998–2001.

Franke, D., Neben, S., Schreckenberger, B., Schulze, A., Stiller, M. and Krawczyk, C.M. 2006. Crustal structure across the Colorado Basin, offshore Argentina. *Geophysical Journal International*. **165**, (3), pp.850–864.

Foulger, G.R., Natland, J.H. and Anderson, D.L. 2007. Genesis of the Iceland melt anomaly by plate tectonic processes. Special Paper 388: Plates, plumes and paradigms. pp.595-625.

Franke, D., Ladage, S., Schnabel, M., Schreckenberger, B., Reichert, C., Hinz, K., Paterlini, M., de Abelleyra, J. and Siciliano, M. 2010. Birth of a volcanic margin off Argentina, South Atlantic. *Geochemistry, Geophysics, Geosystems*. **11**, (2), pp.1-20.

Franke, D. 2013. Rifting, lithosphere breakup and volcanism: Comparison of magma-poor and volcanic rifted margins. *Marine and Petroleum Geology*. **43**, pp.63–87.

Frimmel, H.E., Basei, M.S. and Gaucher, C. 2011. *Neoproterozoic geodynamic evolution of SW-Gondwana: A southern African perspective*.

Funck, T., Erlendsson, Ö., Geissler, W.H., Gradmann, S., Kimbell, G.S., McDermott, K. and Petersen, U.K. 2017. A review of the NE Atlantic conjugate margins based on seismic refraction data. *Geological Society, London, Special Publications*. **447**, (1), pp.171–205.

Funck, T. 2003. Crustal structure of the ocean-continent transition at Flemish Cap: Seismic refraction results. *Journal of Geophysical Research*. **108**, (B11), pp.1–20.

Gaina, C., Gernigon, L. and Ball, P. 2009. Palaeocene-Recent plate boundaries in the NE Atlantic and the formation of the Jan Mayen microcontinent. *Journal of the Geological Society*. **166**, (4), pp.601–616.

García-Senz, J., Pedrera, A., Ayala, C., Ruiz-Constán, A., Robador, A. and Rodríguez-Fernández, L.R. 2019. Inversion of the north Iberian hyperextended margin: the role of exhumed mantle indentation during continental collision. *Geological Society, London, Special Publications*., **490**.

Geoffroy, L., Ravilly, M., Angelier, J., Bonin, B., Cayet, C., Perrot, K. and Bay, B. 2001. Southeast Baffin volcanic margin and the North American-Greenland separation. *Tectonics*. **20**, (4), pp.566–584.

Geoffroy, L. 2005. Volcanic passive margins. *Comptes Rendus Geoscience*. **337**, (16), pp.1395–1408.

Geoffroy, L., Le Gall, B., Daoud, M.A. and Jalludin, M. 2014. Flip-flop detachment tectonics at nascent passive margins in SE Afar. *Journal of the Geological Society*. **171**, (5) pp.689–694.

Geoffroy, L., Burov, E.B. and Werner, P. 2015. Volcanic passive margins: another way to break up continents. *Scientific Reports*. **5**, p.14828.

Gernigon, L., Ringenbach, J.-C., Planke, S. and Le Gall, B. 2004. Deep structures and breakup along volcanic rifted margins: insights from integrated studies along the outer Vøring Basin (Norway). *Marine and Petroleum Geology*. **21**, (3), pp.363–372.

Geyer, A., Álvarez-Valero, A.M., Gisbert, G., Aulinas, M., Hernández-Barreña, D., Lobo, A. and Marti, J. 2019. Deciphering the evolution of Deception Island's magmatic system. *Scientific Reports*. **9**, (1), pp.1–14.

Ghiglione, M.C., Quinteros, J., Yagupsky, D., Bonillo-Martínez, P., Hlebszevtich, J., Ramos, V. a., Vergani, G., Figueroa, D., Quesada, S. and Zapata, Y.T. 2010. Structure and tectonic history of the foreland basins of southernmost South America. *Journal of South American Earth Sciences*. **29**, (2), pp.262–277.

Gillard, M., Autin, J., Manatschal, G., Sauter, D., Munschy, M. and Schaming, M. 2015. Tectonomagmatic evolution of the final stages of rifting along the deep conjugate Australian-Antarctic magma-poor rifted margins: constraints from seismic observations. *Tectonics*., pp.753–783.

Gillard, M., Autin, J. and Manatschal, G. 2016. Fault systems at hyper-extended rifted margins and embryonic oceanic crust: Structural style, evolution and relation to magma. *Marine and Petroleum Geology*. **76**, pp.51–67.

Gillard, M., Manatschal, G. and Autin, J. 2016. How can asymmetric detachment faults generate symmetric Ocean Continent Transitions? *Terra Nova*. **28**, (1), pp.27–34.

Gillard, M., Sauter, D., Tugend, J., Tomasi, S., Epin, M.E. and Manatschal, G. 2017. Birth of an oceanic spreading center at a magma-poor rift system. *Scientific Reports*. **7**, (1), pp.1–6.

Gudmundsson, A. 2012. Magma chambers: Formation, local stresses, excess pressures, and compartments. *Journal of Volcanology and Geothermal Research*. **237**–**238**, pp.19–41.

Harkin, C., Kusznir, N., Tugend, J., Manatschal, G. and McDermott, K. 2019. Evaluating magmatic additions at a magma-poor rifted margin: An East Indian case study. *Geophysical Journal International*. **217**, pp.25–40.

Heine, C., Zoethout, J. and Müller, R.D. 2013. Kinematics of the South Atlantic rift. *Solid Earth*. **4**, (2), pp.215–253.

Henning, A.T., Sawyer, D.S. and Templeton, D.C. 2004. Exhumed upper mantle within the ocean-continent transition on the northern West Iberia margin: Evidence from prestack depth migration and total tectonic subsidence analyses. *Journal of Geophysical Research: Solid Earth*. **109**, (5), pp.1–16.

Hernández-Molina, F.J., Soto, M., Piola, A.R., Tomasini, J., Preu, B., Thompson, P., Badalini, G., Creaser, A., Violante, R.A., Morales, E., Paterlini, M. and De Santa Ana, H. 2016. A contourite depositional system along the Uruguayan continental margin: Sedimentary, oceanographic and paleoceanographic implications. *Marine Geology*. **378**, pp.333–349.

Holbrook, W.S., Larsen, H.C., Korenaga, J., Dahl-Jensen, T., Reid, I.D., Kelemen, P.B., Hopper, J.R., Kent, G.M., Lizarralde, D., Bernstein, S. and Detrick, R.S. 2001. Mantle thermal structure and active upwelling during continental breakup in the North Atlantic. *Earth and Planetary Science Letters*. **190**, (3–4), pp.251–266.

Hopper, J.R., Funck, T., Tucholke, B.E., Larsen, H.C., Holbrook, W.S., Louden, K.E., Shillington, D. and Lau, H. 2004. Continental break-up and the onset of ultraslow seafloor spreading off Flemish Cap on the Newfoundland rifted margin. *Geology*. **32**, (1), pp.93–96.

Huber, C., Townsend, M., Degruyter, W. and Bachmann, O. 2019. Optimal depth of subvolcanic magma chamber growth controlled by volatiles and crust rheology. *Nature Geoscience*. **12**, (9) pp.762–768.

Hunt, T., Sugihara, M., Sato, T. and Takemura, T. 2002. Measurement and use of the vertical gravity gradient in correcting repeat microgravity measurements for the effects of ground subsidence in geothermal systems. *Geothermics*. **31**(5), pp.525–543.

Huppert, H.E. and Sparks, R.S.J. 1980. Contributions to Mineralogy and The Fluid Dynamics of a Basaltic Magma Chamber Replenished by Influx of Hot , Dense Ultrabasic Magma. *Contributions to Mineralogy and Petrology*. **75**, pp.279–289.

Jackson, M.P.., Cramez, C. and Fonck, J.-M. 2000. Role of subaerial volcanic rocks and mantle plumes in creation of South Atlantic margins: implications for salt tectonics and source rocks. *Marine and Petroleum Geology*. **17**, (4), pp.477–498.

Jacques, J. 2003. A tectonostratigraphic synthesis of the Sub-Andean basins: implications for the geotectonic segmentation of the Andean Belt. *Journal of the Geological Society*. **160**, (5), pp.687–701.

Janssen, M.E., Stephenson, R.A. and Cloetingh, S. 1995. Temporal and spatial correlations between changes in plate motions and the evolution of rifted basins in Africa. *Geological Society of America Bulletin*. **107**, (11) pp.1317–1332.

Keeley, M. and Light, M. 1993. Basin evolution and prospectivity of the Argentine continental margin. *Journal of Petroleum Geology*. **16**, (October), pp.451–464.

Keen, C.E., Voogd, B. De, Centre, A.G. and Scotia, N. 1988. The Continent-Ocean Boundary At the Rifted Margin Off Eastern Canada: New Results From Deep Seismic Reflection Studies. **7**, (1), pp.107–124.

Keen, C.E., Dickie, K. and Dafoe, L.T. 2018. Structural characteristics of the ocean-continent transition along the rifted continental margin, offshore central Labrador. *Marine and Petroleum Geology*. **89**, (October 2017), pp.443–463.

Keir, D., Belachew, M., Ebinger, C.J., Kendall, J.M., Hammond, J.O.S., Stuart, G.W., Ayele, A. and Rowland, J. V. 2011. Mapping the evolving strain field during continental breakup from crustal anisotropy in the Afar Depression. *Nature Communications*. **2**, (1).

Keir, D., Bastow, I.D., Corti, G., Mazzarini, F. and Rooney, T.O. 2015. The origin of along-rift variations in faulting and magmatism in the Ethiopian Rift. *Tectonics*.

34, pp.1–14.

Keranen, K., Klemperer, S.L., Gloaguen, R., Asfaw, L., Ayele, a., Ebinger, C., Furman, T., Harder, S., Keler, G.R., Mackenzie, G.D., Maguire, P.K.H. and Stuart, G.W. 2004. Three-dimensional seismic imaging of a protoridge axis in the Main Ethiopian rift. *Geology*. **32**, (11), pp.949–952.

King, Scott D; Anderson, D.. 1998. Edge-driven convection. *Earth and Planetary Science Letters*. **160**, (October), pp.289–296.

Koopmann, H., Brune, S., Franke, D. and Breuer, S. 2014. Linking rift propagation barriers to excess magmatism at volcanic rifted margins. *Geology*. **42**, (October), pp.1–4.

Koopmann, H., Franke, D., Schreckenberger, B., Schulz, H., Hartwig, A., Stollhofen, H. and di Primio, R. 2014. Segmentation and volcano-tectonic characteristics along the SW African continental margin, South Atlantic, as derived from multichannel seismic and potential field data. *Marine and Petroleum Geology*. **50**, pp.22–39.

Korenaga, J. 2004. Mantle mixing and continental breakup magmatism. *Earth and Planetary Science Letters*. **218**, (3–4), pp.463–473.

Kukla, P.A., Strozyk, F. and Mohriak, W.U. 2018. South Atlantic salt basins – Witnesses of complex passive margin evolution. *Gondwana Research*. **53**, pp.41–57.

Kusznir, N.J. and Karner, G.D. 2007. Continental lithospheric thinning and breakup in response to upwelling divergent mantle flow: application to the Woodlark, Newfoundland and Iberia margins. *Geological Society, London, Special Publications*. **282**, (1), pp.389–419.

Kusznir, N.J., Roberts, A.M. and Alvey, A.D. 2018. Crustal structure of the conjugate Equatorial Atlantic Margins, derived by gravity anomaly inversion. *Geological Society, London, Special Publications*. **1**, SP476.5.

Lavier, L.L. and Manatschal, G. 2006. A mechanism to thin the continental lithosphere at magma-poor margins. *Nature*. **440**, (7082), pp.324–328.

Loegering, M.J., Anka, Z., Autin, J., di Primio, R., Marchal, D., Rodriguez, J.F., Franke, D. and Vallejo, E. 2013. Tectonic evolution of the Colorado Basin, offshore Argentina, inferred from seismo-stratigraphy and depositional rates analysis. *Tectonophysics*. **604**, pp.245–263.

Lundin, E.R. and Dore, A.G. 2011. Hyperextension, serpentinization, and weakening: A new paradigm for rifted margin compressional deformation. *Geology*. **39**, (4), pp.347–350.

Lundin, E.R., Doré, A.G. and Redfield, T.F. 2018. Magmatism and extension rates at rifted margins. *Petroleum Geoscience*. **24**, (4), pp.379–392.

Macdonald, D., Gomez-Perez, I., Franzese, J., Spalletti, L., Lawver, L., Gahagan, L., Dalziel, I., Thomas, C., Trewin, N., Hole, M. and Paton, D. 2003. Mesozoic break-up of SW Gondwana: Implications for regional hydrocarbon potential of the southern South Atlantic. *Marine and Petroleum Geology*. **20**, pp.287–308.

Magee, C., Stevenson, C.T.E., Ebmeier, S.K., Keir, D., Hammond, J.O.S., Gottsmann, J.H., Whaler, K.A., Schofield, N., Jackson, C.A.L., Petronis, M.S., O'Driscoll, B., Morgan, J., Cruden, A., Vollgger, S.A., Dering, G., Micklethwaite, S. and Jackson, M.D. 2018. Magma plumbing systems: A geophysical perspective. *Journal of Petrology*. **59** (6), pp.1217–1251.

Manatschal, G., Froitzheim, N., Rubenach, M. and Turrin, B.D. 2001. The role of detachment faulting in the formation of an ocean-continent transition: insights from the Iberia Abyssal Plain. *Geological Society, London, Special Publications*. **187**, (1), pp.405–428.

Manatschal, G. and Müntener, O. 2009. A type sequence across an ancient magma-poor ocean-continent transition: the example of the western Alpine Tethys ophiolites. *Tectonophysics*. **473**, (1–2), pp.4–19.

Manatschal, G., Sauter, D., Karpoff, A.M., Masini, E., Mohn, G. and Lagabrielle, Y. 2011. The Chenaillet Ophiolite in the French/Italian Alps: An ancient analogue for an Oceanic Core Complex? *Lithoshere*. **124**, (3–4), pp.169–184.

Manatschal, G., Lavier, L. and Chenin, P. 2015. The role of inheritance in structuring hyperextended rift systems: Some considerations based on observations and numerical modeling. *Gondwana Research*. **27**, (1), pp.140–164.

Mangipudi, V.R., Goli, A., Desa, M., Tammisetti, R. and Dewangan, P. 2014. Synthesis of deep multichannel seismic and high resolution sparker data: Implications for the geological environment of the Krishna-Godavari offshore, Eastern Continental Margin of India. *Marine and Petroleum Geology*. **58**, (PA), pp.339–355.

Maus, S. *et al.* (2009) 'EMAG2: A 2-arc min resolution Earth Magnetic Anomaly Grid compiled from satellite, airborne, and marine magnetic measurements', *Geochemistry, Geophysics, Geosystems*, **10**, (8)

McCarthy, J., Mutter, J.C., Morton, J.L., Sleep, N.H. and Thompson, G.A. 1988. Relic magma chamber structures preserved within the Mesozoic North Atlantic crust? *Geological Society of America Bulletin*. **100**, (9), pp.1423–1436.

Menzies, M. and Klemperer, S. 2002. Characteristics of volcanic rifted margins. *Geological Society of America Special Papers*. **362**, pp.1–14.

Meyer, R., van Wijk, J. and Gernigon, L. 2007. The North Atlantic Igneous Province: A review of models for its formation. *Special Paper 430: Plates, Plumes and Planetary Processes*. **2430**, (26), pp.525–552.

Milani, E. and Davison, I. 1988. Basement control and transfer tectonics in the Recôncavo-Tucano-Jatobá rift, Northeast Brazil. *Tectonophysics*. **154**.

Milani, E.J., Lana, M.C. and Szatmari, P. 1988. Mesozoic rift basins around the northeast Brazilian microplate (Recôncavo – Tucano – Jatobá, Sergipe – Alagoas). *Developments in Geotectonics*. **22**, (C) pp.833–858.

Mjelde, R., Raum, T., Kandilarov, A., Murai, Y. and Takanami, T. 2009. Crustal structure and evolution of the outer Møre Margin, NE Atlantic. *Tectonophysics*. **468**, (1–4), pp.224–243.

Mohn, G., Manatschal, G., Müntener, O., Beltrando, M. and Masini, E. 2010.

Unravelling the interaction between tectonic and sedimentary processes during lithospheric thinning in the Alpine Tethys margins. *International Journal of Earth Sciences*. **99**, (1) pp.75–101.

Mohriak, W.U., Rosendahl, B.R., Turner, J.P. and Valente, S.C. 2002. Crustal architecture of South Atlantic volcanic margins. *Geological Society of America Special Papers*. **362**, pp.159–202.

Mohriak, W.U., Nobrega, M., Odegard, M.E., Gomes, B.S. and Dickson, W.G. 2010. Geological and geophysical interpretation of the Rio Grande Rise, south-eastern Brazilian margin: extensional tectonics and rifting of continental and oceanic crusts. *Petroleum Geoscience*. **16**, (3) pp.231–245.

Morales, E., Chang, H.K., Soto, M., Corrêa, F.S., Veroslavsky, G., de Santa Ana, H., Conti, B. and Daners, G. 2017. Tectonic and stratigraphic evolution of the Punta del Este and Pelotas basins (offshore Uruguay). *Petroleum Geoscience*. **23**, (4), pp.415–426.

Morley, C.K., Nelson, R. a., Patton, T.L. and Munn, S.G. 1990. Transfer zones in the East African rift system and their relevance to hydrocarbon exploration in rifts. *American Association of Petroleum Geologists Bulletin*. **74**, pp.1234–1253.

Mortimer, E., Paton, D.A., Scholz, C.A., Strecker, M.R. and Blisniuk, P. 2007. Orthogonal to oblique rifting: Effect of rift basin orientation in the evolution of the North basin, Malawi Rift, East Africa. *Basin Research*. **19**, (3) pp.393–407.

Moulin, M., Aslanian, D. and Unternehr, P. 2010. A new starting point for the South and Equatorial Atlantic Ocean. *Earth-Science Reviews*. **98**, (1–2), pp.1–37.

Muirhead, J.D. and Kattenhorn, S.A. 2018. Activation of preexisting transverse structures in an evolving magmatic rift in East Africa. *Journal of Structural Geology*. **106**, (September 2017), pp.1–18.

Müntener, O. and Hermann, J. 2001. The role of lower crust and continental upper mantle during formation of non-volcanic passive margins: evidence from the Alps. *Geological Society, London, Special Publications*. **187**, (1), pp.267–288.

Müntener, O. and Manatschal, G. 2006. High degrees of melt extraction recorded by spinel harzburgite of the Newfoundland margin: The role of inheritance and consequences for the evolution of the southern North Atlantic. *Earth and Planetary Science Letters*. **252**, (3–4), pp.437–452.

Mutter, J., Talwani, M. and Stoffa, P. 1982. Origin of seaward-dipping reflectors in oceanic crust off the Norwegian margin by “subaerial sea-floor spreading”. *Geology*. **10**, pp.353–357.

Mutter, C. 1985. Seaward Dipping Reflectors and the Continent-Ocean boundary at passive continental margins. *Tectonophysics*. **114**, (3634) pp.117–131.

Norcliffe, J.R., Paton, D.A., Mortimer, E.J., McCaig, A.M., Nicholls, H., Rodriguez, K., Hodgson, N. and Van Der Spuy, D. 2018. Laterally Confined Volcanic Successions (LCVS); recording rift-jumps during the formation of magma-rich margins. *Earth and Planetary Science Letters*. **504**, pp.53–63.

Nürnberg, D. and Müller, R.D. 1991. The tectonic evolution of the South Atlantic

from Late Jurassic to present. *Tectonophysics*. **191**, (1–2), pp.27–53.

Osmundsen, P.T. and Redfield, T.F. 2011. Crustal taper and topography at passive continental margins. *Terra Nova*. **23**, (6) pp.349–361.

Osmundsen, P.T. and Péron-Pinvidic, G. 2018. Crustal-Scale Fault Interaction at Rifted Margins and the Formation of Domain-Bounding Breakaway Complexes: Insights From Offshore Norway. *Tectonics*. **37**, (3), pp.935–964.

Oyhantçabal, P., Siegesmund, S., Wemmer, K., Presnyakov, S. and Layer, P. 2009. Geochronological constraints on the evolution of the southern Dom Feliciano Belt (Uruguay). *Journal of the Geological Society, London*. **166**, pp.1075–1084.

Páengaro, F. and Ramos, V.A. 2012. Paleozoic crustal blocks of onshore and offshore central Argentina: New pieces of the southwestern Gondwana collage and their role in the accretion of Patagonia and the evolution of Mesozoic south Atlantic sedimentary basins. *Marine and Petroleum Geology*. **37**, (1), pp.162–183.

Panario, D., Gutiérrez, O., Bettucci, L.S., Peel, E., Oyhantçabal, P. and Rabassa, J. 2014. Ancient landscapes of uruguay *In*: *Gondwana Landscapes in Southern South America: Argentina, Uruguay and Southern Brazil*. pp.161–199.

Pángaro, F., Ramos, V.A. and Pazos, P.J. 2016. The Hesperides basin: a continental-scale upper Palaeozoic to Triassic basin in southern Gondwana. *Basin Research*. **28**, (5) pp.685–711.

Paton, D. a. 2006. Influence of crustal heterogeneity on normal fault dimensions and evolution: southern South Africa extensional system. *Journal of Structural Geology*. **28**, pp.868–886.

Paton, D.A., Mortimer, E.J., Hodgson, N. and Van Der Spuy, D. 2016. The missing piece of the South Atlantic jigsaw - when continental break-up ignores crustal heterogeneity. *Petroleum Geoscience of the West Africa Margin, Geological Society, London, Special Publications*. **438**.

Paton, D.A., Pindell, J., McDermott, K., Bellingham, P. and Horn, B. 2017. Evolution of seaward-dipping reflectors at the onset of oceanic crust formation at volcanic passive margins: Insights from the South Atlantic. *Geology*. **45**, (5), pp.439–442.

Perez-Diaz, L. and Eagles, G. 2014. Constraining South Atlantic growth with seafloor spreading data. *Tectonics*. **33,** (9), pp.1848–1873.

Perez-Gussinye, M. and Reston, T.J. 2001. Rheological evolution during extension at non-volcanic rifted margins: Onset of serpentinization and development of detachments leading to continental breakup. *Journal of Geophysical Research*. **106**, (B3) pp.3961–3975.

Perez-Gussinye, M. 2012. A tectonic model for hyperextension at magma-poor rifted margins: an example from the West Iberia-Newfoundland conjugate margins. *Geological Society, London, Special Publications*. **369**, pp.403–427.

Pérez-Gussinyé, M., Morgan, J.P., Reston, T.J. and Ranero, C.R. 2006. The rift to drift transition at non-volcanic margins: Insights from numerical modelling. *Earth and Planetary Science Letters*. **244**, (1–2), pp.458–473.

Péron-Pinvidic, G., Manatschal, G., Minshull, T.A. and Sawyer, D.S. 2007. Tectonosedimentary evolution of the deep Iberia-Newfoundland margins: Evidence for a complex breakup history. *Tectonics*. **26**, (2) pp.1–19.

Péron-Pinvidic, G. and Manatschal, G. 2009. The final rifting evolution at deep magma-poor passive margins from Iberia-Newfoundland: A new point of view. *International Journal of Earth Sciences*. **98**, (7) pp.1581–1597.

Péron-Pinvidic, G. and Manatschal, G. 2009. The final rifting evolution at deep magma-poor passive margins from Iberia-Newfoundland: A new point of view. *International Journal of Earth Sciences*. **98**, (7) pp.1581–1597.

Péron-Pinvidic, G., Van Wijk, J., Shillington, D.J. and Gernigon, L. 2009. An introduction to the Tectonophysics Special Issue 'Role of magmatism in continental lithosphere extension'. *Tectonophysics*. **468**, (1–4), pp.1–5.

Péron-Pinvidic, G. and Manatschal, G. 2010. From microcontinents to extensional allochthons: Witnesses of how continents rift and break apart. *Petroleum Geoscience*. **16**, (3) pp.189–197.

Peron-Pinvidic, G., Manatschal, G. and Osmundsen, P.T. 2013. Structural comparison of archetypal Atlantic rifted margins: A review of observations and concepts. *Marine and Petroleum Geology*. **43**, pp.21–47.

Pickup, S.L.B., Whitmarsh, R.B., Fowler, C.M.R. and Reston, T.J. 1996. Insight into the nature of the ocean-continent transition off West Iberia from a deep multichannel seismic reflection profile. *Geology*. **24**, (12) pp.1079–1082.

Piqué, A. and Laville, E. 1996. The Central Atlantic rifting: Reactivation of palaeozoic structures *Journal of Geodynamics*. **21**, (3), pp.235–255.

Planke, S. and Symonds, P. 2000. Seismic volcanostratigraphy of large-volume basaltic extrusive complexes on rifted margins. *Journal of Geophysical Research* **105**, (B8) 19,335-19,351.

Planke, S., Jamtveit, B., Malthe-sørenssen, A., Myklebust, R., Svensen, H., Rasmussen, T., Rey, S.S. and Berndt, C. 2003. Volcanic Processes and Deposits on Rifted Margins and in Sedimentary Basins. *Magma*., pp.1–5.

Quirk, D.G., Shakerley, A. and Howe, M.J. 2014. A mechanism for construction of volcanic rifted margins during continental breakup. *Geology*. **42**, (October), pp.1079–1082.

Rabassa, J. 2010. Gondwana paleolandscapes: long-term landscape evolution, genesis, distribution and age. *Geociências (São Paulo)*. **2**, pp.541–570. Rabassa, J. and Ollier, C. 2014. *Gondwana landscapes in southern South America*.

Rabinowitz, P. and LaBrecque, J. 1979. The Mesozoic South Atlantic Ocean and evolution of its continental margins. *Journal of Geophysical Research* **84**, (B11 October 1979).

Ranero, C.R., Reston, T.J., Belykh, I. and Gnibidenko, H. 1997. Reflective oceanic crust formed at a fast-spreading center in the Pacific. *Geology*. **25**, (6) pp.499–502.

Rapela, C.W., Fanning, C.M., Casquet, C., Pankhurst, R.J., Spalletti, L., Poiré, D. and Baldo, E.G. 2011. The Rio de la Plata craton and the adjoining Pan-African/brasiliano terranes: Their origins and incorporation into south-west Gondwana. *Gondwana Research*. **20**, (4), pp.673–690.

Reston, T.J., Ranero, C.R. and Belykh, I. 1999. The structure of Cretaceous oceanic crust of the NW Pacific: Constraints on processes at fast spreading centers. *Journal of Geophysical Research: Solid Earth*. **104**, (B1) pp.629–644.

Reston, T.J. and Morgan, J.P. 2004. Continental geotherm and the evolution of rifted margins. *Geology*. **32**, (2), pp.133–136.

Reston, T.J. 2005. Polyphase faulting during the development of the west Galicia rifted margin. *Earth and Planetary Science Letters*. **237**, (3–4), pp.561–576.

Reston, T.J. 2007. The formation of non-volcanic rifted margins by the progressive extension of the lithosphere: the example of the West Iberian margin. *Geological Society, London, Special Publications*. **282**, (1), pp.77–110.

Reston, T.J. 2009. The structure, evolution and symmetry of the magma-poor rifted margins of the North and Central Atlantic: A synthesis. *Tectonophysics*. **468**, (1–4), pp.6–27.

Reston, T.J. and McDermott, K.G. 2011. Successive detachment faults and mantle unroofing at magma-poor rifted margins. *Geology*. **39**, (11), pp.1071–1074.

Reynisson, R.F., Ebbing, J., Lundin, E. and Osmundsen, P.T. 2011. Properties and distribution of lower crustal bodies on the mid-Norwegian margin. *Geological Society, London, Petroleum Geology Conference series*. **7**, (1), pp.843–854.

Ring, U. 1994. The influence of preexisting structure on the evolution of the Cenozoic Malawi rift (East African rift system). *Tectonics*. **13**, (2), pp.313–326.

Roger, W., Zehnder, C.M., Mutter, J.C. and Buck, W.R. 1988. Convective partial melting: A model for the formation of thick basaltic sequences during the initiation of spreading. *Journal of Geophysical Research*. **93**, (7), pp.1031–1048.

Rooney, T.O., Bastow, I.D. and Keir, D. 2011. Insights into extensional processes during magma assisted rifting: Evidence from aligned scoria cones. *Journal of Volcanology and Geothermal Research*. **201**, (August) pp.83–96.

Rosendahl, B. 1987. Architecture of continental rifts with special reference to East Africa. *Annual Review of Earth and Planetary sciences* **15**, pp.445–503.

Rossello, E.A., Veroslavsky, G., de Santa Ana, H. and Rodríguez, P. 2018. Geology of the Río de la Plata and the surrounding areas of Argentina and Uruguay related to the evolution of the Atlantic margin. *Journal of South American Earth Sciences*. **83**, pp.147–164.

Rubin, A.M. 1992. Dike-induced faulting and graben subsidence in volcanic rift zones. *Journal of Geophysical Research*. **97**, (B2), pp.1839–1858.

Russell, S.M. and Whitmarsh, R.B. 2003. Magmatism at the west Iberia non-volcanic rifted continental margin: Evidence from analyses of magnetic anomalies. *Geophysical Journal International*. **154**, (3), pp.706–730.

Sandwell, D. T. and Smith, W. H. F. (2009) 'Global marine gravity from retracked Geosat and ERS-1 altimetry: Ridge segmentation versus spreading rate', *Journal of Geophysical Research*, **114**, (B1), p. B01411.

Sauter, D., Cannat, M., Rouméjon, S., Andreani, M., Birot, D., Bronner, A., Brunelli, D., Carlut, J., Delacour, A., Guyader, V., MacLeod, C.J., Manatschal, G., Mendel, V., Ménez, B., Pasini, V., Ruellan, E. and Searle, R. 2013. Continuous exhumation of mantle-derived rocks at the Southwest Indian Ridge for 11 million years. *Nature Geoscience*. **6**, (4) pp.314–320.

Seifert, K.E. and Brunotte, D.A. 1997. Evidence from Ocean Drilling Program Leg 149 mafic igneous rocks for oceanic crust in the Iberia Abyssal Plain ocean-continent transition zone. **102**, pp.7915–7928.

Schnabel, M., Franke, D., Engels, M., Hinz, K., Neben, S., Damm, V., Grassmann, S., Pelliza, H. and Dos Santos, P.R. 2008. The structure of the lower crust at the Argentine continental margin, South Atlantic at 44°S. *Tectonophysics*. **454**, (1–4), pp.14–22.

Schofield, N., Holford, S., Millett, J., Brown, D., Jolley, D., Passey, S.R., Muirhead, D., Grove, C., Magee, C., Murray, J., Hole, M., Jackson, C.A.L. and Stevenson, C. 2017. Regional magma plumbing and emplacement mechanisms of the Faroe-Shetland Sill Complex: implications for magma transport and petroleum systems within sedimentary basins. *Basin Research*. **29**, (1), pp.41–63.

Sibuet, J.C., Srivastava, S. and Manatschal, G. 2007. Exhumed mantle-forming transitional crust in the Newfoundland-Iberia rift and associated magnetic anomalies. *Journal of Geophysical Research: Solid Earth*. **112**, (6), pp.1–23.

Sinha, S.T., Nemčok, M., Choudhuri, M., Sinha, N. and Rao, D.P. 2016. The role of break-up localization in microcontinent separation along a strike-slip margin: the East India–Elan Bank case study. *Geological Society, London, Special Publications*. **431**, (1), pp.95–123.

Skogseid, J., Pedersen, T., Eldholm, O. and Larsen, B.T. 1992. Tectonism and magmatism during NE Atlantic continental break-up: the Vøring Margin. *Geological Society, London, Special Publications*. **68**, (1), pp.305–320.

Soto, M., Morales, E., Veroslavsky, G., de Santa Ana, H., Ucha, N. and Rodríguez, P. 2011. The continental margin of Uruguay: Crustal architecture and segmentation. *Marine and Petroleum Geology*. **28**, (9), pp.1676–1689.

Sparks, R.S.J., Meyer, P. and Sigurdsson, H. 1980. Density variation amongst mid-ocean ridge basalts: Implications for magma mixing and the scarcity of primitive lavas. *Earth and Planetary Science Letters*. **46**, (3) pp.419–430.

Stoakes, F.. and Campbell, C. 1991. Seismic Stratigraphic Analysis of the Punta Del Este Basin, Offshore Uruguay, South America (1). *AAPG Bulletin*. **75**, (2) pp.219–240.

Symonds, PA; Planke,S;Frey,O;Skogseid, J. 1998. Volcanic Evolution of the Western Australian Continental Margin and its Implications for Basin Development *In*: *The Sedimentary Basins of Western Australia II*., pp.33–53.

Sutra, E. and Manatschal, G. 2012. How does the continental crust thin in a

hyperextended rifted margin? Insights from the iberia margin. *Geology*. **40**, (2), pp.139–142.

Sutra, E., Manatschal, G., Mohn, G. and Unternehr, P. 2013. Quantification and restoration of extensional deformation along the Western Iberia and Newfoundland rifted margins. *Geochemistry, Geophysics, Geosystems*. **14**, (8), pp.2575–2597.

Talwani, M., Udintsev, G. and White, S. 1976. Introduction and explanatory notes, Leg 38, Deep Sea Drilling Project. *Initial Rep. Deep Sea Drill. Proj*.

Tankard, A.., Uliana, M.A., Welsink, H.J., Ramos, V.A., Tunik, M., Franca, A.B., Milani, E.J., de Brito Neves, B.B., Eyles, N., Skarmeta, J. and Santa Ana et al., H. 1995. Structural and tectonic controls of basin evolution in southwestern Gondwana during the Phanerozoic. *Tectonic controls of basin evolution in southwestern Gondwana, in A.J. Tankard, R. Suarez S., and H.J. Weslsink, Petroleum basins of South America: AAPG Memoir 62*., pp.5–52.

Taposeea, C.A., Armitage, J.J. and Collier, J.S. 2017. Asthenosphere and lithosphere structure controls on early onset oceanic crust production in the southern South Atlantic. *Tectonophysics*. **716**, pp.4-20.

Theissen-Krah, S., Zastrozhnov, D., Abdelmalak, M.M., Schmid, D.W., Faleide, J.I. and Gernigon, L. 2017. Tectonic evolution and extension at the Møre Margin – Offshore mid-Norway. *Tectonophysics*. **721**, (March), pp.227–238.

Thomson, K. and Hutton, D. 2004. Geometry and growth of sill complexes: Insights using 3D seismic from the North Rockall Trough. *Bulletin of Volcanology*. **66**, (4) pp.364–375.

Thybo, H. and Nielsen, C. a 2009. Magma-compensated crustal thinning in continental rift zones. *Nature*. **457**, (7231), pp.873–876.

Thybo, H. and Artemieva, I.M.M. 2013. Moho and magmatic underplating in continental lithosphere. *Tectonophysics*. **609**, pp.605–619.

Tomasini, J., de Santa Ana, H., Conti, B., Ferro, S., Gristo, P., Marmisolle, J., Morales, E., Rodriguez, P., Soto, M. and Veroslavsky, G. 2011. Assessment of Marine Gas Hydrates and Associated Free Gas Distribution Offshore Uruguay. *Journal of Geological Research*. 2011, pp.1–7.

Torsvik, T.H., Rousse, S., Labails, C. and Smethurst, M. a. 2009. A new scheme for the opening of the South Atlantic Ocean and the dissection of an Aptian salt basin. *Geophysical Journal International*. **177**, (3) pp.1315–1333.

Tugend, J., Manatschal, G. and Kusznir, N.J. 2015. Spatial and temporal evolution of hyperextended rift systems: Implication for the nature, kinematics, and timing of the Iberian- European plate boundary. *Geology*. **43**, (1) pp.15–18.

Tugend, J., Gillard, M., Manatschal, G., Nirrengarten, M., Harkin, C., Epin, M., Sauter, D., Autin, J., Kusznir, N. and McDermott, K. 2018. Reappraisal of the magma-rich versus magma-poor rifted margin archetypes. *Geological Society, London, Special Publications*.,**476**, (1) pp.23-47.

Turic, M.A., Nevistic, A. V. and Rebay, G. 1996. *Geologia y recursos naturales de la plataforma continental*.

Uchupi, E. 1989. The tectonic style of the atlantic mesozoic rift system. *Journal of African Earth Sciences*. **8**, (2–4), pp.143–164.

Unternehr, P., Peron-Pinvidic, G., Manatschal, G. and Sutra, E. 2010. Hyper-extended crust in the South Atlantic: in search of a model. *Petroleum Geoscience*. **16,** (3) pp.207–215.

Urien, C.M. and Zambrano, J.J. 1973. The Geology of the Basins of the Argentine Continental Margin and Malvinas Plateau BT - The South Atlantic *In*: A. E. M. Nairn and F. G. Stehli, eds. *The ocean basins and margins* [Online]. Boston, MA: Springer US, pp.135–169.

Van Wijk, J.W.W. and Blackman, D.K.K. 2005. Dynamics of continental rift propagation: the end-member modes. *Earth and Planetary Science Letters*. **229**, (3–4) pp.247–258.

Van Wijk, J., van Hunen, J. and Goes, S. 2008. Small-scale convection during continental rifting: Evidence from the Rio Grande rift. *Geology*. **36**, (7) pp.575–578.

Veroslavsky, G. 2003. Permian sedimentary rocks of the Uruguayan continental shelf: the pre-rift of the Punta del Este basin **34**, pp. 203–206.

Weinberg, R.F., Regenauer-Lieb, K. and Rosenbaum, G. 2007. Mantle detachment faults and the breakup of cold continental lithosphere. *Geology*. **35**, (11) pp.1035–1038.

White, R. and Mckenzie, D. 1989. Magmatism at Rift Zones : The Generation of Volcanic Continental Margins. *Journal of Geophysical Research*. **94**, (B6), pp.7685–7729.

White, R.S., Smith, L.K., Roberts, A.W., Christie, P.A.F., Kusznir, N.J., Roberts, A.M., Healy, D., Spitzer, R., Chappell, A., Eccles, J.D., Fletcher, R., Hurst, N., Lunnon, Z., Parkin, C.J. and Tymms, V.J. 2008. Lower-crustal intrusion on the North Atlantic continental margin. *Nature*. **452**, (7186), pp.460–464.

Whitmarsh, R.B., Miles, P.R. and Mauffret, A. 1990. The ocean–continent boundary off the western continental margin of Iberia. *Geophysical Journal International*. **103,** (2) pp.509–531.

Whitmarsh, R.B., Manatschal, G. and Minshull, T. a 2001. Evolution of magma-poor continental margins from rifting to seafloor spreading. *Nature*. **413**, (September), pp.150–154.

Whitney, D. L. *et al.* 2013. Continental and oceanic core complexes *Bulletin of the Geological Society of America*, **125**, (3–4), pp. 273–298.

Will, T.M. and Frimmel, H.E. 2013. The Influence of Inherited Structures on Dike Emplacement during Gondwana Breakup in Southwestern Africa. *The Journal of Geology*. **121**, (5), pp.455–474.

Will, T.M. and Frimmel, H.E. 2016. Where does a continent prefer to break up? Some lessons from the South Atlantic margins. *Gondwana Research*. **53** pp.9-19.Will, T.M. and Frimmel, H.E. 2018. Where does a continent prefer to break up? Some lessons from the South Atlantic margins. *Gondwana Research*. **53**, pp.9–19.

Wilson, P.G., Turner, J.P. and Westbrook, G.K. 2003. Structural architecture of the ocean-continent boundary at an oblique transform margin through deep-imaging seismic interpretation and gravity modelling: Equatorial Guinea, West Africa. *Tectonophysics*. **374**, (1–2), pp.19–40.

Wright, T.J., Ebinger, C., Biggs, J., Ayele, A., Yirgu, G., Keir, D. and Stork, A. 2006. Magma-maintained rift segmentation at continental rupture in the 2005 Afar dyking episode. *Nature*. **442**, (7100), pp.291–4.

Wright, T.J., Sigmundsson, F., Pagli, C., Belachew, M., Hamling, I.J., Brandsdóttir, B., Keir, D., Pedersen, R., Ayele, A., Ebinger, C., Einarsson, P., Lewi, E. and Calais, E. 2012. Geophysical constraints on the dynamics of spreading centres from rifting episodes on land. *Nature Geoscience*. **5**, (4), pp.242–250.

Yu, X., Chen, L.-H. and Zeng, G. 2015. Growing magma chambers control the distribution of small-scale flood basalts. *Scientific Reports*. **5**, p.16824.

Zambrano, J.J. and Urien, C.M. 1970. Geological outline of the basins in southern Argentina and their continuation off the Atlantic shore. *Journal of Geophysical Research*. **75**, (8), pp.1363–1396.

Zastrozhnov, D., Gernigon, L., Gogin, I., Planke, S., Abdelmalak, M.M., Polteau, S., Faleide, J.I., Manton, B. and Myklebust, R. 2020. Regional structure and polyphased Cretaceous-Paleocene rift and basin development of the mid-Norwegian volcanic passive margin. *Marine and Petroleum Geology*. **115**, (September 2019), p.104269.

Zhang, C., Koepke, J., Kirchner, C., Götze, N. and Behrens, H. 2015. Rapid hydrothermal cooling above the axial melt lens at fast-spreading mid-ocean ridge. *Scientific Reports*. **4**.

Ziegler, P. a. and Cloetingh, S. 2004. Dynamic processes controlling evolution of rifted basins. *Earth-Science Reviews*. **64**, pp.1–50.